Ion-specific particle aggregation probed by different analytical techniques

Oncsik, Tamas

UNIVERSITÉ DE GENÈVE FACULTÉ DE SCIENCES

Section de chimie et biochimie Professeur Michal Borkovec
Département de chimie minérale et analytique

Ion-specific Particle Aggregation Probed by Different Analytical Techniques

THÈSE

présentée à la Faculté des Sciences de l'Université de Genève

pour obtenir le grade de Docteur ès sciences, mention chimie

par

Tamas ONCSIK

de

Orosháza (Hongrie)

Thèse N° 4999

GENÈVE

Atelier ReproMail

2016

UNIVERSITÉ DE GENÈVE

FACULTÉ DES SCIENCES

Doctorat ès sciences
Mention chimie

Thèse de *Monsieur Tamas ONCSIK*

intitulée :

"Ion-specific Effects on Particle Aggregation Probed by Different Analytical Techniques"

La Faculté des sciences, sur le préavis de Monsieur M. BORKOVEC, professeur ordinaire et directeur de thèse (Département de chimie minérale et analytique), Monsieur G. HOPFGARTNER, professeur ordinaire (Département de chimie minérale et analytique) et Monsieur P. J. DYSON, professeur (Laboratoire de chimie organométallique et médicinale, Ecole Polytechnique Fédérale de Lausanne, Suisse), autorise l'impression de la présente thèse, sans exprimer d'opinion sur les propositions qui y sont énoncées.

Genève, le 21 octobre 2016

Thèse - 4999 -

Le Doyen

N.B. - La thèse doit porter la déclaration précédente et remplir les conditions énumérées dans les "Informations relatives aux thèses de doctorat à l'Université de Genève".

Contents

Abstract

This thesis is focusing on comprehensive aggregation studies involving polymeric latex particles and different ionic coagulating agents. In the first chapter a detailed description of the particle aggregation and the principle of the different experimental techniques will be given. Besides, the chapter provides a brief introduction to the colloidal particles and to the ionic liquids used in the different projects.

The second chapter focuses on the aggregation of negatively charged latex particles in the presence of different multivalent salts. We demonstrate the relevance of the counterion valence in the aggregation process, reflecting the well-known Schulze-Hardy rule. A comparison with literature data will reveal that our systems investigated show similar behavior to the ones described earlier. Moreover, we provide an experimental evidence of the slowdown in the aggregation process at elevated electrolyte concentrations, which can be explained by the bigger viscosity of the media under these conditions.

The third chapter presents direct force measurements between negatively charged latex particles in aqueous solutions of electrolytes of different counterion valence in order to investigate the origin of the Schulze-Hardy rule. We show that in case of mono- and divalent counterions, the observed force profiles can be rationalized by the theory of Derjaguin, Landau, Verwey and Overbeek (DLVO) down to few nm. At shorter distances and in case of counterions of higher valence, additional non-DLVO forces are needed to interpret the forces acting between the particles. Based on these force profiles, we were able to calculate aggregation rates which agree reasonably well with the ones independently measured by light scattering.

The fourth chapter reports a study where we show that ions of the same valence can have completely different effects on aggregation of positively and negatively charged latex particles. Depending on the hydration state of the counterion, characteristic shifts in the critical coagulation concentrations (CCC) can be seen. The results reflect the well-known Hofmeister series. Comparison between experimental CCCs and those calculated by the DLVO theory reveals that the different extent of the ion adsorption is the main responsible for the ion-specific effects.

A detailed study with force profiles and aggregation rates involving positive and negative charged polystyrene latex articles is presented in the fifth chapter, where the origin of the Hofmeister effect in particle aggregation is investigated. We demonstrate that the interaction force profiles cannot be described with the pure DLVO theory, an additional attractive short-ranged non-DLVO force must be included. The measured and calculated CCCs including the characteristic shifts due to the Hofmeister effect agree in an excellent fashion in each system.

The sixth chapter presents the extension of the well-known Hofmeister series based on aggregation studies. This project can be considered as the continuation of the one presented in the fourth chapter, since the same particles were investigated. Besides simple monovalent salts, water miscible ionic liquids (ILs) were used as coagulating agents. It will be shown that only small changes in the anion or cation structure can cause huge differences in their coagulating power. Based on the results obtained, we propose an extended Hofmeister series.

The seventh chapter reports an aggregation study of sub-micron and nano-sized latex particles in room temperature ionic liquids and in their water mixtures. In each system, the entire IL concentration range will be explored, starting with dilute solutions through intermediate concentrations to the pure ILs with traces of water. Two different stabilization mechanisms will be suggested, namely viscous and solvation stabilization. While the former one is important in highly viscous ILs, where the diffusion can be hindered due to the increased viscosity of the media, the latter one is system specific, but can lead to significant slowdown in the aggregation process. The knowledge generated from this project has a huge impact in the materials science, cause the ILs are commonly used in nanoparticle synthesis, where the fate of the synthesized particles is crucial for further applications.

The eighth chapter contains the general conclusions of the thesis.

Résumé

Cette thèse se focalise sur l'étude des différents mécanismes d'agrégation entre les particules de latex fonctionnalisées et divers agents de coagulation d'origine ionique. Dans le premier chapitre, une description détaillée sur l'agrégation des particules sera traitée ainsi que le principe des différentes techniques expérimentales utilisées. De plus, ce chapitre introduira les particules colloïdales et les liquides ioniques utilisés dans les différents projets.

Le second chapitre traite de l'agrégation entre deux particules négatives de latex en présence de différents sels multivalents. On démontrera la pertinence de la valence des contre–ions sur le processus d'agrégation, ce qui est traduit par la règle de Schulze–Hardy. Une comparaison entre nos données et ceux de la littérature ont révélée que notre système se comporte de manière similaire à ceux décrit précédemment. Par ailleurs, on montrera des résultats expérimentaux sur le ralentissement du processus d'agrégation aux fortes concentrations d'électrolytes pouvant être expliqué par une plus grande viscosité de la solution sous ces conditions.

Le troisième chapitre présente les mesures de forces entre les particules de latex chargées négativement en solution pour divers électrolytes de valences différentes afin d'étudier l'origine de la règle de Schulze–hardy. On montrera que dans le cas des contre–ions mono- et di-valent, les profiles de forces peuvent être modélisés jusqu'à quelques nanomètres par la théorie de Derjaguin, Landau, Verwey et Overbeek (DLVO). Pour de faibles distances et dans le cas des contre–ions de plus hautes valences, des forces additionnelles d'origine non-DLVO doivent être ajoutées afin d'interpréter les forces agissantes entre les particules. Basé sur ces profiles de force, on a été capable de calculer les constantes d'agrégation dont les résultats obtenus sont en accord avec ceux mesurés par diffusion de la lumière.

Le chapitre quatre traite d'une étude où l'on a mis en évidence que divers ions de même valence peuvent avoir des effets complètement différents sur l'agrégation des particules de latex chargées positivement et négativement. En fonction du degré d'hydratation des contre–ions, un déplacement dans la valeur de la concentration critique de coagulation (CCC) a été observé. Ces résultats traduisent l'effet de la série de Hofmeister. La comparaison entre les CCC déterminées

expérimentalement et calculées par la théorie de DLVO montre que l'adsorption des ions sur les particules est responsable de ces effets spécifiques des ions.

Une étude détaillée sur les profiles de force et sur les constantes d'agrégation entre les particules positive et négative de latex fonctionnalisées par du polystyrène est présentée dans le chapitre cinq où l'effet de la série de Hofmeister est étudiée. On démontrera que les profiles des forces d'interactions ne peuvent pas être décrites par la théorie de DLVO seule et qu'une force attractive supplémentaire d'origine non-DLVO doit être ajoutées. Les CCC mesurées et calculées ainsi que leurs déplacements dus à la série de Hofmeister sont en accord pour chaque système investigués.

Le sixième chapitre présente une extension de la série de Hofmeister basée sur l'étude d'agrégation. Ce projet peut être considéré comme la suite du quatrième chapitre étant donné que les mêmes particules ont été utilisées. En plus des ions monovalents, des liquides ioniques (IL) miscibles dans de l'eau ont été utilisés comme agents de coagulation. On s'efforcera de montrer comment les changements dans la structure des anions ou cations peuvent induire autant de différences dans leur pouvoir de coagulation. Sur la base de ces résultats une extension de la série de Hofmeister sera proposée.

Le septième chapitre traite d'une étude sur l'agrégation des particules de latex de taille micro- et nano-métrique à température ambiante dans des liquides ioniques purs ou dilués avec de l'eau. Dans chaque système, une échelle de concentration des liquides ioniques sera explorée. Elle commencera pour des solutions diluées jusqu'à celle des IL purs présentant des traces d'eau en passant par des concentrations intermédiaires de IL diluées dans de l'eau. Deux mécanismes de stabilisation sera suggérés correspondant à une stabilisation par la viscosité et par la solvatation. La stabilisation par la viscosité est importante pour les IL hautement visqueux car la diffusion peut être annihilée due à l'augmentation de la viscosité de la solution. La stabilisation par la solvatation est dépendent du système mais peut résulter en une diminution significative du processus d'agrégation. Les connaissances générées par ce projet ont un fort impact dans la science des matériaux car les IL sont communément utilisés dans la synthèse des nanoparticules où la caractéristique des nanoparticules synthétisée est cruciale pour divers applications.

Le chapitre huit fournit une conclusion générale de la thèse.

CHAPTER 1

INTRODUCTION

1.1 Particle suspensions and their stability

Particle suspensions represent an important class of materials, which can be found in nature and in numerous manufacturing processes. They are widely used in papermaking, food, cosmetics and paint formulation as well as they can be relevant in biomedical applications (Figure 1).

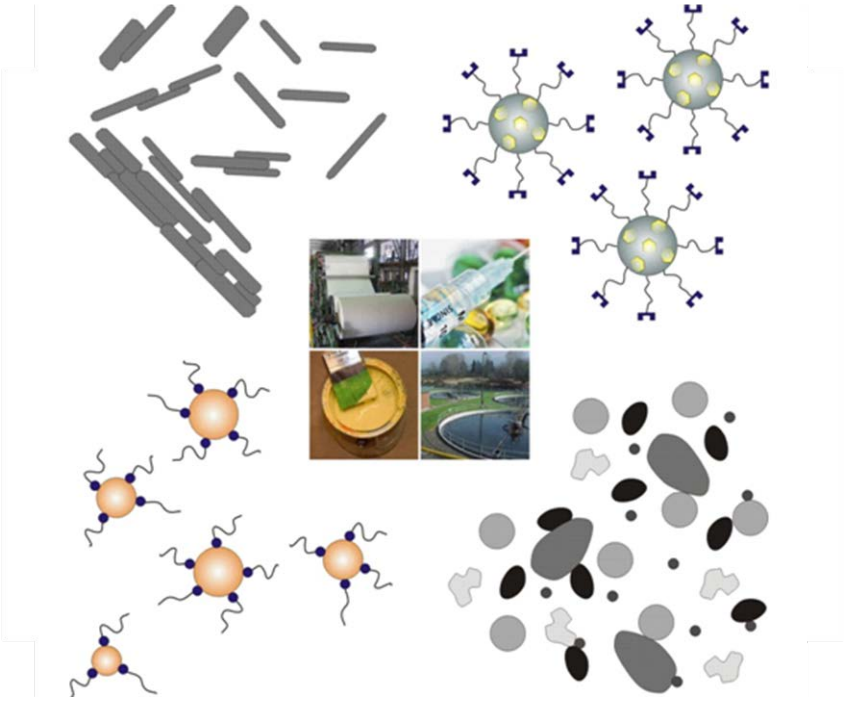

Figure 1 Some applications where suspended particles are important, clockwise, starting from the upper left corner: papermaking, drug and gene delivery, wastewater treatment, and paint formulation.

In papermaking, mixtures of negatively charged cellulose fibers and fillers (calcite, titania) are treated with cationic polyelectrolyte in order to achieve the product desired.[1,2] Paint formulation is another important process dealing with solid particles. Since the development of water-based products, they mainly contain water, pigments, fillers and stabilizing agents. Titania, calcite, clay,

silica or polymeric latex particles are used most frequently, depending on the properties desired.[3,4] Particles can be found in cosmetics and food products. The typical example of such systems is the titania-containing sunscreens due to its advantageous UV-adsorption properties.[5] Particles are commonly used to stabilize food colloids such as emulsions or foams.[6] Destabilization of suspended solid particles is an important phenomena in wastewater treatment. The dust and other particles are aggregated followed by sufficient sedimentation and filtration. Organic polymers or multivalent metal ions are the most frequently used coagulating agents.[7,8] Growing interest in nanoparticle-based systems can be seen in different biomedical applications. Iron-oxide or layered double hydroxide particles are widely used in gene and drug delivery.[9] They have to be specifically modified in order to achieve advantageous properties. The high stability of such systems is crucial due to the complex environment of a biological medium.

The stability of particle suspensions depends on many factors. The size of the suspended particles varies from few nm that one can refer to as nanoparticles, to micrometer range, which represents real colloidal systems. Besides the size of the particles, their composition can substantially differ. In the nature, several metal and oxide particles exist. Another important class of suspensions, where the dispersed particles are of polymeric origin. Regardless of the chemical composition of the dispersed solid phase, particle dispersions can be routinely synthesized in laboratory environments. Due to the huge effort made in the past, the size and the composition as well as the shape of the particles can be precisely controlled during preparation. Besides spherical shape, rod-like elongated particles can be achieved according to the applications desired. The suspended particles are often charged, which can originate from pH-dependent acid-base equilibrium of certain surface functional groups or from adsorption of different additives. Therefore, the charge of the particles always depends on the environmental and experimental conditions, such as pH, ionic strength or type of solvent. One important parameter of such systems is their stability. Stable suspensions refer to a homogenous distribution of primary particles in the liquid medium, while in unstable systems aggregation occurs where the particles initially form doublets, and then higher order aggregates. The words “coagulation”, as well as “flocculation” are also used, but while the first one is a broader term, the latter one refers specifically to systems where the the aggregation is induced by polymers or polyelectrolytes. Accordingly, the materials that can induce aggregation are often referred to as coagulant or flocculant. These can be of different

nature, e.g. simply or complex electrolytes, charged or uncharged oligomers and polymers. When the instable suspension contains only identical colloidal particles, one talks about homoaggregation, while in case of dispersions of dissimilar particles, one can refer to heteroaggregation. Particle aggregation is usually irreversible, meaning that once the aggregates formed, they cannot be easily disrupted. As a consequence of the aggregation process, the larger aggregates may settle to the bottom of the container. This phenomenon is referred to as sedimentation. The course of aggregation can lead to creaming or gel formation depending on material properties and particle concentration.

Stabilization and/or destabilization need to be achieved by appropriately chosen conditions and additives. In order to describe and predict the behavior of the suspensions, the principles of particle aggregation need to be well-understood. In general, the driving force in determining the stability of a suspension is the nature of interparticle interactions. Colloidal particles are always attracted to each other by van der Waals forces. However, due to the charge of the particles, which results in an electrical double layer, repulsion can also be present depending on the conditions applied. The overall force acting between two colloidal particles is the superposition of these two contributions. This theory was elaborated in the 1940s independently by two Russian scientists (Derjaguin, Landau) and two Dutch scientists (Verwey, Overbeek).[10-12] In their honor, one refers to the DLVO theory.

Despite the fact that this theory is relatively old, the applicability of predicting stability of suspensions is still reasonable. It states, that at low ionic strength the particle aggregation rates are small, which then increases with increasing electrolyte concentrations, reaching a plateau value. This refers to as the fast aggregation, where only the diffusion of the particles determines the aggregation. The transition between slow and fast aggregation is often referred to as the critical coagulation concentration (CCC), which separates the two regimes. Detailed description of the DLVO theory will be given in the subchapter 1.2.3.

Due to the relevance of particle suspensions in everyday life, appropriate methods needed to be developed to monitor and describe aggregation processes. There are several techniques which can be routinely used to investigate such systems. In the following, detailed description will be provided about the methods I have been using to probe particle aggregation.

1.2 Methods to probe particle aggregation

Due to its relevance in fundamental as well as in applied research, several techniques have been developed and proposed to study particle aggregation. The aim of the studies can be for different purposes, e.g. precise determination of particle aggregation rates, optimization of the dosage of different additives or assessing the properties of the clusters formed upon aggregation, such as size and density. Besides its high practical impact, the methods developed are essential and of great importance in fundamental studies.

In the following, light scattering methods to determine aggregation rates, electrophoresis to obtain electrokinetic potential and the colloidal probe technique to directly measure interparticle forces will be discussed.

1.2.1 Aggregation rates by light scattering techniques

Destabilization of colloidal suspensions can be achieved by carefully chosen coagulants. Initially, particle doublets form in the early stage of the aggregation, while triplets and higher order aggregates can be found in the later stages of the process. Numerous techniques have been developed to probe particle aggregation.[13] Turbidity measurements can be useful in case of larger particles, however, small particles can only be investigated at higher concentrations where it is difficult to follow the early stages of the coagulation.

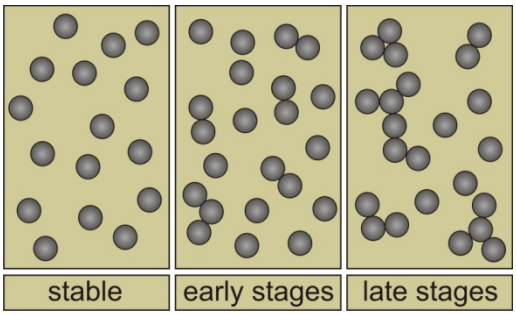

Figure 2 Schematic representation of stable and unstable particle suspensions

Time-resolved light scattering techniques turned out to be excellent tools to monitor this range of the aggregation process. Besides measuring the interaction between colloidal particles, light

scattering methods are useful to evaluate the different parameters of a colloidal suspension, such as particle size, shape or the concentration of the particles. Two types of scattering experiment can be performed, which provide us different valuable information of the systems investigated. Static light scattering (SLS), where the intensity of the scattered light is measured as a function of the scattering angle, provides structural information. Dynamic light scattering (DLS) is the analysis of the scattering intensity fluctuations over time which gives us information about the dynamics of the particles. Both techniques can be used in a time-resolved fashion which allows us to monitor the aggregation state of a colloidal suspension. Even though the particle aggregation is a complex kinetic process, its overall timescale is set by the rate of particle doublet formation.

In general, the elementary step of the particle aggregation is where the primary particles (A) form particle doublets (A_2):

$$A + A \rightarrow A_2 \tag{1}$$

Therefore, the corresponding rate law of this second order kinetic process can be written as:[14]

$$\frac{dN_{A_2}}{dt} = \frac{k}{2} N_A^2 \tag{2}$$

where N_{A_2} and N_A are the number concentration of the doublets and individual particles, respectively and k is the aggregation rate coefficient. If the particle aggregation is controlled entirely by the diffusion, the aggregation rate for doublet formation can be expressed with the Smoluchowski rate as:[13]

$$k = \frac{8k_B T}{3\eta} \tag{3}$$

where k_B is the Boltzmann constant, T is the absolute temperature and η is the dynamic viscosity of the medium. Smoluchowski has also shown that the half-time of aggregation ($T_{1/2}$) in a suspension, which initially contained only primary particles, can be defined as:

$$T_{1/2} = \frac{2}{kN_0} \tag{4}$$

where N_0 is the initial concentration of the particles, i.e., $N_0 = N_A + 2N_{A_2}$ if only doublet formation takes place. This half-time is the characteristic time needed to reduce the total number of primary particles by a factor of two.

The aggregation rates can be determined in SLS measurements by following the initial rate of change in the scattered intensity in time-resolved measurements performed at one or different angles. The intensity of the scattered light (I) originating from a suspension undergone early stages of the aggregation (i.e., only individual particles and doublets are present) can be defined as:[14]

$$I(q,t) = I_{\mathrm{A}}(q)N_{\mathrm{A}}(t) + I_{\mathrm{A}_2}(q)N_{\mathrm{A}_2}(t) \tag{5}$$

where t is the experiment time, I_{A} and I_{A_2} are the scattering intensity of the primary particles and doublets, respectively, whereas q is the magnitude of the scattering vector:

$$q = \frac{4\pi n}{\lambda}\sin\left(\frac{\theta}{2}\right) \tag{6}$$

where n is the refractive index of the medium, λ is the wavelength of the incident light and θ is the scattering angle.

At the beginning of the aggregation process, where the individual particles dominate, the following apparent static rate (Σ) can be calculated by differentiating equation (5) with respect to the time:[14]

$$\Sigma = \frac{1}{I(q,0)}\left(\frac{dI(q,t)}{dt}\right)_{t\to 0} = \left(\frac{I_{\mathrm{A}_2}(q)}{2I_{\mathrm{A}}(q)} - 1\right)kN_0 \tag{7}$$

Using the Rayleigh-Gans-Debye (RGD) theory to describe the form factor of the spherical primary particles of radius R and the doublets, the optical factor can be given by the following expression:[15]

$$\frac{I_{\mathrm{A}_2}(q)}{2I_{\mathrm{A}}(q)} - 1 = \frac{\sin(2Rq)}{2Rq}kN_0 \tag{8}$$

Accordingly, the apparent static rate coefficient can be obtained from the initial slope of the scattering intensity versus time plot by performing a linear fit. Typical curves can be seen in Figure 3.

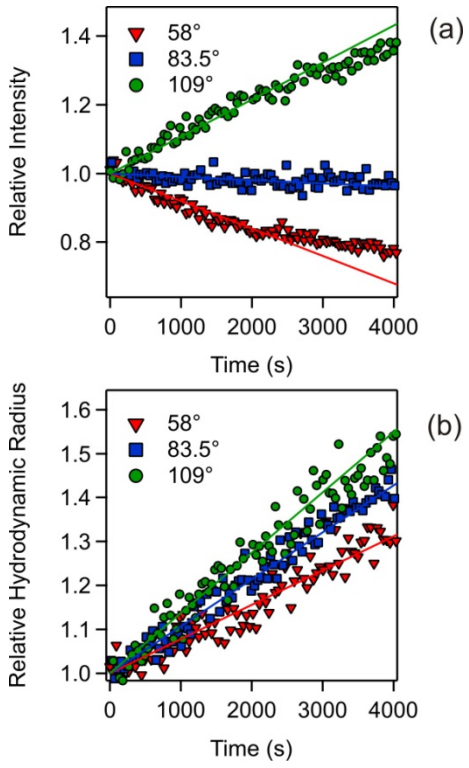

Figure 3 Relative change in the scattering intensity (a) and apparent hydronadynamic radius (b) with time during particle aggregation. The values are normalized to the initial value.[16]

DLS measures the average hydrodynamic radius (R_h) of particles in suspensions.[17] In the presence of primary particles and doublets, which undergo Brownian motion, the average R_h is given as:[18]

$$\frac{1}{R_h(t)} = \frac{I_{\mathrm{A}}(q)N_{\mathrm{A}}(t)/R_{h\mathrm{A}}(t) + I_{\mathrm{A}_2}(q)N_{\mathrm{A}_2}(t)/R_{h\mathrm{A}_2}(t)}{I_{\mathrm{A}}(q)N_{\mathrm{A}}(t) + I_{\mathrm{A}_2}(q)N_{\mathrm{A}_2}(t)} \tag{9}$$

where $R_{h\mathrm{A}}$ and $R_{h\mathrm{A}_2}$ are the hydrodynamic radii of the individual particles and doublets, respectively, and their relation is $R_{h\mathrm{A}_2} = 1.39R_{h\mathrm{A}}$ as calculated from the friction coefficient of a

doublet under laminar flow conditions (ref 4). The apparent dynamic rate (Δ), i.e., initial change of R_h, is written as:

$$\Delta = \frac{1}{R_h(q,0)}\left(\frac{dR_h(q,t)}{dt}\right)_{t\to 0} = \frac{I_{A_2}(q)}{2I_A(q)}\left(1-\frac{R_{hA}}{R_{hA_2}}\right)kN_0 \tag{10}$$

The Δ can be determined from the initial slope of the apparent hydrodynamic radius versus time curve and this quantity depends on the scattering angle. Combining equations (7) and (10), the form factor terms cancel out and one obtains k as:[14,19]

$$kN_0 = \frac{R_{hA_2}}{R_{hA_2}-R_{hA}}\Delta - \Sigma \tag{11}$$

Accordingly, measuring the initial rate of change in the scattered intensity and hydrodynamic radius simultaneously by SLS and DLS, respectively, the aggregation rate coefficients can be determined without knowing the optical properties of the particles.

The rate of aggregation can be also expressed in terms of the stability ratio (W), which is the ratio between the fast aggregation rate coefficient (k_{fast}) and the one (k) measured in the actual experiment:[14,15,20-22]

$$W = \frac{k_{fast}}{k} = \frac{\Sigma_{fast}}{\Sigma} = \frac{\Delta_{fast}}{\Delta} \tag{12}$$

As shown in the above equation, the W can be also determined from the apparent rates (i.e., only from time-resolved SLS or DLS measurements) without knowing the optical and hydrodynamic factors of the primary particles and doublets. In case of slow or reaction limited aggregation, only the $1/W$ fraction of the collisions leads to doublet formation, whereas, all collisions are efficient for the fast aggregation condition, where the aggregation of the particles is controlled entirely by their diffusion. Accordingly, stability ratio close to unity refers to fast aggregation and unstable samples, while higher values indicate slow aggregation and more stable suspensions.[23-29]

In most of the studies to be presented, the critical coagulation concentrations (CCCs) of different particle suspensions were determined. This was possible after measuring the aggregation rates at

several electrolyte concentrations. When one plots the aggregation rates versus the salt concentration in a logarithmic scale, two regimes are usually identified, referring to the slow and fast aggregation processes.[16] The CCC, which separates these two regimes, could be determined from the intercept of the corresponding two straight lines. These values allowed us to directly compare the effectiveness of the different ionic additives in coagulating the dispersion. A schematic representation of the change in the aggregation rates is shown in Figure 4.

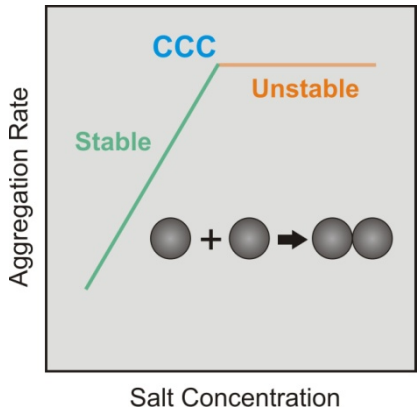

Figure 4 Illustration of the typical salt dependence of the aggregation rates.

1.2.2 Electrophoresis

Immersing a colloidal particle in an electrolyte solution, spatial distribution of the surrounding ions can be seen. This is due to the fact that the particle surface possesses a certain amount of charge. Ions of the same sign of charge as the surface are called coions, while the ones of opposite charge are the counterions. The concentration of counterions near the surface is higher due to electrical attraction, and an exponential decrease can be seen as the distance increases. In case of the coions the situation is the other way around, i.e., the concentration of the coions near the surface is almost negligible, and an exponential increase can be seen as the distance increases. This distribution of the ions originating from the dissolved salts leads to the formation of the electrical double layer (EDL).[30] A schematic representation of the EDL can be seen in the Figure 5.

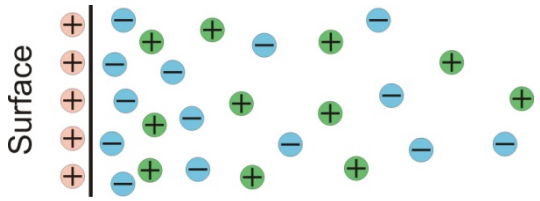

Figure 5 Illustration of EDL for a positively charged surface.

The development of surface charge can be due to different mechanisms, such as ion adsorption or protonation/deprotonation of ionisable acid-base active functional groups. Good example for the latter one is the silica, which at high pH possesses a net negative charge due to deprotonation of the Si-OH surface functional groups. The surface charge is compensated by an accumulation of counterions in the EDL. With respect to the type of interactions, basically two types of ions can be distinguished, namely indifferent ions and specifically adsorbing ions. The former ones adsorb on the surface only weakly due to Coulomb forces, while the latter ones have additional interactions with the surface. In case of huge affinity, ion adsorption can be so pronounced that the surface can be neutralized, or in special cases even overcharged. This means that the sign of the surface charge is reversed upon adsorption.[31,32]

A surface charge results in a surface potential (ψ_0), which is the potential corresponding to the solid surface in contact with the electrolyte solution. The potential at the beginning of the diffuse part of the EDL is called as diffuse layer potential (ψ_D), which has a similar value as the zeta or electrokinetic potential (ζ), as it can be seen in Figure 6.

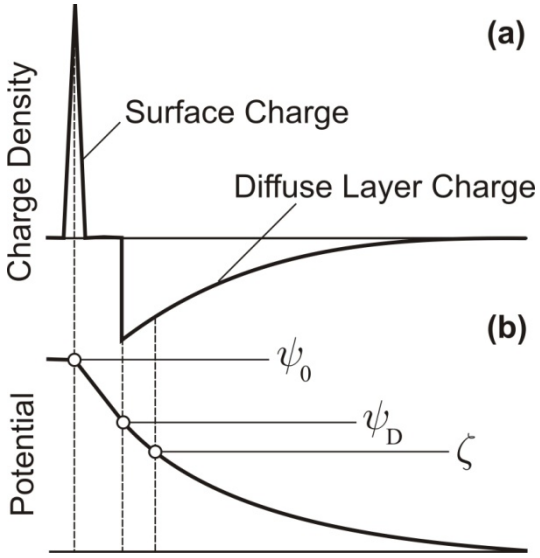

Figure 6 Charge density (a) and electric potential (b) profiles for a positively charged interface.

The latter potential is located at the so-called slip plane or shear plane, which is the distance from the surface at which a hydrodynamically stagnant layer exists. This layer moves together with particle when an external electrical field or mechanical force is applied.[33] In practice, the location of the shear plane is very close to the double layer; therefore, the zeta potential is equal (at low ionic strengths) or a bit smaller (at high ionic strengths) than the diffuse layer potential.

The most frequently used method to determine the zeta potential is the electrophoresis. It has proved to be an excellent tool to characterize the charging properties of the different suspended colloidal particles.[34,35] The method is based on the movement of charged particles dispersed in a liquid under an applied electric field. In practice, two electrodes are used and the positively charged objects move towards the lower potential (i.e., negative electrode) and the negatively charged ones towards the higher potentials. The electrophoretic velocity (υ) is proportional to the electrophoretic mobility (u) as:[30]

$$u = \frac{\upsilon}{E} \tag{13}$$

where E is the magnitude of the electric field strength. The mobility of an isolated single ion of valence V and radius R moving in an electric field is:

$$u = \frac{eV}{6\pi\eta R} \tag{14}$$

where e is the elementary charge. In the electrophoretic mobility experiments, the particles move together with a stagnant layer of ions detailed above and the measured mobility values can be related to the electrokinetic or zeta potentials as follows.

Depending on the particle size and the ionic strength in the suspension, different methods need to be used to convert the electrophoretic mobilities to potentials.[33] In order to choose the most appropriate conversion model, one has to consider the R and κ values. The latter one is the so-called inverse Debye length which contains the contribution of all ionic species as:

$$\kappa = \sqrt{\frac{2N_A e^2 I}{\varepsilon\varepsilon_0 k_B T}} \tag{15}$$

where N_A is the Avogadro number, ε_0 is the permittivity of vacuum, ε is the dielectric constant and I is the ionic strength. As discussed above, charged surface and the neutralizing diffuse layer of counterions form the EDL. The thickness of this layer is in the order of the Debye length. If $\kappa R \gg 1$ (i.e., big particles and/or high ionic strength) and the potential is low ($|\zeta| \leq 50$ mV), the analytical model developed by Helmholtz and Smoluchowski can be used to calculate the electrokinetic potential as:[30]

$$\zeta = \frac{u\eta}{\varepsilon_0 \varepsilon} \tag{16}$$

If $\kappa R \ll 1$ (i.e., small particles and/or low ionic strength), the Hückel-Onsager equation can be applied:

$$\zeta = \frac{3u\eta}{2\varepsilon_0 \varepsilon} \tag{17}$$

For the transition range between low and high κR values, the Henry's formula is appropriate for the conversion as follows:[36]

$$\zeta = \frac{3u\eta}{2\varepsilon_0 \varepsilon} f(\kappa R) \tag{18}$$

where $f(\kappa R)$ is the Henry's function, which varies from 1 to 1.5 depending on the ionic strength in the suspensions. The latter model is limited to low potentials ($|\zeta| \leq 50$ mV). For higher potentials, the more complex O'Brien-White theory is recommended to use in the intermediate κR region.[35] Accordingly, given the size of the particles and the electrolyte concentration in our system, the most suitable model can be selected and good precision can be achieved while converting electrophoretic mobility values to electrokinetic potentials.

Once the electrokinetic potentials are calculated, the corresponding surface charge density of the particles can be estimated. Following the ionic strength dependence of the potentials gives information about the charge density if one uses appropriate model to fit calculated data to the experimental values. In case of planar surfaces, the Gouy-Chapman theory relates the surface charge (σ) to the surface potential, as:[37]

$$\psi_0 = \frac{2k_B T}{e} \operatorname{asinh}\left(\frac{e\sigma}{2k_B T \varepsilon \varepsilon_0 \kappa} \right) \tag{19}$$

This equation is derived from the Poisson-Boltzmann description of the EDL within the DLVO theory to be discussed in detail later.[10-12] However, the surface potential cannot be measured directly, but can be calculated from the electrokinetic or diffuse layer potentials using model assumptions. For spherical ions or colloids, the Debye-Hückel theory describes the decrease of the potential with the distance from the surface as:[38]

$$\sigma = \varepsilon \varepsilon_0 \kappa \psi_0 \tag{20}$$

This equation is the linearized solution of the Poisson-Boltzmann model and it is valid for low potentials (i.e., moderately charged surface).

1.2.3 Atomic Force Microscopy

As discussed in 1.2.1, electric double layer is formed as charged colloidal particles are suspended in an electrolyte solution. This has a huge impact in the stability of the dispersions. When two highly charged particles get close to contact, they repel each other by a built-up osmotic pressure due to the overlap of the double layers. This interaction results in a repulsive interparticle force. Regardless of the magnitude of the surface charge, attractive van der Waals forces are always present, originating from rotating or fluctuating dipoles of atoms and molecules. These two forces are the base of the well-known DLVO theory, which was named after B. Derjaguin, L. Landau, E. Verwey and Th. Overbeek. This theory states that the overall interparticle force can be approximated by the sum of these repulsive and attractive forces.[10-12] However, non-DLVO forces may also be present, which can be induced by surface charge heterogeneities,[39] polymer adsorption,[40,41] or depletion interactions generated by suspended macromolecules.[42]

Applying the Derjaguin approximation,[38,43] which describes the forces between two spheres in terms of the energy per unit area of two flat surfaces and is valid for particles of significantly larger size than the ranges of the forces, the overall interparticle force (F) between two identical particles at a separation distance (h) is:

$$F(h) = F_{\mathrm{vdW}}(h) + F_{\mathrm{DL}}(h) \tag{21}$$

Accordingly, the DLVO theory states that the total force is the sum of the repulsive (by the electrical double layers) and attractive (by van der Waals interactions) contributions (Figure 7).

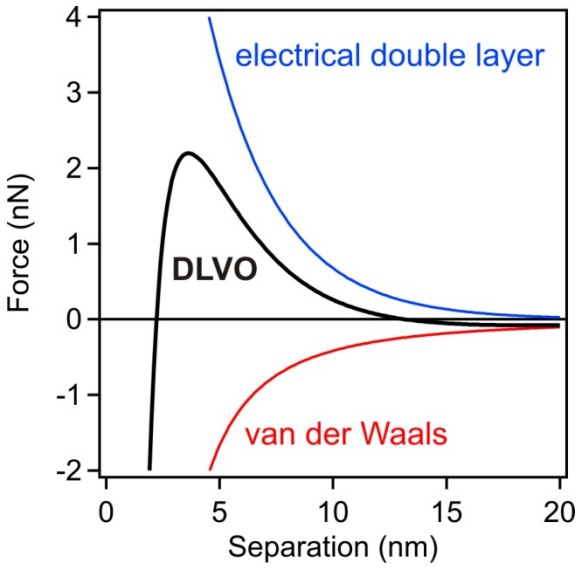

Figure 7 Schematic representation of the DLVO forces[10-12]

The attractive van der Waals forces are always present and they can be calculated with the following equation:

$$F_{\mathrm{vdW}}(h) = -\frac{RH}{12h^2} \tag{22}$$

where H is the Hamaker constant, which mainly depends on the nature of the materials.[38] If the surface charge density is low, the forces originating from the electric double layers can be treated within the Debye-Hückel superposition approximation as:

$$F_{\mathrm{DL}}(h) = 2\pi\varepsilon_0\varepsilon R\psi_0^2 e^{-\kappa h} \tag{23}$$

For higher surface charge densities and smaller surface separations, the Poisson-Boltzmann theory must be used to describe the forces caused by the electrical double layers. The DLVO theory includes also the estimation of the aggregation rates, which can be calculated from the steady-state solution of the forced diffusion equation as:[15]

$$k = \frac{4k_{\mathrm{B}}T}{3\eta R}\left[\int_0^{\infty}\frac{B(h)}{(2R+h)^2}\exp\left[\frac{V(h)}{k_{\mathrm{B}}T}\right]dh\right]^{-1} \tag{24}$$

where $B(h)$ is the hydrodynamic resistance function and $V(h)$ is the potential energy obtained from the analytical integration of the force profile as:

$$V(h) = \int_{h}^{\infty} F(h')dh' \tag{25}$$

As one can realize at this point, if the interparticle forces are determined accurately, the aggregation rates can be calculated and compared to the ones measured independently with other techniques, e.g., with light scattering.[44,45]

Several techniques can be used to directly measure interaction forces between surfaces. The most well-known and applied methods are the following:

- Surface Force Apparatus[46-48]
- Total Internal Reflection Microscopy[49]
- Optical Tweezers[50]
- Colloidal Probe Technique.[51,52]

The Surface Force Apparatus (SFA) measures the forces between two smooth curved mica surfaces of a radius of 1 cm in a crossed cylindrical configuration. Despite the highest distance resolution which is offered by this technique among all, it has several restrictions. Its main drawback is that it requires mica surfaces. In case of the Total Internal Reflection Microscopy (TIRM), the separation distance can be accurately determined between a colloidal particle immersed in a liquid and a transparent plate. It is a sensitive technique by which the interaction potential can be determined by the Boltzmann equation from the equilibrium distribution of the separations. In the optical tweezers, one particle is positioned close to another one, where the interaction force profile can be extracted from their trajectories followed by a video camera. The latter two methods provide an excellent force resolution in the sub-pN regime, however, their positional resolution is only in the nm range.

The latter one can be carried out with an atomic force microscope in different geometries leading to a force resolution of 10-50 pN. In the sphere-plane mode, the probe particle is attached to a tip-less cantilever and it approaches the substrate with an AFM scanner. The force can be converted

from the deflection of the cantilever by measuring the reflection of a light beam focusing on the cantilever. In the sphere-sphere geometry, one of the particles is also attached to the tip-less cantilever, however, the other one is immobilized on the surface of the substrate. The particles have to be centered laterally (e.g., with an optical microscope) and this setup allows investigating interaction forces between the particles directly (Figure 8).

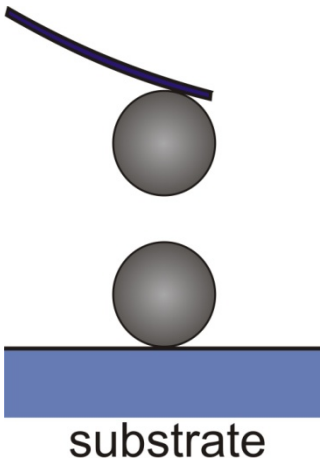

Figure 8 Schematic representation of the geometry applied in the AFM-based colloidal probe experiments

In the multiparticle mode, one works in suspensions of the particles where concentration if the additives can be more precisely adjusted, in addition, the particles are attached in the liquid, thereferore, bubble formation due to the hydrophobicity of the surfaces is negligible. Based on this method, force measurements can be also performed between different particles.[53] In the present thesis, aggregation rates measured for colloidal particles by light scattering will be compared to the rates calculated from the interparticle forces determined by the colloidal probe technique.

1.3 Colloidal Particles

There are several types of particles which can be routinely used for fundamental as well as applied research. The most commonly investigated ones are the following:

- metal: Au, Ag, Pd, Rh nanoparticles;
- metal oxide: Fe_2O_3, TiO_2, WO_3;
- metal hydroxide: $Fe(OH)_3$, layered double hydroxides
- metal halide: AgX, where X can be Cl, Br, I;
- metalloid oxide or sulfide: SiO_2, As_2S_3;
- carbon-based: nanotubes, fullerenes, graphite, graphite-oxide;
- polymer-based: particles of polystyrene or other type of polymers.

Not only the bare particles can be probed, but they can be decorated with grafted chemical groups, proteins, or polymers. Such surface modifications are very important, since in many cases coatings are used to prevent the aggregation of particles, promoting their stability. In the present thesis, differently functionalized polystyrene-based spherical latex particles were investigated. They are surface functionalized commercial products purchased from Interfacial Dynamic Cooperation (Portland, USA). Latex dispersions are widely used in different applications,[54-57] due to their advantageous properties such as tunable surface charge and well-defined size and shape. The chemical composition of their surface is shown in Figure 9.

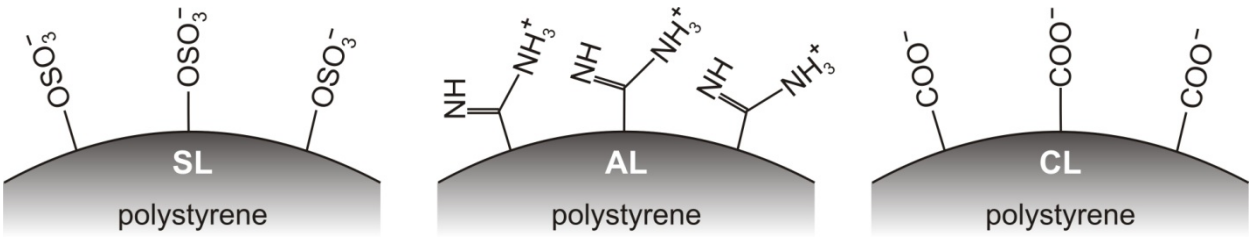

Figure 9 Illustration of the latex particle surfaces. The different particles are functionalized with sulfate (SL), amidine (AL) or carboxylate (CL) groups.

Despite their surface functionalities, they can be considered as hydrophobic, which plays a key role in their stability under the various conditions. Due to the different acid-base properties of the functional groups, their surface charge is pH dependent. The sulfate or carboxylate containing particles possess negative charge at sufficiently high pH, while the amidine terminated particles are positive at low pH. Due to the different nature of these functional groups, pH adjustment needed to be carefully done throughout the different measurements. They are monodisperse, meaning that their particle size distribution is rather narrow. The important parameters of the different particles used are summarized in Table 1.

Table 1 The characteristic parameters of the different latex particles used.

Latex	Surface functionality	Particle Radius (nm)		Polydispersity (%)[a,d]	SCD (mC/m^2)[a,e]
		TEM[a,b]	DLS[c]		
SL100	sulfate	50	58	7.9	-20
SL530	sulfate	265	278	2.0	-77
SL980	sulfate	490	550	2.2	-67
CL1000	carboxylate	500	516	4.5	-127
AL220	amidine	110	117	4.3	+130
AL950	amidine	475	530	3.6	+237

[a]The values were reported by the manufacturer. [b]Determined by transmission electron microscopy. [c]Measured by dynamic light scattering. [d]Coefficient of variation of size obtained by TEM. [e]Surface charge density values of the particles in fully ionized state, measured by conductometric titration.

These particles are most useful to investigate charging, stability and interparticle forces in different ionic environment. The additives used to study ion-specific aggregation include not only commonly used simple electrolytes, such as chloride salts of alkali and alkali earth metals, but complex salts like $[Co(NH_3)_6]Cl_3$ or $[Ru(NH_3)_6]Cl_3$ too. In addition, the effect of a novel type of ionic materials called ionic liquids was also probed. A general description of this compound group will be given in the next subchapter.

1.4 Ionic Liquids

Ionic liquids (ILs) are salts with a melting point below 100 °C. They consist solely of ions resulting in unusual properties such as low vapor pressure, high chemical and thermal stability or wide electrochemical window. They are also called designer solvents due to their variable properties simply by varying the constituent anions and cations.[58,59] They are extensively studied from fundamental perspectives as well as in numerous applications, such as electrochemical devices, biomass production, or nanoparticle synthesis.[60-64]

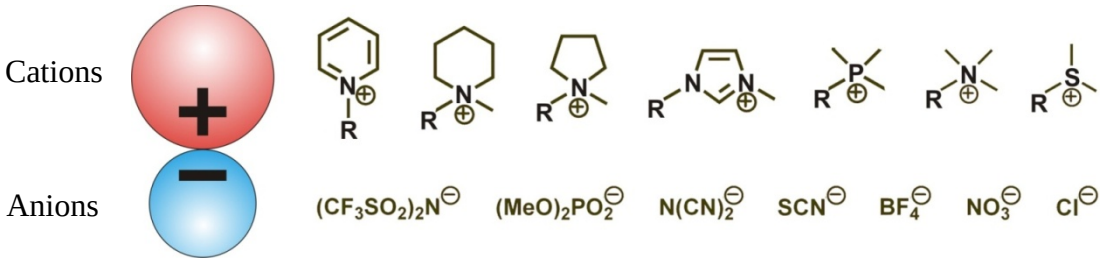

Figure 10 Schematic representation of the most common IL constituent cations and anions

Due to the large combination of salts (theoretically 10^{18} ILs re possible) and their widespread applications, the research efforts on designing task-specific ILs are dynamically increasing.[65]

There are several types of particles which can be successfully synthesized in ILs, such as metal, oxide, or latex particles.[66-70] But one thing is to prepare these suspensions, their applicability strongly depends on the stability of such systems. Therefore, it is necessary to explore their effect on particle aggregation. In the present thesis, two different projects dealing with ILs will be presented. One of them investigates the ion-specific effects of different IL constituent cations and anions, how only small modifications in their structure can cause dramatic changes, resulting in completely different suspension behavior. The other one explores the stability of latex particles in ionic liquids and their binary water mixtures, starting with dilute through intermediate, more concentrated solutions to the pure ILs. In the latter case, different stabilization mechanisms will be proposed.

1.5 Outline of the thesis

In this subchapter, the remaining part of the thesis will be summarized. It consists of different studies on the charging and aggregation of latex particles using electrophoresis and light scattering techniques. In addition, in some cases the interparticle forces will be explored by means of the AFM-based colloidal probe technique.

The **second chapter** deals with the effect of multivalent ions on the charging and aggregation of two negatively charged latex particles. It reveals that the valence of the counterion is highly relevant in determining the stability of a suspension. Multivalent ions tend to adsorb on the oppositely charged surface in a more pronounced way, destabilizing the dispersions more efficiently. This behavior confirms the well-known Schulde-Hardy rule, which states that the critical coagulation concentration (CCC) of a given suspension is inversely proportional to the counterion valence.

$$\mathrm{CCC} \propto \frac{1}{z^n} \tag{26}$$

This rule can be derived from the DLVO theory, where z is the valence of the counterion, $n = 2$ for weakly charged particles, and $n = 6$ for highly charged ones.

An important finding described in this chapter was that the aggregation rates decreased at elevated salt concentrations. This could suggest some kind of restabilization process due to the enhanced adsorption of the counterions. However, the salt level is too high for such phenomenon. This behavior is shown in Figure 11.

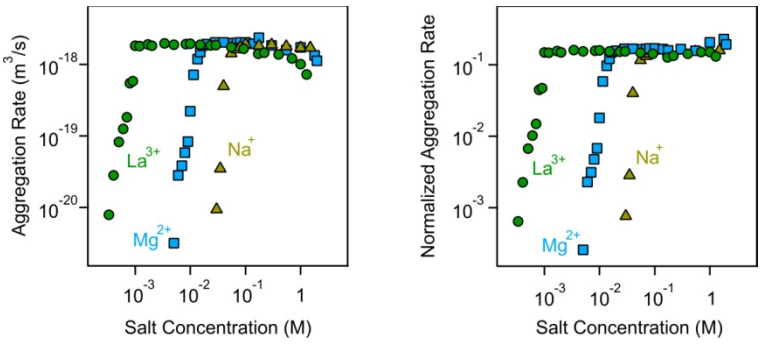

Figure 11 Aggregation behavior of CL1000 at pH 4.0 in case of counterions of different valence. Normalized aggregation rates were calculated with the corresponding Smoluchowski values. More details in the chapter 2.

The decrease can be attributed to the increased viscosity of the medium. The viscosity of electrolyte solutions can be up to a factor of 2-3 higher than the one of water, especially in case of salts containing ions of higher valence, which leads to a slowdown of the diffusion-controlled aggregation process. This effect becomes more obvious, when the normalized aggregation rate coefficients are presented. They can be calculated with respect to the corresponding Smoluchowski values at each salt level investigated. In this representation, the effect of the solution viscosity is factored out, so one can observe that the normalized rates remain constant even at the highest concentrations measured.

At the end of this chapter, a comprehensive comparison with literature was made. We collected relevant data from literature dealing with different types of particles. These data are summarized in Figure 12.

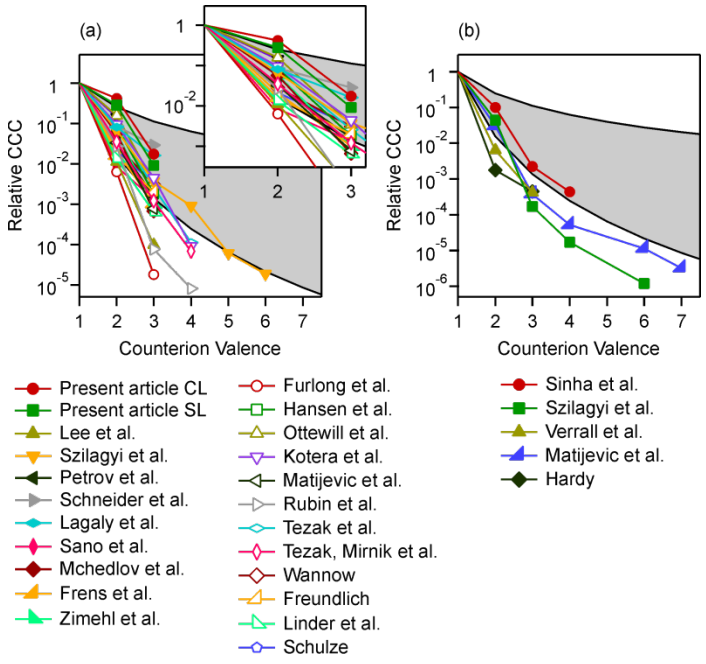

Figure 12 Relative CCCs with respect to its value for monovalent electrolytes for the present systems and others reported in the literature. The expected power law dependence is indicated for $n = 2$ and 6. (a) Cations together with negatively charged particles (with the inset up to trivalent ions) and (b) anions with positively charged particles. Mor details in the second chapter.

One can observe that the CCCs decrease with the valence but there is substantial system specificity. However, several common trends can be seen. First, multivalent anions are more

effective to destabilize colloidal suspensions than are multivalent cations. Second, the power law given by equation (26) describes the data with $n = 6$ relatively well. However, this observed trend reflects the valence-dependence only semiquantitatively. In order to better understand the behavior of the system, some progress could be made by combining aggregation rates with direct force measurements. This combined study will be presented in the next chapter.

In the **third chapter**, the Schulze-Hardy rule is further explored. Besides accurate measurements of aggregation rates by time-resolved light scattering, direct force measurements were also carried out for the better understanding of these interactions. The same CL1000 particles and electrolytes were used in this study for direct comparison of the behavior. The obtained force profiles in the different electrolyte solutions can be seen in Figure 13.

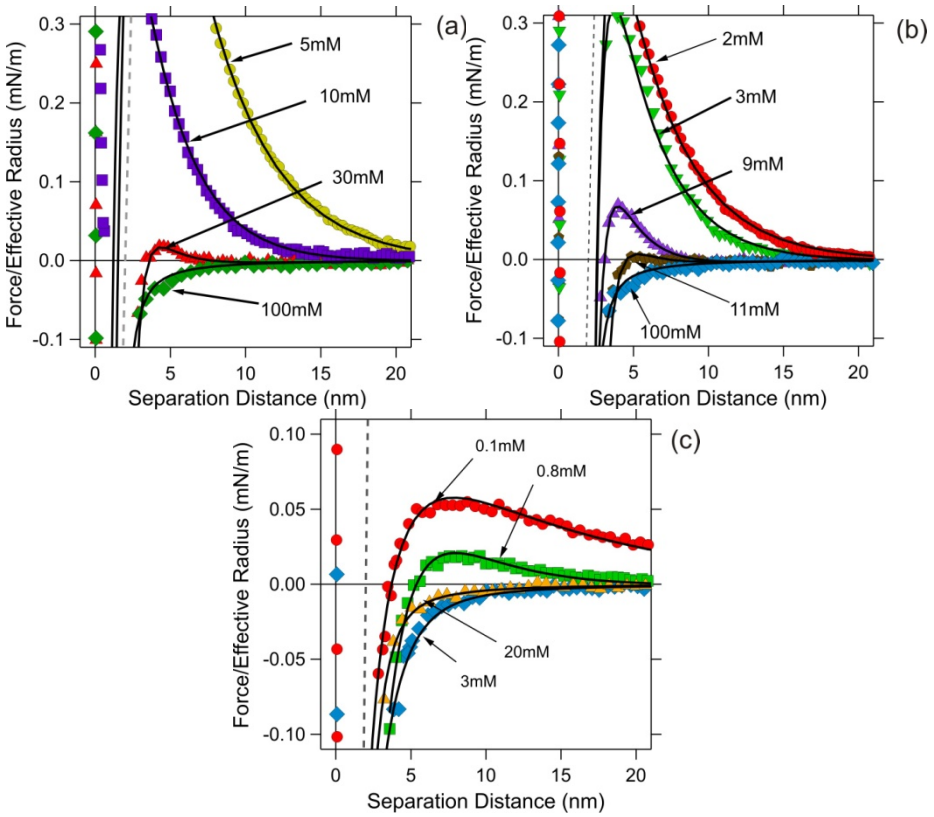

Figure 13 Force profiles between CL1000 particles in different electrolyte solutions at pH 4.0 at the concentrations indicated. (a) KCl, (b) $MgCl_2$, and (c) $LaCl_3$. More details can be found in the third chapter.

In case of KCl at low concentrations the forces are strongly repulsive, reflecting the overlap of the electrical double layers. Increasing the salt concentration, due to the charge screening this

repulsion weakens, and a maximum in the force curves is observed. This maximum is visible at 30 mM KCl concentration. Further increasing the concentration, purely attractive force is acting, which indicates that evanescence of the double layer repulsion. At this stage, only the omnipresent van der Waals interaction determines the interaction. In addition to this, a jump-in at distances of about 2 nm can be observed. In the presence of $MgCl_2$ and $LaCl_3$, the force profiles are qualitatively similar, however, there are quantitative differences. First, purely attractive curves are observed at decreasing concentrations with increasing the valence of the counterion. Second, the maximum in the force curves shifts to larger distances. This can be explained by the fact that an increasing valence of the ions leads to an increasingly important contribution to the ionic strength and thereby to electrostatic screening.

By fitting the obtained data, it has been revealed that the DLVO theory is capable of describing the force profiles rather well in the presence of mono- and divalent ions, even though a non-DLVO exponential short-ranged attraction is present at distances below 2 nm. In case of ions of higher valence, DLVO fails to describe the interaction even at separation distances above 5 nm. This discrepancy originates from the fact that the attractive forces are stronger than the van der Waals force determined in systems containing ions of lower valence. This attraction can be rationalized with an additional exponential attraction of longer range. We suspect that this originates from patch-charge heterogeneities of the substrate, which are amplified in the presence of multivalent ions.

Determining the force profiles of the different systems allowed us to calculate the corresponding aggregation rates, which then could be compared to the ones obtained by time-resolved combined static and dynamic light scattering. Besides all the calculations of the forces with the additional non-DLVO terms, pure DLVO-based aggregation rates were calculated too. In general, salts containing ions of lower valence resemble the classical situation, where at low concentration of the electrolytes stable suspensions are present, while at high concentrations fast aggregation occurs. The characteristic shifts towards lower concentrations can be attributed to the Schulze-Hardy rule. The stability plots are presented in the Figure 14.

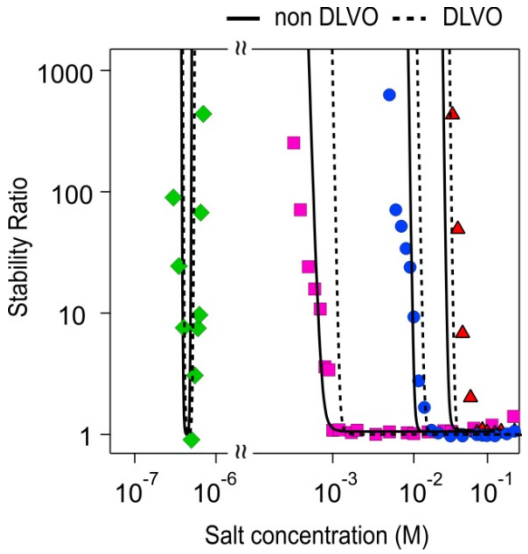

Figure 14 Comparison between stability ratios measured by time-resolved light scattering (symbols) and the ones calculated from direct force measurements. The solid lines include the non-DLVO contributions to the force, while the dashed ones only consider DLVO forces. The different systems from right to left: KCl, $MgCl_2$, $LaCl_3$, $ZrCl_4$. Further information is provided in the third chapter.

In addition to the previously investigated mono-, di- and trivalent ions, in this chapter, $ZrCl_4$ solutions were also used as coagulating agents. Due to the higher valence of this cation, it is obvious that the obtained CCC of this system should be the lowest one. However, the shape of the curve is very atypical. The suspension is stable at low electrolyte concentration, however, it becomes unstable only in a very narrow concentration range. Slight increase in its concentration results in stable suspension again. This behavior can be explained by the formation of a highly charged semihydrolyzed complex $Zr_4(OH)_8^{8+}$.[71] This specie is octavalent, which results in a huge affinity to oppositely charged particles. Therefore, the surface can be neutralized and overcharged already at sufficiently low electrolyte concentration, giving rise to the restabilization of the suspension. Electrophoretic mobility measurements confirmed the behavior of this system. The calculated stability ratios with all the additional non-DLVO contributions agree well with the ones measured experimentally by dynamic light scattering. If these additional attractions are neglected, the overall shape of the curves is still predicted well, however, the stability ratios are overestimated.

After showing that the particle aggregation process is strongly dependent on the valence of the counterion, **chapter four** reveals that ions of the same valence can have different effect and

coagulating power too. The chapter discusses the well-known Hofmeister series, which orders cations and anions according to their stabilization power of protein solutions, namely:

$$CO_3^{2-} < SO_4^{2-} < H_2PO_4^- < F^- < Cl^- < Br^- < NO_3^- < I^- < ClO_4^- < SCN^-$$

Strongly hydrated anions — Weakly hydrated anions

$$N(CH_3)_4^+ < NH_4^+ < Cs^+ < Rb^+ < K^+ < Na^+ < Li^+ < Mg^{2+} < Ca^{2+}$$

Weakly hydrated cations — Strongly hydrated cations

Many other phenomena can be explained by these series, for example, the viscosity or surface tension of electrolyte solutions. The exact origin of these effects is still unclear, however, the hydration state of the different ions is surely relevant. Ions appearing on the left are the strongly hydrated anions and the weakly hydrated cations. They precipitate proteins already at lower salt concentrations, while the ions of the right (weakly hydrated anions, strongly hydrated cations) keep proteins in solution at even elevated concentrations. The order of the anions and cations with respect to the hydration state is reversed, which can be attributed to the different orientation of the water molecules around the hydrated ions. In the original series, ions of higher valence were also quoted. We excluded them here, and focus on monovalent ions, since the multivalent ones primarily follow the Schulze-Hardy rule, as shown in chapter two and three.

Negatively charged SL530 and the positively charged AL220 were used to explore the ion-specific effects on the charging and aggregation. The chemical composition of the electrolytes was systematically varied in the experiments. Accordingly, sodium (NaH_2PO_4, NaF, NaCl, NaBr, $NaNO_3$, and NaSCN) and chloride ($N(CH_3)_4Cl$, NH_4Cl, CsCl, KCl, NaCl, and LiCl) salts were used for both particles in order to probe not only counterion, but co-ion effects too. In addition to the determination of the CCCs, we have investigated, whether there is any ion-specificity in the fast aggregation regime of the different systems.

In conclusion, the variation of the counterions leads to different CCC value due to specific interaction with the particle surface. The trends follow the well-known Hofmeister series of cations for negatively charged SL530 particles, while a reversed order of anions was found for

the positively charged AL220 particles. Varying the co-ions, no specificity was found with exception of the ammonium salts. When viscosity corrections are taken into account, no ion-specificity in the fast aggregation regime can be established either. These findings are summarized in Figure 15.

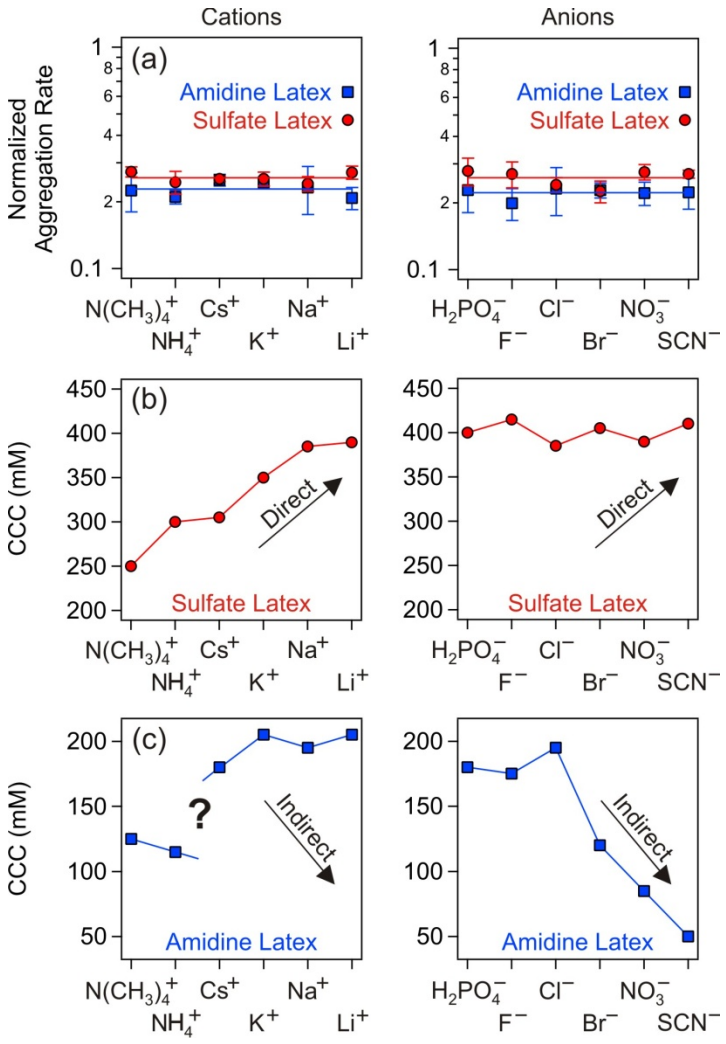

Figure 15 Characteristics of the latex particle aggregation versus the position in the Hofmeister series. The effect of cations is shown in the left coloumn, while the one of the anions, in the right coloumn. (a) Normalized aggregation rate coefficients in the fast regime with respect to the Smoluchowski value. The error bars represent three times the standard deviation. CCCs for (b) sulfate particles (c) amidine particles. The arrows indicate the expected trends from direct or indirect Hofmeister series. Detailed information can be found in the fourth chapter.

The ions interact with the oppositely charged particle surface specifically. This is due to the different extent of their hydration. Poorly hydrated ions, such as $N(CH_3)_4^+$ and SCN^-, tend to

adsorb to the oppositely charged surface more strongly, lowering the magnitude of the surface charge, thus the CCC substantially. On the other hand, strongly hydrated ions, such as Li^+ or F^-, do not adsorb on the particles surface, they only screen the charge of the particles. In some well hydrated counterions, the CCCs remain the same, suggesting that these electrolytes can be considered as indifferent ones.

In order to explore the origin of the interparticle forces in such ion-specific systems, a simplified form of DLVO theory was used to calculate theoretical CCC values at given surface charge densities. This procedure is described in chapter four in detail. The results of the calculations are shown in Figure 16.

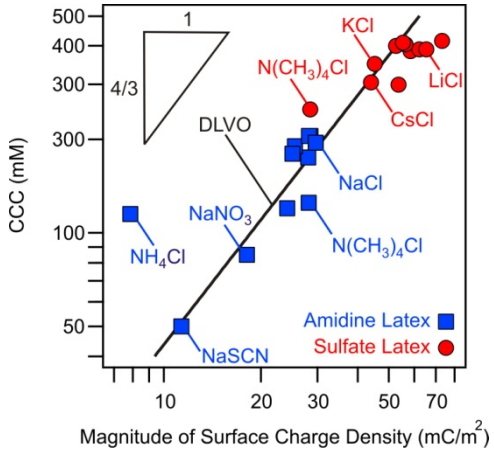

Figure 16 Comparison of experimental CCC values for the sulfate and amidine particles with DLVO theory. The data are plotted versus the magnitude of the surface charge density, which was estimated from the electrophoretic mobility. The DLVO theory uses the superposition approximation to calculate the double layer interactions. Additional information is provided in the chapter four.

The experimental CCCs agree reasonably well with the calculations based on the DLVO theory with the exception of NH_4^+ ion, which is probably influenced by specific interaction between these ions and the amidine groups on the particle surface. The agreement suggests that the main reason for ion-specificity is the modification of the surface charge due to the different extent of adsorption of the ions. However, the fitted Hamaker constant of the particles, which is proportional to the strength of the van der Waals interactions, are substantially larger than the Hamaker constants of similar latex particles that were actually measured by AFM-based colloidal probe technique. This indicates that additional non-DLVO forces are present. A combined study

on Hofmeister effects in the interaction forces and aggregation rates of colloidal latex particles could reveal the origin of these interactions. This will be presented in the next chapter.

Chapter five further explores the Hofmeister effects in the particle aggregation. Just as in chapter three, direct force measurements were carried out to obtain the interaction force profiles. Absolute aggregation rates were determined by light scattering and were directly compared to the ones calculated from the AFM measurements. Two types of latex particle were used to investigate this phenomenon, namely negatively charged SL980 and positively charged AL950. Various electrolytes were used to probe the effect of different monovalent counterions. They were arbitrarily chosen according to their position in the Hofmeister series. The results suggest that the interaction force profiles cannot be described by pure DLVO theory, and an additional exponential attractive short-ranged force must be included. Figure 17 shows some of the obtained forces between pairs of AL950 particles versus the separation distance at pH 4.0.

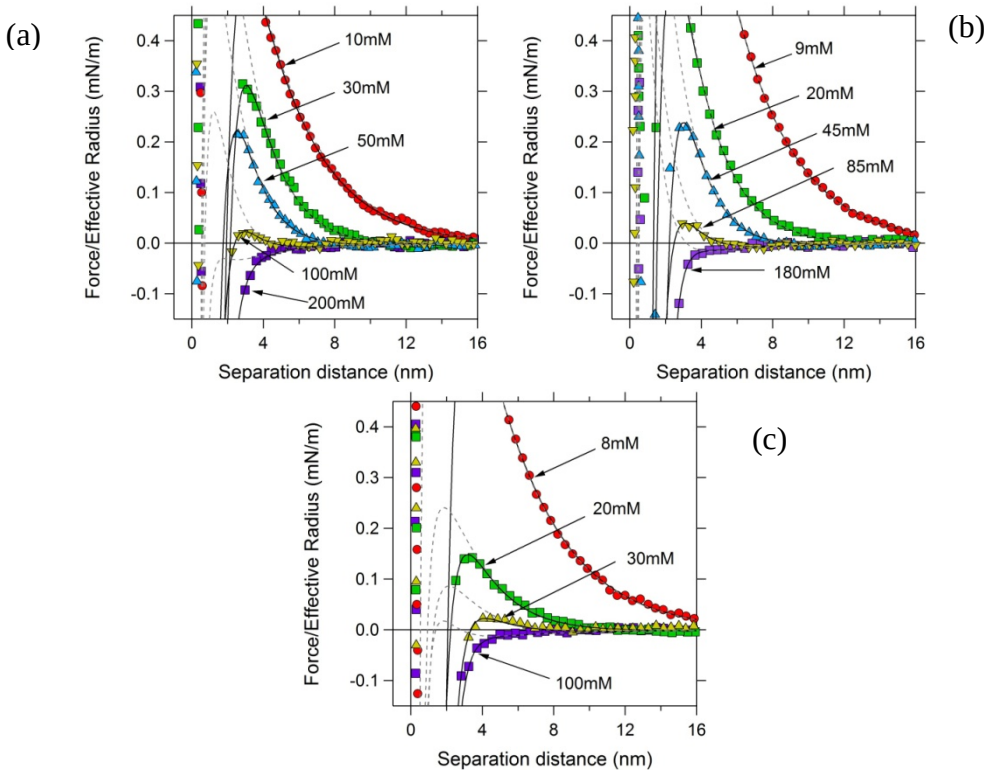

Figure 17 Interaction force profiles of AL950 particles at pH 4.0 in different electrolyte solutions. (a) NaCl, (b) NaBr, and (c) NaSCN. Solid lines show the calculations with the additional non-DLVO force included, while the dashed ones represent the classical DLVO calculations. Further details in chapter five.

In each case, at low salt concentration the forces are strongly repulsive, soft, and long-ranged. At these conditions the dominant force is the double-layer repulsion. Increasing the salt level, the double-layers shrink, and the repulsive forces start to diminish. At sufficiently high concentration, only attractive contributions are present. However, this attraction cannot be attributed only to the van der Waals interactions. Already at intermediate concentrations, an attractive short-range force becomes apparent through the jump-in of the cantilever into contact, which is still present at elevated salt levels. The position of the jump-in is relatively independent of the concentration, but its position somewhat increases in the presence of poorly hydrated ions.

An important finding, that even though the force profiles are qualitatively similar, the transition from repulsion to attraction occurs at progressively lower concentrations in the sequence NaCl > NaBr > NaSCN. This indicates the higher affinity of SCN^- ion to the positively charged particle surface. These ions tend to adsorb on the particle surface more efficiently, lowering the charge of the particle, thus its stability.

Based on the measured force profiles, the aggregation rates could be calculated without adjustable parameters. They were directly compared to aggregation rates measured directly by light scattering. These results are shown in Figure 18.

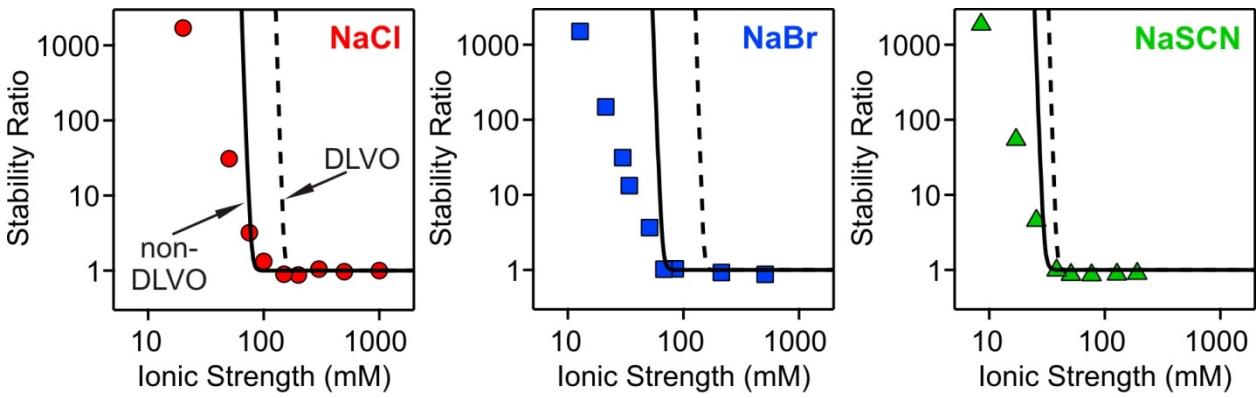

Figure 18 Comparison of measure stability ratios (symbols) with calculated ones based on the force profiles (solid lines). The dashed lines show the results for pure DLVO theory. More information in chapter five.

In conclusion, the measured and calculated stability ratios agree very well in case of the calculations including the short-ranged attractive term. The characteristic shifts in the CCCs, which were predictable after the force measurement, clearly indicate ion-specific interactions.

The results obtained with pure DLVO theory overestimate the stability of the suspensions, leading to unrealistically high CCCs.

The effect of different counterions within the Hofmeister series cannot be simply attributed to the variation of a single quantity. When the ions are less hydrated, they increasingly adsorb on the oppositely charged hydrophobic surface, lowering the magnitude of the surface charge. The additional attractive force varies strongly with the salt level and type of ion, but we are not able to propose a simple interpretation of the observed trends. However, the observed shifts in the critical coagulation concentrations can be well quantified by direct force measurements.

An aggregation study, where the Hofmeister series was extended with additional ions, is presented in the **sixth chapter**. Water-miscible ionic liquids (ILs) were used as additional coagulating agents. The ILs include 1-butyl-3-methylimidazolium as cation with chloride (BMIM-Cl), bromide (BMIM-Br), dicyanoamide (BMIM-$N(CN)_2$) and thiocyanate (BMIM-SCN) ions, 1-butyl-1-methylpyrrolidinium ILs with the same anions (BMPL-Cl, BMPL-Br, BMPL-$N(CN)_2$ and BMPL-SCN) and the chloride salts of 3-methylimidazolium (MIM-Cl), 1 ethyl-3-methylimidazolium (EMIM-Cl), 1-hexyl-3-methylimidazolium (HMIM-Cl), and 1-octyl-3-methylimidazolium (OMIM-Cl) cations. Their structure is shown in Figure 19.

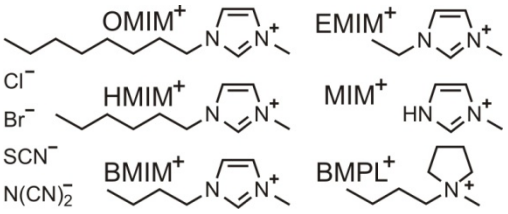

Figure 19 The structure of the different ionic liquids constituents used.

Ionic liquids fully dissociate to ions at lower concentrations, and therefore their behavior can be related to the ones of simple electrolytes. Comparing the results with the previously obtained ones, one can have several remarks. First, despite the significantly different structures of some IL constituents, co-ion specificity cannot be observed in any of the systems investigated. In case of BMIM-Cl and BMPL-Cl, the CCCs of the AL220 particle suspensions are within experimental error the same as in case of simple electrolytes, such as NaCl or KCl. This indicates that the co-

ions play only secondary role in the determination of the suspension stability. This finding can be applied to the negatively charged particles and anions too. The situation becomes more complicated, when none of the constituent ions can be considered indifferent, like in case of BMIM-SCN or BMPL-$N(CN)_2$. The counterions tend to adsorb on the oppositely charged particle surface, however, the particles decorated with less hydrated counterions can promote co-ion adsorption, which can result in higher CCCs. This is why exploring ion-specific interactions needs to be done with carefully chosen electrolytes, otherwise the comparison is really difficult. The combined CCC results of the previous and present studies are presented in the Figure 20.

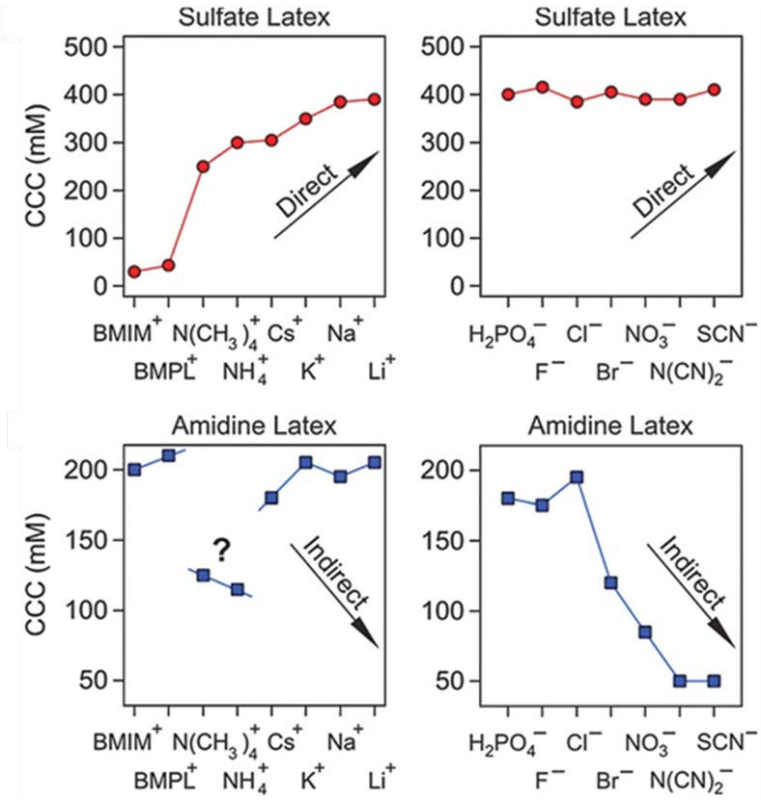

Figure 20 CCC values for SL530 and AL220 in the presence of different chloride salts of cations (left) and sodium salts of anions (right). The arrows indicate the expected trends according to the direct or indirect Hofmeister series. Further details can be found in chapter six.

Another part of this study was to probe the effect of the alkyl chain length of the IL constituent cation. In this case, only the negative SL530 particles were further investigated. The corresponding electrophoretic mobility and aggregation rate values can be seen in Figure 21.

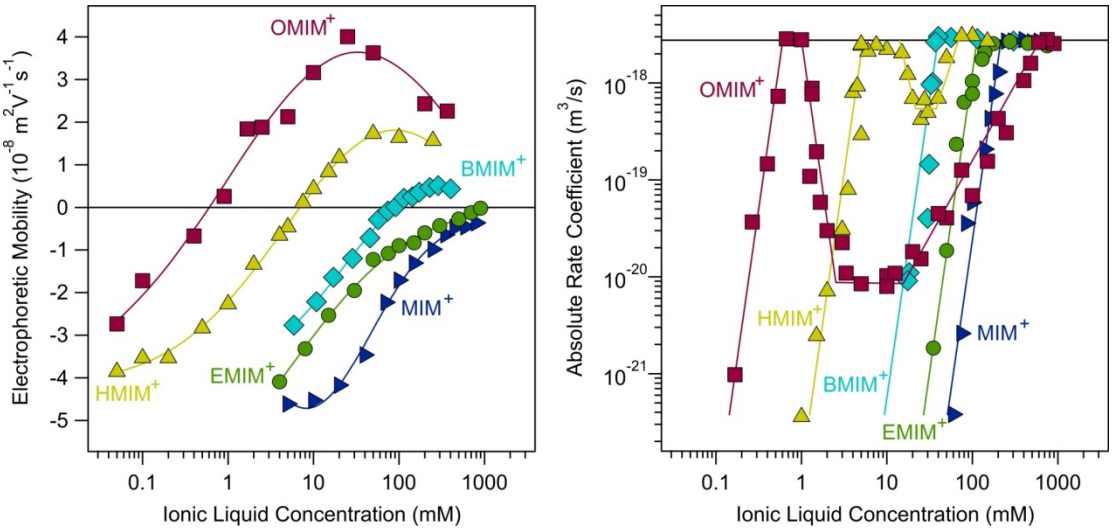

Figure 21 Electrophoretic mobilities and aggregation rates of SL530 particles in the presence of ILs composed of chloride anion and 1-alkyl-3-methylimidazolium cations of different alkyl chains.

The longer the alkyl chain of the cation, the more hydrophobic its character is, which suggests completely different affinity to the hydrophobic particle surface. This is reflected by the results obtained by electrophoresis. Accordingly, in case of MIM-Cl screening and weaker adsorption can be observed, but the particles remain negative throughout the whole concentration range investigated. The extent of MIM^+ adsorption is comparable to the one of $N(CH_3)_4^+$. In case of EMIM-Cl the cation neutralizes the surface at sufficiently high concentration. $BMIM^+$ not only neutralizes the particle surface, but slightly overcharging it. However, the adsorption of $HMIM^+$ and $OMIM^+$ is so pronounced that it induces a significant charge reversal already at low concentrations. In both cases, further increasing the IL concentration, a decrease in the mobilities can be observed due to the screening of the Cl^- ions that act as new counterion in the case of overcharged particles.

The corresponding aggregation rates reflect well the charging behavior of the particles in each system. MIM^+, $EMIM^+$ and $BMIM^+$ cations show the classical behavior of slow aggregation at low IL concentrations and fast aggregation at elevated ones. Systematic decrease in the CCCs can be seen in case of increasing alkyl chain length. This can be explained by the different adsorption strength due to increasing hydrophobicity. In case of $BMIM^+$ the overcharging occurs at too high IL concentrations, so there is no possibility for any kind of restabilization process. However, $HMIM^+$ and $OMIM^+$ overcharge the particles at sufficiently low IL concentrations, giving rise to

real restabilization. While in case of $HMIM^+$ this effect is observed at a narrow concentration range, the $OMIM^+$ containing system can be restabilized over three orders of magnitude in concentration. Table 2 contains the most important effects of the different IL constituent cations.

Table 2 Effects on the charging and aggregation of the IL contsituent cations.

	MIM^+	**$EMIM^+$**	**$BMIM^+$**	**$HMIM^+$**	**$OMIM^+$**
Screening					
Neutralization					
Overcharging					
Restabilization					

From the studies performed on negatively charged SL530 particles, the Hofmeister series for the cations may be extended as:

$$OMIM^+ < HMIM^+ < BMIM^+ < BMPL^+ < EMIM^+ < MIM^+ < N(CH_3)_4^+ < NH_4^+ < Cs^+ < K^+ < Na^+ < Li^+$$

The more hydrophobic ions on the left hand side lead to the lowest CCCs, while ions of more hydrophilic character on the right hand side bear with lowest coagulating power, thus with the highest CCCs. Since these results originate from salts containing indifferent Cl^- ion in each case, the direct comparison of the CCCs could be arbitrarily made.

In the previous chapter, it was demonstrated that varying the ionic liquid constituents can lead to completely different aggregation behaviour of aqueous dispersions. However, ILs are used in nanoparticle synthesis in pure state, i.e., the stability of these suspensions can be crucial for further applications. Therefore, the description of particle aggregation mechanisms in different ionic liquids is necessary. The **seventh chapter** presents a study involving the same type of particles (SL530, AL220) as in chapter six, but from a different perspective. Starting from dilute

solutions of ionic liquids through intermediate concentrations to the pure ILs, we explored the whole range of IL concentration, in order to describe the systems systematically. Five different ionic liquids were chosen for this study, whose anions and cations were systematically varied. All are room temperature, water miscible ILs. Their structure is shown in Figure 22.

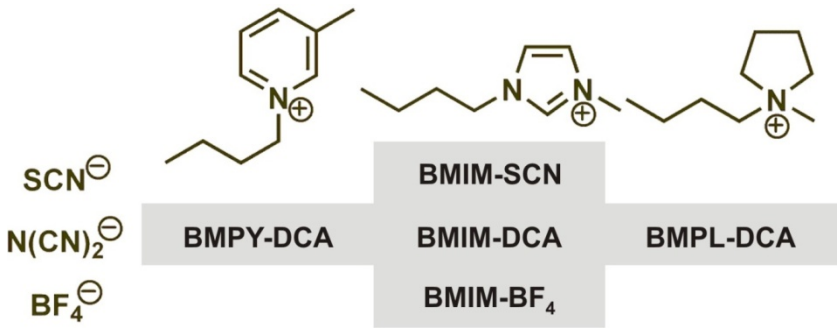

Figure 22 The structures and abbreviations of the different ILs used in this study.

Prior the light scattering measurements, the properties of the IL-water mixtures, such as density, viscosity and refractive index, had to be determined. This is crucial for appropriate data interpretation. The values were determined with standard techniques. The data obtained are shown in Figure 23.

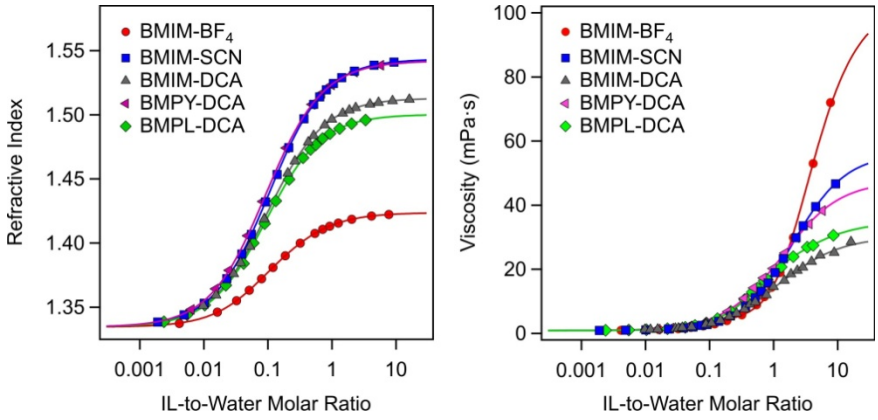

Figure 23 Properties of ILs, refractive indices measured at 533 nm and the corresponding shear viscosities. Additional information can be found in chapter seven.

Once the physicochemical properties were determined, the aggregation study could be performed. General conclusion is that each IL behaves similarly. A representative figure of the suspension behaviour in case of AL220 in BMIM-DCA is shown in Figure 24.

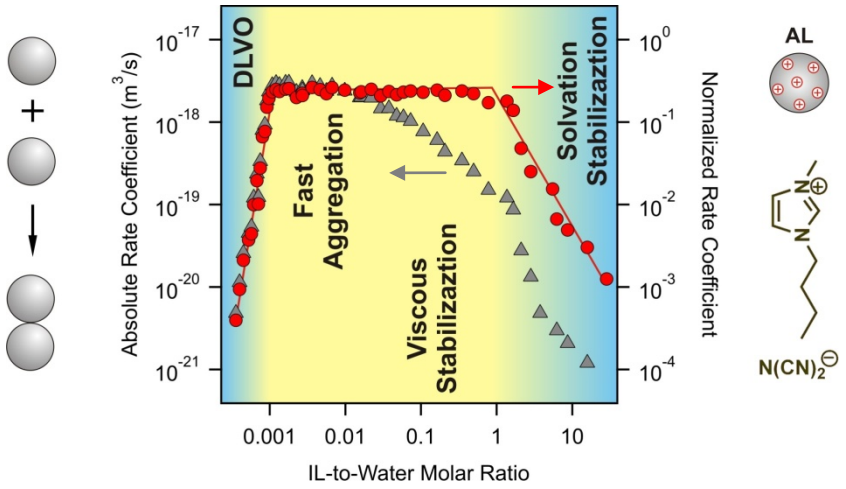

Figure 24 Aggregation rates of AL220 suspensions in the presence of BMIM-DCA.

In each case, three regimes could be identified. First, at low IL content, the classical DLVO behaviour can be seen, i.e., the aggregation rates are small initially, while they start to increase as the IL content increases. This is mainly due to the progressive screening of the double layer of the particles. At a certain concentration, the aggregation rates reach a plateau value. This corresponds to the fast aggregation regime, where the aggregation is controlled solely by the diffusion. Second regime can be assigned to the intermediate IL content, where a gradual decrease in the aggregation rates can be observed. This originates from the elevated viscosity of the medium. Even though the process is still diffusion-controlled, the higher viscosity of the IL-water mixtures hinders the aggregation. This mechanism can slow down the coagulation process by almost two orders of magnitude. This regime is referred to as viscous stabilization. Such an effect can be confirmed by comparing the aggregation rate coefficients to the corresponding Smoluchowski values. The latter ones take into account the viscosity of the medium, i.e., in this case the decrease in the calculated rates should be reflected. The normalized aggregation rates remain constant throughout the entire intermediate concentration regime, which confirms that the aggregation is diffusion-controlled. Further increase in the IL content, reaching pure ILs where only small amount of water is present, the aggregation rates decrease rapidly. This can be attributed to the layering of the ionic liquid constituents on the particle surface, which results in an overall repulsive interparticle force, which then prevents the suspensions from aggregation. This type of solvation stabilization is not related, or just secondarily, to the viscosity of the medium, because even the normalized aggregation rates are systematically smaller than the one

corresponds to fast aggregation. Such structuring was observed by X-ray reflectivity, and the corresponding forces could be measured using SFA or AFM.[72-74]. The aforementioned two stabilization mechanisms are suspected to be generic, as they are operational in different ILs and for particles of different surface functionalities and of different size.

References

1. Nasser, M. S.; Twaiq, F. A.; Onaizi, S. A., Effect of polyelectrolytes on the degree of flocculation of papermaking suspensions. *Sep. Purif. Technol.* **2013,** 103, 43-52.
2. Porubska, J.; Alince, B.; van de Ven, T. G. M., Homo- and heteroflocculation of papermaking fines and fillers. *Colloid Surf. A* **2002,** 210, 223-230.
3. Tiarks, F.; Frechen, T.; Kirsch, S.; Leuninger, J.; Melan, M.; Pfau, A.; Richter, F.; Schuler, B.; Zhao, C. L., Formulation effects on the distribution of pigment particles in paints. *Prog. Org. Coat.* **2003,** 48, 140-152.
4. Jadhav, R. S.; Patil, K. J.; Hundiwale, D. G.; Mahulikar, P. P., Synthesis of waterborne nanopolyanilne latexes and application of nanopolyaniline particles in epoxy paint formulation for smart corrosion resistivity of carbon steel. *Polym. Adv. Technol.* **2011,** 22, 1620-1627.
5. Farrokhpay, S., A review of polymeric dispersant stabilisation of titania pigment. *Adv. Colloid Interface Sci.* **2009,** 151, 24-32.
6. Dickinson, E., Food emulsions and foams: Stabilization by particles. *Curr. Opin. Colloid Interface Sci.* **2010,** 15, 40-49.
7. Bolto, B.; Gregory, J., Organic polyelectrolytes in water treatment. *Water Res.* **2007,** 41, 2301-2324.
8. Honda, R. J.; Keene, V.; Daniels, L.; Walker, S. L., Removal of TiO2 Nanoparticles During Primary Water Treatment: Role of Coagulant Type, Dose, and Nanoparticle Concentration. *Environ. Eng. Sci.* **2014,** 31, 127-134.
9. Xu, Z. P.; Zeng, Q. H.; Lu, G. Q.; Yu, A. B., Inorganic nanoparticles as carriers for efficient cellular delivery. *Chem. Eng. Sci.* **2006,** 61, 1027-1040.
10. Derjaguin, B., On the repulsive forces between charged colloid particles and on the theory of slow coagulation and stability of lyophobe sols. *Trans. Faraday Soc.* **1940,** 35, 0203-0214.
11. Verwey, E. J. W.; Overbeek, J. T. G., *Theory of Stability of Lyophobic Colloids*. Elsevier: Amsterdam, 1948.
12. Derjaguin, B., A theory of interaction of particles in presence of electric double-layers and the stability of lyophobe colloids and disperse systems. *Prog. Surf. Sci.* **1993,** 43, 1-14.
13. Gregory, J., Monitoring particle aggregation processes. *Adv. Colloid Interface Sci.* **2009,** 147-48, 109-123.
14. Holthoff, H.; Egelhaaf, S. U.; Borkovec, M.; Schurtenberger, P.; Sticher, H., Coagulation rate measurements of colloidal particles by simultaneous static and dynamic light scattering. *Langmuir* **1996,** 12, 5541-5549.
15. Elimelech, M.; Gregory, J.; Jia, X.; Williams, R. A., *Particle Deposition and Aggregation: Measurement, Modeling, and Simulation*. Butterworth-Heinemann Ltd.: Oxford, 1995.
16. Trefalt, G.; Szilagyi, I.; Oncsik, T.; Sadeghpour, A.; Borkovec, M., Probing Colloidal Particle Aggregation by Light Scattering. *Chimia* **2013,** 67, 772-776.
17. Hassan, P. A.; Rana, S.; Verma, G., Making Sense of Brownian Motion: Colloid Characterization by Dynamic Light Scattering. *Langmuir* **2015,** 31, 3-12.
18. Zaccone, A.; Crassous, J. J.; Beri, B.; Ballauff, M., Quantifying the reversible association of thermosensitive nanoparticles. *Phys. Rev. Lett.* **2011,** 107.

19. Schneider, C.; Hanisch, M.; Wedel, B.; Jusufi, A.; Ballauff, M., Experimental study of electrostatically stabilized colloidal particles: Colloidal stability and charge reversal. *J. Colloid Interface Sci.* **2011,** 358, 62-67.
20. Chen, K. L.; Mylon, S. E.; Elimelech, M., Enhanced aggregation of alginate-coated iron oxide (hematite) nanoparticles in the presence of, calcium, strontium and barium cations. *Langmuir* **2007,** 23, 5920-5928.
21. Meng, Z. Y.; Hashmi, S. M.; Elimelech, M., Aggregation rate and fractal dimension of fullerene nanoparticles via simultaneous multiangle static and dynamic light scattering measurement. *J. Colloid Interface Sci.* **2013,** 392, 27-33.
22. Owczarz, M.; Motta, A. C.; Morbidelli, M.; Arosio, P., A Colloidal Description of Intermolecular Interactions Driving Fibril-Fibril Aggregation of a Model Amphiphilic Peptide. *Langmuir* **2015,** 31, 7590-7600.
23. Sadeghpour, A.; Seyrek, E.; Szilagyi, I.; Hierrezuelo, J.; Borkovec, M., Influence of the Degree of Ionization and Molecular Mass of Weak Polyelectrolytes on Charging and Stability Behavior of Oppositely Charged Colloidal Particles. *Langmuir* **2011,** 27, 9270-9276.
24. Seyrek, E.; Hierrezuelo, J.; Sadeghpour, A.; Szilagyi, I.; Borkovec, M., Molecular mass dependence of adsorbed amount and hydrodynamic thickness of polyelectrolyte layers. *Phys. Chem. Chem. Phys.* **2011,** 13, 12716-12719.
25. Szilagyi, I.; Rosicka, D.; Hierrezuelo, J.; Borkovec, M., Charging and stability of anionic latex particles in the presence of linear poly(ethylene imine). *J. Colloid Interface Sci.* **2011,** 360, 580-585.
26. Sadeghpour, A.; Szilagyi, I.; Borkovec, M., Charging and Aggregation of Positively Charged Colloidal Latex Particles in Presence of Multivalent Polycarboxylate Anions. *Z. Phys. Chemie-Int. J. Res. Phys. Chem. Chem. Phys.* **2012,** 226, 597-612.
27. Szilagyi, I.; Sadeghpour, A.; Borkovec, M., Destabilization of Colloidal Suspensions by Multivalent Ions and Polyelectrolytes: From Screening to Overcharging. *Langmuir* **2012,** 28, 6211-6215.
28. Szilagyi, I.; Polomska, A.; Citherlet, D.; Sadeghpour, A.; Borkovec, M., Charging and aggregation of negatively charged colloidal latex particles in the presence of multivalent oligoamine cations. *J. Colloid Interface Sci.* **2013,** 392, 34-41.
29. Cao, T.; Szilagyi, I.; Oncsik, T.; Borkovec, M.; Trefalt, G., Aggregation of Colloidal Particles in the Presence of Multivalent Colons: The Inverse Schulze-Hardy Rule. *Langmuir* **2015,** 31, 6610-6614.
30. Evans, D. F.; Wennerstrom, H., *The Colloidal Domain*. John Wiley: New York, 1999.
31. Lyklema, J., Overcharging, charge reversal: Chemistry or physics? *Colloid Surf. A* **2006,** 291, 3-12.
32. Quesada-Perez, M.; Gonzalez-Tovar, E.; Martin-Molina, A.; Lozada-Cassou, M.; Hidalgo-Alvarez, R., Overcharging in colloids: Beyond the Poisson-Boltzmann approach. *ChemPhysChem* **2003,** 4, 235-248.
33. Delgado, A. V.; Gonzalez-Caballero, F.; Hunter, R. J.; Koopal, L. K.; Lyklema, J., Measurement and interpretation of electrokinetic phenomena. *J. Colloid Interface Sci.* **2007,** 309, 194-224.

34. Delgado, A. V.; Gonzalez-Caballero, E.; Hunter, R. J.; Koopal, L. K.; Lyklema, J., Measurement and interpretation of electrokinetic phenomena - (IUPAC technical report). *Pure Appl. Chem.* **2005,** 77, 1753-1805.
35. O'Brien, R. W.; White, L. R., Electrophoretic mobility of a spherical colloidal particle. *J. Chem. Soc.-Faraday Trans.* **1978,** 74, 1607-1626.
36. Deshiikan, S. R.; Papadopoulos, K. D., Modified Booth equation for the calculation of zeta potential. *Colloid Polym. Sci.* **1998,** 276, 117-124.
37. Horváth, E.; Grebikova, L.; Maroni, P.; Szabó, T.; Magrez, A.; Forró, L.; Szilagyi, I., Dispersion Characteristics and Aggregation in Titanate Nanowire Colloids. *ChemPlusChem* **2014,** 79, 592-600.
38. Russel, W. B.; Saville, D. A.; Schowalter, W. R., *Colloidal Dispersions*. Cambridge University Press: Cambridge, 1989.
39. Popa, I.; Papastavrou, G.; Borkovec, M., Charge regulation effects on electrostatic patch-charge attraction induced by adsorbed dendrimers. *Phys. Chem. Chem. Phys.* **2010,** 12, 4863-4871.
40. Fritz, G.; Schadler, V.; Willenbacher, N.; Wagner, N. J., Electrosteric stabilization of colloidal dispersions. *Langmuir* **2002,** 18, 6381-6390.
41. Illes, E.; Tombacz, E., The effect of humic acid adsorption on pH-dependent surface charging and aggregation of magnetite nanoparticles. *J. Colloid Interface Sci.* **2006,** 295, 115-123.
42. Zaccone, A.; Wu, H.; Lattuada, M.; Morbidelli, M., Correlation between colloidal stability and surfactant adsorption/association phenomena studied by light scattering. *J. Phys. Chem. B* **2008,** 112, 1976-1986.
43. Israelachvili, J., *Intermolecular and Surface Forces*. 3 ed.; Academic Press: London, 2011.
44. Sinha, P.; Szilagyi, I.; Ruiz-Cabello, F. J. M.; Maroni, P.; Borkovec, M., Attractive Forces between Charged Colloidal Particles Induced by Multivalent Ions Revealed by Confronting Aggregation and Direct Force Measurements. *J. Phys. Chem. Lett.* **2013,** 4, 648–652.
45. Finessi, M.; Szilagyi, I.; Maroni, P., Dendrimer induced interaction forces between colloidal particles revealed by direct force and aggregation measurements. *J. Colloid Interface Sci.* **2014,** 417, 346-355.
46. Shubin, V. E.; Kekicheff, P., Electrical double-layer structure revisited via a surface force apparatus. Mica interfaces in lithium-nitrate solutions. *J. Colloid Interface Sci.* **1993,** 155, 108-123.
47. Gebbie, M. A.; Valtiner, M.; Banquy, X.; Fox, E. T.; Henderson, W. A.; Israelachvili, J. N., Ionic liquids behave as dilute electrolyte solutions. *Proc. Natl. Acad. Sci. U. S. A.* **2013,** 110, 9674-9679.
48. Espinosa-Marzal, R. M.; Arcifa, A.; Rossi, A.; Spencer, N. D., Microslips to "Avalanches" in Confined, Molecular Layers of Ionic Liquids. *J. Phys. Chem. Lett.* **2014,** 5, 179-184.
49. Prieve, D. C., Measurement of colloidal forces with TIRM. *Adv. Colloid Interface Sci.* **1999,** 82, 93-125.
50. Elmahdy, M. M.; Gutsche, C.; Kremer, F., Forces within Single Pairs of Charged Colloids in Aqueous Solutions of Ionic Liquids as Studied by Optical Tweezers. *J. Phys. Chem. C* **2010,** 114, 19452-19458.
51. Butt, H. J., Measuring electrostatic, van der Waals, and hydration forces in electrolyte solutions with an atomic force microscope. *Biophys. J.* **1991,** 60, 1438-1444.

52. Ducker, W. A.; Senden, T. J.; Pashley, R. M., Direct measurement of colloidal forces using an atomic force microscope. *Nature* **1991,** 353, 239-241.
53. Montes Ruiz-Cabello, F. J.; Trefalt, G.; Maroni, P.; Borkovec, M., Accurate predictions of forces in the presence of multivalent ions by Poisson-Boltzmann theory. *Langmuir* **2014,** 30, 4551-4555.
54. Xia, Y. N.; Gates, B.; Yin, Y. D.; Lu, Y., Monodispersed colloidal spheres: Old materials with new applications. *Adv. Mater.* **2000,** 12, 693-713.
55. Ianchis, R.; Donescu, D.; Corobea, M. C.; Petcu, C.; Ghiurea, M.; Serban, S.; Radovici, C., Synthesis of polystyrene/polybutylacrylate/layered silicate nanocomposites in aqueous medium. *Colloid Polym. Sci.* **2010,** 288, 1215-1224.
56. Mballa, M. A. M.; Ali, S. I.; Heuts, J. P. A.; van Herk, A. M., Control of the anisotropic morphology of latex nanocomposites containing single montmorillonite clay particles prepared by conventional and reversible addition-fragmentation chain transfer based emulsion polymerization. *Polym. Int.* **2012,** 61, 861-865.
57. Ramos, J.; Forcada, J.; Hidalgo-Alvarez, R., Cationic Polymer Nanoparticles and Nanogels: From Synthesis to Biotechnological Applications. *Chem. Rev.* **2014,** 114, 367-428.
58. Freemantle, M., Designer solvents: ionic liquids may boost clean technology development. *Chem. Eng. News* **1998,** 76, 32-37.
59. Forsyth, S. A.; Pringle, J. M.; MacFarlane, D. R., Ionic liquids - An overview. *Aust. J. Chem.* **2004,** 57, 113-119.
60. Armand, M.; Endres, F.; MacFarlane, D. R.; Ohno, H.; Scrosati, B., Ionic-liquid materials for the electrochemical challenges of the future. *Nat. Mater.* **2009,** 8, 621-629.
61. Fujita, K.; MacFarlane, D. R.; Forsyth, M., Protein solubilising and stabilising ionic liquids. *Chem. Commun.* **2005**, 4804-4806.
62. Hayes, R.; Warr, G. G.; Atkin, R., Structure and Nanostructure in Ionic Liquids. *Chem. Rev.* **2015,** 115, 6357-6426.
63. MacFarlane, D. R.; Tachikawa, N.; Forsyth, M.; Pringle, J. M.; Howlett, P. C.; Elliott, G. D.; Davis, J. H.; Watanabe, M.; Simon, P.; Angell, C. A., Energy applications of ionic liquids. *Energy Environ. Sci.* **2014,** 7, 232-250.
64. Tan, S. S. Y.; MacFarlane, D. R., Ionic Liquids in Biomass Processing. *Top. Curr. Chem.* **2009,** 290, 311-339.
65. Rogers, R. D.; Seddon, K. R., Ionic liquids - Solvents of the future? *Science* **2003,** 302, 792-793.
66. Itoh, H.; Naka, K.; Chujo, Y., Synthesis of gold nanoparticles modified with ionic liquid based on the imidazolium cation. *J. Am. Chem. Soc.* **2004,** 126, 3026-3027.
67. Lazarus, L. L.; Riche, C. T.; Malmstadt, N.; Brutchey, R. L., Effect of Ionic Liquid Impurities on the Synthesis of Silver Nanoparticles. *Langmuir* **2012,** 28, 15987-15993.
68. Ramalakshmi, M.; Shakkthivel, P.; Sundrarajan, M.; Chen, S. M., Novel method of room temperature ionic liquid assisted Fe3O4 nanocubes and nanoflakes synthesis. *Mater. Res. Bull.* **2013,** 48, 2758-2765.
69. Vanecht, E.; Binnemans, K.; Patskovsky, S.; Meunier, M.; Seo, J. W.; Stappers, L.; Fransaer, J., Stability of sputter-deposited gold nanoparticles in imidazolium ionic liquids. *Phys. Chem. Chem. Phys.* **2012,** 14, 5662-5671.

70. Zhou, Y.; Antonietti, M., Synthesis of very small TiO_2 nanocrystals in a room-temperature ionic liquid and their self-assembly toward mesoporous spherical aggregates. *J. Am. Chem. Soc.* **2003,** 125, 14960-14961.
71. Baes, C. F.; Mesmer, R. E., *The Hydrolysis of Cations*. Krieger Publishing: Malabar 1976.
72. Mezger, M.; Schroder, H.; Reichert, H.; Schramm, S.; Okasinski, J. S.; Schoder, S.; Honkimaki, V.; Deutsch, M.; Ocko, B. M.; Ralston, J.; Rohwerder, M.; Stratmann, M.; Dosch, H., Molecular layering of fluorinated ionic liquids at a charged sapphire (0001) surface. *Science* **2008,** 322, 424-428.
73. Segura, J. J.; Elbourne, A.; Wanless, E. J.; Warr, G. G.; Voïtchovsky, K.; Atkin, R., Adsorbed and near surface structure of ionic liquids at a solid interface. *Phys. Chem. Chem. Phys.* **2013,** 15, 3320-3328.
74. Horn, R.; Evans, D.; Ninham, B., Double-layer and solvation forces measured in a molten salt and its mixtures with water. *J. Phys. Chem.* **1988,** 92, 3531-3537.

CHAPTER 2

Aggregation of Negatively Charged Colloidal Particles in the Presence of Multivalent Cations

Oncsik, T.; Trefalt, G.; Csendes, Z.; Szilagyi, I.; Borkovec, M.

Langmuir **2014,** 30, 733-741.

Langmuir

Article

pubs.acs.org/Langmuir

Aggregation of Negatively Charged Colloidal Particles in the Presence of Multivalent Cations

Tamas Oncsik, Gregor Trefalt, Zita Csendes, Istvan Szilagyi, and Michal Borkovec*

Department of Inorganic and Analytical Chemistry, University of Geneva, Sciences II, Quai Ernest-Ansermet 30, 1205 Geneva, Switzerland

ABSTRACT: The aggregation and charging behavior of sulfate and carboxyl latex particles in the presence of different multivalent salts was studied. Time-resolved light scattering and electrophoresis are the main experimental techniques used. In particular, the influence of the type of counterion is investigated. The main conclusion is that the valence of the counterion is highly relevant in determining the aggregation behavior, whereas its chemical nature is rather unimportant. Multivalent ions of higher valence destabilize the suspensions more effectively, in particular, by shifting the critical coagulation concentration (CCC) to lower values. This behavior reflects the classical Schulze−Hardy rule. Comparison with literature data reveals that the presently investigated systems behave similarly to the ones described earlier, but the observed dependence on valence is weaker than in some other systems. Moreover, we observe a slowdown of the aggregation at high electrolyte concentrations. This slowdown can be explained by the greater viscosity of the electrolyte solutions under these conditions.

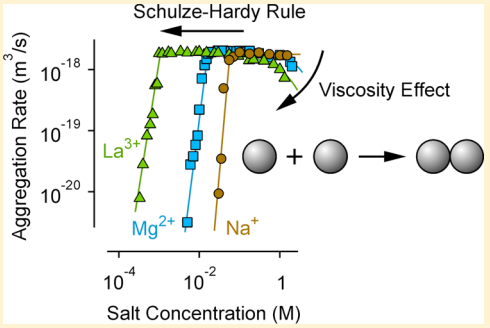

INTRODUCTION

More than a century ago, Schulze and Hardy recognized that salts containing multivalent ions are much more efficient in coagulating colloidal suspensions than monovalent ones.[1−3] This fact has been established empirically by studying the stability of colloidal suspensions in the presence of various salts. The theoretical explanation of this rule had to await the development of the theory by Derjaguin, Landau, Verwey, and Overbeek (DLVO).[4] This theory assumes that the interaction potential of two colloidal particles is dominated by electric double layer repulsions and van der Waals attractions. This energy profile is then used to calculate the aggregation rate of two colloidal particles. In agreement with experiment, this theory predicts that charged particle suspensions are stable at low salt concentrations and become unstable at higher ones. The transition between these two regimes is rather sudden and is referred to as the critical coagulation concentration (CCC). On the basis of DLVO theory, one can show that[4,5]

$$\mathrm{CCC} \propto \frac{1}{z^n} \tag{1}$$

where z is the valence of the counterion, $n = 2$ for weakly charged particles, and $n = 6$ for highly charged ones. Matijevic, Tezak, and their co-workers have tested the validity of this rule with a large number of cations and anions with silver halide particles.[6−8] Back then, however, these researchers were able to determine only the CCC, but they could not measure the absolute aggregation rate coefficients. In the meantime, these questions were revisited in a wide range of systems, including silver halides,[9] latexes,[10−14] clay minerals,[15] oxides,[16,17] fullerenes,[18,19] carbon nanotubes,[20] and bacteria.[21] Other studies have addressed the effect of variable charge on particle aggregation.[22−24]

More recently, the role of multivalent ions in interactions between colloidal particles has received renewed attention. This interest was triggered by the discovery that the Poisson−Boltzmann approximation that is used to treat the interaction between electric double layers may fail in the presence of multivalent ions.[25,26] In fact, such ions may induce attractive interactions in situations where classical Poisson−Boltzmann theory would predict repulsion. Such attractions are accompanied by the charge reversal of the surface due to the adsorption of these ions. These effects were suggested to originate from correlations between the highly charged ions, which are not considered within the mean-field approximation that is inherent in Poisson−Boltzmann theory. Ion correlation effects were studied theoretically in substantial detail, and effects of the size and shape of the ions were considered.[27−30] On the experimental side, numerous reports exist on the charge reversal induced by multivalent ions, even though the role of ion correlations continues to be discussed.[31−34] However, the presence of additional attractive forces is less established.[35−37] The forces were compatible with DLVO theory in some systems,[35,37] whereas an additional attractive force was reported in others.[36]

When additional attractive forces are induced by multivalent ions, these forces may also have an effect on particle aggregation rates. This aspect was investigated recently by some of us, and more rapid aggregation rates than the ones

Received: December 4, 2013
Revised: January 8, 2014
Published: January 8, 2014

expected from DLVO theory were indeed found.[33,34,38] Although charge reversal and a strong adsorption of multivalent ions could be established, it was not clear whether the adsorption occurs as a result of short-ranged specific interactions or ion correlation forces. This aspect can be addressed when various types of multivalent ions of the same charge are investigated.

Such an investigation is the aim of the present article. We study the aggregation of negatively charged colloidal particles in the presence of salts containing different types of multivalent counterions. In particular, we address whether the interactions depend on the type of ions of the same valence and to what extent their chemical nature is important.

EXPERIMENTAL SECTION

Materials. Carboxylate- and sulfate-functionalized polystyrene particles were purchased from Invitrogen Corporation. The mean diameter and polydispersity of the carboxylated latex was 1.0 μm and the coefficient of variation was 0.05, whereas for the sulfate latex these numbers were 0.53 μm and 0.02. The surface charge densities were -127 mC/m^2 for the carboxylated particles and -77 mC/m^2 for the sulfate particles. These characteristics were determined by the manufacturer by transmission electron microscopy and conductivity titrations, respectively. Stock particle suspensions were prepared by dialyzing the suspensions obtained from the manufacturer with a cellulose ester membrane against Milli-Q water until the conductivity stabilized at the conductivity of the Milli-Q water used. Milli-Q water was used throughout. Particle concentrations in the dialyzed stock suspensions were determined by static light scattering by comparing the scattering intensity with the original particle suspension of known concentration, and they were around 100 mg/L. Analytical-grade inorganic salts NaCl, CsCl, $LaCl_3{\cdot}7H_2O$, and $Co(NH_3)_6Cl_3$ were purchased from Sigma; KCl, $MgCl_2{\cdot}7H_2O$, and $BaCl_2{\cdot}2H_2O$, from Acros; $CaCl_2{\cdot}6H_2O$, from Fluka; and $Ru(NH_3)_6Cl_3$, from Strem Chemicals.

The salt solutions were prepared by dissolving the amount of solid salt needed in water adjusted to pH 4.0. Before sample preparation, both the salt solution and the water were filtered with a 0.1 μm Durapore filter (Merck). The pH was adjusted to 4.0 with dilute HCl. Under these conditions, the carboxyl particles are only weakly charged as a result of the weak ionization of the carboxyl groups.[24] The sulfate particles are expected to remain highly charged. All measurements were carried out at a temperature of 25.0 $\pm$ 0.2 °C.

Viscosity. Dynamic viscosities of $[Co(NH_3)_6]Cl_3$ and $[Ru(NH_3)_6]Cl_3$ solutions were determined with a Brookfield viscometer (DV-II Pro) up to a concentration of 0.2 M. The samples were prepared by mixing the appropriate volume of concentrated salt solution and Milli-Q water. Up to the concentrations investigated, the viscosity remained within 5% of the viscosity of water. The viscosities of the other electrolytes were taken from the literature.[39] The experimental viscosities η were fitted to the relation[40]

$$\frac{\eta}{\eta_0} = 1 + A\sqrt{c} + Bc + Dc^2 \qquad (2)$$

where $\eta_0 = 8.90 \times 10^{-4}$ Pa s is the viscosity of water at 25 °C and A, B, and D are constants that are summarized in Table 1. The respective dependencies are shown in Figure 1. The theoretical value for constant A was used, which was based on Debye–Hückel theory.[40] Constants B and D were obtained by a least-squares fit of the data. The former ones were in good agreement with the expected theoretical values based on the ionic radii.[40]

Light Scattering. Two different goniometer setups were used to carry out the light scattering experiments. The first instrument is a multiangle goniometer with eight fiber-optic detectors (ALV/CGS-8F) with a solid-state laser having a wavelength of 532 nm. The second instrument is a compact single-angle goniometer (ALV/CGS-3) with a He/Ne laser with a wavelength of 633 nm.

Table 1. Constants in Equation 2 Describing the Concentration Dependence of the Viscosities of Electrolyte Solutions Used

electrolyte	A ($M^{-1/2}$)	B (M^{-1})	D (M^{-2})
NaCl	0.0062	0.0614	0.0211
KCl	0.0052	−0.0248	0.0084
CsCl	0.0049	−0.0710	0.0138
$MgCl_2$	0.0168	0.2540	0.2010
$CaCl_2$	0.0156	0.1957	0.1110
$BaCl_2$	0.0201	0.1732	0.0765
$LaCl_3$	0.0285	0.5126	0.3086

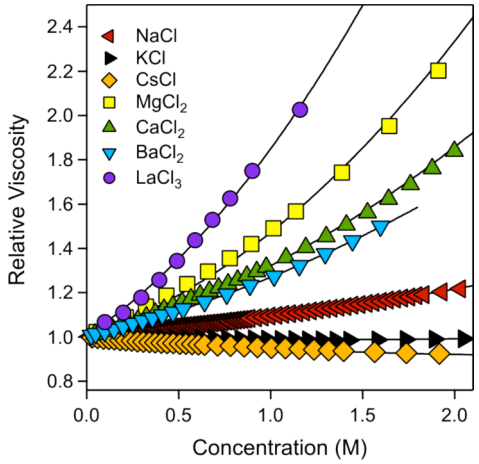

Figure 1. Relative viscosities of the electrolyte solutions used together with the best fit to eq 2. The coefficients are given in Table 1.

Particles in stable suspensions were characterized by light scattering as follows. The particle suspensions were prepared at a particle concentration of 4.5 mg/L and adjusted to pH 4.0. The angular dependence of the static scattering intensity was measured with the multiangle goniometer. The scattering profiles were fitted to the form factor of polydisperse spheres based on Mie theory including the back-reflection correction and the refractive index of polystyrene of 1.59 as known from the literature.[41] The best fits are shown in Figure 2. They

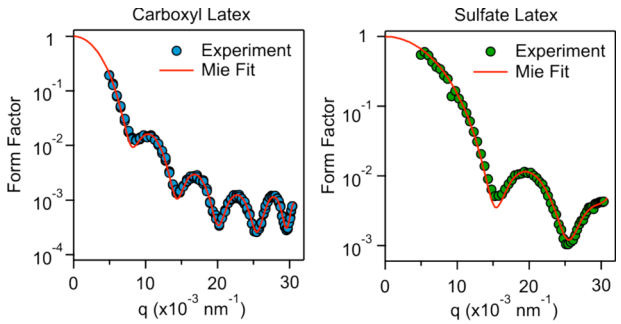

Figure 2. Particle form factors vs the magnitude of the scattering vector q for the carboxyl latex (left) and sulfate latex (right) measured in dilute suspensions by static light scattering and best fit with Mie theory.

yield an average diameter of 0.97 μm and a coefficient of variation of 0.029 for the carboxyl particles and 0.53 μm and 0.038 for the sulfate particles. The reflection coefficient was around 0.03. Dynamic light scattering at a scattering angle of 90° yields a diameter of 1.04 μm for the carboxyl latex and a diameter of 0.58 μm for the sulfate latex. The latter values are slightly higher than those obtained by the manufacturer as a result of polydispersity effects.

dx.doi.org/10.1021/la4046644 | Langmuir 2014, 30, 733−741

Absolute aggregation rates were measured with the multiangle goniometer. Light scattering cuvettes were cleaned prior to use in hot Piranha solution, which is a mixture of 98% H_2SO_4 and 30% H_2O_2 in a ratio of 3:1. The cuvettes were then washed with Milli-Q water and dried in a dust-free oven. The experiments were carried out in quartz cuvettes filled with particle suspensions in a 1.0 M KCl solution at particle concentrations of 2−5 mg/L. The experiment was initiated by adding the particle suspension to the electrolyte solution in the cuvette, followed by rapid mixing. The correlation functions were accumulated for 30 s, and the hydrodynamic radius was obtained from a second-order cumulant fit. The time evolution of the scattering intensity and of the hydrodynamic radius was followed over 100−400 consecutive measurements.

The absolute aggregation rate coefficient k, which characterizes the rate of the aggregation process, was obtained from the evolution of the static light scattering intensity $I(q, t)$ and of the apparent hydrodynamic radius r_h (q, t), where t is the time and q is the magnitude of the scattering vector. For short times, where monomers and dimers dominate, the rate of the relative change in the scattering intensity, which is also referred to as the apparent static rate, can be expressed as[42]

$$S = \frac{1}{I(q,0)}\frac{\mathrm{d}I(q,t)}{\mathrm{d}t}\bigg|_{t\to 0} = kN_0\left(\frac{I_2(q)}{2I_1(q)} - 1\right) \tag{3}$$

where k is the aggregation rate coefficient, N_0 is the initial particle number concentration, and $I_1(q)$ and $I_2(q)$ are the scattering intensities of the monomers and dimers, respectively. For short times, the relative rate of change in the hydrodynamic radius, which is also referred to as the apparent dynamic rate, is given by[42]

$$D = \frac{1}{r_h(q,0)}\frac{\mathrm{d}r_h(q,t)}{\mathrm{d}t}\bigg|_{t\to 0} = kN_0\left(1 - \frac{1}{\alpha}\right)\frac{I_2(q)}{2I_1(q)} \tag{4}$$

where $\alpha = r_{h,2}/r_{h,1}$ with $r_{h,1}$ and $r_{h,2}$ being the hydrodynamic radii of the monomer and the dimer, respectively. By combining eqs 3 and 4, one obtains a linear relationship

$$S = \left(1 - \frac{1}{\alpha}\right)^{-1} D - kN_0 \tag{5}$$

Therefore, a scatter plot of the two quantities S and D measured at different scattering angles gives a straight line. The absolute aggregation rate coefficient can be obtained from its intercept, and the slope yields the hydrodynamic factor α. From this representation, the errors in these quantities can also be obtained. The fact that only the early stages of the aggregation process are being probed can be ascertained by assuring that the initial hydrodynamic radius is within the experimental error of the one measured in a stable suspension and that the apparent hydrodynamic radius does not increase more than 20% during these measurements.

In all other situations, the aggregation rates were determined by time-resolved dynamic light scattering at a scattering angle of 90°. Typical time dependencies of the apparent hydrodynamic radius are shown for different electrolytes and concentrations in Figure 3. The resulting apparent dynamic rate was normalized by the apparent dynamic rate determined in a 1 M KCl reference solution. The absolute rate coefficient was then obtained by multiplying the ratio of the apparent rates by the absolute rate coefficient measured by the multiangle technique in the same reference solution. The samples were prepared similarly to the method described above in borosilicate glass cuvettes at particle concentrations of 80 mg/L for the carboxyl particles and 20 mg/L for the sulfate particles. The errors in the rate coefficients obtained in this fashion are about 50% larger than the ones obtained from the scatter plot.

Electrophoresis. A ZetaSizer Nano ZS (Malvern Instruments) was used to measure the electrophoretic mobility of the particles in aqueous solutions. The electrophoretic mobility represents the ratio between the travel velocity of the particle relative to the applied electric field. The samples were prepared by mixing the appropriate amount of the electrolyte solution with a diluted particle stock suspension in order to achieve the desired electrolyte and particle concentrations. The particle concentration was 80 mg/L for the carboxylated particles and 20 mg/L for sulfate particles. Before the measurement, the samples were equilibrated for 1 min, and the measurement was repeated several times.

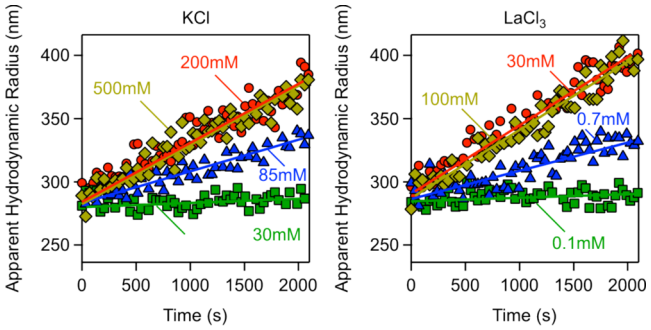

Figure 3. Time dependence of the apparent hydrodynamic radius measured at a scattering angle of 90° for the sulfate latex particles at different electrolyte concentrations in KCl (left) and $LaCl_3$ (right). Note that the data are overlaid in the fast aggregation regime.

RESULTS

We study the aggregation rates of two types of negatively charged latex particles in the presence of various counterions of different valence. Although some of the trivalent cations lead to a charge reversal at higher concentrations, this accumulation of charge does not lead to any slowdown in the aggregation.

Absolute Rate Coefficients. Absolute aggregation rate coefficients were determined from the multiangle measurements in 1.0 M KCl solutions with time-resolved simultaneous static and dynamic light scattering. These conditions correspond to the fast aggregation regime. The scatter plot of the apparent static versus dynamic rate is shown in Figure 4a. From the fit to straight lines as given in eq 5, one obtains aggregation rate coefficients of $(2.0 \pm 0.2) \times 10^{-18}$ m^3/s for the carboxylate particles and $(3.3 \pm 0.1) \times 10^{-18}$ m^3/s for the sulfate particles. The corresponding measured hydrodynamic factors are 1.40 ± 0.05 and 1.31 ± 0.03. The latter numbers are in good agreement with the theoretical value of 1.39 obtained from low Reynolds number hydrodynamics.[43] Figure 4b illustrates that the angular dependence of the ratio $I_2(q)/[2I_1(q)]$ can be well modeled with T-matrix theory.[44] Note that the classical theory by Rayleigh, Debye, and Gans (RDG)[14,36,37] provides only a poor description of the form factor of the particles used here. Apparent dynamic rates under other conditions were obtained from time-resolved DLS measurements at a scattering angle of 90° as shown in Figure 3. These rates were converted to absolute rate coefficients by normalization to the respective measurement at 1 M KCl.

The aggregation rate coefficient in the fast regime can be compared to the value obtained by Smoluchowski for hard-core interactions, but neglecting hydrodynamic forces[4,45]

$$k_S = \frac{8k_BT}{3\eta} = 1.23 \times 10^{-17}\ \frac{\mathrm{m}^3}{\mathrm{s}} \tag{6}$$

where T is the absolute temperature, k_B is the Boltzmann constant, and η is the viscosity of the liquid. The numerical value refers to water at a temperature of 25 °C. The measured rate coefficients are about 4−6 times smaller than the Smoluchowski value. This discrepancy mainly originates from

dx.doi.org/10.1021/la4046644 | Langmuir 2014, 30, 733−741

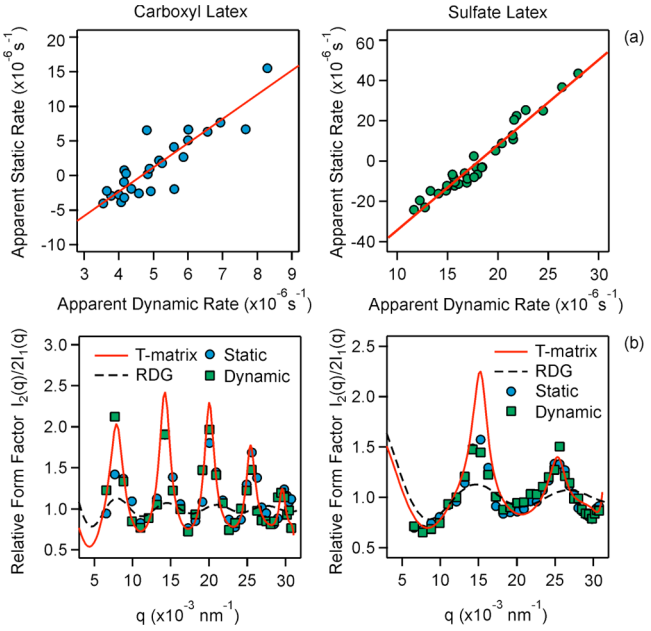

Figure 4. Determination of the absolute aggregation rate coefficients with time-resolved multiangle light scattering for the carboxyl latex (left) and sulfate latex (right) in 1 M KCl solution at particle concentrations of 8.6×10^{12} and 2.3×10^{13} m^{-3}, respectively. (a) Scatter plot of the apparent static and dynamic rates that allows the determination of the absolute rate coefficients. (b) Dimer form factors vs the magnitude of the scattering vector q compared to the T matrix and Rayleigh, Debye, and Gans (RDG) theory.

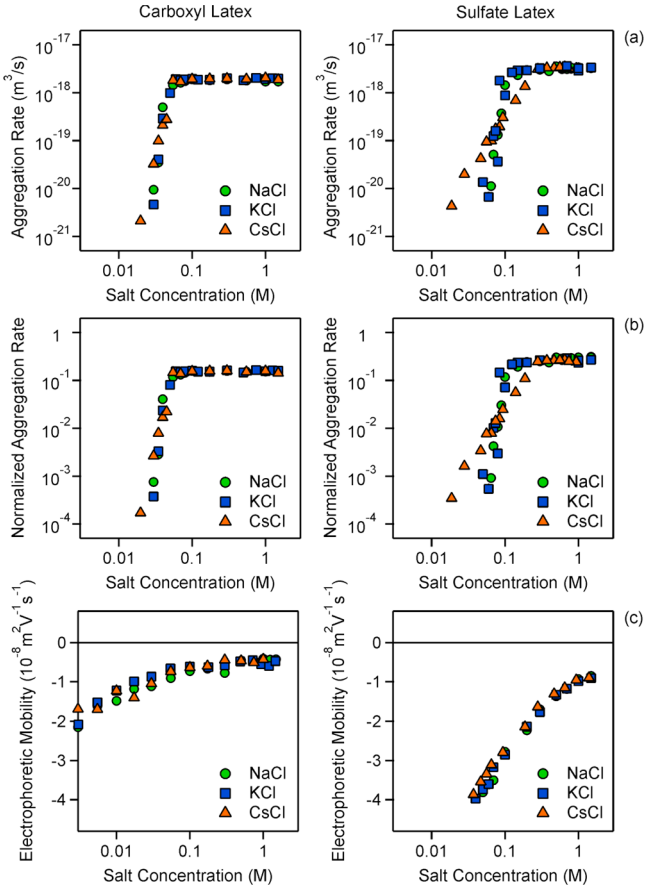

Figure 5. Aggregation and charging behavior in the presence of monovalent counterions for carboxyl (left) and sulfate latex particles (right). (a) Absolute aggregation rates, (b) rates normalized to the Smoluchowski value, and (c) electrophoretic mobility.

the fact that the Smoluchowski theory neglects van der Waals forces between particles and hydrodynamic interactions.

Influence of the Ion Type on Particle Aggregation. Let us now focus on the dependence of the aggregation rates and electrophoretic mobilities on the electrolyte concentration. Figure 1 shows that the viscosities of the electrolyte solutions may become significantly larger than for pure water at higher electrolyte concentrations; therefore, we have also considered the aggregation rate to be normalized to the Smoluchowski value, k/k_S. This representation removes the dependence of the aggregation rate on the viscosity of the solution in the fast aggregation regime.

Figure 5 shows the situation with monovalent Na^+, K^+, and Cs^+ counterions. The two columns refer to the carboxyl and sulfate latex particles with diameters of 1.0 and 0.53 μm, respectively. Figure 5a illustrates the typical dependence of the absolute aggregation rate on the electrolyte concentration. At low concentrations, the aggregation rate is small but increases rapidly with increasing concentration. This regime is referred to as slow aggregation. At higher concentrations, the aggregation rate is constant, and this regime is referred to as fast aggregation. These two regimes are separated by the CCC. Figure 5b shows the aggregation rate normalized to the Smoluchowski rate. The overall appearance of this graph is very similar to the absolute aggregation rate because the viscosities of monovalent salt solutions up to the solubility limit and of pure water do not differ more than 15%.

Figure 5c summarizes the electrophoretic mobility of these particles under the same conditions. One observes that the mobility decreases with decreasing salt concentration. At even lower salt concentrations than shown in the figure, there is a minimum in the mobility plot that can also be predicted with the standard electrokinetic model.[46,47]

The carboxyl latex particles have a CCC value of around 0.05 M. This low value reflects the relatively small charge of the particles, which is also confirmed by the low magnitudes of the electrophoretic mobility. The sulfate particles show a substantially higher CCC, which lies between 0.1 and 0.3 M depending on the type of counterion. These particles also have mobilities of much higher magnitudes. These observations indicate that the sulfate particles are much more strongly charged than the carboxyl particles under the conditions investigated. This aspect is corroborated by the fact that in the slow aggregation regime the dependence on the salt concentration is very strong for the carboxyl particles but less so for the sulfate particles. This dependence was related to the position of the barrier in the mutual energy profile between two particles at the CCC.[24] At low salt levels, this barrier is located at larger distances, and the salt dependence is strong, as predicted by DLVO theory. At higher salt levels, the barrier is at subnanometer distances and the local surface heterogeneities become important and lead to a faster aggregation rate. In this situation, the aggregation rate also depends on the type of cations. This dependence could be related to different affinities of the cations to surface heterogeneities.

The effects of divalent ions Mg^{2+}, Ca^{2+}, and Ba^{2+} are summarized in Figure 6. There is no hydrolysis of these ions under any conditions investigated.[48] The aggregation rates

dx.doi.org/10.1021/la4046644 | Langmuir 2014, 30, 733−741

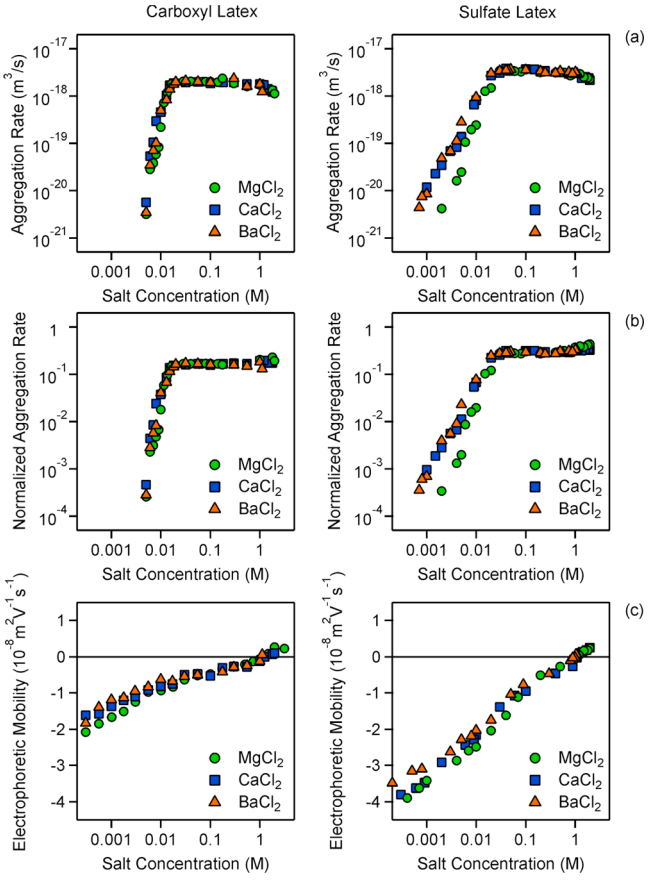

Figure 6. Aggregation and charging behavior in the presence of divalent counterions for carboxyl (left) and sulfate latex particles (right). (a) Absolute aggregation rates, (b) rates normalized to the Smoluchowski value, and (c) electrophoretic mobility.

shown in Figure 6a again illustrate the characteristic slow and fast regimes, but for the divalent ions, the CCCs are now substantially smaller than for the monovalent ions. This trend reflects the Schulze–Hardy rule, which states that the CCC decreases with increasing valence of the counterion. However, the aggregation rates decrease significantly at high electrolyte concentrations.

This decrease in the aggregation rate at high salt concentrations is due to an increase in the viscosity of the electrolyte solution. The viscosity of the electrolyte solution increases with increasing salt concentration as shown in Figure 1. This increase can be up to a factor of 2 for electrolyte solutions containing divalent ions. This effect leads to a slowdown of the diffusion-controlled aggregation process. The correctness of this interpretation becomes obvious when one inspects Figure 6b, where the normalized aggregation rate coefficient with respect to the Smoluchowski value is presented. In this representation, the effect of the solution viscosity is factored out, and one observes that the normalized rate remains constant all the way to the highest concentrations measured.

One might be tempted to associate the slowdown of the aggregation rate at high salt concentrations to an electrostatic stabilization of the particles induced by the charge reversal. Such a charge reversal can be indeed evidenced by the electrophoretic mobility data shown in Figure 6c. At low salt concentrations, the particle mobility is negative, but the electrophoretic mobility becomes positive at elevated concentrations. This charge reversal originates from the adsorption of the counterions to the particle surface. However, the salt concentrations are so high that such a charge reversal does not become noticeable. In fact, when one estimates the surface potentials (ζ potentials) with Smoluchowski's electrokinetic relation, one always finds values below 10 mV, which is not sufficient to obtain a significant slowdown of the aggregation rate due to double-layer repulsion at the salt levels in question.[5]

The CCC of the carboxyl latex particles is around 0.02 M, which is again lower than the CCC of sulfate particles, which is around 0.03 M. This situation again reflects the lower charge density of the carboxyl latex. However, the difference is much smaller than for the monovalent ions, which indicates that the divalent ions adsorb to the surface more strongly. This point is also illustrated by the electrophoretic mobility, which is less disparate for the divalent cations than for the monovalent cations. Aggregation of the carboxyl latex again shows very little ion specificity. For the sulfate latex, Mg^{2+} leads to slightly smaller aggregation rates than for Ca^{2+} and Ba^{2+} in the slow aggregation regime. Still, there is only a small effect of the type of counterion on the aggregation behavior.

The corresponding situation with trivalent cations La^{3+}, $[Co(NH_3)_6]^{3+}$, and $[Ru(NH_3)_6]^{3+}$ is shown in Figure 7. Speciation calculations again indicate that that these ions do not hydrolyze and that they maintain their charge under the conditions investigated.[48−50] The only exception is La^{3+}, which forms $LaCl^{2+}$ complexes to some extent at elevated concentrations. However, these complexes are negligible near the CCC.

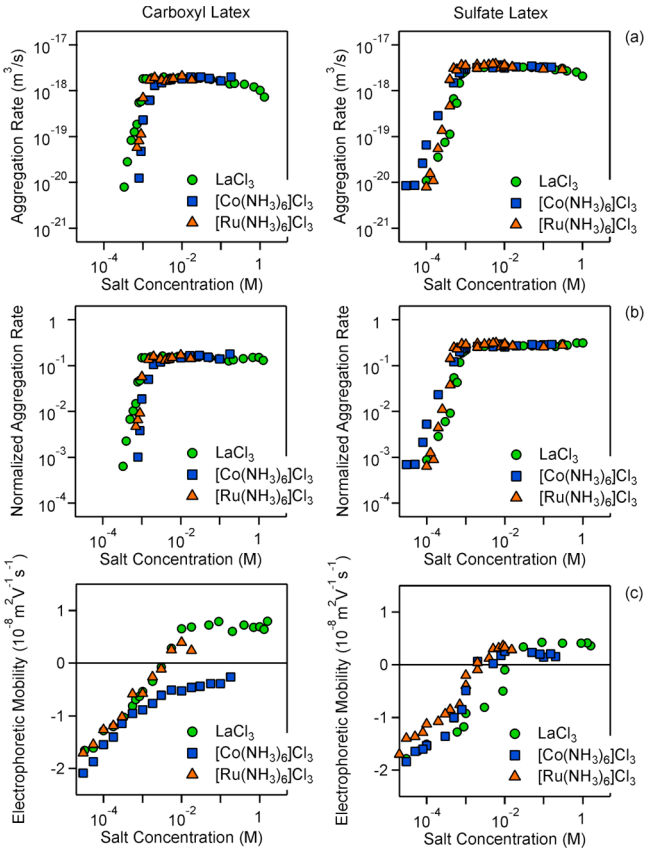

Figure 7. Aggregation and charging behavior in the presence of trivalent counterions for carboxyl (left) and sulfate latex particles (right). (a) Absolute aggregation rates, (b) rates normalized to the Smoluchowski value, and (c) electrophoretic mobility.

dx.doi.org/10.1021/la4046644 | Langmuir 2014, 30, 733−741

The aggregation rates shown in Figure 7a again feature the characteristic slow and fast aggregation regimes. The corresponding CCCs lie in the range of $(0.7-2.0) \times 10^{-3}$ M, and they are now shifted to even lower concentrations than for the divalent ions in accordance with the Schulze–Hardy rule. Now, there is little difference between the sulfate and carboxyl particles, indicating an even stronger interaction of the trivalent ions with the surface than for the divalent ions. The mobilities are also very similar in both cases.

The aggregation rate slows down significantly at high La^{3+} concentration. An inspection of the normalized rate again reveals that this slowdown is due to the increase in the viscosity of the $LaCl_3$ solution and is not due to the charge reversal. The normalized rate coefficient shown in Figure 7b is constant within the experimental error, which indicates that the slowdown is caused by the viscosity increase. Figure 7c shows the corresponding electrophoretic data. Although La^{3+} induces a substantial charge reversal, especially for the carboxyl particles, this charge reversal is too weak to induce a slowdown in aggregation. The corresponding ζ potential is around 5 mV, which is again too low to induce any stabilization due to double-layer repulsion.[5] Although $[Co(NH_3)_6]^{3+}$ does not lead to charge reversal for the carboxylate particles, the other cations induce a weak but clear charge reversal. Nevertheless, this phenomenon has no effect on the aggregation behavior. We observe again that the type of counterion has little effect on the aggregation behavior.

Schulze–Hardy Rule. The present aggregation data with sulfate latex particles illustrate this rule nicely. For the monovalent counterions, the CCCs is around 0.1 M; for divalent counterions, 0.03 M; and for trivalent counterions, 0.001 M. The corresponding CCC data are shown in Figure 8a. The data for the carboxyl latex follow a very similar trend.

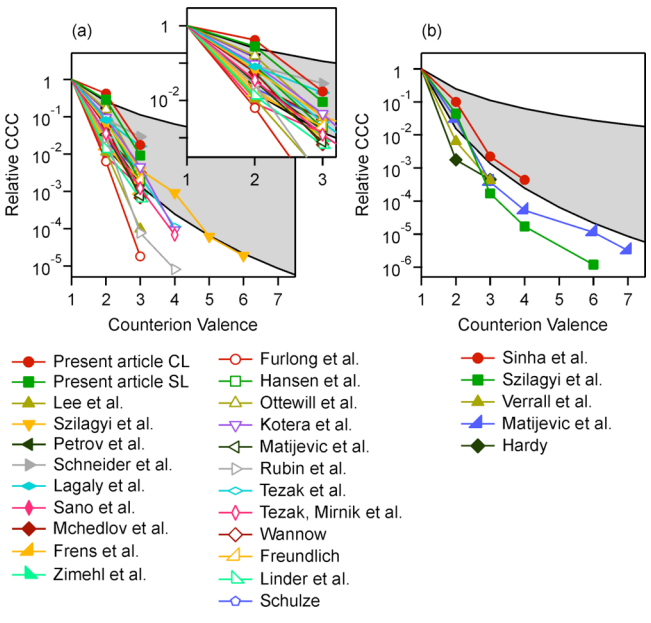

Figure 8. Relative critical coagulation concentration (CCC) with respect to its value for monovalent electrolytes for the present systems and others reported in the literature. The expected power-law dependence given by eq 1 is indicated for $n = 2$ and 6. The respective systems are summarized in Table 2. (a) Cations together with negatively charged particles (with the inset up to trivalent cations) and (b) anions with positively charged particles.

These trends are compared to other negatively charged particles involving multivalent cations taken from the literature. Only systems involving valences higher than 2 were considered. One observes that the CCCs do decrease with the valence but that there is substantial system specificity. Very similar behavior can be found for positively charged particles involving multivalent anions shown in Figure 8b. The individual systems, CCCs, and references are summarized in Table 2.

In spite of some variability due to system specificity, one can recognize several common trends. First, multivalent anions are more effective at destabilizing colloidal suspensions than are multivalent cations. Second, the power law given in eq 1 describes the data with $n = 6$ relatively well. Although this law can also be derived from DLVO theory for highly charged substrates, the observed agreement is likely to be only fortuitous. In those systems where the electric surface potentials at the CCC are known, one finds that their magnitudes are relatively low.[14,36,37] When the surface potential is low, eq 1 applies as well, but rather with $n = 2$. At the same time, however, the CCC also strongly increases with the diffuse layer potential ψ_D, leading to the overall dependence[5]

$$\mathrm{CCC} \propto \frac{\psi_D^4}{z^2} \tag{7}$$

for symmetric electrolytes. For the more common asymmetric electrolytes, the situation is similar.[5] However, the valence of the ions also influences the extent of the adsorption of these ions and thereby modifies the surface potential. The present observations and several other studies[9,14,36,37] point to the fact that the surface potential decreases with increasing valence. Therefore, the dependence of the CCC on the valence also reflects this variation, and one expects stronger dependencies on the valence than with $n = 2$. The stronger dependencies observed for the anions probably result from their greater affinity for the surface.

From the data summarized in Figure 8, one observes that the simple Schulze–Hardy rule reflects only the observed trends with valence semiquantitatively. Substantial system-specific variations remain. At this point, however, a quantitative analysis of these trends is lacking. Some progress could be made by combining aggregation rates with direct force measurements.[36,37] In the case of multivalent cations as investigated here, it was found that DLVO theory is capable of describing the forces and aggregation rates reasonably well. In the case of multivalent anions, additional attractive non-DLVO forces could be established by direct force measurements, but these forces were not sufficient to explain the more rapid aggregation rates observed. The explanation of these discrepancies is probably related to surface charge heterogeneities. However, the nature of these forces is not fully clear, and further research is necessary to clarify these questions.

CONCLUSIONS

We present accurate aggregation rate measurements of sulfate and carboxyl latex particles in the presence of different monovalent, divalent, and trivalent counterions. Although these rates strongly depend on the valence of the counterion, only a weak dependence on this type of ion is observed. The strongest ion specificity is observed for monovalent cations and highly charged sulfate particles.

At high salt concentrations, however, the increased viscosity of the solution may lead to a slowdown in the aggregation rates.

dx.doi.org/10.1021/la4046644 | Langmuir 2014, 30, 733–741

Table 2. CCCs of Various Colloidal Systems in the Presence of Multivalent Ions in Inverse Chronological Order

particles	ion and CCC (M)	reference	particles	ion and CCC (M)	reference
carboxyl latex	K^+ 5.1×10^{-2}, Mg^{2+} 2.1×10^{-2}, La^{3+} 8.8×10^{-4}	present article, CL	silver iodide	K^+ 2.0×10^{-1}, Ba^{2+} 4.2×10^{-3}, La^{3+} 2.0×10^{-4}	Frens et al.[9]
carboxyl latex	Na^+ 6.1×10^{-2}, Ca^{2+} 1.4×10^{-2}, $[Co(NH_3)_6]^{3+}$ 2.0×10^{-3}	present article, not shown[a]	anionic latex	Na^+ 4.4×10^{-1}, Ba^{2+} 2.5×10^{-2}, La^{3+} 4.2×10^{-4}	Zimehl et al.[13]
carboxyl latex	Cs^+ 5.0×10^{-2}, Ba^{2+} 1.8×10^{-2}, $[Ru(NH_3)_6]^{3+}$ 1.3×10^{-3}	present article, not shown[a]	platinum sol	Na^+ 1.0×10^{-1}, Mg^{2+} 6.3×10^{-4}, Al^{3+} 1.8×10^{-6}	Furlong et al.[51]
sulfate latex	K^+ 1.1×10^{-1}, Mg^{2+} 3.1×10^{-2}, La^{3+} 9.9×10^{-4}	present article, SL	anionic latex	K^+ 1.03×10^{-1}, Ca^{2+} 8.61×10^{-3}, La^{3+} 1.85×10^{-4}	Hansen et al.[12]
sulfate latex	Na^+ 1.2×10^{-1}, Ca^{2+} 3.2×10^{-2}, $[Co(NH_3)_6]^{3+}$ 8.7×10^{-4}	present article, not shown[a]	anionic latex	Na^+ 4.7×10^{-2}, Ba^{2+} 7.4×10^{-3}, Al^{3+} 1.6×10^{-4}	Ottewill et al.[11]
sulfate latex	Cs^+ 2.5×10^{-1}, Ba^{2+} 2.4×10^{-2}, $[Ru(NH_3)_6]^{3+}$ 7.2×10^{-4}	present article, not shown[a]	polystyrene latex	K^+ 7.0×10^{-2}, Ba^{2+} 6.6×10^{-3}, La^{3+} 3.1×10^{-5}, Th^{4+} 6.3×10^{-6}	Kotera et al.[10]
amidine latex	Cl^- 1.3×10^{-1}, SO_4^{2-} 1.3×10^{-2}, $[Fe(CN)_6]^{3-}$ 2.9×10^{-4}, $[Fe(CN)_6]^{4-}$ 5.7×10^{-5}	Sinha et al.[36]	silver bromide	Na^+ 6.05×10^{-2}, Ca^{2+} 2.01×10^{-3}, La^{3+} 4.72×10^{-5}	Matijevic et al.[52]
wood resin	Na^+ 7.2×10^{-1}, Ca^{2+} 8.0×10^{-3}, Al^{3+} 7.0×10^{-5}	Lee et al.[53]	*E. coli* bacteria	Na^+ 3.4×10^{-1}, Mg^{2+} 9.0×10^{-3}, La^{3+} 2.6×10^{-5}, Th^{4+} 2.72×10^{-6}	Rubin et al.[21]
amidine latex[b]	C1 1.7×10^{-1}, C2 7.6×10^{-3}, C3 2.9×10^{-5}, C4 2.9×10^{-6}, C6 2.0×10^{-7}	Szilagyi et al.[34]	silver bromide	NO_3^- 2.1×10^{-2}, SO_4^{2-} 6.3×10^{-4}, $citrate^{3-}$ 7.9×10^{-6}, $SiW_{12}O_{40}^{4-}$ 1.1×10^{-6}, $P_2W_{16}O_{62}^{6-}$ 2.4×10^{-7}, $PW_{12}O_{42}^{7-}$ 6.7×10^{-8}	Matijevic et al.[54]
carboxyl latex[c]	N1 3.0×10^{-1}, N2 2.0×10^{-2}, N3 1.1×10^{-3}, N4 2.7×10^{-4}, N5 1.8×10^{-5}, N6 5.6×10^{-6}	Szilagyi et al.[34]	silver iodide	Cs^+ 4.6×10^{-2}, Ba^{2+} 1.74×10^{-3}, Al^{3+} 3.68×10^{-5}	Tezak et al.[7]
tungsten oxide	Na^+ 3.2×10^{-2}, Ba^{2+} 9.9×10^{-4}, La^{3+} 5.1×10^{-5}	Petrov et al.[17]	silver bromide	Na^+ 1.0×10^{-1}, Ca^{2+} 3.48×10^{-3}, Al^{3+} 1.2×10^{-4}, Th^{4+} 6.81×10^{-6}	Tezak, Mirnik et al.[55]
sulfate latex	K^+ 3.5×10^{-1}, Mg^{2+} 3.0×10^{-2}, La^{3+} 1.0×10^{-2}	Schneider et al.[14]	arsenic sulfide	Cs^+ 2.9×10^{-2}, Ca^{2+} 8.3×10^{-4}, La^{3+} 8.8×10^{-5}	Wannow[56]
montmorillonite	Na^+ 5.0×10^{-3}, Ca^{2+} 4.0×10^{-4}, Al^{3+} 8.0×10^{-5}	Lagaly et al.[15]	arsenic sulfide	NH_4^+ 5.1×10^{-2}, UO_2^{2+} 8.0×10^{-4}, Ce^{3+} 1.0×10^{-4}	Freundlich[57]
carbon nanotubes	Na^+ 3.7×10^{-2}, Mg^{2+} 3.10×10^{-4}, La^{3+} 5.0×10^{-5}	Sano et al.[20]	ferric hydrate	Cl^- 5.6×10^{-1}, SO_4^{2-} 1.0×10^{-3}, $citrate^{3-}$ 2.5×10^{-4}	Hardy[2]
hematite	Cl^- 6.2×10^{-2}, SO_4^{2-} 4.0×10^{-4}, $[Fe(CN)_6]^{3-}$ 2.6×10^{-5}	Verrall et al.[16]	arsenic sulfide	K^+ 9.8×10^{-2}, Ca^{2+} 1.3×10^{-3}, Al^{3+} 6.2×10^{-5}	Linder et al.[58]
fullerene	Na^+ 8.5×10^{-2}, Mg^{2+} 4.75×10^{-3}, La^{3+} 5.6×10^{-5}	McHedlov et al.[18]	arsenic sulfide	K^+ 9.8×10^{-2}, Ca^{2+} 2.06×10^{-3}, Cr^{3+} 3.16×10^{-4}	Schulze[1]

[a]Data are not shown in Figure 8. [b]Dissociated acetic acid (C1), glutaric acid (C2), and oligomers of poly(acrylic acid) (C3–C6). [c]Ionized methylamine (N1), ethylenediamine (N2), diethylenetriamine (N3), triethylenetetramine (N4), tetraethylenepentamine (N5), and pentaethylenehexamine (N6).

dx.doi.org/10.1021/la4046644 | Langmuir 2014, 30, 733−741

However, this effect is relatively minor, and overall the valence of the counterions mainly dictates the aggregation rates whereas the chemical nature of the ion is less important. The presently observed values for the CCCs are well in line with other data available from the literature, even though the dependence on valence may vary from system to system. We suspect that multivalent ions adsorb strongly to the substrates and reduce the magnitude of the surface potential.

AUTHOR INFORMATION

Corresponding Author

*E-mail: michal.borkovec@unige.ch.

Notes

The authors declare no competing financial interest.

ACKNOWLEDGMENTS

This research was supported by the Swiss National Science Foundation, Swiss Scientific Exchange Program, and University of Geneva.

REFERENCES

(1) Schulze, H. Schwefelarsen in wässriger Lösung. *J. Prakt. Chem.* **1882**, *25*, 431−452.

(2) Hardy, W. B. A preliminary investigation of the conditions which determine the stability of irreversible hydrosols. *Proc. R. Soc. London* **1900**, *66*, 110−125.

(3) Vincent, B. Early (pre-DLVO) studies of particle aggregation. *Adv. Colloid Interface Sci.* **2012**, *170*, 56−67.

(4) Russel, W. B.; Saville, D. A.; Schowalter, W. R. *Colloidal Dispersions*; Cambridge University Press: Cambridge, U.K., 1989.

(5) Trefalt, G.; Szilagyi, I.; Borkovec, M. Poisson-Boltzmann description of interaction forces and aggregation rates involving charged colloidal particles in asymmetric electrolytes. *J. Colloid Interface Sci.* **2013**, *406*, 111−120.

(6) Matijevic, E.; Shulz, K.; Mirnik, M.; Herak, J.; Vouk, V. B.; Slunjski, M.; Babic, S.; Kratohvil, J.; Palmar, T. The mechanism of coagulation of lyophobic sols as revealed through investigations of silver halide sols in statu nascendi. *J. Phys. Chem.* **1953**, *57*, 301−307.

(7) Tezak, B.; Matijevic, E.; Schulz, K. F. Coagulation of hydrophobic sols in statu nascendi 3. The influence of the ionic size and valency of the counterion. *J. Phys. Chem.* **1955**, *59*, 769−773.

(8) Matijevic, E.; Broadhurst, D.; Kerker, M. On coagulation effects of highly charged counterions. *J. Phys. Chem.* **1959**, *63*, 1552−1557.

(9) Frens, G.; Heuts, J. J. F. G. The double layer potential as a rate determining factor in the coagulation of electrocratic colloids. *Colloids Surf.* **1988**, *30*, 295−305.

(10) Kotera, A.; Furusawa, K.; Kudo, K. Colloid chemical studies of polystyrene latices polymerized without any surface-active agents 0.2. Coagulation into secondary minimum. *Kolloid Z.* **1970**, *240*, 837−842.

(11) Ottewill, R. H.; Rance, D. G. Studies on polytetrafluoroethylene lattices Part 1. Coagulation by non-hydrolyzed electrolytes. *Croat. Chem. Acta* **1977**, *50*, 65−75.

(12) Hansen, F. K.; Matijevic, E. Heterocoagulation 5. Adsorption of a carboxylated polymer latex on monodispersed hydrated metal oxides. *J. Chem. Soc., Faraday Trans. 1* **1980**, *76*, 1240−1262.

(13) Zimehl, R.; Lagaly, G. Coagulation of latex dispersions by inorganic salts: structural effects. *Prog. Colloid Polym. Sci.* **1986**, *72*, 28−36.

(14) Schneider, C.; Hanisch, M.; Wedel, B.; Jusufi, A.; Ballauff, M. Experimental study of electrostatically stabilized colloidal particles: colloidal stability and charge reversal. *J. Colloid Interface Sci.* **2011**, *358*, 62−67.

(15) Lagaly, G.; Ziesmer, S. Colloid chemistry of clay minerals: the coagulation of montmorillonite dispersions. *Adv. Colloid Interface Sci.* **2003**, *100*, 105−128.

(16) Verrall, K. E.; Warwick, P.; Fairhurst, A. J. Application of the Schulze-Hardy rule to haematite and haematite/humate colloid stability. *Colloids Surf., A* **1999**, *150*, 261−273.

(17) Petrov, Y. Y.; Avvakumova, S. Y.; Sidorova, M. P.; Ermakova, L. E.; Voitylov, V. V.; Voitylov, A. V. Stability of tungsten(VI) oxide dispersions in electrolyte solutions. *Colloid J.* **2011**, *73*, 834−840.

(18) McHedlov-Petrossyan, N. O.; Klochkov, V. K.; Andrievsky, G. V. Colloidal dispersions of fullerene C-60 in water: some properties and regularities of coagulation by electrolytes. *J. Chem. Soc., Faraday Trans.* **1997**, *93*, 4343−4346.

(19) Chen, K. L.; Elimelech, M. Aggregation and deposition kinetics of fullerene (C_{60}) nanoparticles. *Langmuir* **2006**, *22*, 10994−11001.

(20) Sano, M.; Okamura, J.; Shinkai, S. Colloidal nature of single-walled carbon nanotubes in electrolyte solution: the Schulze-Hardy rule. *Langmuir* **2001**, *17*, 7172−7173.

(21) Rubin, A. J.; Hayden, P. L.; Hanna, G. P. Coagulation of escherichia coli by neutral salts. *Water Res.* **1969**, *3*, 843−852.

(22) Ehrl, L.; Jia, Z.; Wu, H.; Lattuada, M.; Soos, M.; Morbidelli, M. Role of counterion association in colloidal stability. *Langmuir* **2009**, *25*, 2696−2702.

(23) Metcalfe, I. M.; Healy, T. W. Charge regulation modeling of the Schulze-Hardy rule and related coagulation effects. *Faraday Discuss.* **1990**, 335−344.

(24) Behrens, S. H.; Christl, D. I.; Emmerzael, R.; Schurtenberger, P.; Borkovec, M. Charging and aggregation properties of carboxyl latex particles: experiments versus DLVO theory. *Langmuir* **2000**, *16*, 2566−2575.

(25) Guldbrand, L.; Jonsson, B.; Wennerstrom, H.; Linse, P. Electrical double-layer forces: a Monte-Carlo study. *J. Chem. Phys.* **1984**, *80*, 2221−2228.

(26) Kjellander, R.; Marcelja, S. Correlation and image charge effects in electric double-layers. *Chem. Phys. Lett.* **1984**, *112*, 49−53.

(27) Ennis, J.; Marecelja, S.; Kjellander, R. Effective surface charge for symmetric electrolytes in the primitive model double layer. *Electrochim. Acta* **1996**, *41*, 2115−2124.

(28) Kjellander, R. Intricate coupling between ion-ion and ion-surface correlations in double layers as illustrated by charge inversion-combined effects of strong coulomb correlations and excluded volume. *J. Phys.: Condens. Matter* **2009**, *21*, 424101.

(29) Bohinc, K.; Grime, J. M. A.; Lue, L. The interactions between charged colloids with rod-like counterions. *Soft Matter* **2012**, *8*, 5679−5686.

(30) Sjostrom, L.; Akesson, T.; Jonsson, B. Charge reversal in electrical double layers: a balance between energy and entropy. *Ber. Bunsen-Ges.* **1996**, *100*, 889−893.

(31) Besteman, K.; Van Eijk, K.; Lemay, S. G. Charge inversion accompanies DNA condensation by multivalent ions. *Nat. Phys.* **2007**, *3*, 641−644.

(32) Martin-Molina, A.; Quesada-Perez, M.; Galisteo-Gonzalez, F.; Hidalgo-Alvarez, R. Primitive models and electrophoresis: An experimental study. *Colloids Surf., A* **2003**, *222*, 155−164.

(33) Szilagyi, I.; Polomska, A.; Citherlet, D.; Sadeghpour, A.; Borkovec, M. Charging and aggregation of negatively charged colloidal latex particles in presence of multivalent polyamine cations. *J. Colloid Interface Sci.* **2013**, *392*, 34−41.

(34) Szilagyi, I.; Sadeghpour, A.; Borkovec, M. Destabilization of colloidal suspensions by multivalent ions and polyelectrolytes: from screening to overcharging. *Langmuir* **2012**, *28*, 6211−6215.

(35) Besteman, K.; Zevenbergen, M. A. G.; Heering, H. A.; Lemay, S. G. Direct observation of charge inversion by multivalent ions as a universal electrostatic phenomenon. *Phys. Rev. Lett.* **2004**, *93*, 170802.

(36) Sinha, P.; Szilagyi, I.; Montes Ruiz-Cabello, F. J.; Maroni, P.; Borkovec, M. Attractive forces between charged colloidal particles induced by multivalent ions revealed by confronting aggregation and direct force measurements. *J. Phys. Chem. Lett.* **2013**, *4*, 648−652.

(37) Montes Ruiz-Cabello, F. J.; Trefalt, G.; Csendes, Z.; Sinha, P.; Oncsik, T.; Szilagyi, I.; Maroni, P.; Borkovec, M. Predicting aggregation rates of colloidal particles from direct force measurements. *J. Phys. Chem. B* **2013**, *117*, 11853−11862.

(38) Sadeghpour, A.; Szilagyi, I.; Borkovec, M. Charging and aggregation of positively charged colloidal latex particles in presence of multivalent polycarboxylate anions. *Z. Phys. Chem.* **2012**, *226*, 597−612.
(39) Weast, R. C.; Astle, M. J. *CRC Handbook of Chemistry and Physics*, 60th ed.; CRC Press: New York, 1980.
(40) Jenkins, H. D. B.; Marcus, Y. Viscosity B-coefficients of ions in solution. *Chem. Rev.* **1995**, *95*, 2695−2724.
(41) Ma, X. Y.; Lu, J. Q.; Brock, R. S.; Jacobs, K. M.; Yang, P.; Hu, X. H. Determination of complex refractive index of polystyrene microspheres from 370 to 1610 nm. *Phys. Med. Biol.* **2003**, *48*, 4165−4172.
(42) Lin, W.; Kobayashi, M.; Skarba, M.; Mu, C.; Galletto, P.; Borkovec, M. Heteroaggregation in binary mixtures of oppositely charged colloidal particles. *Langmuir* **2006**, *22*, 1038−1047.
(43) Yu, W. L.; Matijevic, E.; Borkovec, M. Absolute hetero-aggregation rate constants by multiangle static and dynamic light scattering. *Langmuir* **2002**, *18*, 7853−7860.
(44) Galletto, P.; Lin, W.; Mishchenko, M. I.; Borkovec, M. Light scattering form factors of asymmetric particle dimers from heteroaggregation experiments. *J. Chem. Phys.* **2005**, *292*, 139−147.
(45) Elimelech, M.; Gregory, J.; Jia, X.; Williams, R. A. *Particle Deposition and Aggregation: Measurement, Modeling, and Simulation*. Butterworth-Heinemann: Oxford, U.K., 1995.
(46) O'Brien, R. W.; White, L. R. Electrophoretic mobility of a spherical colloidal particle. *J. Chem. Soc., Faraday Trans. 2* **1978**, *74*, 1607−1626.
(47) Borkovec, M.; Behrens, S. H.; Semmler, M. Observation of the mobility maximum predicted by the standard electrokinetic model for highly charged amidine latex particles. *Langmuir* **2000**, *16*, 5209−5212.
(48) Baes, C. F.; Mesmer, R. E. *The Hydrolysis of Cations*; Krieger Publishing: Malabar, FL, 1976.
(49) Bjerrum, J.; McReynolds, J. P. Hexammine cobalt (III) salts. *Inorg. Synth.* **1946**, *2*, 216−221.
(50) Lever, F. M.; Powell, A. R. Ammine complexes of ruthenium. *J. Chem. Soc. A* **1969**, 1477−1482.
(51) Furlong, D. N.; Launikonis, A.; Sasse, W. H. F.; Sanders, J. V. Colloidal platinum sols: preparation characterization and stability towards salt. *J. Chem. Soc., Faraday Trans. 1* **1984**, *80*, 571−588.
(52) Matijevic, E.; Allen, L. H. Interactions of colloidal dispersions with electrolytes. *Environ. Sci. Technol.* **1969**, *3*, 264−268.
(53) Lee, R.; Stack, K.; Richardson, D.; Lewis, T.; Garnier, G. Effect of shear, temperature and pH on the dynamics of salt induced coagulation of wood resin colloids. *Colloids Surf., A* **2012**, *396*, 106−114.
(54) Matijevic, E.; Kerker, M. The charge of some heteropoly anions in aqueous solutions as determined by coagulation effects. *J. Phys. Chem.* **1958**, *62*, 1271−1276.
(55) Tezak, B.; Matijevic, E.; Shulz, K.; Mirnik, M.; Herak, J.; Vouk, V. B.; Slunjski, M.; Babic, S.; Kratohvil, J.; Palmar, T. The mechanism of coagulation of lyophobic sols as revealed through investigations of silver halide sols in statu-nascendi. *J. Phys. Chem.* **1953**, *57*, 301−307.
(56) Wannow, H. A. Über eine neue methode zur quantitativen koagulationsmessung. *Kolloidchem. Beih.* **1939**, *50*, 367−472.
(57) Freundlich, H. Die bedeutung der adsorption bei der fällung der suspensionskolloide. *Z. Chem. Ind. Kolloide* **1910**, *7*, 193−195.
(58) Linder, S. E.; Picton, H. Solution and pseudo-solution: part II. Some physical properties of arsenious suphide and ofther solutions. *J. Chem. Soc.* **1882**, *67*, 63−74.

CHAPTER 3

Predicting Aggregation Rates of Colloidal Particles from Direct Force Measurements

Ruiz-Cabello, F. J. M.; Trefalt, G.; Csendes, Z.; Sinha, P.; Oncsik, T.; Szilagyi, I.; Maroni, P.; Borkovec, M.

J. Phys. Chem. B **2013,** 117, 11853-11862.

THE JOURNAL OF PHYSICAL CHEMISTRY B

Article

pubs.acs.org/JPCB

Predicting Aggregation Rates of Colloidal Particles from Direct Force Measurements

F. Javier Montes Ruiz-Cabello, Gregor Trefalt, Zita Csendes, Prashant Sinha, Tamas Oncsik, Istvan Szilagyi, Plinio Maroni, and Michal Borkovec*

Department of Inorganic and Analytical Chemistry, University of Geneva, Sciences II, Quai Ernest-Ansermet 30, 1205 Geneva, Switzerland

ABSTRACT: Direct force measurements between negatively charged colloidal latex particles of a diameter of 1 μm were carried out in aqueous solutions of various inorganic monovalent and multivalent cations with the multiparticle colloidal probe technique based on the atomic force microscope (AFM). The observed force profiles were rationalized within the theory of Derjaguin, Landau, Verwey, and Overbeek (DLVO). In the presence of monovalent and divalent cations, this theory was capable to describe the force profiles correctly down to distances of a few nm. At shorter distances, however, a strong non-DLVO attraction was identified. For more highly charged cations, an additional and more long-ranged non-DLVO attractive force is observed, and it was interpreted by surface charge heterogeneities. On the basis of these force profiles, the aggregation rates, which were independently measured by light scattering, can be predicted relatively well. The main conclusion of this study is that, in the present system, direct force measurements do capture the principal interactions driving aggregation in colloidal suspensions.

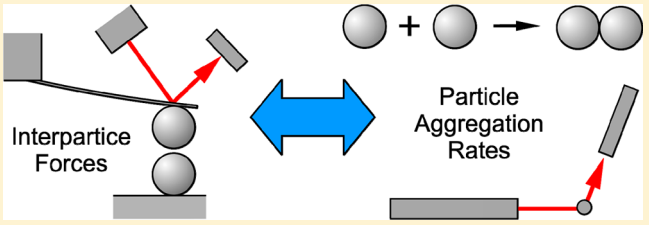

INTRODUCTION

The discovery that the popular Poisson−Boltzmann (PB) description of the electrical double layer may fail in the presence of multivalent ions triggered renewed interest in the interaction of multivalent ions with interfaces and their influence on interparticle forces.[1,2] In the meantime, numerous theoretical as well as experimental studies involving multivalent ions were carried out in order to understand the role of ion correlations in more detail.[3−6] The most surprising finding that emerged from these investigations was that in the presence of multivalent ions forces between similarly charged water−solid interfaces may become attractive, whereby the classical PB theory would predict purely repulsive forces in such situations. Such attractive forces were surmised to be responsible for the collapse of clays, condensation of DNA, and cement hardening.[4,7−11]

To clarify the importance of such additional forces more directly, effects of multivalent ions on interactions between water−solid interfaces were investigated with the surface forces apparatus (SFA),[12−14] the colloidal probe technique based on the atomic force microscope (AFM),[15] or video microscopy combined with optical tweezers.[16] Many of these studies confirmed that the PB model provides a good description of the force profiles down to distances of a few nm.[12−16] However, some reports revealed the characteristic charge reversal[15] and additional attractive forces.[14]

In spite of all this recent activity, the question how multivalent ions affect interaction forces between colloidal particles was investigated for a long time. The Schulze−Hardy rule, which was discovered about a century ago, states that multivalent ions are much more effective in destabilizing colloidal suspensions than monovalent ones.[17] More precisely, this rule states that the critical coagulation concentration (CCC), which separates the regions of slow and rapid aggregation, scales with the inverse sixth power of the valence of the counterion. The triumph of the famous theory put forward by Derjaguin, Landau, Verwey, and Overbeek (DLVO) was to derive this rule by assuming that interparticle forces can be approximated by a superposition of attractive van der Waals interactions and repulsive forces due to the overlap of the electrical double layers.[18,19] Nevertheless, this characteristic dependence remains puzzling even today, as its derivation within DLVO theory assumes very high diffuse layer potentials. Such high potentials are unrealistic, since more recent adsorption studies of multivalent ions on charged water−oxide interfaces have revealed that relatively low surface potentials are the rule.[20−22] Moreover, formation of hydroxo and multicenter metal complexes complicates the picture further.[23,24]

While forces acting between colloidal particles determine the suspension stability, direct measurements of forces and colloidal aggregation rates were hardly carried out in the same system. The reasons are probably technical. Direct force measurements with the colloidal probe[25−27] or optical tweezers techniques[16,28,29] are typically carried out with particles of several μm in diameter. On the other hand, aggregation rate

Received: June 19, 2013
Revised: August 5, 2013
Published: September 9, 2013

   dx.doi.org/10.1021/jp406061f | J. Phys. Chem. B 2013, 117, 11853−11862

measurements are normally done with substantially smaller particles.[30−33] To circumvent this problem, particles of different size but of similar surface functionalities have been used in order to compare forces and aggregation rates.[33] Thereby, the larger particles were used in the colloidal probe experiment, and smaller ones in the aggregation studies.

We are now capable of measuring forces between particles from the same batch as used for aggregation rate measurements. Such experiments became possible due to two important developments. With multiangle static and dynamic light scattering experiments, one can reliably measure absolute aggregation rate coefficients just below 1 μm in size.[34−36] Furthermore, the recently developed multiparticle colloidal probe technique enables us to carry out direct force measurements between two micrometer-sized particles.[37,38] We have adapted both techniques to investigate particles of 1 μm in diameter. A report on direct force measurements and aggregation studies with positively charged particles in the presence of multivalent anions has appeared.[39] In the case of trivalent and tetravalent anions, this system displayed a characteristic reentrant behavior due to charge reversal. In the present article, we investigate the practically more relevant case of negatively charged particles in the presence of multivalent cations. Such studies are essential to give new insights on how multivalent ions influence interparticle forces and aggregation rates between colloidal particles.

DLVO THEORY

Forces acting between colloidal particles across aqueous solutions are typically described in terms of the DLVO theory. This theory stipulates that the total force $F(h)$, which depends on the surface separation h, can be represented as a sum of two contributions[40]

$$F = F_{vdW} + F_{dl} \tag{1}$$

where F_{vdW} is the attractive van der Waals force and F_{dl} is the repulsion force due to the overlap of electrical double layers. Neglecting retardation effects, the van der Waals force can be approximated by[40]

$$F_{vdW}(h) = -\frac{Hr}{12h^2} \tag{2}$$

where H is the Hamaker constant and r is the particle radius. This expression invokes the Derjaguin approximation, which will be used throughout. The double-layer force F_{dl} is evaluated from the electrical potential profile $\psi(x)$ between two charged plates by numerically solving the PB equation[40]

$$\frac{d^2\psi}{dx^2} = -\frac{q}{\varepsilon_0\varepsilon}\sum_i z_i c_i e^{-z_i\beta q\psi} \tag{3}$$

where z_i and c_i are the valence and bulk concentration of ion type i, respectively, q is the elementary charge, ε_0 the dielectric permittivity of vacuum, ε the dielectric constant, and $\beta = 1/(k_B T)$ the inverse thermal energy, where T is the absolute temperature and k_B is the Boltzmann constant. The PB equation is solved numerically for the two plates situated at $x = \pm h/2$ subject to the boundary conditions[41]

$$\pm\varepsilon_0\varepsilon \left.\frac{d\psi}{dx}\right|_{x=\pm h/2} = \sigma - C_I[\psi(\pm h/2) - \psi_D] \tag{4}$$

where ψ_D is the diffuse layer potential and C_I is the inner layer capacitance. We prefer to express the inner capacitance in terms of the regulation parameter

$$p = \frac{C_D}{C_D + C_I} \tag{5}$$

where C_D is the diffuse layer capacitance of an isolated plate. For constant charge (CC) boundary conditions, one has $p = 1$ while for constant potential (CP) conditions $p = 0$. The interaction force is evaluated from the swelling pressure

$$\Pi = k_B T \sum_i c_i (e^{-z_i\beta q\psi} - 1) - \frac{\varepsilon_0\varepsilon}{2}\left(\frac{d\psi}{dx}\right)^2 \tag{6}$$

Finally, the forces are calculated by numerical integration of the swelling pressure according to

$$F_{dl}(h) = \pi r \int_h^\infty \Pi(h')\, dh' \tag{7}$$

For larger distances, the force decays exponentially as[40]

$$F_{dl} = 2\pi r\varepsilon_0\varepsilon\kappa\psi_{eff}^{\ 2} e^{-\kappa h} \tag{8}$$

where ψ_{eff} is the effective potential and κ^{-1} is the Debye length, which can be expressed as

$$\kappa^2 = \frac{2\beta q^2 I}{\varepsilon_0\varepsilon} \tag{9}$$

where the ionic strength is given by

$$I = \frac{1}{2}\sum_i z_i^2 c_i \tag{10}$$

Early stage aggregation between colloidal particles can be quantified by the kinetic rate law of dimer formation

$$\frac{dN_2}{dt} = \frac{k}{2}N_1^{\ 2} \tag{11}$$

where N_1 and N_2 are the number concentrations of the monomers and dimers, respectively, and k is the aggregation rate coefficient. This rate coefficient can be obtained from the steady-state solution of the pair diffusion equation subject to the force given by eq 1. The result reads[40,42]

$$k = \frac{4}{3\beta\eta r}\left[\int_0^\infty \frac{B(h/r)}{(2r+h)^2}\exp[\beta V(h)]\, dh\right]^{-1} \tag{12}$$

where $V(h)$ is the interaction potential energy and $B(x)$ is the hydrodynamic resistance function that can be approximated by[43,44]

$$B(x) = \frac{6x^2 + 13x + 2}{6x^2 + 4x} \tag{13}$$

The interaction potential energy can be obtained from the force profile by an additional integration

$$V(h) = \int_h^\infty F(h')\, dh' \tag{14}$$

We will report the corresponding rate coefficients as a dimensionless stability ratio. This ratio is defined as

$$W = \frac{k_{fast}}{k} \tag{15}$$

dx.doi.org/10.1021/jp406061f | J. Phys. Chem. B 2013, 117, 11853−11862

where k_{fast} is the aggregation rate coefficient at a suitably chosen reference condition. This condition is chosen in the fast aggregation region where the repulsive double layer contribution is negligible.

EXPERIMENTAL SECTION

Materials. Carboxyl-terminated surfactant-free colloidal particles were purchased as aqueous suspensions from Interfacial Dynamics Corporation. The manufacturer characterized these particles with transmission electron microscopy, and they report a mean diameter of 1.0 μm and a polydispersity with a coefficient of variation of 0.045. The suspension was purified in a cellulose ester membrane with a molecular mass cutoff of 300 kg/mol (Spectrum) by dialysis against Milli-Q water. The procedure was carried out for at least 3 days until the conductivity of the dialysate was the same as the one of Milli-Q water. The particle concentrations after dialysis were obtained by their light scattering intensity. The surface of these particles was relatively smooth, as revealed by the mean square roughness of 0.39 nm measured by tapping mode AFM in air.

Colloidal suspensions with a particle concentration of 80 mg/L were prepared by mixing the stock particle suspension with appropriate amounts of corresponding salt solutions of KCl, $MgCl_2$, $LaCl_3$, and $ZrCl_4$ (Acros, Aldrich). When experiments were carried out with other particle concentrations, this fact is indicated in the text. Solutions were prepared with Milli-Q water (Millipore) and adjusted to pH 4.0 with HCl (Sigma-Aldrich). The prevalent species in the electrolyte solutions were estimated by solving the chemical equilibrium conditions subject to mass conservation. In KCl and $MgCl_2$ solutions, the hydrated K^+ and Mg^{2+} ions are the dominant species in the entire concentration range considered. In $LaCl_3$ solution, the formation of the chloro-complex was considered according to the reaction[45]

$$La^{3+} + Cl^- \rightleftharpoons LaCl^{2+} \qquad K = 0.8 \tag{16}$$

where the corresponding equilibrium constant is indicated. Molar concentration units are used throughout. The distribution of these species is given in Figure 1a. One observes that La^{3+} is the major species below 10^{-2} M. In the case of $ZrCl_4$ solution, the relevant equilibria are[45]

$$Zr^{4+} + OH^- \rightleftharpoons ZrOH^{3+} \qquad K = 0.3$$
$$4Zr^{4+} + 8OH^- \rightleftharpoons Zr_4(OH)_8^{8+} \qquad K' = 2 \times 10^8 \tag{17}$$

Figure 1b illustrates that, for most conditions considered, $Zr_4(OH)_8^{8+}$ is the principal species. Note that the actual composition might be somewhat different due to the slow formation kinetics of some of these species.

Direct Force Measurements. Forces between the particles were measured with a closed-loop AFM (MFP-3D, Asylum Research) mounted on an inverted optical microscope (Olympus IX 70). Prior to the force measurements, the glass plate fitting the fluid cell was cleaned overnight with hot Piranha solution, which consists of a mixture of H_2SO_4 98% and H_2O_2 30% in a ratio of 3:1. Subsequently, it was rinsed with Milli-Q water and dried with nitrogen. The glass plate and the tip-less AFM cantilever (NSC 12, μMash, Estonia) were further cleaned in air plasma cleaner (PDC-32G, Harrick, New York) for 20 min. The glass plate and the cantilever were silanized in an evacuated airtight container aside of a drop of 3-ethoxydimethylsilylpropyl amine (Sigma-Aldrich). The silanized glass plate and the cantilever were then mounted in the AFM fluid cell and the cantilever holder, and the cell was flushed with the appropriate suspension of a particle concentration of 80 mg/L. The particles were allowed to settle for about 2 h, and the cell was then rinsed with the electrolyte solution or the suspension supernatant. The supernatant was used for $LaCl_3$ and $ZrCl_4$ solutions and was obtained by filtering the suspension with a 0.1 μm polyvinylidene difluoride (PVDF) membrane filter (Millex VV-33, Millipore).

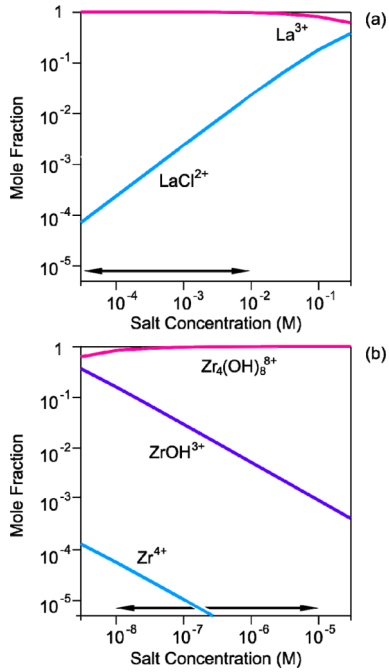

Figure 1. Estimated solution speciation at pH 4. The double arrow indicates the concentration range investigated. (a) $LaCl_3$ and (b) $ZrCl_4$.

A colloidal particle was attached to the tip-less cantilever by pressing the particle against the substrate with the cantilever. This particle was then centered with respect to another particle immobilized on the glass surface with the optical microscope with a lateral precision of about 50 nm. Interaction forces between the particles were measured with repeated vertical approach/retraction cycles at a frequency of 0.5 Hz, velocity of 300 nm/s, and sampling rate of 5 kHz. The probe was approached until the constant compliance region was reached. The onset of this region was used to determine the zero separation with a precision of about 0.5 nm. A jump-out was observed upon retraction. The interaction forces were obtained from the cantilever deflection in the approach part and the spring constant of the cantilever. They were measured through the amplitude of the thermal noise[38] and the geometrical dimensions of the cantilever[46] and were in the range 0.1−0.3 N/m. Each force curve was time-averaged in intervals of 0.3 ms, and about 100 such force curves obtained from different approach−retraction cycles averaged again. This procedure leads to a force resolution of about 3 pN and a distance resolution of 0.15 nm. After a measurement sequence, the particle used was detached from the cantilever and another particle attached. In this way, interaction forces between different pairs of particles could be measured under the same conditions. In some cases, the forces were well reproducible between different particle pairs, while in others they were less so. Figure 2 gives respective examples. In the following, we will always report force profiles that have been obtained from the

dx.doi.org/10.1021/jp406061f | J. Phys. Chem. B 2013, 117, 11853−11862

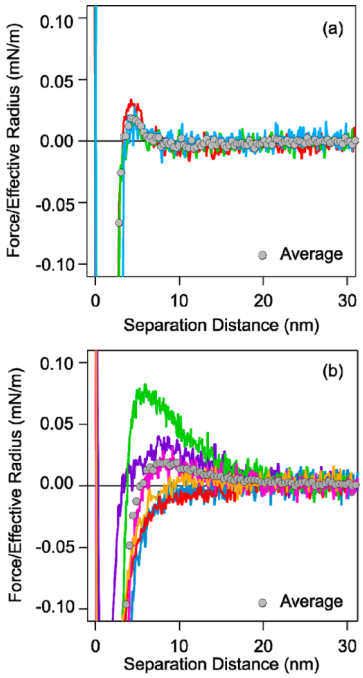

Figure 2. Variation between force profiles measured between different pairs of particles and the corresponding averaged profile. Solution of (a) 30 mM KCl and (b) 0.8 mM $LaCl_3$.

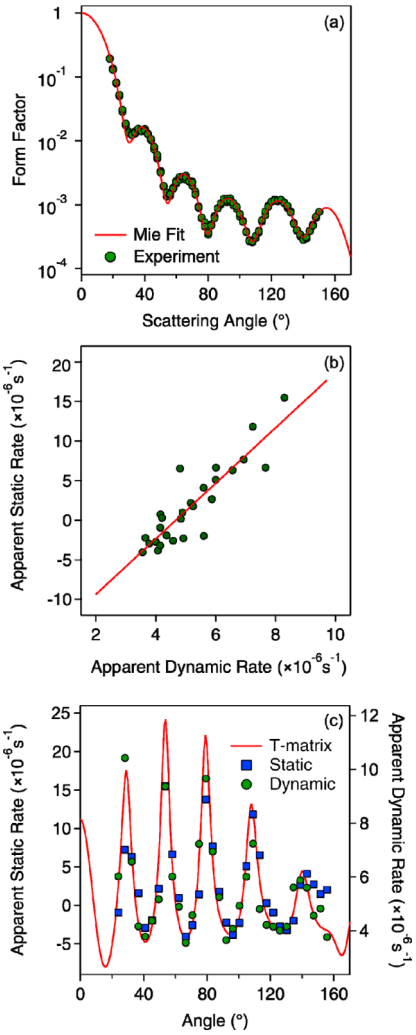

Figure 3. Light scattering experiments in latex particle suspensions at a particle concentration of 4.5 mg/L and pH 4.0. (a) Scattering intensity in a stable suspension with no additional salt added and the fit with Mie theory including polydispersity. (b) Scatter plot of the apparent static and dynamic rates from which the absolute aggregation rate coefficient has been determined. (c) Angular dependence of apparent static and dynamic rates and the corresponding calculation with T-matrix theory.

average of the forces involving at least three different pairs of particles. Adhesion forces were measured from the maximum deflection of the cantilever during retraction.

Light Scattering. Experiments were carried out with two different instruments. The multiangle light scattering instrument has eight fiber-optic photomultiplier detectors (ALV/CGS-8, Langen, Germany) and a solid state laser with a wavelength of 532 nm (Verdi V2, Coherent, Inc.). The compact goniometer (ALV/CGS-3, Langen, Germany) uses an avalanche photodiode as a detector and a He−Ne laser of 633 nm wavelength as the light source.

Stable particle suspensions were characterized with static and dynamic light scattering with the multiangle instrument. The measured angular dependence of the scattering intensity in an aqueous suspension adjusted to pH 4.0 at a particle concentration of 4.5 mg/L was fitted to the expected form factor of polydisperse spheres obtained from Mie theory (Figure 3a). The best fit yields an average diameter of 0.97 μm and a polydispersity characterized by a coefficient variation of 0.029 in good agreement with the values provided by the manufacturer quoted above. We have used the known refractive index of 1.59 for polystyrene.[47] Dynamic light scattering at a scattering angle of 90° yields a diameter of 1.04 μm. For subsequent analysis of the force curves and calculations of aggregation rate constants, a particle diameter of 1.0 μm was used.

Absolute aggregation rate constant measurements were carried out with the multiangle goniometer. Each correlation function was accumulated for 30 s, and second cumulant fit was used to obtain the apparent hydrodynamic radius. The time dependence of the scattering intensity and of the hydrodynamic radius was estimated from 100−400 consecutive measurements.

From the time dependence of the static light scattering intensity $I(q, t)$ and of the apparent hydrodynamic radius $r_h(q, t)$, the absolute aggregation rate coefficient k was obtained. In the early stages of the aggregation process, the rate of change of the static intensity, denoted as the static signal S, is given by[34,35]

$$S = \frac{1}{I(q, 0)} \cdot \frac{\mathrm{d}I(q, t)}{\mathrm{d}t}\bigg|_{t\to 0} = kN_0\left(\frac{I_2(q)}{2I_1(q)} - 1\right) \quad (18)$$

where N_0 is the initial particle number concentration, q is the magnitude of the scattering vector, and $I_1(q)$ and $I_2(q)$ are the scattering intensities of the monomers and dimers, respectively. The initial rate of change of the hydrodynamic radius, denoted as the dynamic signal D, is given by[34,35]

$$D = \frac{1}{r_h(q, 0)} \cdot \frac{\mathrm{d}r_h(q, t)}{\mathrm{d}t}\bigg|_{t\to 0} = kN_0\left(1 - \frac{1}{\alpha}\right)\frac{I_2(q)}{2I_1(q)} \quad (19)$$

where $\alpha = r_{h,2}/r_{h,1}$ is the ratio of the hydrodynamic radii $r_{h,1}$ and $r_{h,2}$ which refer to the monomer and the dimer, respectively. Equations 1 and 2 yield a linear relationship between the dynamic and static signals, namely,

dx.doi.org/10.1021/jp406061f | J. Phys. Chem. B 2013, 117, 11853−11862

$$S = \left(1 - \frac{1}{\alpha}\right)^{-1} D - kN_0 \quad (20)$$

A plot of the static versus dynamic signal yields a straight line, and from its intercept, the absolute aggregation rate coefficient can be obtained. The data measured in 1 M KCl solution at a particle concentration of 4.5 mg/L (8.2×10^{12} m^{-3}) are shown in Figure 3b and yield an aggregation rate coefficient of 2.0×10^{-18} m^3/s. The slope yields the hydrodynamic factor of 1.40, which is in excellent agreement with the value of 1.39 obtained from low Reynolds number hydrodynamics.[48] The angular dependence could be well described with calculations of the doublet form factors with T-matrix theory (Figure 3c). Note that the simplified theory by Rayleigh, Debye, and Gans provides a poor description of the optical response of the particles used here.

Stability ratios were measured on the compact goniometer by dynamic light scattering at a scattering angle of 90° at a particle concentration of 80 mg/L. The 1 M KCl solution is used as the reference for fast aggregation.

Electrophoresis. The laser velocimetry setup ZetaNano ZS (Malvern Instruments, Worcestershire, UK) was used to measure the electrophoretic mobility of the particles at electric field strengths of 4 kV/m. The suspensions were prepared at a particle concentration of about 80 mg/L and equilibrated about half a day prior to measurement. Some electrophoresis measurements were also carried out at 200 mg/L. Electrokinetic potentials (ζ-potentials) were obtained from the electrophoretic mobilities as follows. For potentials of magnitude below 30 mV, Henry theory was used for the conversion, while, for potentials of higher magnitude, the theory of O'Brien and White was used.[40,49]

RESULTS AND DISCUSSION

Direct force measurements between carboxylated colloidal particles of diameter 1.0 μm were performed with the AFM in aqueous solution of pH 4.0 containing KCl, $MgCl_2$, $LaCl_3$, and $ZrCl_4$ electrolytes. The force profiles were fitted quantitatively with modified DLVO theory, and these fits were used to predict the aggregation rate coefficients. These predictions were compared with aggregation rate coefficients measured by light scattering.

Direct Force Measurements. The multiparticle colloidal probe technique was used to measure forces between pairs of particles. The force curves strongly depend on the type of salt and its concentration.

Figure 4a shows the force profiles in monovalent KCl solutions. At low concentrations, the forces are strongly repulsive, reflecting the overlap of the electrical double layers. With increasing concentrations, the repulsion weakens, and a maximum in the force curve is observed. This maximum is visible in Figure 4a for a KCl concentration of 30 mM. At even higher concentrations, a purely attractive force is acting, which reflects the omnipresent van der Waals interaction. One observes a jump-in at distances of about 2 nm. The force profiles in $MgCl_2$ and $LaCl_3$ solutions shown in Figure 4b,c are qualitatively similar, but there are two quantitative differences. First, the transition to attractive forces occurs at increasingly lower concentration with increasing valence. Second, the maxima in the force curves shift to larger distances. These trends are mainly related to the fact that an increasing valence of the ions leads to an increasingly important contribution to the ionic strength and thereby to electrostatic screening.

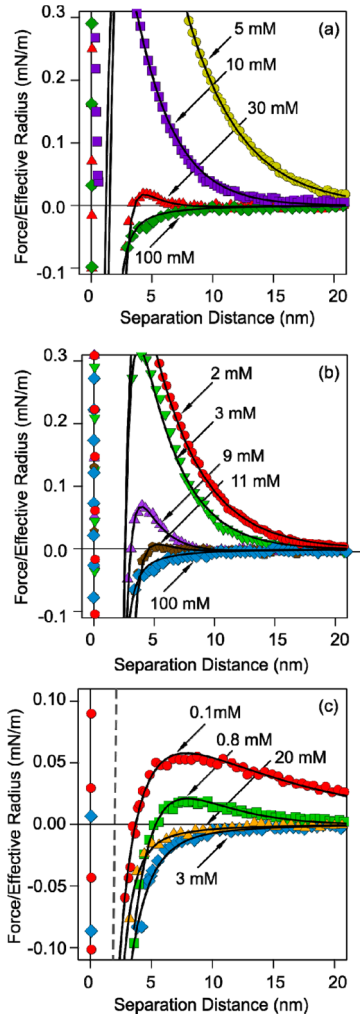

Figure 4. Force profiles between carboxylated latex particles of 1.0 μm in diameter in different electrolyte solutions at pH 4.0 at the concentrations indicated. Solid lines are fits to the modified DLVO theory. (a) KCl, (b) $MgCl_2$, and (c) $LaCl_3$.

Figure 5 shows the force profiles in $ZrCl_4$ solutions. With increasing concentration, one observes the forces to become increasingly attractive, but then they become repulsive again. As suggested by the chemical equilibrium calculations shown in Figure 1b, $Zr_4(OH)_8^{8+}$ has a high valence and is likely the prevalent species in solution. The observed trend in the force profiles can be explained by adsorption of this positively charged species and a subsequent charge reversal. While the jump-in at short distances is observed at small concentrations, the jump-in disappears at higher concentrations.

The force profiles in KCl and $MgCl_2$ shown in Figure 4a and b can be very well quantified with classical DLVO theory at distances larger than 5 nm. By fitting the van der Waals expression given in eq 2 to purely attractive profiles, one finds a Hamaker constant of $(3.5 \pm 0.8) \times 10^{-21}$ J. This value is in reasonable agreement with the theoretical estimate of 9.0×10^{-21} J for polystyrene,[50] and the discrepancy between these values is probably due to surface roughness. The measured force profiles were fitted to DLVO force profiles given by eq 1 for distances down to 5 nm by fixing the Hamaker constant to $H = 3.5 \times 10^{-21}$ J. Thereby, the nonlinear PB model and the CR approximation were used. This model is solved numerically for the appropriate mixture of the eventually asymmetric

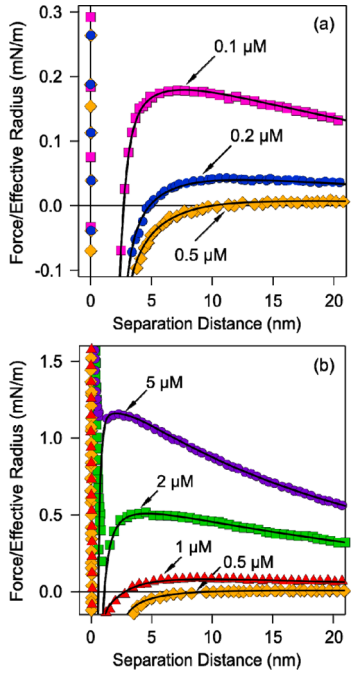

Figure 5. Force profiles between carboxylated latex particles of 1.0 μm in diameter in $ZrCl_4$ solution at pH 4.0 at the concentrations indicated. Solid lines are fits with the modified DLVO theory. Concentrations (a) below and at the charge reversal point and (b) at this point and above.

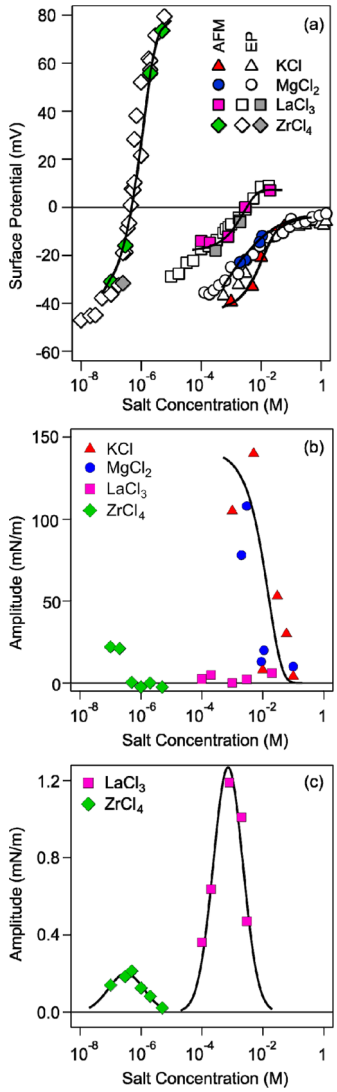

Figure 6. Concentration dependence of the parameters derived from the force profiles. Solid lines are empirical fitting functions. (a) Surface potentials refer to diffuse layer potentials determined by AFM and ζ-potentials obtained from electrophoresis at particle concentrations of 80 mg/L (white symbols) and 200 mg/L (gray symbols). Amplitudes (b) of the short-range attraction and (c) the longer-ranged patch-charge attraction. The latter is only present in the $LaCl_3$ and $ZrCl_4$ systems.

electrolyte and the known concentration of the monovalent electrolyte HCl. Three parameters enter this PB model, namely, the electrolyte concentration, the diffuse layer potential, and the regulation parameter. The fitted electrolyte concentration was always found to be within 10% of the analytical concentration of the solution. The regulation parameter was found to fluctuate somewhat, and its mean with standard deviation was 0.41 ± 0.09. We have fixed the regulation parameter to its mean value of $p = 0.41$, and refitted all force curves. The resulting diffuse layer potentials are shown in Figure 6a. This figure also demonstrates that the diffuse layer potentials determined by AFM agree relatively well with the electrokinetic ζ-potentials measured by electrophoresis.

In KCl and $MgCl_2$ electrolyte solutions, DLVO theory works well beyond distances of 5 nm but fails to describe the strong attraction acting at distances of 2–3 nm. In order to describe the force curves in these regimes as well, we have modified the force profile with a short-ranged attractive exponential term

$$F = F_{dl} + F_{vdW} - A_s e^{-q_s h} \quad (21)$$

The experimental force curves were refitted for all measured separation distances whereby $H = 3.5 \times 10^{-21}$ J and $p = 0.41$ were kept fixed to the same values as determined above. This modified model rationalizes the forces over the whole experimentally accessible distance range, and we found that the decay length q_s^{-1} fluctuates around the average value of 0.49 ± 0.07 nm. The final fit of these force curves was obtained by also fixing the decay length to $q_s^{-1} = 0.49$ nm, and in this fashion, one obtains the amplitudes shown in Figure 6b. The diffuse layer potentials obtained from this fit are very similar to the ones obtained from the fits at larger distances. These amplitudes are very comparable in the KCl and $MgCl_2$ systems, and they decrease within increasing salt level. This short-ranged non-DLVO force is probably a hydrophobic attraction due to the nonpolar nature of polystyrene.

The force profiles in $LaCl_3$ and $ZrCl_4$ solutions in Figures 4c and 5 cannot be reconciled with the classical DLVO theory even at separation distances above 5 nm. This disparity originates from the fact that the attractive forces are stronger than van der Waals force determined in systems of lower valence. This attraction cannot be explained by regulation effects but can be rationalized with an additional exponential attraction. The observed force profiles are thus fitted to

$$F = F_{dl} + F_{vdW} - A_s e^{-q_s h} - A_p e^{-q_p h} \quad (22)$$

where the first exponential term corresponds to the short-range attraction, while the second term reflects the additional attraction of longer range.

dx.doi.org/10.1021/jp406061f | J. Phys. Chem. B 2013, 117, 11853–11862

We suspect that this additional attraction originates from patch-charge heterogeneities of the substrate, for which an exponential dependence was predicted.[51] Moreover, when these heterogeneities are arranged on a square-lattice, the range q_p^{-1} of the patch-charge attraction can be expressed as

$$q_p^{\ 2} = \kappa^2 + (2\pi/a)^2 \tag{23}$$

where a is the lattice spacing. By invoking the patch-charge model, the number of fitting parameters can be reduced further. The force profiles were now fitted by fixing $H = 3.5 \times 10^{-21}$ J, $p = 0.41$, and $q_s^{-1} = 0.49$ nm, which were the vales determined in the systems of low valence. The remaining parameters, namely, the diffuse layer potential, the salt concentration, the amplitudes of the exponential terms A_s and A_p, and the lattice spacing a were fitted to the experimental force curves. The data were well consistent with the model, and the lattice spacing did fluctuate with a mean and a standard deviation of 13 ± 5 nm. No systematic differences of this value between the $LaCl_3$ and $ZrCl_4$ systems could be observed. The data were therefore refitted by taking a fixed value of a = 13 nm. The remaining parameters could be determined well from the force profiles, and they are summarized in Figure 6.

When the observed decay lengths of the electrostatic double-layer repulsion in $LaCl_3$ solutions are interpreted with the Debye–Hückel equation (eq 9), one obtains La^{3+} concentrations that are about 20% lower. This discrepancy might be caused by a decrease of the solution concentration by adsorption of La^{3+} to the particle surface or formation of $LaCl^{2+}$ complexes, which would lead to a reduction of the ionic strength (Figure 1). In $ZrCl_4$, the decay lengths agreed well with the expected values, since the ionic strength is dominated by the monovalent HCl electrolyte, which was used to adjust the pH. The previously determined regulation parameter of 0.41 was found to be consistent with the force profiles observed in these systems as well.

The corresponding diffuse layer potentials are summarized in Figure 6a. For $LaCl_3$ and $ZrCl_4$, one observes a charge reversal, which is weak in the case of $LaCl_3$ and very pronounced for $ZrCl_4$. The pronounced nature of the charge reversal in the latter system can be explained by the adsorption of the highly charged species $Zr_4(OH)_8^{8+}$. This charge reversal is also confirmed by electrophoresis, and the corresponding ζ-potentials. Since the highly charged ions adsorb to the particle surface, the corresponding solution concentration might be decreased. Such partitioning effects between dissolved and adsorbed species were further investigated for the more highly charged ions by varying the particle concentration in the electrophoresis experiments.[52,53] For $LaCl_3$ and $ZrCl_4$, only a weak dependence of the mobility on the particle concentration was observed, from which we conclude that the solution concentrations change only weakly during the adsorption process. This conclusion is further supported by the fact that in the $LaCl_3$ system the solution concentrations estimated from the decay lengths agree within 20% with the total concentrations.

The amplitudes of the exponential short-ranged and long-ranged non-DLVO attractive forces are summarized in Figure 6b and c, respectively. The amplitude of the short-range attraction is much smaller in the presence of the highly charged ions than for monovalent and divalent ones. This finding suggests that the adsorption of multivalent ions makes the particle surfaces more hydrophilic. The amplitudes of the long-ranged attractive force go through a characteristic maximum, and they are larger in the $LaCl_3$ system.

We suspect that the additional long-ranged attractive forces do not originate from ion–ion correlations but from surface charge heterogeneities. Computer simulations and density functional theories predict that the range of attractive forces induced by ion–ion correlations lies well within the sub-nanometer regime.[6,54] Forces acting over such a small range would be hidden by the jump-in instability of the cantilever, and they cannot be resolved with the presently used colloidal probe technique. On the other hand, surface charge heterogeneities are known to induce attractive forces acting at larger distances.[55−57] The existence of patch-change heterogeneities is further supported by the variability of the force profiles observed between different pairs of particles (Figure 2b) and the fact that the existence of such heterogeneities on similar latex particles has been demonstrated with rotational electrophoresis.[58] The reason why the role of these heterogeneities is more important for the multivalent ions is probably related to the fact that these ions preferentially adsorb to patches of higher charge.

Adhesion forces were similar in all situations investigated, whereby the average was 0.6 nN. In $ZrCl_4$ solutions, the adhesion was weaker, and short pulling events were observed. We suspect that these effects are caused by the formation of linear Zr–OH–Zr multicenter hydroxo complexes forming on the particle surface.

Particle Aggregation Rates. Particle aggregation was monitored with time-resolved combined static and dynamic light scattering. The aggregation rates are presented as stability ratios in Figure 7. In KCl, $MgCl_2$, and $LaCl_3$ solutions, one observes the classical situation, where high salt concentrations induce fast aggregation, while at lower concentrations the aggregation suddenly slows down. The onset of the slow aggregation is referred to as the critical coagulation concentration (CCC). The CCC shifts toward lower concentrations, as suggested by the Schulze–Hardy rule. For $ZrCl_4$ solutions, however, the suspension becomes unstable only in a very narrow concentration range. This behavior is consistent with the presence of the highly charged species $Zr_4(OH)_8^{8+}$ and the pronounced charge reversal observed by electrophoresis. A minor slowdown of the aggregation is also observed at higher concentration in the $LaCl_3$ solutions, which

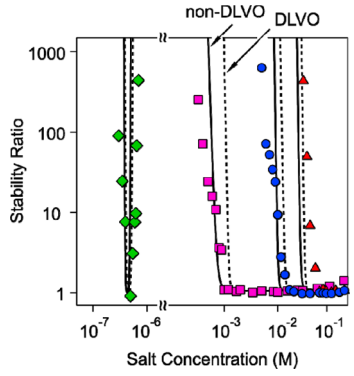

Figure 7. Comparison between stability ratios measured by time-resolved light scattering and the ones calculated form direct force measurements. The solid lines include the non-DLVO contributions to the force, while the dashed ones only consider DLVO forces.

is probably also related by the weak charge reversal observed by electrophoresis.

The solid lines shown in Figure 7 are predictions of the stability ratios calculated from the force profiles measured by the AFM. These predictions contain no adjustable parameters, and they were obtained as follows. The concentration dependence of the parameters entering the interpretation of the force curves in terms of modified DLVO theory was approximated by the empirical fitting functions shown as solid lines in Figure 6. These functions were used to calculate the concentration dependence of the respective parameters. These parameters were then inserted into the modified DLVO theory to calculate the aggregation rate coefficient with eq 12, which was converted to the stability ratio. While an attempt was made to interpret the force profile with a physically reasonable model, the real aim was to obtain a smooth interpolation function of the measured force profiles that can be used to calculate the stability ratios. The predicted stability ratios are independent of the exact nature of the model used to fit the force data.

The calculated stability ratios agree very well with the stability ratios measured experimentally with dynamic light scattering. Overall, the predicted salt dependence in the slow aggregation region is slightly stronger. The prediction in KCl solutions is shifted to lower concentrations, which is probably related to inaccuracies in the force profiles at small separation distances. Figure 7 also reports the results obtained by the DLVO theory, where all non-DLVO contributions are neglected. While the overall shape of the stability curves is still predicted well, by excluding the non-DLVO contributions, the stability ratios are overestimated.

The predicted absolute aggregation rate of 6.8×10^{-18} m^3/s compares with the experimentally determined one of 2.0×10^{-18} m^3/s. By excluding the non-DLVO contributions, one obtains the same value as given above. Since the force profile is known from the AFM experiments, the discrepancy is probably related to inaccuracies in the hydrodynamic resistance function at small separations.

Figure 8 provides additional information on the comparison of experimental and calculated aggregation rates. Figure 8a summarizes the experimental CCCs versus the counterion valence together with the calculated ones that include all non-DLVO contributions and those that consider the DLVO contributions only. In the $ZrCl_4$ system, lower CCC and the valence of the highly charged species $Zr_4(OH)_8^{8+}$ were considered. Given the large range of the concentrations reported, the non-DLVO contributions do not appear to be extremely important. The trend in the CCCs agrees reasonably well with the classical Schulze–Hardy rule that states that the CCCs should scale with the inverse of the sixth power of the valence. The fact that the $ZrCl_4$ fits well into this trend supports the conclusion that the principal species in this solution is much more highly charged than Zr^{4+}.

Figure 8b summarizes the separation distance of the maximum in the interaction potential $V(h)$ at CCC. For the monovalent and divalent systems, these distances are below 3 nm. For the more highly charged ions, these distances move to substantially larger separations. The non-DLVO patch-charge contributions shift these distances to 8–12 nm. When one considers the DLVO contributions only, these distances become substantially smaller.

Comparison with Other Systems. One should compare these results with a similar study presented recently, where positively charged particles were investigated in the presence of

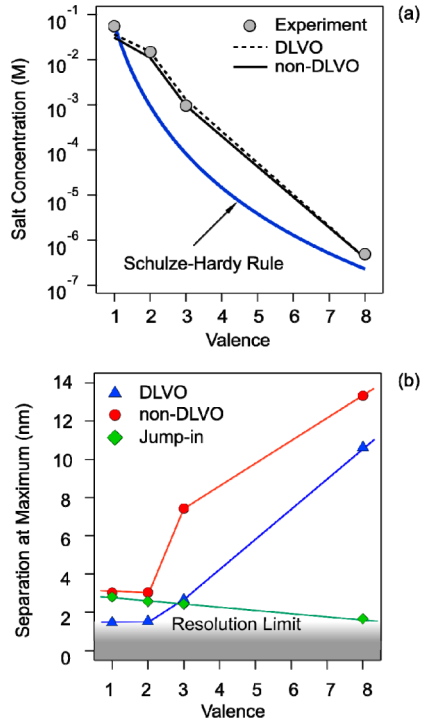

Figure 8. Summary of CCCs and separation distances at CCC versus the valence. (a) Comparison of experimental and calculated CCCs with the trend expected from the Schulze–Hardy rule. (b) Calculated separation distances of the energy maximum at CCC and the average position of the jump-ins. The distance resolution is also indicated.

multivalent anions.[39] Attractive non-DLVO forces with a range of several nm were also observed in the presence of highly charged ions, and these forces were also interpreted as originating from surface charge heterogeneities. The predicted aggregation rates agreed well with the experimental ones for monovalent and divalent ions, but for trivalent and tetravalent ions, they were substantially larger than the ones observed experimentally. This discrepancy was also attributed to additional attractive forces induced by surface charge heterogeneities. Since these deviations are absent in the present study, we suspect that relative contribution from these patch-charge forces is less important in the present system. This conclusion is equally supported by the fact that the magnitude of the additional non-DLVO forces in the presence of multivalent ions measured with the colloidal probe is about a factor of 2 smaller in the present system.

A less direct comparison can be made with electrophoresis and aggregation studies of substantially smaller charged latex particles in the presence of oppositely charged linear chain oligomers.[53,59,60] In particular, negatively charged carboxyl particles were investigated in the presence of aliphatic polyamines. In close analogy to the $LaCl_3$ system, a weak charge reversal was observed for the trivalent cation, and no restabilization region was observed.[60] A pronounced over-charging was only observed for hexavalent ions, which supports the existence of a highly charged species in the $ZrCl_4$ system. Anionic oligomers of poly(acrylic acid) are more effective to induce a charge reversal of amidine latex particles, whereby the reversal already happens for the divalent ion.[53,59]

dx.doi.org/10.1021/jp406061f | J. Phys. Chem. B 2013, 117, 11853–11862

CONCLUSIONS

Measurements of force profiles and of aggregation rates involving negatively charged colloidal particles in the presence of monovalent and multivalent inorganic cations were carried out. DLVO theory is capable of describing the force profiles rather well in the presence of monovalent and divalent cations, even though a non-DLVO short-ranged attraction is present at distances below 2 nm. For more highly charged ions, an additional and more long-ranged attractive force is observed, and is attributed to surface charge heterogeneities. From these force profiles, the observed aggregation rates can be predicted relatively well. We conclude that direct force measurements capture the principal interactions driving the aggregation in the colloidal suspensions correctly.

Ion−ion correlations seem not to be directly responsible for the additional non-DLVO forces observed in the presence of multivalent ions. While additional attractive forces are observed, their range is substantially larger than the range of attractive forces induced by ion−ion correlations.[6,54] We rather suspect that the observed attractive forces are caused by patch-charge heterogeneities, which are amplified in the presence of multivalent ions. On the other hand, ion−ion correlations are probably responsible for the charge reversal observed in the presence of ions of higher valence. An analogous scenario was suggested on the basis of similar experiments with positively charged particles in the presence of multivalent ions.[39]

AUTHOR INFORMATION

Corresponding Author

*E-mail: michal.borkovec@unige.ch.

Notes

The authors declare no competing financial interest.

ACKNOWLEDGMENTS

This research was supported by the Swiss National Science Foundation, University of Geneva, COST Action CM1101, Swiss Secretariat of Education and Research, and the Swiss Scientific Exchange Program. Useful discussions with Mihail Popescu are acknowledged.

REFERENCES

(1) Guldbrand, L.; Jonsson, B.; Wennerstrom, H.; Linse, P. Electrical Double-layer Forces: A Monte-Carlo Study. *J. Chem. Phys.* **1984**, *80*, 2221−2228.

(2) Kjellander, R.; Marcelja, S. Correlation and Image Charge Effects in Electric Double-layers. *Chem. Phys. Lett.* **1984**, *112*, 49−53.

(3) Grosberg, A. Y.; Nguyen, T. T.; Shklovskii, B. I. Colloquium: The Physics of Charge Inversion in Chemical and Biological Systems. *Rev. Mod. Phys.* **2002**, *74*, 329−345.

(4) Nguyen, T. T.; Grosberg, A. Y.; Shklovskii, B. I. Screening of a Charged Particle by Multivalent Counterions in Salty Water: Strong Charge Inversion. *J. Chem. Phys.* **2000**, *113*, 1110−1125.

(5) Forsman, J. Simple Correlation-Corrected Theory of Systems Described by Screened Coulomb Interactions. *Langmuir* **2007**, *23*, 5515−5521.

(6) Bohinc, K.; Grime, J. M. A.; Lue, L. The Interactions between Charged Colloids with Rod-like Counterions. *Soft Matter* **2012**, *8*, 5679−5686.

(7) Kjellander, R.; Marcelja, S.; Pashley, R. M.; Quirk, J. P. Double-layer Ion Correlation Forces Restrict Calcium Clay Swelling. *J. Phys. Chem.* **1988**, *92*, 6489−6492.

(8) Segad, M.; Jonsson, B.; Akesson, T.; Cabane, B. Ca/Na Montmorillonite: Structure Forces and Swelling Properties. *Langmuir* **2010**, *26*, 5782−5790.

(9) Jonsson, B.; Nonat, A.; Labbez, C.; Cabane, B.; Wennerstrom, H. Controlling the Cohesion of Cement Paste. *Langmuir* **2005**, *21*, 9211−9221.

(10) Khan, M. O.; Mel'nikov, S. M.; Jonsson, B. Anomalous Salt Effects on DNA Conformation: Experiment and Theory. *Macromolecules* **1999**, *32*, 8836−8840.

(11) Besteman, K.; Van Eijk, K.; Lemay, S. G. Charge Inversion Accompanies DNA Condensation by Multivalent Ions. *Nat. Phys.* **2007**, *3*, 641−644.

(12) Kohonen, M. M.; Karaman, M. E.; Pashley, R. M. Debye Length in Multivalent Electrolyte Solutions. *Langmuir* **2000**, *16*, 5749−5753.

(13) Pashley, R. M.; Israelachvili, J. N. DLVO and Hydration Forces between Mica Surfaces in Mg^{2+}, Ca^{2+}, Sr^{2+}, and Ba^{2+} Chloride Solutions. *J. Colloid Interface Sci.* **1984**, *97*, 446−455.

(14) Kjellander, R.; Marcelja, S.; Pashley, R. M.; Quirk, J. P. A Theoretical and Experimental Study of Forces between Charged Mica Surfaces in Aqueous $CaCl_2$ Solutions. *J. Chem. Phys.* **1990**, *92*, 4399−4407.

(15) Besteman, K.; Zevenbergen, M. A. G.; Heering, H. A.; Lemay, S. G. Direct Observation of Charge Inversion by Multivalent Ions as a Universal Electrostatic Phenomenon. *Phys. Rev. Lett.* **2004**, *93*, 170802.

(16) Gutsche, C.; Keyser, U. F.; Kegler, K.; Kremer, F. Forces between Single Pairs of Charged Colloids in Aqueous Salt Solutions. *Phys. Rev. E* **2007**, *76*, 031403.

(17) Evans, D. F.; Wennerstrom, H. *The Colloidal Domain*; John Wiley: New York, 1999.

(18) Derjaguin, B.; Landau, L. D. Theory of the Stability of Strongly Charged Lyophobic Sols and of the Adhesion of Strongly Charged Particles in Solutions of Electrolytes. *Acta Phys. Chim.* **1941**, *14*, 633−662.

(19) Verwey, E. J. W.; Overbeek, J. T. G. *Theory of Stability of Lyophobic Colloids*; Elsevier: Amsterdam, The Netherlands, 1948.

(20) James, R. O.; Healy, T. W. Adsorption of Hydrolyzable Metal Ions at Oxide-water Interface 2. Charge Teversal of SiO_2 and TiO_2 Colloids by Adsorbed Co(II), La(III), and Th(IV) as Model Systems. *J. Colloid Interface Sci.* **1972**, *40*, 53−64.

(21) Venema, P.; Hiemstra, T.; van Riemsdijk, W. H. Interaction of Cadmium with Phosphate on Goethite. *J. Colloid Interface Sci.* **1997**, *192*, 94−103.

(22) Schneider, C.; Hanisch, M.; Wedel, B.; Jusufi, A.; Ballauff, M. Experimental Study of Electrostatically Stabilized Colloidal Particles: Colloidal Stability and Charge Reversal. *J. Colloid Interface Sci.* **2011**, *358*, 62−67.

(23) Tezak, B.; Matijevic, E.; Schulz, K. F. Coagulation of Hydrophobic Sols in Statu Nascendi 3. The Influence of the Ionic Size and Valency of the Counterion. *J. Phys. Chem.* **1955**, *59*, 769−773.

(24) Matijevic, E.; Broadhurst, D.; Kerker, M. On Coagulation Effects of Highly Charged Counterions. *J. Phys. Chem.* **1959**, *63*, 1552−1557.

(25) Ducker, W. A.; Senden, T. J.; Pashley, R. M. Direct Measurement of Colloidal Forces using an Atomic Force Microscope. *Nature* **1991**, *353*, 239−241.

(26) Butt, H. J.; Cappella, B.; Kappl, M. Force Measurements with the Atomic Force Microscope: Technique, Interpretation and Applications. *Surf. Sci. Rep.* **2005**, *59*, 1−152.

(27) Toikka, G.; Hayes, R. A.; Ralston, J. Surface Forces between Spherical ZnS Particles in Aqueous Electrolyte. *Langmuir* **1996**, *12*, 3783−3788.

(28) Crocker, J. C.; Grier, D. G. Microscopic Measurement of the Pair Interaction Potential of Charge-stabilized Colloid. *Phys. Rev. Lett.* **1994**, *73*, 352−355.

(29) Baumgartl, J.; Arauz-Lara, J. L.; Bechinger, C. Like-charge Attraction in Confinement: Myth or Truth? *Soft Matter* **2006**, *2*, 631−635.

(30) Kihira, H.; Ryde, N.; Matijevic, E. Kinetics of Heterocoagulation 2. The Effect of the Discreteness of Surface Charge. *J. Chem. Soc., Faraday Trans.* **1992**, *88*, 2379−2386.

(31) van Zanten, J. H.; Elimelech, M. Determination of Absolute Coagulation Rate Constants by Multiangle Light-scattering. *J. Colloid Interface Sci.* **1992**, *154*, 1−7.

(32) Behrens, S. H.; Borkovec, M.; Schurtenberger, P. Aggregation in Charge-stabilized Colloidal Suspensions Revisited. *Langmuir* **1998**, *14*, 1951−1954.
(33) Chen, K. L.; Mylon, S. E.; Elimelech, M. Enhanced Aggregation of Alginate-coated Iron Oxide (Hematite) Nanoparticles in the Presence of Calcium, Strontium, and Barium Cations. *Langmuir* **2007**, *23*, 5920−5928.
(34) Holthoff, H.; Egelhaaf, S. U.; Borkovec, M.; Schurtenberger, P.; Sticher, H. Coagulation Rate Measurements of Colloidal Particles by Simultaneous Static and Dynamic Light Scattering. *Langmuir* **1996**, *12*, 5541−5549.
(35) Lin, W.; Kobayashi, M.; Skarba, M.; Mu, C.; Galletto, P.; Borkovec, M. Heteroaggregation in Binary Mixtures of Oppositely Charged Colloidal Particles. *Langmuir* **2006**, *22*, 1038−1047.
(36) Xu, S. H.; Sun, Z. W. Progress in Coagulation Rate Measurements of Colloidal Dispersions. *Soft Matter* **2011**, *7*, 11298−11308.
(37) Popa, I.; Gillies, G.; Papastavrou, G.; Borkovec, M. Attractive Electrostatic Forces between Identical Colloidal Particles Induced by Adsorbed Polyelectrolytes. *J. Phys. Chem. B* **2009**, *113*, 8458−8461.
(38) Borkovec, M.; Szilagyi, I.; Popa, I.; Finessi, M.; Sinha, P.; Maroni, P.; Papastavrou, G. Investigating Forces between Charged Particles in the Presence of Oppositely Charged Polyelectrolytes with the Multi-particle Colloidal Probe Technique. *Adv. Colloid Interface Sci.* **2012**, *179*−*182*, 85−98.
(39) Sinha, P.; Szilagyi, I.; Montes Ruiz-Cabello, F. J.; Maroni, P.; Borkovec, M. Attractive Forces between Charged Colloidal Particles Induced by Multivalent Ions Revealed by Confronting Aggregation and Direct Force Measurements. *J. Phys. Chem. Lett.* **2013**, *4*, 648−652.
(40) Russel, W. B.; Saville, D. A.; Schowalter, W. R. *Colloidal Dispersions*; Cambridge University Press: Cambridge, U.K., 1989.
(41) Behrens, S. H.; Borkovec, M. Electric Double Layer Interaction of Ionizable Surfaces: Charge Regulation for Arbitrary Potentials. *J. Chem. Phys.* **1999**, *111*, 382−385.
(42) Kobayashi, M.; Skarba, M.; Galletto, P.; Cakara, D.; Borkovec, M. Effects of Heat Treatment on the Aggregation and Charging of Stöber-type Silica. *J. Colloid Interface Sci.* **2005**, *292*, 139−147.
(43) Honig, E. P.; Roebersen, G. J.; Wiersema, P. H. Effect of Hydrodynamic Interaction on Coagulation Rate of Hydrophobic Colloids. *J. Colloid Interface Sci.* **1971**, *36*, 97−102.
(44) Elimelech, M.; Gregory, J.; Jia, X.; Williams, R. A. *Particle Deposition and Aggregation: Measurement, Modeling, and Simulation*; Butterworth-Heinemann Ltd.: Oxford, U.K., 1995.
(45) Baes, C. F.; Mesmer, R. E. *The Hydrolysis of Cations*; Krieger Publishing: Malabar, FL, 1976.
(46) Sader, J. E.; Chon, J. W. M.; Mulvaney, P. Calibration of Rectangular Atomic Force Microscope Cantilevers. *Rev. Sci. Instrum.* **1999**, *70*, 3967−3969.
(47) Ma, X. Y.; Lu, J. Q.; Brock, R. S.; Jacobs, K. M.; Yang, P.; Hu, X. H. Determination of Complex Refractive Index of Polystyrene Microspheres from 370 to 1610 nm. *Phys. Med. Biol.* **2003**, *48*, 4165−4172.
(48) Yu, W. L.; Matijevic, E.; Borkovec, M. Absolute Hetero-aggregation Rate Constants by Multiangle Static and Dynamic Light Scattering. *Langmuir* **2002**, *18*, 7853−7860.
(49) O'Brien, R. W.; White, L. R. Electrophoretic Mobility of a Spherical Colloidal Particle. *J. Chem. Soc., Faraday Trans. 2* **1978**, *74*, 1607−1626.
(50) Bevan, M. A.; Prieve, D. C. Direct Measurement of Retarded van der Waals Attraction. *Langmuir* **1999**, *15*, 7925−7936.
(51) Miklavic, S. J.; Chan, D. Y. C.; White, L. R.; Healy, T. W. Double Layer Forces between Heterogeneous Charged Surfaces. *J. Phys. Chem.* **1994**, *98*, 9022−9032.
(52) Mezei, A.; Meszaros, R. Novel Method for the Estimation of the Binding Isotherms of Ionic Surfactants on Oppositely Charged Polyelectrolytes. *Langmuir* **2006**, *22*, 7148−7151.
(53) Sadeghpour, A.; Szilagyi, I.; Borkovec, M. Charging and Aggregation of Positively Charged Colloidal Latex Particles in Presence of Multivalent Polycarboxylate Anions. *Z. Phys. Chem.* **2012**, *226*, 597−612.
(54) Forsman, J. A simple Correlation-Corrected Poisson-Boltzmann Theory. *J. Phys. Chem. B* **2004**, *108*, 9236−9245.
(55) Popa, I.; Papastavrou, G.; Borkovec, M. Charge Regulation Effects on Electrostatic Patch-charge Attraction Induced by Adsorbed Dendrimers. *Phys. Chem. Chem. Phys.* **2010**, *12*, 4863−4871.
(56) Silbert, G.; Ben-Yaakov, D.; Dror, Y.; Perkin, S.; Kampf, N.; Klein, J. Long-ranged Attraction between Disordered Heterogeneous Surfaces. *Phys. Rev. Lett.* **2012**, 109.
(57) Lund, M.; Jungwirth, P. Ion Specific Protein Assembly and Hydrophobic Surface Forces. *Phys. Rev. Lett.* **2008**, *100*, 258105.
(58) Feick, J. D.; Velegol, D. Measurements of Charge Non-uniformity on Polystyrene Latex Particles. *Langmuir* **2002**, *18*, 3454−3458.
(59) Szilagyi, I.; Sadeghpour, A.; Borkovec, M. Destabilization of Colloidal Suspensions by Multivalent Ions and Polyelectrolytes: From Screening to Overcharging. *Langmuir* **2012**, *28*, 6211−6215.
(60) Szilagyi, I.; Polomska, A.; Citherlet, D.; Sadeghpour, A.; Borkovec, M. Charging and Aggregation of Negatively Charged Colloidal Latex Particles in Presence of Multivalent Polyamine Cations. *J. Colloid Interface Sci.* **2013**, *392*, 34−41.

CHAPTER 4

Specific Ion Effects on Particle Aggregation Induced by Monovalent Salts within the Hofmeister Series

Oncsik, T.; Trefalt, G.; Borkovec, M.; Szilagyi, I.

Langmuir **2015,** 31, 3799-3807.

Langmuir

Article

pubs.acs.org/Langmuir

Specific Ion Effects on Particle Aggregation Induced by Monovalent Salts within the Hofmeister Series

Tamas Oncsik, Gregor Trefalt, Michal Borkovec, and Istvan Szilagyi*

Department of Inorganic and Analytical Chemistry, University of Geneva, 30 Quai Ernest-Ansermet, 1205 Geneva, Switzerland

Supporting Information

ABSTRACT: Ion specific effects of monovalent salts on charging and aggregation for two types of polystyrene latex particles were investigated by electrophoresis and time-resolved light scattering. The chemical composition of the electrolytes was systematically varied in the experiments. Accordingly, NaH_2PO_4, NaF, NaCl, NaBr, $NaNO_3$, and NaSCN were used to vary the anions and $N(CH_3)_4Cl$, NH_4Cl, CsCl, KCl, NaCl, and LiCl for the cations. The salt concentration dependence of the electrophoretic mobilities indicates that the surface charge was screened by the counterions when their concentrations increased. For the SCN^- ions, adsorption on positively charged particles leads to charge reversal. The aggregation rates are small at low electrolyte concentrations indicating stable dispersions under these conditions, and they increase with the salt concentration. When viscosity corrections are taken into account, no ion specific effects in the fast aggregation regime can be established. The slow and fast aggregation regimes are separated by the critical coagulation concentration (CCC). Within the experimental error, the CCCs are the same in systems containing different co-ions but the same counterions, with the exception of ammonium salts. However, the variation of counterions leads to different CCC values due to specific interaction of the counterions with the surface. These values follow the Hofmeister series for negatively charged sulfate latex particles, while the reversed order was observed for positively charged amidine latex. Comparison between experimental CCCs and those calculated by the theory of Derjaguin, Landau, Verwey, and Owerbeek reveals that variations in the surface charge due to ionic adsorption are mainly responsible for the ion specific effects in the aggregation process.

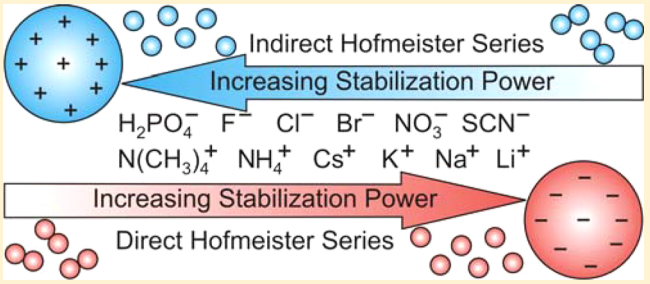

INTRODUCTION

While the Hofmeister series has been known for more than a century, the molecular mechanisms governing this characteristic sequence in the ionic specificities are still not fully clarified.[1−3] The Hofmeister series was discovered in protein precipitation experiments, and this series classifies ions according to their increasing stabilization power of protein solutions, namely,

$$CO_3^{2-} < SO_4^{2-} < H_2PO_4^- < F^- < Cl^- < Br^- < NO_3^- < I^- < ClO_4^- < SCN^-$$

$$N(CH_3)_4^+ < NH_4^+ < Cs^+ < Rb^+ < K^+ < Na^+ < Li^+ < Mg^{2+} < Ca^{2+}$$

This sequence states that solutions of negatively charged proteins remain stable even at high salt concentrations in solutions containing the ions appearing in the right, while they precipitate already at lower salt concentrations containing the ions appearing on the left. Numerous other phenomena can be ordered according to the same sequence, for example, surface tension or viscosities of electrolyte solutions, dissolution heats of salts, binding of ligands, and charging of proteins or polyelectrolytes.[2−13]

Here, we focus on the relation between the Hofmeister series and colloidal particle aggregation.[14−27] This question has also been pursued for quite some time, whereby that community rather used the term *lyotropic series*. Particle aggregation is known to be fast at high salt concentrations or for weakly charged particles, while it slows down at low salt concentrations or highly charged particles.[15,28] The transition between these two regimes is denoted as the critical coagulation concentration (CCC). The ionic valence induces an important dependence, which is referred to as the Schulze−Hardy rule.[15,25,26,29] This rule states that the CCC strongly decreases with an increase in the valence of the counterions. Thereby, multivalent cations are relevant for negatively charged particles, while multivalent anions, for positively charged ones.

However, even ions of the same valence may lead to different CCCs.[17−25] The respective shifts can be normally classified according to the Hofmeister series. Negatively charged particles typically follow the *direct Hofmeister series* quoted earlier. Thereby, the ions on the left induce lower CCCs, while the ions on the right, higher ones. On the other hand, positively charged particles follow the *indirect Hofmeister series*. The latter series maintains the same sequence of ions, but ions on the left induce higher CCCs, while the ions on the right, a lower one. However, ions of higher valence quoted within the Hofmeister

Received: January 20, 2015
Revised: March 15, 2015
Published: March 16, 2015

DOI: 10.1021/acs.langmuir.5b00225
Langmuir 2015, 31, 3799−3807

series should be excluded from this reasoning, since they primarily follow the Schulze−Hardy rule. Therefore, we only focus on monovalent ions here.

The classical theory of Derjaguin, Landau, Verwey, and Overbeek (DLVO) of colloidal aggregation surmises that the interactions between particles are described by a superposition of attractive van der Waals forces and repulsive double layer forces across an indifferent electrolyte solution.[15,28] The fast aggregation regime is governed by an attractive interaction potential, while the slow regime is characterized by a thermally activated energy barrier crossing. The DLVO theory suggests that the CCC is a sharp transition between these two regimes. A strong decrease of the CCC with ionic valence is equally predicted, in accordance to the Schulze−Hardy rule. Aggregation rates calculated with DLVO theory show reasonable agreement with experimental data, especially for weakly charged particles.[30−32]

However, this classical theory cannot directly rationalize any trends in particle aggregation rates within the Hofmeister series, as it considers no other ionic properties than the valence. Ionic specificity can be introduced into DLVO theory by assuming that ions are no longer indifferent. This picture supposes that ions adsorb specifically to the particle surfaces, thereby modifying the surface charge and thus the double layer force.[33−38] This simple approach qualitatively rationalizes the observed dependencies of the CCC.[3,39,40] The Hofmeister series also reflects the size and hydration of ions. Small and strongly hydrated anions, such as F^- and Cl^-, appear on the left, while large and poorly hydrated ones, such as SCN^- and I^-, on the right. The cations are arranged in the opposite way. On the left, one finds large and poorly hydrated cations, such as $N(CH_3)_4^+$ and Cs^+, while strongly hydrated ones, such as Na^+ and Li^+, are situated on the right. Suppose that the particle surface is hydrophobic and poorly hydrated. Poorly hydrated ions will adsorb to such surfaces more strongly than well hydrated ones (i.e., like-seeks-like). Binding of cations to a negatively charged surface will neutralize the surface charge and thus leads to a decrease of the CCC. Adsorption of anions will increase the magnitude of the surface charge and lead to a larger CCC. Analogous reasoning applies to positively charged particles. Adsorption of anions will neutralize the surface, while adsorption of cations will lead to increase of surface charge. Therefore, negatively charged hydrophobic particles follow the direct Hofmeister series, while positively charged ones, the indirect series. Similar arguments can be put forward for particles with a hydrophilic or well hydrated surface. Well hydrated ions will adsorb more strongly on such a hydrated substrate than poorly hydrated ions, and the situation is reversed. Stability of negatively charged hydrophilic particles should rather follow the indirect Hofmeister series, while positively charged ones, the direct series. This picture may be further complicated by additional forces induced by the adsorbed ions. Such short-ranged forces are normally not included in the DLVO theory. These forces are typically introduced into a modified treatment of the electric double layer where one introduces additional ion−substrate interactions (e.g., hydration, van der Waals, and image charges).[40−42] While such additional forces may modify the sequences within the series, the qualitative picture remains similar.

Particle surface charge density has often been found to vary systematically with the type of ions, as one would expect for a hydrophobic surface. The charge of positively charged alumina decreased in the $Cl^- > Br^- > I^-$ order following the indirect Hofmeister series.[33] The same trend was reported for positively charged latex particles as revealed by electrophoresis.[17,19,20,43] The charge density of negatively charged alumina particles would decrease from Cs^+ to Na^+ with the direct Hofmeister series.[33] Similar trends were observed for negatively charged hematite, titania, and silica.[36,44,45] However, the behavior of the mentioned silica sample seems atypical, since other authors reported the charge density of silica to follow the indirect Hofmeister series as one would expect for a hydrophilic substrate.[34,35,46] Analogous behavior was reported for silver halide.[47]

Many trends in the observed CCCs are also consistent with the fact that surfaces of colloidal particles are hydrophobic. Negatively charged polystyrene and clay mineral particles follow the direct Hofmeister series, while positively charged metal oxides and polystyrene particles follow the indirect one.[17,19−21,23,24] While the same trend was observed for negatively charged silver halide particles,[25] the behavior of this system seems atypical, since the surface charge densities follow the reverse trend.[47] For polystyrene particles, however, only a few cations were investigated so far. The opposite dependence was observed for protein-coated latex or calcined titania, as one would expect for hydrophilic surfaces.[18,19,21−23] However, ion specific effects on particle aggregation were absent for weakly charged iron oxide, titania, and carboxylated latex particles.[21,23,26]

A transition between the direct and indirect Hofmeister series was observed for CCCs of titania after a heat treatment.[21] The native particles followed the indirect series in basic conditions, as one would expect for a hydrophilic surface. After heat treatment, the surface becomes hydrophobic, and the direct series is observed. A similar transition between the direct and indirect Hofmeister series was also evidenced for the water−silica interface upon pH variations through electric surface potentials obtained from direct force measurements.[38] In acidic conditions, the silica surface is more hydrophobic and thus follows the direct series. In basic conditions, the surface becomes more hydrophilic due to the ionization of the silanol groups and, therefore, reflects the indirect Hofmeister series. The observations that the charge density of silica may follow the direct[45] or the indirect[34,35,46] Hofmeister series could also be related to this hydrophobic to hydrophilic transition. In some situations, partial reversal of Hofmeister series was equally reported,[21,23,34,48] and this possibility was confirmed by computer simulations.[39]

The present work investigates how the position of monovalent ions within the Hofmeister series affects the aggregation of negatively and positively charged polystyrene latex particles. Absolute aggregation rate coefficients were measured by combining time-resolved static light scattering (SLS) and dynamic light scattering (DLS). Similar light scattering techniques were used to study particle aggregation earlier.[27,49−52] The surface charging properties were investigated by electrophoresis. The present study explores a larger number of ions than the previous investigations, especially cations. Moreover, the use of the indifferent chloride allows addressing the specific effect of different cations unequivocally. In addition, the variation of the absolute aggregation rate constant in the fast aggregation regime with the type of salt and particles is studied for the first time.

DOI: 10.1021/acs.langmuir.5b00225
Langmuir 2015, 31, 3799−3807

EXPERIMENTAL SECTION

Materials. Polystyrene latex particles that were functionalized with amidine or sulfate groups on their surface were purchased from Invitrogen Corp. The particle size and the surface charge density of the particles were determined by the manufacturer by transmission electron microscopy (TEM) and conductometric titration. The sulfate latex has a mean radius of 265 nm, a polydispersity expressed as a coefficient of variation (CV) of 2.0%, and a surface charge density of −77 mC/m^2. In the case of the amidine latex, the corresponding quantities are 110 nm, 4.3%, and +132 mC/m^2. The same particles were used by us in a previous publication,[53] and their size was determined by SLS and DLS in stable suspensions. SLS measurements were analyzed using the Mie theory for spheres[54] and yield the mean radius of 263 nm for the sulfate latex and 110 nm for the amidine latex. The measured polydispersity expressed as the CV were 3.8% and 7.1%. All of these values obtained by SLS are in very good agreement with TEM. DLS yields slightly larger average radii, namely, 278 and 117 nm, probably due to polydispersity and hydration effects. The sulfate latex particles were dialyzed with cellulose ester membrane against pure water until the conductivity value was less than 8×10^{-5} S/m, while for the amidine particles a polyvinylidene fluoride membrane was used. The particle concentrations of the dialyzed stock suspensions were determined by static light scattering by calibrating the scattering intensity with the original particle suspension of known concentration. The concentration of the sulfate latex stock suspension was 65 g/L, while the one of amidine latex, around 7 g/L. Analytical grade NaCl, KCl, CsCl, NH_4Cl, NaSCN (Sigma-Aldrich), LiCl, NaH_2PO_4 (Acros Organics), NaF, NaBr, $NaNO_3$, and $N(CH_3)_4Cl$ (Fluka) were dissolved in pure water, adjusted to pH 4.0 with HCl and filtered with a 0.1 μm syringe filter (Millipore). All experiments were performed in a thermostated environment at a temperature of 25.0 ± 0.2 °C. Milli-Q water (Millipore) was used throughout.

Electrophoretic Mobility. ZetaSizer Nano ZS (Malvern) equipped with a He/Ne laser operating at 633 nm as a light source and an avalanche photodiode as a detector was used to measure the electrophoretic mobility of the particles in an electric field of 4 kV/m. The suspensions needed for the measurements were prepared by mixing the appropriate salt solutions with a particle stock suspension, with final particle concentration of 50 mg/L for the sulfate latex and 5 mg/L for the amidine latex. The suspensions were equilibrated for 1 min prior to the measurements. Five runs were performed for each sample, and averaged.

Aggregation Rates by Light Scattering. Absolute aggregation rates were determined in 1.0 M KCl by combined time-resolved SLS and DLS on the multiangle goniometer (ALV/CGS-8F). This goniometer uses eight fiber-optic detectors and solid state laser of a wavelength of 532 nm. Quartz cuvettes were first cleaned in piranha solution, which is a mixture of concentrated H_2SO_4 and 30% H_2O_2 at a volume ratio of 3:1, then rinsed with water, and dried in a dust-free oven at 60 °C. The particle concentration was 4 mg/L (4.9×10^{13} m^{-3}) for the sulfate latex, and 1 mg/L (1.7×10^{14} m^{-3}) for the amidine latex. The stable particle stock suspension was injected into the salt solution in the cuvette, mixed, and immediately monitored by light scattering. The intensity and the correlation function were accumulated for 20 s, and the apparent hydrodynamic radius was calculated from the second order cumulant fit. This quantity was recorded as a function of time until the initial radius increased by about 40%. To determine the absolute aggregation rate coefficient, the SLS intensity $I(q,t)$ and the apparent hydrodynamic radius $r_h(q,t)$ were followed with time, t, at different magnitudes of the scattering vector, q. For short times, relative change of the scattering intensity can be written as[55]

$$\Sigma = \frac{1}{I(q,0)}\frac{\mathrm{d}I(q,t)}{\mathrm{d}t}\bigg|_{t\to 0} = kN_0\left(\frac{I_2(q)}{2I_1(q)} - 1\right) \quad (1)$$

where k is the aggregation rate coefficient and N_0 is the initial particle number concentration while $I_1(q)$ and $I_2(q)$ are the scattering intensities of the monomers and dimers, respectively. The corresponding expression for the relative rate of change of the hydrodynamic radius is[55]

$$\Delta = \frac{1}{r_h(q,0)}\frac{\mathrm{d}r_h(q,t)}{\mathrm{d}t}\bigg|_{t\to 0} = kN_0\left(1 - \frac{1}{\alpha}\right)\frac{I_2(q)}{2I_1(q)} \quad (2)$$

where $\alpha = r_{h,2}/r_{h,1}$ with $r_{h,1}$ and $r_{h,2}$ being the hydrodynamic radii of the monomer and the dimer. Combining eqs 1 and 2, one obtains

$$\Sigma = \left(1 - \frac{1}{\alpha}\right)^{-1}\Delta - kN_0 \quad (3)$$

A scatter plot of the relative rates Σ and Δ gives a straight line, whereby the slope yields the hydrodynamic factor α and the absolute aggregation rate coefficient follows from the intercept. The respective experimental results obtained in 1.0 M KCl solutions are shown in Figure 1. The aggregation rate coefficient for the sulfate latex was (3.3 ± 0.2) × 10^{-18} m^3/s and for the amidine latex (3.0 ± 0.2) × 10^{-18} m^3/s. These aggregation rate coefficients agree within experimental error with our previous measurements with time-resolved SLS for the same particles at pH 5.0 in 1.0 M KCl.[53] The hydrodynamic factors α were for the sulfate latex 1.37 ± 0.02 and for the amidine 1.31 ± 0.02. These values compare reasonably well with the theoretical value of 1.39, which can be calculated from low Reynolds number hydrodynamics.[56]

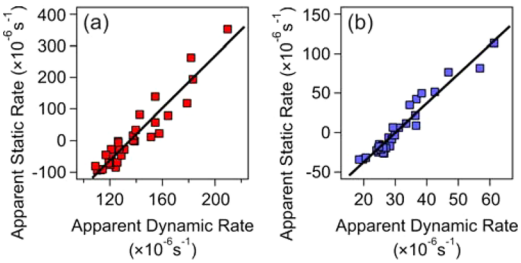

Figure 1. Scatter plot of the apparent static and dynamic rates for different latex particles for determination of the absolute rate coefficients in 1 M KCl solution: (a) sulfate latex and (b) amidine latex.

For other conditions, the aggregation rate was measured by time-resolved DLS with the compact single-angle goniometer (ALV/CGS-3) with a He/Ne laser of a wavelength of 633 nm. The hydrodynamic radius was monitored at a scattering angle of 90° in the same fashion as described previously. The particle concentration was chosen in the range of 50−200 mg/L for the sulfate latex and in the range of 2−10 mg/L for the amidine latex. The relative rate coefficient was obtained from the relative increase of the hydrodynamic radius. Absolute rate coefficients were obtained by dividing the apparent rate coefficient by the apparent rate coefficient in 1.0 M KCl at the same particle concentration and by multiplying this ratio by the absolute aggregation rate coefficient in 1.0 M KCl.

RESULTS

Charging and aggregation of negatively charged sulfate latex particles and positively charged amidine particles were investigated in monovalent electrolyte solutions at pH 4.0 by electrophoresis and time-resolved DLS. The solution composition was systematically varied, whereby $N(CH_3)_4Cl$, NH_4Cl, CsCl, KCl, NaCl, and LiCl were used to vary cations, while the anions were investigated with NaH_2PO_4, NaF, NaCl, NaBr, $NaNO_3$, and NaSCN. In this way, the influence of both counter- and co-ions could be addressed. Since these ions are situated within the Hofmeister series, the relation between particle aggregation rates and the position within this series will be clarified.

DOI: 10.1021/acs.langmuir.5b00225
Langmuir 2015, 31, 3799−3807

General Trends. The electrophoretic mobility of the particles is shown versus the salt concentration for the sulfate particle in Figures 2a and 3a, while for the amidine particles, in Figures 4a and 5a. The magnitude of electrophoretic mobility typically decreases with the salt concentration due to screening of the surface charge. At low salt concentrations, negative and positive mobilities were observed for the sulfate and amidine latex particles, respectively. This sign reflects the charge of the ionized surface functional groups at pH 4.0. The actual values of the electrophoretic mobilities depend on the type of ions, and these trends will be discussed later.

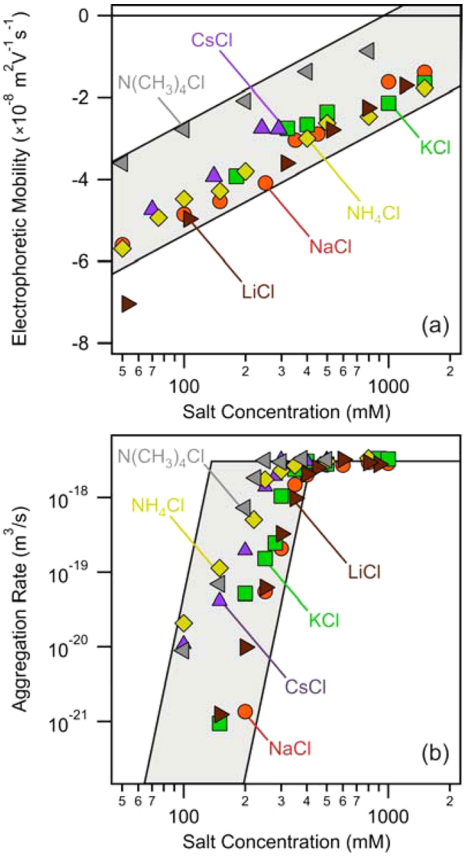

Figure 2. Charging and aggregation of negatively charged sulfate latex particles as a function of the concentration of various monovalent chloride salts of different cations: (a) electrophoretic mobilites and (b) aggregation rate coefficients. The gray region represents an envelope of all experimental data points.

Absolute particle aggregation rate coefficients are shown versus the salt concentration for the sulfate particle in Figures 2b and 3b and for the amidine particles in Figures 4b and 5b. At low salt concentration, the absolute aggregation rates are small. This behavior is referred to as the slow or reaction controlled regime, and the rate coefficients increase with the salt concentration strongly. At higher salt concentrations, the aggregation rate coefficients become large. Here, one has the fast or diffusion controlled regime, and the rate coefficients are almost independent of the salt level. The critical coagulation concentration was identified as the transition point between the slow and fast aggregation regimes. While the CCC depends sensitively on the type of ion present, no systematic trends concerning the aggregation rates in the slow regime could be established.

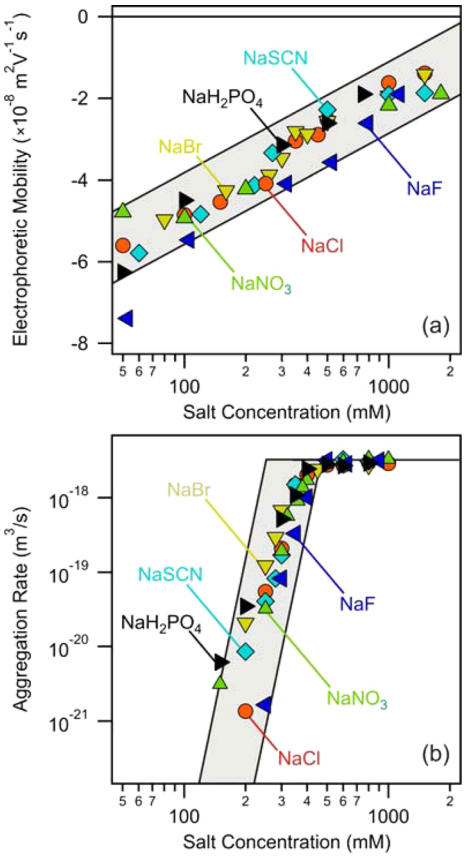

Figure 3. Charging and aggregation of negatively charged sulfate latex particles as a function of the concentration of various monovalent sodium salts of different anions: (a) electrophoretic mobilites and (b) aggregation rate coefficients. The gray region represents an envelope of all experimental data points.

Fast Aggregation Regime. When investigating eventual ion specific effects on aggregation rates at high electrolyte concentrations, one must realize that viscosities of concentrated electrolyte solution may significantly deviate from the one of pure water. The rate coefficients in the diffusion controlled regime may therefore vary, since the diffusion coefficient of the particles depends on the solution viscosity. In order to take this effect into account, known dynamic viscosities, η, of the salt solutions investigated here were considered.[57,58] To simplify the data analysis, the experimental viscosity data were represented with the relation[10]

$$\eta/\eta_0 = 1 + A\sqrt{c} + Bc + Dc^2 \quad (4)$$

where $\eta_0 = 8.90 \times 10^{-4}$ Pa·s is the dynamic viscosity of water at 25 °C while A, B, and D are constants. The constant A was calculated from the Debye–Hückel theory,[10] while B and D were obtained by least-squares fits to the experimental viscosity data. The resulting constants are reported in Supporting Information Table S1. To compare the experimental aggregation rates, the aggregation rate coefficients were normalized with the diffusion controlled aggregation rate coefficient, k_S, obtained from Smoluchowski's theory[15,28]

$$k_S = \frac{8k_BT}{3\eta} = 1.23 \times 10^{-17}\ \mathrm{m^3/s} \quad (5)$$

where k_B is the Boltzmann constant, T is the absolute temperature, and the numerical value refers to water at 25 °C.

DOI: 10.1021/acs.langmuir.5b00225
Langmuir 2015, 31, 3799–3807

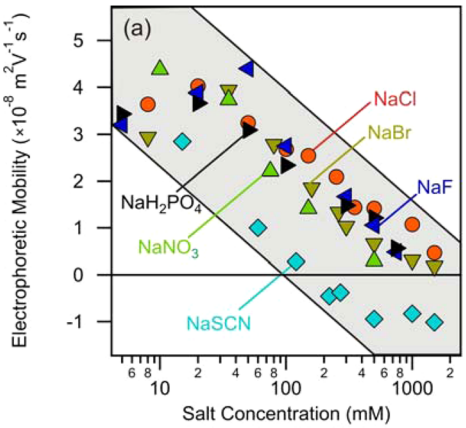

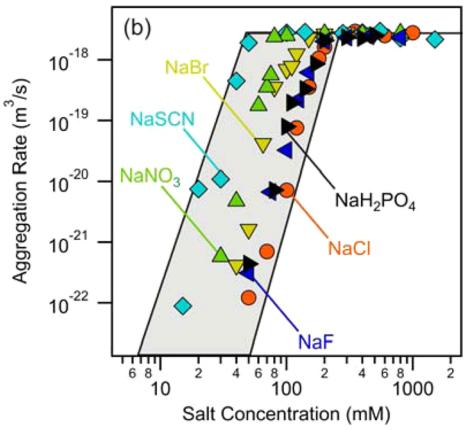

Figure 4. Charging and aggregation of positively charged amidine latex particles as a function of the concentration of various monovalent sodium salts of different anions: (a) electrophoretic mobilites and (b) aggregation rate coefficients. The gray region represents an envelope of all experimental data points.

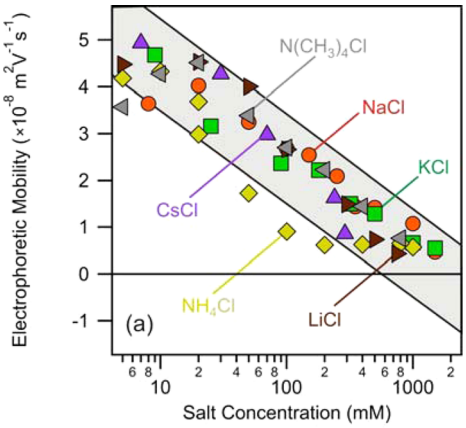

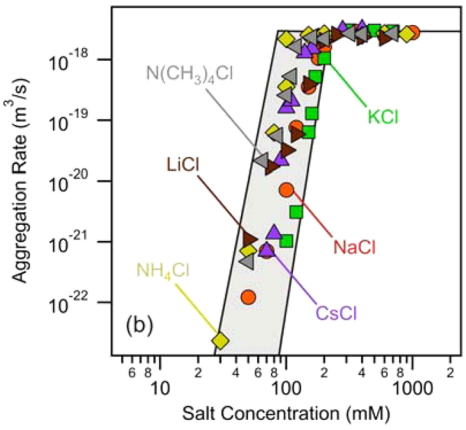

Figure 5. Charging and aggregation of positively charged amidine latex particles as a function of the concentration of various monovalent chloride salts of different cations: (a) electrophoretic mobilites and (b) aggregation rate coefficients. The gray region represents an envelope of all experimental data points.

The averaged normalized rate coefficients k/k_S above the CCC are shown in Figure 6a. These normalized rates are independent of the type of ions within the experimental error. Moreover, these normalized coefficients are very similar for the two types of particles used, namely, 0.26 ± 0.01 for the sulfate latex and 0.23 ± 0.01 for the amidine latex. However, this normalized coefficient may depend on the type of particle used. This point was established by reanalyzing fast aggregation rates of latex particles in nine different salt solutions, which include multivalent ions, which were published earlier by us.[26] These data include carboxyl and sulfate latex particles. The latter sulfate latex particles are different from the one used here. When the aggregation rate coefficients are normalized by Smoluchowski's rates including the correct viscosities, we find again no dependence on the type of ions present. However, the normalized rate coefficients differ from the values reported earlier. For the carboxyl latex particles, one finds 0.16 ± 0.01, while for the latter sulfate particles 0.29 ± 0.01. The fact that the normalized aggregation rates vary with the particle type somewhat is probably related to their variable polymeric compositions, which originates from the differing conditions during synthesis. Differences in surface roughness may equally contribute.[59] However, when the same type of particles is considered, the normalized fast aggregation rate coefficients are independent of the type of salt. This observation suggests that attractive forces acting in the fast aggregation regime are not influenced by the nature of the ions present. These experimental results should be contrasted with earlier reports, where a modest variation of the fast aggregation rate on the type of salt was reported.[17,51] In our view, however, these results are hardly conclusive, since viscosity corrections were not considered in these studies.

Specific Ion Effects on Negatively Charged Sulfate Latex. The electrophoretic mobility at given salt concentrations decreases with the type of cation from $N(CH_3)_4^+$ to Li^+. This sequence reflects the expected direct Hofmeister series; namely, $N(CH_3)_4^+ < NH_4^+ < Cs^+ < K^+ < Na^+ < Li^+$ (Figure 2a). This trend in the electrophoretic mobility reflects the affinity of the different cations to the surface. Therefore, poorly hydrated $N(CH_3)_4^+$ ion adsorbs most strongly to the hydrophobic latex particle surface and, hence, reduces the magnitude of the surface charge and of the mobility. The strongly hydrated Li^+ ion adsorbs weakly on the particle surface, or not at all, and the magnitudes of the surface charge and of the mobility are therefore the largest.

The CCC, which reflects the transition between the fast and slow regime, systematically varies with the type of cation (Figure 2b). The CCC shifts from low to high values following the direct Hofmeister series; namely, $N(CH_3)_4^+ < NH_4^+ < Cs^+ < K^+ < Na^+ < Li^+$ (Figure 6b). This trend is expected for a negatively charged hydrophobic surface. The poorly hydrated $N(CH_3)_4^+$ ion adsorbs strongly to the surface, thereby reducing the magnitude of surface charge, and therefore the CCC. On the other hand, well hydrated Li^+ ion induces the highest CCC,

DOI: 10.1021/acs.langmuir.5b00225
Langmuir 2015, 31, 3799−3807

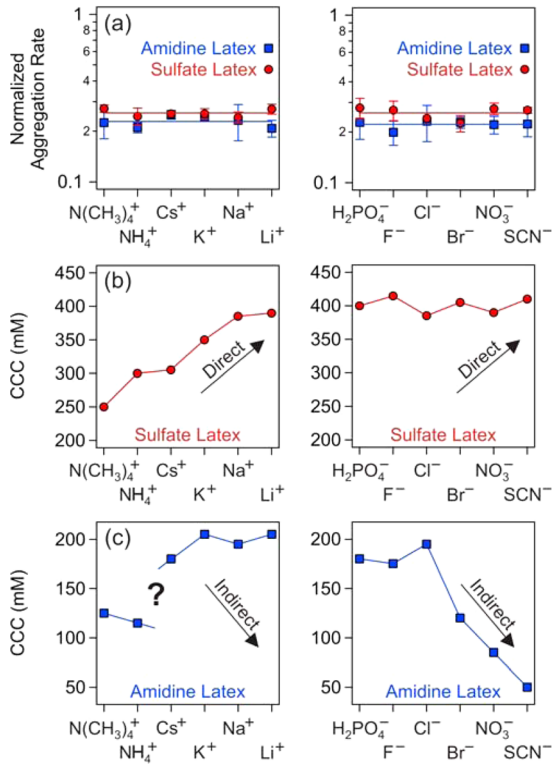

Figure 6. Characteristics of the latex particle aggregation versus the position in the Hofmeister series. The effect of cations is shown in the left column, while of the anions, in the right column. (a) Aggregation rate coefficients in the fast regime normalized by the Smoluchowski value. The error bars represent three times the standard deviation. CCCs for (b) sulfate particles and (c) amidine particles. The arrows indicate the expected trends from direct or indirect Hofmeister series. The lines serve to guide the eye only.

since the surface charge is high due to weak adsorption of this ion. These results are in agreement with molecular dynamic simulations at hydrophobic surfaces.[40] One further observes that the CCCs for Li^+ and Na^+ are almost identical, suggesting that these two ions do not adsorb to the surface at all. Similar trends in the CCCs following the direct Hofmeister series as typical for a negatively charged hydrophobic substrate were previously reported for various systems, including montmorillonite, silver iodide, and heat-treated titania.[21,24,25] The same trend was also documented for negatively charged polystyrene latex, but with Na^+ and NH_4^+ ions only.[18,20] When the particles are weakly charged, there are no ion specific effects on the charging and aggregation behavior in the presence of Na^+, K^+, and Cs^+ for iron oxide, titania, and carboxylate latex.[21,23,26] In this situation, the cations do not interact with the surface specifically.

Co-ions have no effect on the charging and aggregation of the sulfate latex particles (Figure 3). The electrophoretic mobilities are similar for all ions investigated, with the exception of F^-, which induces somewhat lower mobilities. The CCCs are identical within experimental error, and they have the value of 400 ± 10 mM (Figure 6b). One might expect that the CCCs also follow the direct Hofmeister series $H_2PO_4^-$, F^-, Cl^-, Br^-, NO_3^-, and SCN^-. The poorly hydrated anions, such as NO_3^- and SCN^-, should adsorb more strongly to the negatively charged hydrophobic latex surface and induce an even higher magnitude of charge. However, such dependencies can be evidenced neither from the electrophoresis nor from the CCCs. Therefore, we conclude that these anions do not adsorb on the particle surface, due to its high negative surface charge. The present observations are similar to earlier studies, where only a weak dependence of the CCC of sulfate latex particles with the type of anion was found.[17,18,20]

To investigate ion specific effects on charging and aggregation of negatively charged particles, an indifferent anion must be chosen. As will become obvious in the next section, such an anion is the chosen Cl^-. Anions that are strongly interacting with the particle surface, such as NO_3^-, make the interpretation more difficult.[18]

Specific Ion Effects on Positively Charged Amidine Latex. At sufficiently low salt concentration, the electrophoretic mobility at given concentration decreases approximately in the sequence $H_2PO_4^- > F^- > Cl^- > Br^- > NO_3^- > SCN^-$, reflecting the indirect Hofmeister series (Figure 4a). This trend in the electrophoretic mobility was also found for other positively charged latex particles[17,19,20] and reflects the affinity of the different anions to the surface. Strongly hydrated anions, such as $H_2PO_4^-$ or F^-, interact weakly with the hydrophobic latex particle surface. The poorly hydrated anions, such as NO_3^- or SCN^-, interact more strongly with the surface, and their adsorption reduces the surface charge. The adsorption of SCN^- is so pronounced that a charge reversal is induced. Such charge reversal has been observed for highly charged multivalent ions[60,61] but also for other strongly adsorbing monovalent ions.[19,43]

The CCCs decrease in the same sequence reflecting the expected indirect Hofmeister series (Figures 4b and 6c). However, a pronounced decrease of the CCC is only observed in the series $Cl^- > Br^- > NO_3^- > SCN^-$, while in the presence of $H_2PO_4^-$, F^-, and Cl^- the CCC remains practically constant. This constancy indicates that the latter ions are basically indifferent and do not adsorb on the particle surface. Similar specificities involving Cl^-, NO_3^-, and SCN^- ions were also reported for the CCCs for sulfate latex particles earlier.[17,18,20] However, the indifference for the other ions was not reported for latex so far, but only for weakly charged titania.[21] The observed trends in the CCCs agree with the ones predicted theoretically based on the ionic polarizability, except that the positions of Br^- and NO_3^- are reversed.[41]

In the presence of various co-ions, namely, Cs^+, K^+, Na^+, and Li^+, the measured electrophoretic mobilities and CCCs were very similar (Figures 5 and 6c). Since the affinity of these ions toward the surface decreases in the same sequence, one would expect that the CCCs follow the indirect Hofmeister series. However, no systematic dependence could be established, and the CCC remains constant at 200 ± 10 mM. We suspect that these ions interact with the highly positively charged surface too weakly. Nitrogen-containing ions, namely, $N(CH_3)_4^+$ and NH_4^+, behave irregularly. The indirect Hofmeister series would suggests higher CCCs, but the measured values are substantially lower than for the remaining cations within the series. This discrepancy could be probably related to a specific interaction between the amidine groups on the particle surfaces and the nitrogen-containing ions (e.g., hydrogen bonding). These findings are similar to previous measurements of the CCCs for positively charged latex particles, where small shifts between Na^+ and NH_4^+ were reported.[18,20]

Origin of Interparticle Forces. A simplified form of DLVO theory was used to clarify ion specific effects on the CCCs. Electrophoretic mobilites, u, were converted to diffuse layer potentials, ψ_D, with the Smoluchowski equation[15]

DOI: 10.1021/acs.langmuir.5b00225
Langmuir 2015, 31, 3799−3807

$$u = \frac{\varepsilon\varepsilon_0}{\eta}\psi_D \tag{6}$$

where ε_0 is the permittivity of vacuum and ε is the dielectric constant. We have $\varepsilon = 80$ for water at room temperature. The accuracy of the Smoluchowski equation was checked with the standard electrokinetic model.[62] For the particles and concentration range considered, both models agreed within 3%. The surface charge density σ was determined by fitting ψ_D at different salt levels with the Debye−Hückel charge-potential relationship[15,28]

$$\sigma = \varepsilon\varepsilon_0\kappa\psi_D \tag{7}$$

where κ is the inverse Debye length defined by

$$\kappa^2 = \frac{2N_A e^2 c}{\varepsilon\varepsilon_0 k_B T} \tag{8}$$

where c is the molar concentration of the monovalent electrolyte, N_A the Avogadro number, and e the elementary charge. While the resulting charge densities reflect the extent of the ion adsorption, an eventual influence of the variation of the position of the shear plane with the type of ions is neglected.[28,63] The CCC was estimated from DLVO theory, which assumes that the total interaction energy can be written as a superposition of electrostatic double layer energy, V_{dl}, and the van der Waals energy, V_{vdW}; namely,

$$V = V_{dl} + V_{vdW} \tag{9}$$

By invoking the Derjaguin and superposition approximations, one has[15,28]

$$V_{dl} = 2\pi r\varepsilon\varepsilon_0{\psi_D}^2 \exp(-\kappa h) \tag{10}$$

where r is the particle radius and h is the separation distance between particle surfaces. The van der Waals interaction energy is approximated with the nonretarded expression

$$V_{vdW} = -\frac{Hr}{12h} \tag{11}$$

where H is the Hamaker constant. The CCC can be located by assuming that the energy barrier just vanishes[15]

$$V(h_{max}) = 0 \quad \text{and} \quad \left.\frac{dV}{dh}\right|_{h=h_{max}} = 0 \tag{12}$$

where h_{max} is the separation at the energy barrier. Combining eqs 9−12, one can express the CCC as[15,29]

$$CCC = \frac{0.365}{N_A L_B}(H\varepsilon\varepsilon_0)^{-2/3}\sigma^{4/3} \tag{13}$$

where $L_B = e^2/(4\pi\varepsilon\varepsilon_0 k_B T)$ is the Bjerrum length, which is 0.72 nm at room temperature in water. Note that the preceding relation is only approximate, since accurate DLVO calculations show that the energy barrier does not quite vanish at CCC.[29]

The calculated and experimental data given in Supporting Information Table S2 and Figure 7 show indeed a good correlation between the CCCs and the surface charge density. The straight line obtained from DLVO theory agrees with the experimental data reasonably well with the exception of the NH_4^+ ion which is probably influenced by specific interactions with the amidine groups on the particle surface. By fitting eq 13 to the data, a Hamaker constant of $H = 1.2 \times 10^{-20}$ J is found. The charge density for the sulfate latex measured by conductometric titration is −77 mC/m^2 and agrees quite well

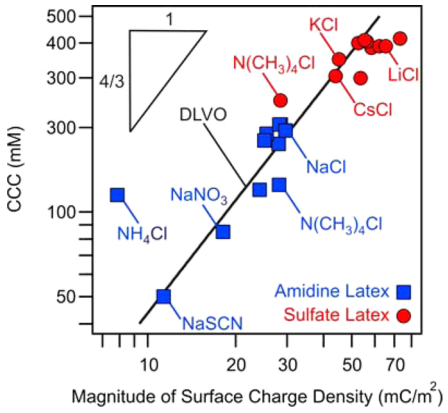

Figure 7. Comparison of experimental CCC values for the sulfate and amidine latex particles with DLVO theory. The data are plotted versus the magnitude of surface charge density, which was estimated from the electrophoretic mobility. The DLVO theory uses the superposition approximation to calculate the double layer interactions.

in magnitude with the highest charge densities reported in Figure 7, which refer to indifferent ions. On the other hand, the titrated charge of the amidine latex of +132 mC/m^2 reported by the manufacturer is probably too high, since Figure 7 rather suggests a charge density around +30 mC/m^2.

The relatively good agreement between experimental data and DLVO theory indicates that the main reason for the ionic specificity is the modification of the surface charge through adsorption of these ions. Poorly hydrated counterions adsorb strongly on the hydrophobic latex particle surface, thereby decrease the magnitude of the surface charge and the CCC. Well hydrated counterions adsorb weakly, or not at all, and they hardly influence the surface charge and typically lead to high CCCs. The co-ions do not adsorb, and they influence the surface charge and the CCC only slightly. Similar trends were observed for charging of oxide particles,[33,36] while the reverse trends were obtained for silica at high pH.[34,35,38]

The fitted Hamaker constant $H = 1.2 \times 10^{-20}$ J is in good agreement with the value of 1.0×10^{-20} J that is obtained from the full Lifshitz calculation.[59,64] However, these values are factors of 3−5 larger than the Hamaker constants of similar latex particles that were actually measured with the colloidal probe technique.[59] The reduction of these values is probably due to surface roughness. When one assumes that the presently used latex particles have comparably smaller Hamaker constants, the observed values of the CCCs indicate the presence of additional attractive non-DLVO forces. The substantial scatter of the data points in Figure 7 also points toward possible variation of the distance of the shear plane with the nature of the ion, or the importance of additional forces, which are most probably of hydrophobic nature.[65]

CONCLUSION

Surface charge and aggregation of anionic and cationic polystyrene latex particles were investigated in the presence of various monovalent electrolytes by electrophoresis and time-resolved light scattering. Sodium salts of $H_2PO_4^-$, F^-, Cl^-, Br^-, NO_3^-, and SCN^- were used to probe the effect of anions, while with chloride salts of $N(CH_3)_4^+$, NH_4^+, Cs^+, K^+, Na^+, and Li^+ the cations were varied. These ions interact with oppositely charged particle surfaces specifically. They normally adsorb, and thereby modify, the surface charge and the CCC. Poorly hydrated counterions, such as $N(CH_3)_4^+$ and SCN^-, adsorb to

DOI: 10.1021/acs.langmuir.5b00225
Langmuir 2015, 31, 3799−3807

the oppositely charged surfaces more strongly, and they lower the magnitude of the surface charge and the CCC substantially. Strongly hydrated counterions, such as Li^+ or F^-, do not adsorb, and lead to high magnitudes of the surface charge and high CCCs. For some well hydrated counterions, the CCC remains independent of the type of ion. In this regime, we suspect that these ions do not adsorb to the particle surface at all. On the other hand, these ions interact only weakly with equally charged surfaces, and the CCCs are basically independent of the nature of the co-ion. Moreover, we have demonstrated that the aggregation rate in the fast regime does not depend on the type of ions present but only on the type of particles.

DLVO theory can be used to confirm that the principal mechanism responsible for the shifts of the CCCs originates from modification of the surface charge. The dependence of the CCC on the surface charge density obtained from electrophoresis agrees well with DLVO theory. However, the Hamaker constant obtained by fitting the experimental CCC data is probably somewhat high, indicating the presence of additional non-DLVO forces.

■ ASSOCIATED CONTENT

Supporting Information

Tables S1 and S2 with viscosity coefficients and experimental CCCs. This material is available free of charge via the Internet at http://pubs.acs.org.

■ AUTHOR INFORMATION

Corresponding Author

*E-mail: istvan.szilagyi@unige.ch.

Notes

The authors declare no competing financial interest.

■ ACKNOWLEDGMENTS

This research was supported by the Swiss National Science Foundation, the University of Geneva and the COST Action MP1106.

■ REFERENCES

(1) Jungwirth, P.; Cremer, P. S. Beyond Hofmeister. *Nat. Chem.* **2014**, *6*, 261−263.

(2) Zhang, Y. J.; Cremer, P. S. Chemistry of Hofmeister anions and osmolytes. *Annu. Rev. Phys. Chem.* **2010**, *61*, 63−83.

(3) Lo Nostro, P.; Ninham, B. W. Hofmeister phenomena: An update on ion specificity in biology. *Chem. Rev.* **2012**, *112*, 2286−2322.

(4) Weissenborn, P. K.; Pugh, R. J. Surface tension of aqueous solutions of electrolytes: Relationship with ion hydration, oxygen solubility, and bubble coalescence. *J. Colloid Interface Sci.* **1996**, *184*, 550−563.

(5) Matubayasi, N.; Yamamoto, K.; Yamaguchi, S. I.; Matsuo, H.; Ikeda, N. Thermodynamic quantities of surface formation of aqueous electrolyte solutions—III. Aqueous solutions of alkali metal chloride. *J. Colloid Interface Sci.* **1999**, *214*, 101−105.

(6) Diehl, A.; dos Santos, A. P.; Levin, Y. Surface tension of an electrolyte-air interface: A Monte Carlo study. *J. Phys.: Condens. Matter* **2012**, 24.

(7) Nihonyanagi, S.; Yamaguchi, S.; Tahara, T. Counterion effect on interfacial water at charged interfaces and its relevance to the Hofmeister series. *J. Am. Chem. Soc.* **2014**, *136*, 6155−6158.

(8) Pozar, J.; Bohinc, K.; Vlachy, V.; Kovacevic, D. Ion-specific and charge effects in counterion binding to poly(styrene sulfonate) anions. *Phys. Chem. Chem. Phys.* **2011**, *13*, 15610−15618.

(9) Salomaki, M.; Tervasmaki, P.; Areva, S.; Kankare, J. The Hofmeister anion effect and the growth of polyelectrolyte multilayers. *Langmuir* **2004**, *20*, 3679−3683.

(10) Jenkins, H. D. B.; Marcus, Y. Viscosity B-coefficients of ions in solution. *Chem. Rev.* **1995**, *95*, 2695−2724.

(11) dos Santos, A. P.; Diehl, A.; Levin, Y. Surface tensions, surface potentials, and the Hofmeister series of electrolyte solutions. *Langmuir* **2010**, *26*, 10778−10783.

(12) Sowmiya, M.; Tiwari, A. K.; Sonu; Eranna, G.; Sharma, A. K.; Saha, S. K. Study of the binding interactions of a hemicyanine dye with nanotubes of beta-cyclodextrin and effect of a Hofmeister series of potassium salts. *J. Phys. Chem. C* **2014**, *118*, 2735−2748.

(13) Medda, L.; Barse, B.; Cugia, F.; Bostrom, M.; Parsons, D. F.; Ninham, B. W.; Monduzzi, M.; Salis, A. Hofmeister challenges: Ion binding and charge of the BSA protein as explicit examples. *Langmuir* **2012**, *28*, 16355−16363.

(14) Merk, V.; Rehbock, C.; Becker, F.; Hagemann, U.; Nienhaus, H.; Barcikowski, S. In situ non-DLVO stabilization of surfactant-free plasmonic gold nanoparticles: Effect of Hofmeister's anions. *Langmuir* **2014**, *30*, 4213−4222.

(15) Evans, D. F.; Wennerstrom, H. *The Colloidal Domain*; John Wiley: New York, 1999.

(16) Wang, D. W.; Tejerina, B.; Lagzi, I.; Kowalczyk, B.; Grzybowski, B. A. Bridging interactions and selective nanoparticle aggregation mediated by monovalent cations. *ACS Nano* **2011**, *5*, 530−536.

(17) Lopez-Leon, T.; Ortega-Vinuesa, J. L.; Bastos-Gonzalez, D. Ion-specific aggregation of hydrophobic particles. *ChemPhysChem* **2012**, *13*, 2382−2391.

(18) Lopez-Leon, T.; Santander-Ortega, M. J.; Ortega-Vinuesa, J. L.; Bastos-Gonzalez, D. Hofmeister effects in colloidal systems: Influence of the surface nature. *J. Phys. Chem. C* **2008**, *112*, 16060−16069.

(19) Lopez-Leon, T.; Jodar-Reyes, A. B.; Ortega-Vinuesa, J. L.; Bastos-Gonzalez, D. Hofmeister effects on the colloidal stability of an IgG-coated polystyrene latex. *J. Colloid Interface Sci.* **2005**, *284*, 139−148.

(20) Lopez-Leon, T.; Jodar-Reyes, A. B.; Bastos-Gonzalez, D.; Ortega-Vinuesa, J. L. Hofmeister effects in the stability and electrophoretic mobility of polystyrene latex particles. *J. Phys. Chem. B* **2003**, *107*, 5696−5708.

(21) Dumont, F.; Warlus, J.; Watillon, A. Influence of the point of zero charge of titanium-dioxide hydrosols on the ionic adsorption sequences. *J. Colloid Interface Sci.* **1990**, *138*, 543−554.

(22) Peula-Garcia, J. M.; Ortega-Vinuesa, J. L.; Bastos-Gonzalez, D. Inversion of Hofmeister series by changing the surface of colloidal particles from hydrophobic to hydrophilic. *J. Phys. Chem. C* **2010**, *114*, 11133−11139.

(23) Dumont, F.; Watillon, A. Stability of ferric oxide hydrosols. *Discuss. Faraday Soc.* **1971**, *52*, 352−380.

(24) Tian, R.; Yang, G.; Li, H.; Gao, X. D.; Liu, X. M.; Zhu, H. L.; Tang, Y. Activation energies of colloidal particle aggregation: Towards a quantitative characterization of specific ion effects. *Phys. Chem. Chem. Phys.* **2014**, *16*, 8828−8836.

(25) Tezak, B.; Matijevic, E.; Schulz, K. F. Coagulation of hydrophobic sols in statu nascendi. III. The influence of the ionic size and valency of the counterion. *J. Phys. Chem.* **1955**, *59*, 769−773.

(26) Oncsik, T.; Trefalt, G.; Csendes, Z.; Szilagyi, I.; Borkovec, M. Aggregation of negatively charged colloidal particles in the presence of multivalent cations. *Langmuir* **2014**, *30*, 733−741.

(27) Schneider, C.; Hanisch, M.; Wedel, B.; Jusufi, A.; Ballauff, M. Experimental study of electrostatically stabilized colloidal particles: Colloidal stability and charge reversal. *J. Colloid Interface Sci.* **2011**, *358*, 62−67.

(28) Elimelech, M.; Gregory, J.; Jia, X.; Williams, R. A. *Particle Deposition and Aggregation: Measurement, Modeling, and Simulation*; Butterworth-Heinemann: Oxford, U.K., 1995.

(29) Trefalt, G.; Szilagyi, I.; Borkovec, M. Poisson-Boltzmann description of interaction forces and aggregation rates involving charged colloidal particles in asymmetric electrolytes. *J. Colloid Interface Sci.* **2013**, *406*, 111−120.

DOI: 10.1021/acs.langmuir.5b00225
Langmuir 2015, 31, 3799−3807

(30) Behrens, S. H.; Borkovec, M.; Schurtenberger, P. Aggregation in charge-stabilized colloidal suspensions revisited. *Langmuir* **1998**, *14*, 1951−1954.
(31) Lin, W.; Galletto, P.; Borkovec, M. Charging and aggregation of latex particles by oppositely charged dendrimers. *Langmuir* **2004**, *20*, 7465−7473.
(32) Kobayashi, M.; Skarba, M.; Galletto, P.; Cakara, D.; Borkovec, M. Effects of heat treatment on the aggregation and charging of Stöber-type silica. *J. Colloid Interface Sci.* **2005**, *292*, 139−147.
(33) Sprycha, R. Electrical double-layer at alumina electrolyte interface 1. Surface-charge and zeta potential. *J. Colloid Interface Sci.* **1989**, *127*, 1−11.
(34) Tadros, T. F.; Lyklema, J. Adsorption of potential determining ions at silica-aqueous electrolyte interface and role of some cations. *J. Electroanal. Chem.* **1968**, *17*, 267−275.
(35) Abendroth, R. P. Behavior of a pyrogenic silica in simple electrolytes. *J. Colloid Interface Sci.* **1970**, *34*, 591−596.
(36) Breeuwsma, A.; Lyklema, J. Interfacial electrochemistry of hematite (α-Fe_2O_3). *Discuss. Faraday Soc.* **1971**, *52*, 324−333.
(37) Dishon, M.; Zohar, O.; Sivan, U. From repulsion to attraction and back to repulsion: The effect of NaCl, KCl, and CsCl on the force between silica surfaces in aqueous solution. *Langmuir* **2009**, *25*, 2831−2836.
(38) Morag, J.; Dishon, M.; Sivan, U. The governing role of surface hydration in ion specific adsorption to silica: An AFM-based account of the Hofmeister universality and its reversal. *Langmuir* **2013**, *29*, 6317−6322.
(39) Schwierz, N.; Horinek, D.; Netz, R. R. Reversed anionic Hofmeister series: The interplay of surface charge and surface polarity. *Langmuir* **2010**, *26*, 7370−7379.
(40) Schwierz, N.; Horinek, D.; Netz, R. R. Anionic and cationic Hofmeister effects on hydrophobic and hydrophilic surfaces. *Langmuir* **2013**, *29*, 2602−2614.
(41) dos Santos, A. P.; Levin, Y. Ion specificity and the theory of stability of colloidal suspensions. *Phys. Rev. Lett.* **2011**, 106.
(42) Huang, H. H.; Ruckenstein, E. Effect of hydration of ions on double-layer repulsion and the Hofmeister series. *J. Phys. Chem. Lett.* **2013**, *4*, 3725−3727.
(43) Calero, C.; Faraudo, J.; Bastos-Gonzalez, D. Interaction of monovalent ions with hydrophobic and hydrophilic colloids: Charge inversion and ionic specificity. *J. Am. Chem. Soc.* **2011**, *133*, 15025−15035.
(44) Yates, D. E.; Healy, T. W. Titanium-dioxide electrolyte interface 2. Surface-charge (titration) studies. *J. Chem. Soc., Faraday Trans. 1* **1980**, *76*, 9−18.
(45) Franks, G. V. Zeta potentials and yield stresses of silica suspensions in concentrated monovalent electrolytes: Isoelectric point shift and additional attraction. *J. Colloid Interface Sci.* **2002**, *249*, 44−51.
(46) Dove, P. M.; Craven, C. M. Surface charge density on silica in alkali and alkaline earth chloride electrolyte solutions. *Geochim. Cosmochim. Acta* **2005**, *69*, 4963−4970.
(47) Bijsterbosch, B. H.; Lyklema, J. Interfacial electrochemistry of silver iodide. *Adv. Colloid Interface Sci.* **1978**, *9*, 147−251.
(48) Yang, Z.; Li, Q. F.; Chou, K. C. Structures of water molecules at the interfaces of aqueous salt solutions and silica: Cation effects. *J. Phys. Chem. C* **2009**, *113*, 8201−8205.
(49) Abe, T.; Kobayashi, S.; Kobayashi, M. Aggregation of colloidal silica particles in the presence of fulvic acid, humic, acid or alginate: Effects of ionic composition. *Colloids Surf., A* **2011**, *379*, 21−26.
(50) Chen, K. L.; Mylon, S. E.; Elimelech, M. Enhanced aggregation of alginate-coated iron oxide (hematite) nanoparticles in the presence of, calcium, strontium and barium cations. *Langmuir* **2007**, *23*, 5920−5928.
(51) Holthoff, H.; Egelhaaf, S. U.; Borkovec, M.; Schurtenberger, P.; Sticher, H. Coagulation rate measurements of colloidal particles by simultaneous static and dynamic light scattering. *Langmuir* **1996**, *12*, 5541−5549.
(52) Sandkuhler, P.; Lattuada, M.; Wu, H.; Sefcik, J.; Morbidelli, M. Further insights into the universality of colloidal aggregation. *Adv. Colloid Interface Sci.* **2005**, *113*, 65−83.
(53) Szilagyi, I.; Szabo, T.; Desert, A.; Trefalt, G.; Oncsik, T.; Borkovec, M. Particle aggregation mechanisms in ionic liquids. *Phys. Chem. Chem. Phys.* **2014**, *16*, 9515−9524.
(54) Mishchenko, M. I.; Travis, L. D.; Lacis, A. A. *Scattering, Absorption, and Emission of Light by Small Particles*; University Press: Cambridge, U.K., 2002.
(55) Lin, W.; Kobayashi, M.; Skarba, M.; Mu, C.; Galletto, P.; Borkovec, M. Heteroaggregation in binary mixtures of oppositely charged colloidal particles. *Langmuir* **2006**, *22*, 1038−1047.
(56) Yu, W. L.; Matijevic, E.; Borkovec, M. Absolute hetero-aggregation rate constants by multiangle static and dynamic light scattering. *Langmuir* **2002**, *18*, 7853−7860.
(57) Desnoyers, J. E.; Perron, G. The viscosity of aqueous solutions of alkali and tetraalkylammonium halides at 25 degrees C. *J. Solution Chem.* **1972**, *1*, 199−212.
(58) Weast, R. C.; Astle, M. J. *CRC Handbook of Chemistry and Physics*, 60th ed.; CRC Press: New York, 1980.
(59) Elzbieciak-Wodka, M.; Popescu, M.; Montes Ruiz-Cabello, F. J.; Trefalt, G.; Maroni, P.; Borkovec, M. Measurements of dispersion forces between colloidal latex particles with the atomic force microscope and comparison with Lifshitz theory. *J. Chem. Phys.* **2014**, *140*, No. 104906.
(60) Sadeghpour, A.; Szilagyi, I.; Borkovec, M. Charging and aggregation of positively charged colloidal latex particles in presence of multivalent polycarboxylate anions. *Z. Phys. Chem.* **2012**, *226*, 597−612.
(61) Sinha, P.; Szilagyi, I.; Montes Ruiz-Cabello, F. J.; Maroni, P.; Borkovec, M. Attractive forces between charged colloidal particles induced by multivalent ions revealed by confronting aggregation and direct force measurements. *J. Phys. Chem. Lett.* **2013**, *4*, 648−652.
(62) O'Brien, R. W.; White, L. R. Electrophoretic mobility of a spherical colloidal particle. *J. Chem. Soc., Faraday Trans. 2* **1978**, *74*, 1607−1626.
(63) Diehl, A.; Levin, Y. Smoluchowski equation and the colloidal charge reversal. *J. Chem. Phys.* **2006**, *125*, No. 054902.
(64) Bevan, M. A.; Prieve, D. C. Direct measurement of retarded van der Waals attraction. *Langmuir* **1999**, *15*, 7925−7936.
(65) Montes Ruiz-Cabello, F. J.; Trefalt, G.; Csendes, Z.; Sinha, P.; Oncsik, T.; Szilagyi, I.; Maroni, P.; Borkovec, M. Predicting aggregation rates of colloidal particles from direct force measurements. *J. Phys. Chem. B* **2013**, *117*, 11853−11862.

DOI: 10.1021/acs.langmuir.5b00225
Langmuir 2015, 31, 3799−3807

CHAPTER 5

Interaction Forces and Aggregation Rates of Colloidal Latex Particles in the Presence of Monovalent Counterions

Ruiz-Cabello, F. J. M.; Trefalt, G.; Oncsik, T.; Szilagyi, I.; Maroni, P.; Borkovec, M.

J. Phys. Chem. B **2015,** 119, 8184-8193.

THE JOURNAL OF PHYSICAL CHEMISTRY B

Article

pubs.acs.org/JPCB

Interaction Forces and Aggregation Rates of Colloidal Latex Particles in the Presence of Monovalent Counterions

F. Javier Montes Ruiz-Cabello, Gregor Trefalt, Tamas Oncsik, Istvan Szilagyi, Plinio Maroni, and Michal Borkovec*

Department of Inorganic and Analytical Chemistry, University of Geneva, Quai Ernest-Ansermet 30, 1205 Geneva, Switzerland

ABSTRACT: Force profiles and aggregation rates involving positively and negatively charged polystyrene latex particles are investigated in monovalent electrolyte solutions, whereby the counterions are varied within the Hofmeister series. The force measurements are carried out with the colloidal probe technique, which is based on the atomic force microscope (AFM), while the aggregation rates are measured with time-resolved multiangle light scattering. The interaction force profiles cannot be described by classical DLVO theory, but an additional attractive short-ranged force must be included. An exponential force profile with a decay length of about 0.5 nm is consistent with the measured forces. Furthermore, the Hamaker constants extracted from the measured force profiles are substantially smaller than the theoretical values calculated from dielectric spectra. The small surface roughness of the latex particles (below 1 nm) is probably responsible for this deviation. Based on the measured force profiles, the aggregation rates can be predicted without adjustable parameters. The measured absolute aggregation rates in the fast regime are somewhat lower than the calculated ones. The critical coagulation concentration (CCC) agrees well with the experiment, including the respective shifts of the CCC within the Hofmeister series. These shifts are particularly pronounced for the positively charged particles. However, the consideration of the additional attractive short-ranged force is essential to quantify these shifts correctly. In the slow regime, the calculated rates are substantially smaller than the experimental ones. This disagreement is probably related to surface charge heterogeneities.

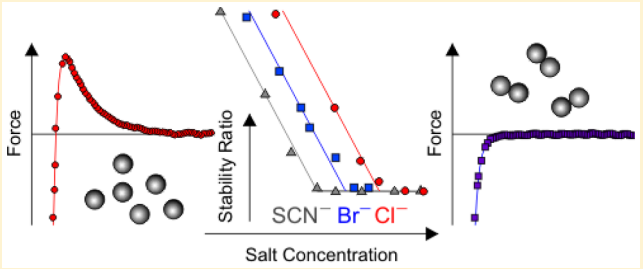

INTRODUCTION

Particle aggregation controls numerous processes in colloidal suspensions, including their stability, sedimentation, or rheology.[1−6] While the growth of larger colloidal aggregates is a complex kinetic process, its overall time scale is set by the rate of particle doublet formation. When this kinetic process is fast, particle aggregation is diffusion controlled, while a slower process is reaction controlled, due to the presence of a reaction barrier in the interaction potential.[1,7] The transition between these two regimes is normally rather sharp and is referred to as the critical coagulation concentration (CCC). This behavior is well established experimentally, since several techniques are available to follow the particle aggregation in its early stages, for example, time-resolved light scattering, turbidity measurements, or single particle counting.[6,8−10]

Formation of particle doublets mainly occurs at early stages of the aggregation, and its rate is governed by the interaction potential acting between a pair of particles and the respective hydrodynamic drag.[1,7] While the hydrodynamics of a particle pair is relatively well understood, there are substantial uncertainties concerning the conservative forces acting between particles, even in aqueous media.[11,12] The classical theory of Derjaguin, Landau, Verwey, and Overbeek (DLVO) provides a good approximation of these forces at larger distances, which typically exceed several nanometers. At shorter distances, several additional contributions to the interaction forces may come into play, such as charge regulation, ion−ion correlations, specific ion effects, and hydrophobic or hydration forces.[11,13−16] These effects are expected to be particularly relevant for highly charged particles suspended in monovalent electrolytes, which feature high CCCs. Under these conditions, the energy barrier is located at small surface separations, typically few nanometers or less. An indication that non-DLVO forces should be relevant is the dependence of the CCC on the type of counterions, normally following the Hofmeister series.[17,18] Such ionic specificity could also be explained within DLVO theory, as the electric surface potential might be modified due to the different extent of the adsorption of these ions to the particle surface.[13,19]

Until recently, it was basically impossible to pinpoint the nature of forces acting between a pair of colloidal particles, especially at separations of few nanometers. However, due to rapid progress in the experimental techniques, these forces can be now directly measured with good precision. The two noteworthy techniques include optical tweezers and the colloidal probe technique.[20,21] While the optical tweezers operate truly *in situ*, the separation distances are determined by video microscopy, which limits the distance resolution. The

Received: March 17, 2015
Revised: April 24, 2015
Published: May 25, 2015

DOI: 10.1021/acs.jpcb.5b02556
J. Phys. Chem. B 2015, 119, 8184−8193

colloidal probe technique, which is based on the atomic force microscope (AFM), offers the necessary distance resolution for some time but was hampered by complications of the fabrication of the colloidal probe.[22,23] The classical approach consisted in gluing colloidal particles to the cantilever and the substrate in the dry state, whereby proper rewetting and sample contamination frequently posed problems. These problems can nowadays be largely circumvented with the multiparticle colloidal probe technique, whereby the particles are directly mounted within the liquid suspension to a functionalized cantilever and substrate.[20] The multiparticle colloidal probe technique can be thus routinely used to measure interaction forces between pairs of colloidal particles with the necessary distance resolution and has the potential to directly clarify the various contributions to the forces in the particle aggregation process. The corresponding particle aggregation rates can be measured with the same particles by means of time-resolved light scattering techniques.

The present article describes direct force measurements between colloidal particles in order to obtain more detailed insight into the respective aggregation rates in different monovalent electrolytes. We find that the observed particle aggregation rates can be rationalized by means of the measured force profiles. However, these forces cannot be well described with classical DLVO theory, and additional attractive forces must be included at shorter distances. These short-range non-DLVO forces also have important implications on the particle aggregation rates. While some of us have published similar studies involving multivalent ions,[24,25] the present work addresses specific ion effects in monovalent electrolytes within the Hofmeister series.

THEORY

Forces acting between particles are modeled within DLVO theory, but an additional short-ranged attractive force is equally included. The aggregation rates are then directly evaluated from this force profile by including the hydrodynamic interaction.

Conservative Forces. The force F acting between two particles is assumed to have the following contributions, namely

$$F = F_{vdW} + F_{dl} + F_s \tag{1}$$

where F_{vdW} is the attractive van der Waals force, F_{dl} the repulsive double-layer force, and F_s an attractive short-ranged force. The first two contributions are included in the classical DLVO theory, while the last one is an additional non-DLVO term.

The nonretarded van der Waals force is used, which is expressed within the Derjaguin approximation as[7]

$$F_{vdW} = -\frac{HR_{eff}}{6h^2} \tag{2}$$

where H is the Hamaker constant, R_{eff} is the effective radius, and h is the surface separation. In the symmetric sphere−sphere situation considered here, $R_{eff} = R/2$ where R is the particle radius.

The double-layer force is calculated from the PB theory of an electrolyte solution between two identically charged parallel plates. The electric potential profile $\psi(x)$ depends on the position x in between the plates located at $\pm h/2$ and satisfies the PB equation[26]

$$\frac{d^2\psi}{dx^2} = \frac{\kappa^2}{\beta e}\sinh(\beta e\psi) \tag{3}$$

where e is the elementary charge and

$$\kappa^2 = \frac{2\beta e^2 c}{\varepsilon_0 \varepsilon} \tag{4}$$

whereby κ^{-1} is the Debye length. The above relation introduces the number concentration c of the monovalent electrolyte, the permittivity of vacuum ε_0, and the dielectric constant ε. We use $\varepsilon = 80$ as appropriate for water at room temperature. The parameter $\beta = 1/(k_B T)$ is the inverse thermal energy, where k_B is the Boltzmann constant and T the absolute temperature. Equation 3 is solved within the constant regulation (CR) approximation, which implies the boundary condition

$$\pm\varepsilon_0\varepsilon\frac{d\psi}{dx}\bigg|_{x=\pm h/2} = \sigma - C_I[\psi(\pm h/2) - \psi_D] \tag{5}$$

where the + and − signs refer to the right and left plate, respectively, C_I is the inner capacitance, σ is the surface charge density, and ψ_D the diffuse layer potential. The latter two quantities are related by the Gouy−Chapman equation

$$\sigma = \frac{2\varepsilon_0\varepsilon\kappa}{\beta e}\sinh\left(\frac{\beta e\psi_D}{2}\right) \tag{6}$$

Instead of reporting the inner capacitance, we use the regulation parameter defined as[26]

$$p = \frac{C_D}{C_D + C_I} \tag{7}$$

where C_D is the diffuse layer capacitance given by

$$C_D = \varepsilon_0\varepsilon\kappa\cosh\left(\frac{\beta e\psi_D}{2}\right) \tag{8}$$

The advantage of the regulation parameter is that it assumes simple values for the classical boundary conditions, namely $p = 1$ for constant charge (CC) and $p = 0$ for constant potential (CP). The double-layer force is calculated from the swelling pressure that can be obtained from

$$\Pi = 2c\beta^{-1}[\cosh(\beta e\psi_m) - 1] \tag{9}$$

where $\psi_m = \psi(0)$ is the electric potential at the midplane. Once the pressure profile $\Pi(h)$ is known, one obtains the force by integration

$$F_{dl} = 2\pi R_{eff}\int_h^\infty \Pi(h')\,dh' \tag{10}$$

The additional attractive non-DLVO force is modeled by a simple exponential[15,16]

$$\frac{F_s}{R_{eff}} = -A_s e^{-q_s h} \tag{11}$$

where q_s^{-1} characterizes its range, while the amplitude A_s defines its strength ($A_s > 0$). The same amplitude A_s of the exponential force introduced earlier[24] was defined in the same fashion as in eq 11. However, the definition given in that reference is incorrect due to a typing error. The position of the jump-in was calculated from the relation[27]

DOI: 10.1021/acs.jpcb.5b02556
J. Phys. Chem. B 2015, 119, 8184−8193

$$\frac{dF}{dh} + k_{sp} = 0 \tag{12}$$

where k_{sp} is the spring constant of the cantilever.

Aggregation Rates. When forces are sufficiently attractive, a colloidal suspension will be destabilized by forming particle dimers from particle monomers according to the rate law[7]

$$\frac{dN_2}{dt} = \frac{k}{2}N_1^2 \tag{13}$$

where k is the aggregation rate coefficient and N_1 and N_2 are the number concentrations of monomers and dimers. The rate coefficient can be obtained from the pair diffusion equation and is given by[7]

$$k = \frac{4}{3\beta\eta R}\left[\int_0^\infty \frac{B(h/R)}{(2R+h)^2}\exp[\beta V(h)]\,dh\right] \tag{14}$$

where η is the dynamic viscosity, $V(h)$ is the interaction potential energy, and $B(y)$ is the hydrodynamic resistance function. The potential energy is obtained by integrating the force profile

$$V(h) = \int_h^\infty F(h')\,dh' \tag{15}$$

while the hydrodynamic resistance function is approximated as

$$B(y) = \frac{6y^2 + 13y + 2}{6y^2 + 4y} \tag{16}$$

For hard-sphere interactions and neglecting the effect of the hydrodynamic function, the rate simplifies to the Smoluchowski's value

$$k_{Sm} = \frac{8}{3\beta\eta} \tag{17}$$

Instead of reporting the rate coefficient, we will rather discuss the stability ratio defined as

$$W = \frac{k_{fast}}{k} \tag{18}$$

where k_{fast} is the rate coefficient in the fast aggregation regime, which is encountered at high salt concentrations.

EXPERIMENTAL SECTION

Materials. Two different types of polystyrene latex particles supplied as aqueous suspensions by Invitrogen (Life Technologies Corporation) were used in this study, namely amidine latex (AL) and sulfate latex (SL). The average radius and polydispersity determined by transmission electron microscopy by the manufacturer are given in Table 1. The particles were dialyzed against pure water for about 1 week using a cellulose ester membrane (Spectrum) with a molecular mass cutoff of 300 kg/mol. The final particle concentrations were determined by comparing the light scattering intensity with the undialyzed stock suspension. In the dialyzed samples, the particle concentrations were 130 g/L for SL and 43 g/L for AL.

Various monovalent electrolytes were used, namely NaBr (Fluka), NaCl (Sigma-Aldrich), NaSCN (Sigma-Aldrich), KCl (Acros Organics), and CsCl (Acros Organics). The electrolytes were mixed with the dialyzed latex suspension. The viscosities of the electrolyte solutions were estimated with the relation

Table 1. Properties of the Latex Particles Used

	radius (μm)			polydispersity (%)[a]			
particle	TEM[d]	SLS[e]	DLS[f]	TEM[d]	SLS[e]	roughness RMS[b] (nm)	Hamaker const H^c ($\times 10^{-21}$ J)
AL	0.48	0.47	0.53	3.6	3.6	0.50	2.8
SL	0.49	0.49	0.55	2.2	2.9	0.85	2.4

[a]Coefficient of variation. [b]Particle root-mean-square (RMS) roughness determined with AFM imaging over an area of 0.5 × 0.5 μm^2. [c]Extracted from force profiles at high salt concentration. [d]Determined by transmission electron microscopy (TEM) by the manufacturer. [e]Determined by static light scattering (SLS). [f]Hydrodynamic radius determined by dynamic light scattering (DLS).

$$\frac{\eta}{\eta_0} = 1 + A\sqrt{c} + Bc + Dc^2 \tag{19}$$

where $\eta_0 = 8.9 \times 10^{-4}$ Pa·s is the viscosity of water at 25 °C. The constants A, B, and D were taken from the literature.[28−30] Prior to use, all solutions or suspensions were adjusted to pH 4.0 with HCl (Sigma-Aldrich). Milli-Q (Millipore) water was used throughout. In the systems studied, the concentration of the added electrolyte always largely exceeds the concentration of the counterions that neutralize the charge of the colloidal particles (i.e., high salt regime).[19,31]

Colloidal Probe Technique. Force measurements between individual colloidal particles were carried out with the multiparticle colloidal probe technique.[20,32] A closed-loop AFM (MFP-3D, Asylum Research) mounted on an inverted optical microscope (Zeiss Axiovert 200) was used together with tip-less cantilevers (NSC 12, μMash, Estonia). The glass plate sealing the bottom of the fluid cell was cleaned for 1 h with piranha solution, which consists of a mixture of H_2SO_4 (98%) and H_2O_2 (30%) in a volumetric ratio 3:1. The plate was subsequently rinsed with water and dried in a flow of nitrogen. The plate and the cantilever were then treated with air plasma for 20 min (PDC-32G, Harrick) and silanized in an evacuated container aside of a small sessile drop of an appropriate silane. For the SL particles, 20 μL of 3-(ethoxydimethylsilyl)-propylamine (Sigma-Aldrich) was used, while for the AL particles 100 μL of 3-glycidoxypropyldimethylethoxysilane (Sigma-Aldrich). The silanized glass plate was inserted in the fluid cell, and a particle suspension having a particle concentration of about 100 mg/L in pure water was injected and allowed to settle for 2 h. During this time, particles attach to the glass plate. Subsequently, the fluid cell was rinsed with the appropriate electrolyte solution adjusted to pH 4.0. The cantilever was then introduced into the fluid cell, and a colloidal particle was attached to the cantilever by pressing the cantilever against a fixed particle on the substrate. This particle was centered over another deposited particle by observing the interference pattern in the optical microscope with a lateral precision of about 100 nm. About 200 approach−retraction cycles were recorded between the centered particles with a velocity of 300 nm/s and a repeat frequency of 0.5 Hz. The data were acquired with 5 kHz, and the trigger was fixed to 60 mV which correspond to a maximum load F/R_{eff} of typically 50 mN/m. The forces were extracted from the approach part of the force profiles. The zero separation distance was obtained from the constant compliance region with an accuracy of about 0.2 nm. The force was calculated from the deflection of the cantilever by means of its spring constant. The spring constant

DOI: 10.1021/acs.jpcb.5b02556
J. Phys. Chem. B 2015, 119, 8184−8193

of the cantilever was measured by the method Sader et al.[33] This method uses the frequency response of the cantilever and its lateral geometrical dimensions. The spring constants were in the range 0.19 ± 0.05 N/m. The respective values were in good agreement with the ones measured through the thermal fluctuations of the cantilever.[34] To obtain the final force curve, at least 120 cycles were averaged, and the result was down sampled to 200 Hz. The resulting force resolution was around 0.6 pN. The same sequence was repeated with three pairs of different particles, and good reproducibility was generally found. The experiments were carried out at room temperature of 23 ± 2 °C.

Particle Roughness. The root-mean-square (RMS) particle roughness was obtained by AFM. The roughness of the particles was determined by imaging the surface of the particles in solution with the AFM (Cypher, Asylum Research, Santa Barbara, CA) operating in amplitude modulation mode. BioLever mini cantilevers (AC40TS, Olympus, Japan) with a tip radius of 9 nm and a resonance frequency around 25 kHz in water were used. As substrates, we used a piranha-cleaned 1 cm square glass plates that were silanized in the same fashion as the glass of the fluid cell for each type of particle. A drop of a colloidal suspension of concentration 100 mg/L in water was deposited on the glass for few hours, and subsequently the liquid was exchanged with a solution of 10 mM NaCl. This way, the particles that did not adhere to the substrate were eliminated. The scan size was 0.5 × 0.5 μm^2, the scan rate 2 Hz, and the free oscillation amplitude (FOA) 20 nm. The set point was fixed around 70% of the FOA.

Light Scattering. Stable particle suspensions were characterized by static and dynamic light scattering using a multiangle light scattering instrument (ALV/CGS-8, Langen, Germany) with a solid state laser operating at a wavelength of 532 nm (Verdi V2, Coherent, Inc.). The suspensions were prepared in pure water at a particle concentration of 4 mg/L and adjusted to pH 4.0. The experiments were carried out in quartz cuvettes. Prior to experiments, the cuvettes were cleaned in piranha solution, rinsed with water, and dried in a dust-free oven at 60 °C. Mie theory including particle polydispersity and back-reflection correction was used to fit the static light scattering data.[35] Figure 1a shows the excellent agreement with experiment. The extracted values of mean particle diameter and the polydispersity are in good agreement with the values obtained by electron microscopy (Table 1). The hydrodynamic particle radius was further measured by dynamic light scattering at a scattering angle of 90°. The correlation function was analyzed with a second cumulant fit. The resulting radii were slightly larger than obtained from the other two techniques, probably due to polydispersity and hydration effects.

The absolute rate coefficient in the fast aggregation regime was determined with time-resolved static light scattering with the multiangle light scattering instrument. The aggregation was initiated by injecting an appropriate amount of the particle suspension into a 1.0 M NaCl solution of pH 4.0 resulting into a particle concentration of 4.0 mg/L, which corresponds to about 8 × 10^{13} m^{-3}. The suspension was mixed and the scattering intensity was monitored with a time resolution of 20 s, and the apparent initial rate was measured, namely

$$\frac{1}{I(q,0)}\frac{dI(q,t)}{dt}\bigg|_{t\to 0} = kN_0\left(\frac{I_2(q)}{2I_1(q)} - 1\right) \quad (20)$$

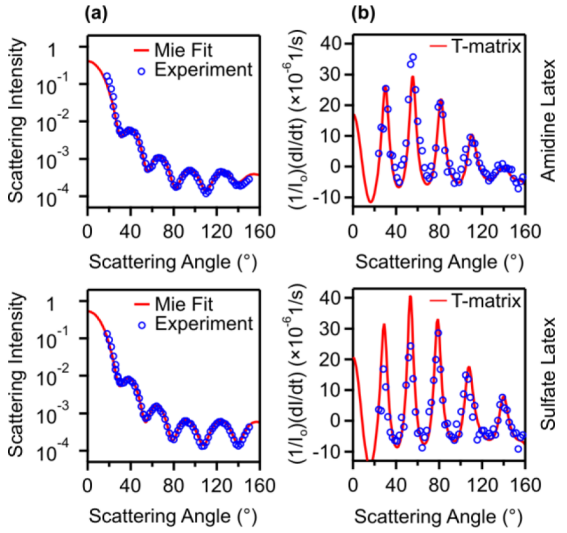

Figure 1. Static light scattering results for the latex particle suspensions used. Data for amidine latex are shown in the top row, while for sulfate latex in the bottom row. (a) Scattering intensity versus the scattering angle of a stable suspension of 4.0 mg/L at pH 4.0 without salt added. The solid line is the best fit with Mie theory including polydispersity and back-reflection. (b) Relative rate of change of the scattering intensity in an aggregating suspension in 1.0 M NaCl. The solid line is prediction of the T-matrix theory. The respective model parameters are summarized in Table 1.

This rate is proportional to the aggregation rate coefficient k, the initial particle number density N_0, and the optical factor, where the scattering intensities $I_1(q)$ and $I_2(q)$ of the monomer and dimer enter. These intensities depend on the magnitude of the scattering vector

$$q = \frac{4\pi n}{\lambda}\sin\left(\frac{\theta}{2}\right) \quad (21)$$

where n is the refractive index of the suspension, λ the wavelength of the light in vacuum, and θ is the scattering angle. The scattering intensity of the monomer can be evaluated with Mie theory, while the corresponding quantity for the dimer was obtained from the exact T-matrix theory.[35] Figure 1b shows the experimental dependence of the apparent rate on the scattering angle and the best theoretical fits. The aggregation rates were extracted from these fits. These experiments were carried out at 25 ± 1 °C.

One can equally evaluate the absolute aggregation rate coefficients by combing time-resolved static and dynamic light scattering measurements. While this technique is normally easier to use, in the present case, the particle concentration must be increased about 5-fold in order to sufficiently reduce the noise in the dynamic light scattering data. The resulting absolute aggregation rate coefficients are about 2 times smaller than with the ones obtained with the T-matrix method. We suspect that these deviations are caused by multiple scattering effects, which start to become important at the concentrations used. For this reason, the absolute aggregation rate coefficients obtained with the T-matrix method are judged to be more reliable, and they are used in the following.

The stability ratios were measured with time-resolved dynamic light scattering on compact goniometer system (ALV/CGS-3, Langen, Germany) operating with a He/Ne laser of a wavelength of 633 nm at a scattering angle of 90°. Piranha-cleaned boroslicate glass cuvettes were used. The

DOI: 10.1021/acs.jpcb.5b02556
J. Phys. Chem. B 2015, 119, 8184−8193

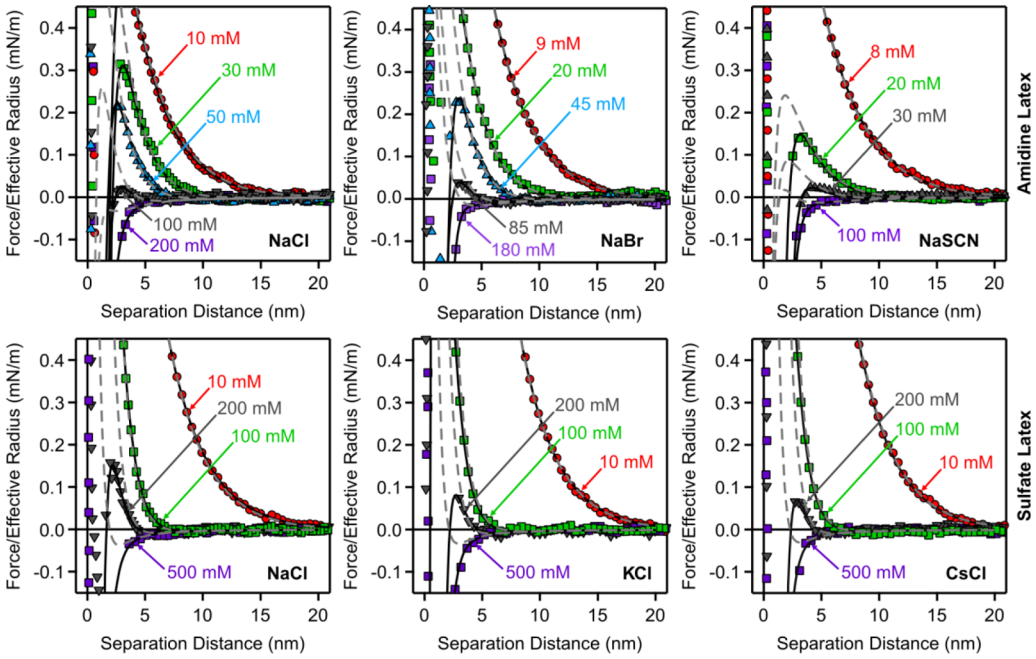

Figure 2. Forces between pairs of latex particles versus the surface separation in different salt solutions indicated in each graph. They are compared with calculations based on DLVO theory including an additional attractive non-DLVO force with q_s^{-1} = 0.49 nm (full lines). The remaining parameters are given in Tables 1 and 2 and Figure 4. The result of DLVO theory only is shown for comparison (dashed lines). Data for amidine latex are shown in the top row, while for sulfate latex in the bottom row.

experiment was started by injecting the particle suspension into the respective electrolyte solution. Particle concentrations of 50−200 mg/L or (1−4) × 10^{14} m^{-3} were used. The correlation function was collected for 20 s, and a second-order cumulant fit was used to obtain the hydrodynamic radius. The initial rate of the increase of the hydrodynamic radius was determined by measuring this quantity during 0.5−8 h. The stability ratio W was obtained by normalizing this rate by the corresponding quantity measured in 1.0 M NaCl solution. The fast aggregation rates for the other salt solutions were obtained by respective normalization of single angle measurements to the value obtained with NaCl.

Electrophoresis. The electrophoretic mobility of the particles was determined with ZetaSizer Nano ZS (Malvern). The latex suspensions were prepared at a particle concentration of 80 mg/L. The samples were equilibrated for a minute prior to the measurement. The mobility of each sample was measured five times and averaged. The standard electrokinetic model was used to convert the electrophoretic mobility to the electric surface potential (ζ-potential).[36]

RESULTS AND DISCUSSION

Forces between charged latex particles are directly measured with the colloidal probe technique. The measured force profiles are quantitatively interpreted with DLVO theory, where an additional exponential short-range attraction is included. Based on these force profiles, the aggregation rate coefficients can be predicted and compared with experiment.

Direct Force Measurements. The multiparticle colloidal probe technique was used to measure forces between pairs of similar particles, which originate from the same stock suspension. Two types of polystyrene particles were investigated, namely positively charged amidine latex (AL) and negatively charged sulfate latex (SL). They both have a diameter around 1.0 μm, and their surface is rather smooth, featuring a maximum RMS surface roughness of 0.8 nm. Further properties of these particles are given in Table 1. All experiments were carried out in various monovalent electrolyte solutions at pH 4.0.

Figure 2 shows a selection of the measured force profiles for the two types of particles investigated, namely AL in the top row and SL in the bottom row. The columns show the results for different monovalent electrolytes, where the counterions were systematically varied according to their position in the Hofmeister series. For AL, we used Cl^-, Br^-, and SCN^- as anions, while the cation was Na^+. For SL, the cations Na^+, K^+, and Cs^+ were used, and the anion was Cl^-. The ions Na^+ and Cl^- were chosen as common ions since they are indifferent. The given series quote the strongly hydrated ions first, while the weakly hydrated ones last. The left column shows the force profiles of both particles in NaCl solution.

Let us first discuss the evolution of the forces profiles qualitatively. To this aim, we focus on the results of AL in NaCl electrolyte (top, left). However, both types of particles behave similarly in all the different electrolytes. At low salt concentration, the force is strongly repulsive, soft, and long-ranged. At these conditions, the double-layer repulsion dominates the force profiles. As the salt concentration is increased, the range of the double-layer force decreases, since the range of this force is determined by the Debye length κ^{-1}. At the same time, an attractive short-range force becomes apparent through the jump-in of the cantilever into contact. With increasing salt concentration, the force profile becomes less repulsive, and a more long ranged attractive force can be evidenced at salt concentrations around 100 mM or above, but the jump-in still occurs at similar distances. The longer ranged part of the attractive force corresponds to the van der Waals attraction. The latter can be seen more clearly in Figure 3, which shows the same force profiles in NaCl, NaSCN, and CsCl on a larger scale. No data points are shown in the

DOI: 10.1021/acs.jpcb.5b02556
J. Phys. Chem. B 2015, 119, 8184−8193

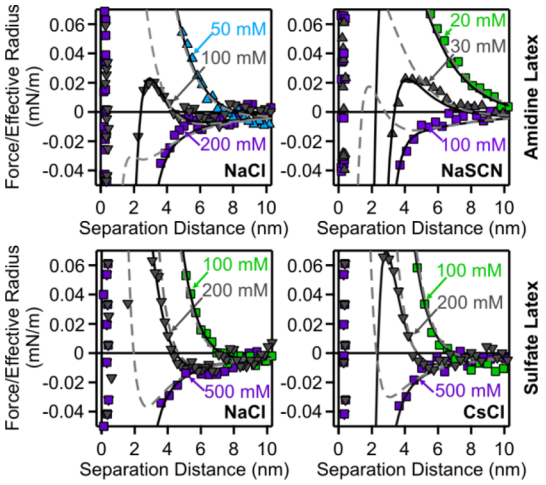

Figure 3. Detailed representation of forces between pairs of latex particles versus the surface separation in different salt solutions indicated in each graph. The lines are the same as in Figure 2. Data for amidine latex are shown in the top row, while for sulfate latex in the bottom row. The jump-in occurs after the leftmost point shown on the force curve.

mechanical instability region. This jump-in occurs at distances of 2−3 nm. The position of the jump-in is relatively independent of the salt concentration, but its position increases in the presence of poorly hydrated ions somewhat (Table 2).

The force profiles can be quantitatively interpreted by means of DLVO theory and modifications thereof. Our approach relies on the Derjaguin approximation, a nonretarded van der Waals force, and the exact solution of the PB equation within the constant regulation (CR) approximation. The experimental results are compared with the classical DLVO theory, as well as with a modified DLVO theory, which includes an attractive exponential non-DLVO force.

The model parameters were determined as follows. The Hamaker constant H was obtained by fitting the force profiles in the range of 4−20 nm for salt concentrations >100 mM with eq 2. This value is around 2.6×10^{-21} J and is independent of the salt used within about 10%. These values were kept constant in all further calculations. The Hamaker constants for AL and SL were slightly different, which is probably related to the different surface roughness (Table 1). For latex particles of similar surface roughness the apparent Hamaker constant was shown to be reduced to similar values as quoted above. These values are substantially smaller than the value of 1.4×10^{-20} J for a smooth substrate.[37,38]

The regulation parameters p were obtained by fitting the force profiles at salt concentrations up to 3 mM with the PB model. The fitted salt concentrations agreed within 10% to the nominal ones. The regulation parameters obtained from the force profiles at different salt concentrations were constant within 10%. Therefore, the regulation parameters fixed to the respective average values, and the force profiles were fitted again. The appropriate values of the regulation parameter p are given in Table 2, and they depend not only on the type of particle but also on the nature of the salt. This variation is not surprising, since the counterions adsorb on the particle surface and thereby modify the inner-layer capacitance. With these fixed regulation parameters, the fits remained of excellent quality. Double-layer forces in similar systems could be equally rationalized with regulation parameters that were independent of salt concentration.[25,37,39,40]

Once the values of the Hamaker constant and the regulation parameter are established, the force curves were refitted in the entire distance range down to the jump-in. When only DLVO forces are being considered, the force profile at shorter distances tends to be more repulsive and the jump-in is predicted at smaller distances than observed experimentally (Figure 3). These deficiencies can be reconciled with an additive non-DLVO exponential force profile given in eq 11. This additional contribution is probably mainly determined by the hydrophobic force, but additional contributions from short-ranged hydration or solvation forces are equally possible.[15,16] When one attempts to determine the amplitude A_s of this force and its range q_s^{-1} from a least-squares fit, one finds that these two parameters are cross-correlated, but only if q_s^{-1} is chosen in the interval of 0.1−0.8 nm. Fitting both parameters, A_s and q_s^{-1}, leads to an average q_s^{-1} of 0.49 ± 0.06 nm. We found that the observed forces can be consistently fitted by fixing q_s^{-1} to this average value. In this fashion, we are able to fit the force profile over the entire distance range with two adjustable parameters, namely the diffuse layer potential ψ_D and the amplitude of the exponential force A_s. The resulting fits shown in Figures 2 and 3 are indeed most satisfactory. The corresponding DLVO contributions are equally shown. The fitted force profiles predict the position of the jump-in rather well, including their increase with decreasing degree of ionic hydration (Table 2). The additional non-DLVO attraction is essential, as pure DLVO theory predicts unrealistically small positions of the jump-in. The observed jump-in occurs somewhat at larger distances than the calculated ones, possibly due to the assumption of the exponential short-ranged force profile.

Table 2. Characteristics of Force Curves in Different Salt Solutions

			jump-in distance (nm)		
particle	salt	regulation[a] p	exp[b]	non-DLVO[c]	DLVO[d]
AL	NaCl	0.20	2.5 ± 0.2	2.0 ± 0.2	0.91 ± 0.04
	NaBr	0.57	2.8 ± 0.2	2.1 ± 0.2	0.84 ± 0.05
	NaSCN	0.33	3.0 ± 0.2	2.3 ± 0.2	0.97 ± 0.03
SL	NaCl	0.28	2.2 ± 0.2	1.7 ± 0.2	0.5 ± 0.1
	KCl	0.45	2.4 ± 0.2	1.9 ± 0.2	0.5 ± 0.1
	CsCl	0.54	2.5 ± 0.3	1.9 ± 0.2	0.4 ± 0.1

[a]Regulation parameter determined from force measurements at low salt concentration. [b]Experimental jump-in distance of the cantilever with standard deviation. [c]Jump-in distance calculated from DLVO theory with exponential attraction force. The error bars reflect the minor variation with the salt concentration. [d]Jump-in distance calculated from DLVO theory without the exponential attraction force. The error bars reflect the minor variation with the salt concentration.

DOI: 10.1021/acs.jpcb.5b02556
J. Phys. Chem. B 2015, 119, 8184−8193

The resulting values of the diffuse layer potential ψ_D and the amplitude of the exponential force A_s are shown in Figure 4.

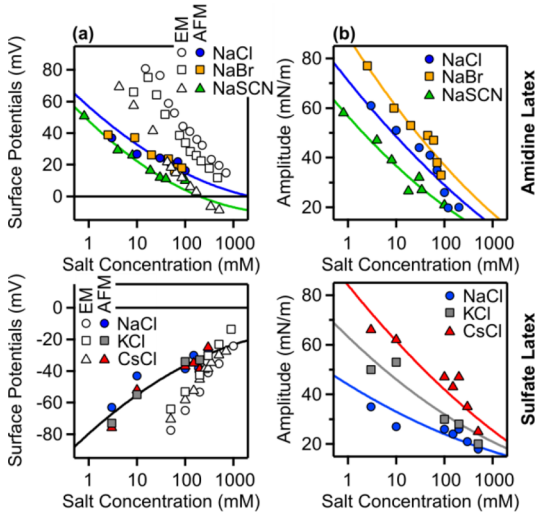

Figure 4. Parameters determined from the force measurements by AFM and electrophoresis versus the salt concentration. Solid lines represent fits by empirical functions to interpolate the data. Data for amidine latex are shown in the top row, while for sulfate latex in the bottom row. (a) Electric surface potentials are shown in the left column, whereby the diffuse layer potential ψ_D are determined from the force measurements (AFM, filled symbols) and the ζ-potentials from electrophoretic mobility (EM, open symbols). (b) Amplitude A_s of the attractive non-DLVO force is shown in the left column.

The fitted diffuse layer potentials are compared with the ζ-potential obtained from electrophoresis in Figure 4a. Note that the sign of the electric potential cannot be extracted from the forces profiles, and it was adjusted to match the sign of the electrophoresis results. The magnitude of the diffuse layer potentials decreases with increasing salt level as one expects from eq 6. The potentials obtained from electrophoresis are systematically higher in magnitude than the ones from AFM. This trend could be due to lateral heterogeneities of the particles.[41] The existence of such charge heterogeneities was independently confirmed by rotational electrophoresis of latex particle doublets.[42] These heterogeneities might introduce additional rotational motion of the particles in the electrophoresis experiment, which would lead to an enhancement of the mobility of the particle. However, this explanation is tentative, and the discrepancies might be also related to variations in position of the plane of shear or to surface roughness effects.

The diffuse layer potentials also vary somewhat with the type of counterion. The Hofmeister series suggests that for such hydrophobic substrate the ions should progressively adsorb with decreasing degree of hydration. Therefore, the diffuse layer potential for AL should decrease with the anion sequence Cl^-, Br^-, and SCN^-, while they should increase for SL with the cation sequence Na^+, K^+, and Cs^+. These trends can be clearly seen in the electrophoretic data, where the affinity of the SCN^- anion to the surface even leads to a charge reversal. The same dependence is probably also inherent to the diffuse layer potentials measured by the AFM, but the scatter of the data points is probably comparable to the effect itself. The scatter originates less from the accuracy by which the diffuse layer potential can be extracted from the force curves, but rather due to the small variability of the force profiles between different pairs of particles. The regulation parameter increases with the mentioned sequence of the cations for SL particles. For AL

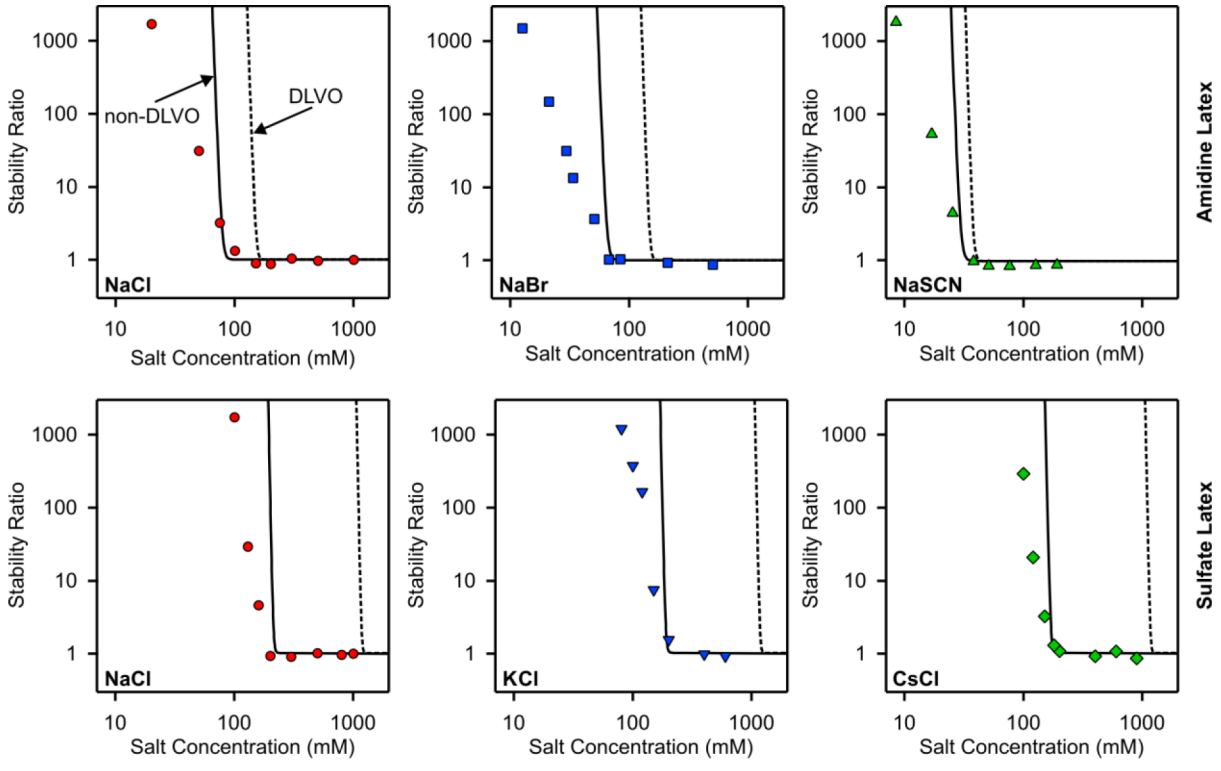

Figure 5. Comparison of measured stability ratios (symbols) with calculated ones based on the force measurements (solid lines). The results for DLVO theory are shown for comparison (dashed line). Data for amidine latex are shown in the top row, while for sulfate latex in the bottom row.

DOI: 10.1021/acs.jpcb.5b02556
J. Phys. Chem. B 2015, 119, 8184−8193

Table 3. Characteristics of Aggregation Rate Coefficients in Different Salt Solutions

		CCC (M)			normalized rate k/k_{Sm}		
particle	salt	exp[a]	non-DLVO[b]	DLVO[c]	exp[a]	non-DLVO[b]	DLVO[c]
AL	NaCl	0.106 ± 0.009	0.084	0.16	0.32 ± 0.02	0.54	0.54
	NaBr	0.078 ± 0.006	0.081	0.18	0.31 ± 0.03	0.54	0.54
	NaSCN	0.045 ± 0.004	0.034	0.042	0.33 ± 0.02	0.54	0.54
SL	NaCl	0.19 ± 0.01	0.23	1.3	0.35 ± 0.01	0.53	0.53
	KCl	0.21 ± 0.02	0.20	1.3	0.34 ± 0.01	0.53	0.53
	CsCl	0.18 ± 0.01	0.19	1.4	0.32 ± 0.03	0.53	0.53

[a]Experimental values with standard deviation. [b]Calculated values using DLVO theory with exponential attraction force. [c]Calculated values using DLVO theory without the exponential attraction force.

particles the same trend could be present, but the SCN^- ion behaves differently.

The value of the range of the non-DLVO attractive force q_s^{-1} of 0.49 nm is in agreement with other estimates of the same quantity.[15,16,24,43] The previously reported values situate in the range of 0.3−1 nm. The amplitude of this force also decreases with increasing salt level as shown in Figure 4b. Furthermore, this amplitude decreases for AL in the sequence Br^-, Cl^-, and SCN^-, while it increases for SL in the series Na^+, K^+, and Cs^+. The latter trend for SL can be simply explained. The cations are progressively less hydrated within the series, and therefore one expects that the strength of hydrophobic interactions increase. The sequence for the AL particle reflects a partial reversal of the Hofmeister series, and the strength of the additional attractive force is weakest for the most weakly hydrated anion, SCN^-. Eventually, the latex particle surface is even less hydrated than this anion, and the adsorption of this anion makes the surface less hydrophobic. Another explanation for the partial reversal of the Hofmeister series could be the coupling between ion correlations and specific interactions between the ions and the surface.[31]

These findings are in line with previous force measurements between latex particles. In particular, measurements involving carboxylated latex particles also show a jump-in at 2−3 nm, which cannot be explained by DLVO theory alone.[24] This additional attraction could be equally rationalized by an additional exponential attraction with a range of 0.4 nm and comparable strength. Earlier force measurements involving amidine latex particles did not show this additional attraction,[25] but later investigations with a new batch of similar amidine particles revealed the presence a similar short-ranged attraction as the one reported here.[39] Possibly, differences in the synthesis of earlier amidine latex sample or the presence of contaminations could be the reason for the different behavior.

Particle Aggregation Rates. Time-resolved light scattering techniques were used to measure the early stage particle aggregation rate. These results are presented as the stability ratios versus the salt concentration in Figure 5. All measurements show similar trends. At high salt concentration, the stability ratio is unity. This situation reflects the fast aggregation regime. With decreasing salt concentration, the stability ratio suddenly increases, indicating the slow aggregation regime. The transition point between the slow and fast aggregation is referred to as the critical coagulation concentration (CCC). The absolute aggregation rate in the fast regime was also measured. Since the rate depends on the viscosity, we eliminate this effect by reporting the rate in the fast regime relative to the Smoluchowski rate given in eq 17. Table 3 shows the CCCs and the normalized rates k_{fast}/k_{Sm}.

On the basis of the Hofmeister series, one expects that the CCC decreases for AL in the sequence Cl^-, Br^-, and SCN^- and for SL in the sequence Na^+, K^+, and Cs^+. The naive reason for such behavior is that the diffuse layer potential is decreasing in magnitude within the same sequence, since the ions adsorb more strongly to the particles surface in the same progression. One observes that this trend can be clearly identified for the AL particles, but the CCC is basically independent of the type of cation for the SL particles. The same lack of dependence on the type of monovalent cations was established for carboxyl latex particles due to their small surface charge.[29] On the other hand, the expected Hofmeister series was established for the CCC of more highly charged sulfate latex particles.[30] One further observes that the normalized absolute rates are independent of the type of counterions within the experimental error. However, this normalized rate depends weakly on the type of particle, and they are 0.32 ± 0.02 for AL particles and 0.34 ± 0.02 for SL. Somewhat smaller normalized aggregation rates in the range of 0.16−0.26 were reported for various smaller latex particles.[30] The reason for the difference between the particles used here and the smaller ones is currently unclear to us.

The solid lines shown in Figure 5 are predictions of the aggregation rates as deduced from the experimental force profiles discussed above. The salt dependence of the diffuse layer potentials and of the amplitudes of the short-ranged force was interpolated with simple empirical functions, which are shown as solid lines in Figure 4. The other parameters, such as the Hamaker constant and regulation parameters, were kept constant. This model provides an accurate description of the measured force profiles over the entire range of salt concentrations investigated. The interaction potential was then obtained from the force profile with eq 15, and this potential was then used in eq 14 to calculate the rate constant. The rate constant was converted to the stability ratio by means of eq 18. When only the DLVO potential is being used, and one neglects the short-ranged contribution, the resulting stability ratio is also shown for comparison. The calculated CCCs and the normalized absolute rates in the fast regime are given in Table 3.

The predicted stability ratios based on the direct force measurements agree reasonably well with the experiment. In particular, the position of the CCC is predicted quite well (see also Table 3). However, there are discrepancies in the slope of the stability plot in the slow regime. These discrepancies are more pronounced for AL than for SL. Similar discrepancies were reported earlier when measured stability ratios were compared with calculations.[1,44] These discrepancies might originate from the existence of lateral charge heterogeneities of the latex particles that are not included in the model. The presence of such heterogeneities is in line with minor small

DOI: 10.1021/acs.jpcb.5b02556
J. Phys. Chem. B 2015, 119, 8184−8193

variations in the force profiles for different pairs of particles and the observed discrepancies between electric surface potentials extracted from direct force measurements and electrophoresis. The effect of such heterogeneities was approximated by considering a distribution of surface potentials, and such calculations were able to explain the weaker salt dependence observed experimentally quite well.[44,45]

Comparison of the classical DLVO predictions with the ones where the additional attractive non-DLVO force is included reveals that the additional short-ranged force is essential to obtain the correct prediction of the CCC. The DLVO force profile alone leads to a too high CCC, which is in line with the presence of an additional attraction. The counterion specificity on the CCC turns out to be more complicated than what one might expect from the Hofmeister series, as it represents contributions from the DLVO double-layer force and the non-DLVO attraction. For the AL particles, the contribution from the short-ranged forces is the weakest for the SCN^- anion. In the fast regime, the DLVO theory predicts the normalized rates to be somewhat higher than the experimental values (Table 3). The additional attraction is unimportant in this regime. We suspect that this discrepancy between the experimental and calculated value is related to inaccuracies in the hydrodynamic function.

These results shed somewhat different light on the quantitative interpretation aggregation rate constants of latex particles with respect to previous work. In the past, two different approaches were pursued. Some authors advocated the validity of classical DLVO theory.[1,45,46] In this case, the Hamaker constant is being fitted to the CCC or the theoretical value is being used, leading to the apparently consistent values in the range of $(1.5 \pm 0.5) \times 10^{-20}$ J. While this approach is normally capable to capture the CCC reasonably well, it is flawed because of cancellation of opposing errors. On one hand, the Hamaker constant is actually substantially smaller (typically by a factor 4−10) due to roughness effects.[24,25,37] On the other hand, the additional short-ranged non-DLVO force must be considered. Clearly, this cancellation of errors cannot be easily identified without the availability of force curves between the latex particles. Other authors have considered the presence of additional forces, but without their direct measurement, their quantification remained problematic.[47,48]

CONCLUSION

The present study shows that aggregation rates of polystyrene latex particles can be reliably predicted based on directly measured force profiles. We investigate monovalent electrolytes with different counterions within the Hofmeister series. The main conclusion is that the interaction force profiles cannot be described by classical DLVO theory and that additional attractive non-DLVO force with a range of about 0.5 nm must be included. Moreover, Hamaker constants are about 2.6×10^{-21} J as obtained from direct force measurements by the AFM. This value is substantially smaller than the calculated values for smooth polystyrene due to surface roughness. The CCCs can only be correctly predicted when the additional attractive non-DLVO force and the appropriate Hamaker constant are included. Consideration of DLVO forces only leads to unrealistically high CCCs.

The effect of different counterion types within the Hofmeister series cannot be simply traced to the variation of a single quantity. When the counterions become more weakly hydrated, they increasingly adsorb to the hydrophobic surface, and they lower the magnitude of the surface charge. This effect is weak, especially for the sulfate latex, and it cannot be easily identified in the direct force measurements. The additional attractive force varies strongly with the salt level and type of ion, but we are unable to propose a simple interpretation of the observed trends. However, the observed CCC shifts within the Hofmeister series can be well quantified by the measured variation of the double layer and the short-ranged forces. On the other hand, the measured absolute aggregation rates are somewhat lower than calculated ones.

The dependence of the aggregation rate on the salt concentration observed experimentally in the slow regime is weaker than the one predicted by DLVO theory. The consideration of the attractive non-DLVO force weakens this dependence somewhat, but the prediction still remains far from the experiment. A likely interpretation of this discrepancy is due to the presence of surface charge heterogeneities. The presence of such heterogeneities is further suggested by the variation of the force profiles for different particle pairs and the discrepancies between the electric surface potentials obtained from direct force measurements and electrokinetics. The experimental aggregation rates constants in the fast regime are somewhat smaller than the predicted ones. At this point, we have little information concerning the origin of these discrepancies.

AUTHOR INFORMATION

Corresponding Author

*E-mail michal.borkovec@unige.ch (M.B.).

Present Address

F.J.M.R.-C.: Biocolloid and Fluid Physics Group, Applied Physics Department, Faculty of Sciences, University of Granada, 18071 Granada, Spain.

Notes

The authors declare no competing financial interest.

ACKNOWLEDGMENTS

This research was supported by the Swiss National Science Foundation, University of Geneva, COST Action CM1101, and the Swiss Secretariat of Education and Research.

REFERENCES

(1) Behrens, S. H.; Borkovec, M.; Schurtenberger, P. Aggregation in charge-stabilized colloidal suspensions revisited. *Langmuir* **1998**, *14*, 1951−1954.

(2) Wu, H.; Lattuada, M.; Sandkuhler, P.; Sefcik, J.; Morbidelli, M. Role of sedimentation and buoyancy on the kinetics of diffusion limited colloidal aggregation. *Langmuir* **2003**, *19*, 10710−10718.

(3) Fritz, G.; Schadler, V.; Willenbacher, N.; Wagner, N. J. Electrosteric stabilization of colloidal dispersions. *Langmuir* **2002**, *18*, 6381−6390.

(4) Hierrezuelo, J.; Sadeghpour, A.; Szilagyi, I.; Vaccaro, A.; Borkovec, M. Electrostatic stabilization of charged colloidal particles with adsorbed polyelectrolytes of opposite charge. *Langmuir* **2010**, *26*, 15109−15111.

(5) Ehrl, L.; Jia, Z.; Wu, H.; Lattuada, M.; Soos, M.; Morbidelli, M. Role of counterion association in colloidal stability. *Langmuir* **2009**, *25*, 2696−2702.

(6) Sandkuhler, P.; Lattuada, M.; Wu, H.; Sefcik, J.; Morbidelli, M. Further insights into the universality of colloidal aggregation. *Adv. Colloid Interface Sci.* **2005**, *113*, 65−83.

(7) Russel, W. B.; Saville, D. A.; Schowalter, W. R. *Colloidal Dispersions*; Cambridge University Press: Cambridge, 1989.

DOI: 10.1021/acs.jpcb.5b02556
J. Phys. Chem. B 2015, 119, 8184−8193

(8) Holthoff, H.; Schmitt, A.; Fernandez-Barbero, A.; Borkovec, M.; Cabrerizo-Vilchez, M. A.; Schurtenberger, P.; Hidalgo-Alvarez, R. Measurement of absolute coagulation rate constants for colloidal particles: Comparison of single and multiparticle light scattering techniques. *J. Colloid Interface Sci.* **1997**, *192*, 463−470.
(9) Xu, S. H.; Sun, Z. W. Progress in coagulation rate measurements of colloidal dispersions. *Soft Matter* **2011**, *7*, 11298−11308.
(10) Puertas, A.; Maroto, J. A.; de las Nieves, F. J. Theoretical description of the absorbance versus time curve in a homocoagulation process. *Colloids Surf., A* **1998**, *140*, 23−31.
(11) Popa, I.; Sinha, P.; Finessi, M.; Maroni, P.; Papastavrou, G.; Borkovec, M. Importance of charge regulation in attractive double-layer forces between dissimilar surfaces. *Phys. Rev. Lett.* **2010**, *104*, 228301.
(12) Israelachvili, J. *Intermolecular and Surface Forces*, 2nd ed.; Academic Press: London, 1992.
(13) Morag, J.; Dishon, M.; Sivan, U. The governing role of surface hydration in ion specific adsorption to silica: An AFM-based account of the Hofmeister universality and its reversal. *Langmuir* **2013**, *29*, 6317−6322.
(14) Kilpatrick, J. I.; Loh, S. H.; Jarvis, S. P. Directly probing the effects of ions on hydration forces at interfaces. *J. Am. Chem. Soc.* **2013**, *135*, 2628−2634.
(15) Tabor, R. F.; Wu, C.; Grieser, F.; Dagastine, R. R.; Chan, D. Y. C. Measurement of the hydrophobic force in a soft matter system. *J. Phys. Chem. Lett.* **2013**, *4*, 3872−3877.
(16) Donaldson, S. H.; Royne, A.; Kristiansen, K.; Rapp, M. V.; Das, S.; Gebbie, M. A.; Lee, D. W.; Stock, P.; Valtiner, M.; Israelachvili, J. Developing a general interaction potential for hydrophobic and hydrophilic interactions. *Langmuir* **2015**, *31*, 2051−2064.
(17) Tezak, B.; Matijevic, E.; Schulz, K. F. Coagulation of hydrophobic sols in statu nascendi 3. The influence of the ionic size and valency of the counterion. *J. Phys. Chem.* **1955**, *59*, 769−773.
(18) Lopez-Leon, T.; Jodar-Reyes, A. B.; Bastos-Gonzalez, D.; Ortega-Vinuesa, J. L. Hofmeister effects in the stability and electrophoretic mobility of polystyrene latex particles. *J. Phys. Chem. B* **2003**, *107*, 5696−5708.
(19) Schwierz, N.; Netz, R. R. Effective interaction between two ion-adsorbing plates: Hofmeister series and salting-in/salting-out phase diagrams from a global mean-field analysis. *Langmuir* **2012**, *28*, 3881−3886.
(20) Popa, I.; Gillies, G.; Papastavrou, G.; Borkovec, M. Attractive electrostatic forces between identical colloidal particles induced by adsorbed polyelectrolytes. *J. Phys. Chem. B* **2009**, *113*, 8458−8461.
(21) Gutsche, C.; Keyser, U. F.; Kegler, K.; Kremer, F. Forces between single pairs of charged colloids in aqueous salt solutions. *Phys. Rev. E* **2007**, *76*, 031403.
(22) Ducker, W. A.; Senden, T. J.; Pashley, R. M. Direct measurement of colloidal forces using an atomic force microscope. *Nature* **1991**, *353*, 239−241.
(23) Butt, H. J.; Cappella, B.; Kappl, M. Force measurements with the atomic force microscope: Technique, interpretation and applications. *Surf. Sci. Rep.* **2005**, *59*, 1−152.
(24) Montes Ruiz-Cabello, F. J.; Trefalt, G.; Csendes, Z.; Sinha, P.; Oncsik, T.; Szilagyi, I.; Maroni, P.; Borkovec, M. Predicting aggregation rates of colloidal particles from direct force measurements. *J. Phys. Chem. B* **2013**, *117*, 11853−11862.
(25) Sinha, P.; Szilagyi, I.; Montes Ruiz-Cabello, F. J.; Maroni, P.; Borkovec, M. Attractive forces between charged colloidal particles induced by multivalent ions revealed by confronting aggregation and direct force measurements. *J. Phys. Chem. Lett.* **2013**, *4*, 648−652.
(26) Behrens, S. H.; Borkovec, M. Electrostatic interaction of colloidal surfaces with variable charge. *J. Phys. Chem. B* **1999**, *103*, 2918−2928.
(27) Israelachvili, J. *Intermolecular and Surface Forces*, 3rd ed.; Academic Press: London, 2011.
(28) Jenkins, H. D. B.; Marcus, Y. Viscosity B-coefficients of ions in solution. *Chem. Rev.* **1995**, *95*, 2695−2724.
(29) Oncsik, T.; Trefalt, G.; Csendes, Z.; Szilagyi, I.; Borkovec, M. Aggregation of negatively charged colloidal particles in the presence of multivalent cations. *Langmuir* **2014**, *30*, 733−741.
(30) Oncsik, T.; Trefalt, G.; Borkovec, M.; Szilagyi, I. Specific ion effects on particle aggregation induced by monovalent salts within the Hofmeister series. *Langmuir* **2015**, *31*, 3799−3807.
(31) Forsman, J. Ion adsorption and lamellar-lamellar transitions in charged bilayer systems. *Langmuir* **2006**, *22*, 2975−2978.
(32) Borkovec, M.; Szilagyi, I.; Popa, I.; Finessi, M.; Sinha, P.; Maroni, P.; Papastavrou, G. Investigating forces between charged particles in the presence of oppositely charged polyelectrolytes with the multi-particle colloidal probe technique. *Adv. Colloid Interface Sci.* **2012**, *179−182*, 85−98.
(33) Sader, J. E.; Chon, J. W. M.; Mulvaney, P. Calibration of rectangular atomic force microscope cantilevers. *Rev. Sci. Instrum.* **1999**, *70*, 3967−3969.
(34) Hutter, J. L.; Bechhoefer, J. Calibration of atomic force microscope tips. *Rev. Sci. Instrum.* **1993**, *64*, 1868−1873.
(35) Holthoff, H.; Borkovec, M.; Schurtenberger, P. Determination of light-scattering form factors of latex particle dimers with simultaneous static and dynamic light scattering in an aggregating suspension. *Phys. Rev. E* **1997**, *56*, 6945−6953.
(36) O'Brien, R. W.; White, L. R. Electrophoretic mobility of a spherical colloidal particle. *J. Chem. Soc., Faraday Trans. 2* **1978**, *74*, 1607−1626.
(37) Elzbieciak-Wodka, M.; Popescu, M.; Montes Ruiz-Cabello, F. J.; Trefalt, G.; Maroni, P.; Borkovec, M. Measurements of dispersion forces between colloidal latex particles with the atomic force microscope and comparison with Lifshitz theory. *J. Chem. Phys.* **2014**, *140*, 104906.
(38) Bevan, M. A.; Prieve, D. C. Direct measurement of retarded van der Waals attraction. *Langmuir* **1999**, *15*, 7925−7936.
(39) Montes Ruiz-Cabello, F. J.; Trefalt, G.; Maroni, P.; Borkovec, M. Accurate predictions of forces in the presence of multivalent ions by Poisson-Boltzmann theory. *Langmuir* **2014**, *30*, 4551−4555.
(40) Montes Ruiz-Cabello, F. J.; Trefalt, G.; Maroni, P.; Borkovec, M. Electric double layer potentials and surface regulation properties measured by colloidal probe atomic force microscopy. *Phys. Rev. E* **2014**, *90*, 012301.
(41) Anderson, J. L. Effect of nonuniform zeta potential on particle movement in electric-fields. *J. Colloid Interface Sci.* **1985**, *105*, 45−54.
(42) Feick, J. D.; Velegol, D. Measurements of charge nonuniformity on polystyrene latex particles. *Langmuir* **2002**, *18*, 3454−3458.
(43) Kaggwa, G. B.; Nalam, P. C.; Kilpatrick, J. I.; Spencer, N. D.; Jarvis, S. P. Impact of hydrophilic/hydrophobic surface chemistry on hydration forces in the absence of confinement. *Langmuir* **2012**, *28*, 6589−6594.
(44) Schudel, M.; Behrens, S. H.; Holthoff, H.; Kretzschmar, R.; Borkovec, M. Absolute aggregation rate constants of hematite particles in aqueous suspensions: A comparison of two different surface morphologies. *J. Colloid Interface Sci.* **1997**, *196*, 241−253.
(45) Kihira, H.; Ryde, N.; Matijevic, E. Kinetics of heterocoagulation 2. The effect of the discreteness of surface charge. *J. Chem. Soc., Faraday Trans.* **1992**, *88*, 2379−2386.
(46) Schneider, C.; Hanisch, M.; Wedel, B.; Jusufi, A.; Ballauff, M. Experimental study of electrostatically stabilized colloidal particles: Colloidal stability and charge reversal. *J. Colloid Interface Sci.* **2011**, *358*, 62−67.
(47) Peula, J. M.; Fernandez-Barbero, A.; Hidalgo-Alvarez, R.; de las Nieves, F. J. Comparative study on the colloidal stability mechanisms of sulfonate latexes. *Langmuir* **1997**, *13*, 3938−3943.
(48) Hidalgo-Alvarez, R.; Martin, A.; Fernandez, A.; Bastos, D.; Martinez, F.; de las Nieves, F. J. Electrokinetic properties, colloidal stability and aggregation kinetics of polymer colloids. *Adv. Colloid Interface Sci.* **1996**, *67*, 1−118.

DOI: 10.1021/acs.jpcb.5b02556
J. Phys. Chem. B 2015, 119, 8184−8193

CHAPTER 6

Charging and Aggregation of Latex Particles in Aqueous Solutions of Ionic Liquids: Towards an Extended Hofmeister Series

Oncsik, T.; Desert, A.; Trefalt, G.; Borkovec, M.; Szilagyi, I.

Phys. Chem. Chem. Phys. **2016,** 18, 7511-7520

PCCP

PAPER

View Article Online
View Journal | View Issue

Cite this: *Phys. Chem. Chem. Phys.*, 2016, **18**, 7511

Charging and aggregation of latex particles in aqueous solutions of ionic liquids: towards an extended Hofmeister series

Tamas Oncsik, Anthony Desert,† Gregor Trefalt, Michal Borkovec and Istvan Szilagyi*

Received 24th November 2015,
Accepted 7th February 2016

DOI: 10.1039/c5cp07238g

www.rsc.org/pccp

The effect of ionic liquid (IL) constituents and other monovalent salts on the stability of polystyrene latex particles was studied by electrophoresis and light scattering in dilute aqueous suspensions. The surface charge and the aggregation rate were both sensitive to the type of ion leading to different critical coagulation concentration (CCC) values. Systematic variation of the type of IL cation and anion allows us to place these ions within the Hofmeister series. We find that the dicyanoamide anion should be placed between iodide and thiocyanate, while all 1-alkyl-3-methylimidazolium cations can be positioned to the left of the tetramethylammonium and ammonium ions. The hydrophobicity of the 1-butyl-1-methylpyrrolidinium ($BMPL^+$) ion is intermediate between 1-ethyl-3-methylimidazolium ($EMIM^+$) and 1-butyl-3-methylimidazolium ($BMIM^+$). With increasing alkyl chain length, the 1-alkyl-3-methylimidazolium cations adsorb on the latex particles very strongly, and 1-hexyl-3-methylimidazolium ($HMIM^+$) and 1-octyl-3-methylimidazolium ($OMIM^+$) lead to pronounced charge reversal and to an intermediate restabilization region.

1. Introduction

Ionic liquids (ILs) consist entirely of cations and anions, and these systems became the focus of intense research recently, mainly due to their uncommon properties, such as low vapour pressure or wide electrochemical window.[1–3] These aspects make ILs promising media in material science applications, including energy storage, extraction of minerals or biomolecules and electrodeposition.[2–8] An important class of materials in these applications are particle suspensions in ILs, as they are relevant in nanoparticle synthesis, catalysis, solar cells, or printing inks.[9–13] For example, numerous researchers have synthesized novel metal nanoparticles in ILs and they could relate the stability of these suspensions to their catalytic activity.[11,14–17] In this context, the stability of these suspensions plays a key role, and therefore particle aggregation in ILs was investigated recently.[18–23]

Such particle aggregation studies also focused on IL–water mixtures, and it was quickly realized that on the water-rich side the IL fully dissociates into ions, and that aqueous solutions of ILs closely resemble simple electrolytes.[19,20,24] A good understanding of the influence of the presence of water in ILs is further important, since most ILs contain water to a certain extent.

Studies of colloidal particle aggregation in simple electrolyte solutions have a long history, including the landmark development of the Derjaguin, Landau, Verwey, and Overbeek (DLVO) theory.[25] This theory predicts, in agreement with experiment, that the aggregation of charged colloidal particles is slow at low salt concentrations, while at higher concentrations it becomes rapid. The sharp transition between these two regimes occurs at the so-called critical coagulation concentration (CCC). The CCC represents an important characteristic concerning the destabilization power of a given salt, or more precisely of the constituent ions. A major achievement of the DLVO theory was to rationalize the Schulze–Hardy rule, which states that multivalent counterions strongly lower the CCC.[25–27]

However, the CCC can be also influenced by other ionic properties than their valence. A well-studied aspect represents the Hofmeister series, which orders ions according to their hydrophobicity.[28] This series was originally developed to account for the stabilization power of protein solutions, namely

$$CO_3^{2-} < SO_4^{2-} < H_2PO_4^- < F^- < Cl^- < Br^- < NO_3^- < I^- < ClO_4^- < SCN^-$$

Department of Inorganic and Analytical Chemistry, University of Geneva, 30 Quai Ernest-Ansermet, CH-1205 Geneva, Switzerland.
E-mail: istvan.szilagyi@unige.ch; Tel: +41 22 3796031
† Present address: École normale supérieure de Lyon, CNRS, Université de Lyon 1, Laboratoire de Chimie (UMR 5182), 46 Allée d'Italie, F-69364 Lyon, France.

$$N(CH_3)_4^+ < NH_4^+ < Cs^+ < Rb^+ < K^+ < Na^+ < Li^+ < Mg^{2+} < Ca^{2+}$$

The series indicates that negatively charged proteins form stable solutions even in the presence of high concentration of ions located on the right hand side, while the ions of the left hand side induce their precipitation already at low concentrations. Typically, particle aggregation follows the same series.[29–33] In particular, negatively charged particles follow the (above) direct Hofmeister series, whereby the ions on the left induce lower CCCs, while the ones on the right, higher ones. On the other hand, positively charged particles follow the (reversed) indirect Hofmeister series. Thereby, the ions on the left lead to higher CCCs, while the ones on the right, to lower ones. The role of divalent ions is more complicated, since their effect on particle aggregation is greatly influenced by the increased valence as described by the Schulze–Hardy rule.[25–27] Therefore, divalent ions are not considered here.

The position of an ion in the Hofmeister series can be qualitatively correlated with its hydrophobicity or its degree of solvation.[34,35] Hydrophilic and well-solvated anions, such as F^- or Cl^-, appear on the left, while hydrophobic and poorly hydrated anions, such as I^- or SCN^-, on the right. The cations are arranged in the opposite way. The hydrophilic cations, such as Li^+ or Na^+, appear on the right, while the hydrophobic ones, such as $N(CH_3)_4^+$ or NH_4^+, on the left. Many colloidal particles have a hydrophobic surface (*e.g.*, polystyrene latex) and the hydrophobic ions will adsorb more strongly to these surfaces than the hydrophilic ones. Therefore, CCC will be lower in the presence of hydrophobic counterions than in the presence of hydrophilic ones. Conversely, the CCC will be higher in the presence of hydrophobic coions than in the presence of hydrophilic ones. In the latter situation, however, electrostatic repulsion between the coions and the charged particle may lead to very weak adsorption, and these effects may not be noticeable. In general, the CCCs will decrease with increasing hydrophobicity of cations for negatively charged hydrophobic particles (direct Hofmeister series), while they will also decrease with decreasing hydrophobicity of cations for positively charged particles (indirect Hofmeister series). The reverse argumentation applies to hydrophilic particles (*e.g.*, silica). These trends have been confirmed by CCC measurements in numerous systems experimentally.[29,31,32,36–38]

In the present study, we investigate charging and aggregation of polystyrene latex particles in aqueous solutions of ILs. From the concentration dependence of the aggregation rate, one can extract the CCC, and the observed sequences in these quantities can be used to place the IL constituents into the Hofmeister series. The present investigation is related to an earlier study published by us, which focused on simple monovalent ions only.[29] That study used the same particles as the present one, thus facilitating a direct comparison of both. While ion specific effects on protein solubilisation and enzymatic activity in aqueous solutions of ILs were studied with a similar aim,[39–43] we believe that the determination of the CCC for uniform particles provides a reliable measure concerning the position of IL constituents within the Hofmeister series.

2. Experimental

2.1 Materials

Sulfate and amidine functionalized polystyrene latex particles were purchased from Invitrogen Corporation. The size and polydispersity of the particles were determined by interpreting static light scattering (SLS) data in stable suspensions using Mie theory.[44] Very good agreement was found with the values obtained in transmission electron microscopy (TEM) measurements by the manufacturer (Table 1). Dynamic light scattering (DLS) yielded slightly higher hydrodynamic radii, probably due to sample polydispersity. The same particles were used in our previous study,[29] where further properties of these particles are given. Prior to the experiments, the particles were dialyzed against ultrapure water until the conductivity remained constant and below 0.8 $\mu S\ cm^{-1}$. For the dialysis, cellulose ester and polyvinylidene fluoride membranes (Spectrum Rancho) were used for the sulfate and amidine modified latex suspensions, respectively. The particle concentrations in the dialyzed stock suspensions were determined by SLS, whereby a calibration curve of the scattering intensity obtained with the original particle suspensions of known concentration was used. Typical concentrations in these stock suspensions were 65 and 7 $g\ L^{-1}$ for sulfate and amidine particles, respectively. Ultrapure Milli-Q water (Millipore) was used throughout.

ILs used in this study were purchased from IoLiTech and they include 1-butyl-3-methylimidazolium as a cation with chloride (BMIM–Cl), bromide (BMIM–Br), dicyanoamide (BMIM–$N(CN)_2$) and thiocyanate (BMIM–SCN) ions, 1-butyl-1-methylpyrrolidinium ILs as the same anions (BMPL–Cl, BMPL–Br, BMPL–$N(CN)_2$ and BMPL–SCN) and the chloride salts of 3-methylimidazolium (MIM–Cl), 1-ethyl-3-methylimidazolium (EMIM–Cl), 1-hexyl-3-methylimidazolium (HMIM–Cl) and 1-octyl-3-methylimidazolium cations (OMIM–Cl) (Fig. 1). The ILs were dried under vacuum at 50 °C for one day and Karl-Fischer titration (Metrohm) was performed to determine their final water content, which was always below 1 $g\ L^{-1}$. The dried ILs were handled in a glove box. In some cases, mixing the ILs with water resulted in the formation of precipitates due to the presence of impurities, which could be detected by light scattering. These precipitates were removed by allowing the aqueous solutions to stand overnight and filtering with a 0.1 μm syringe filter (Millipore). Inorganic salts of analytical grade were purchased from Sigma Aldrich (NaCl, $NaN(CN)_2$ and NaSCN) and Fluka (NaBr). Their solutions were prepared by mixing the calculated amount of solid salt with ultrapure water. All stock solutions and water

Table 1 Characteristic size values of the sulfate and amidine functionalized polystyrene latex particles used in the present study

	Average radius (nm)			Polydispersity[c] (%)	
Latex particles	TEM[a]	SLS[b]	DLS[b]	TEM[a]	SLS[b]
Sulfate	265	263	278	2.0	3.8
Amidine	110	110	117	4.3	7.1

[a] Measured by the manufacturer. [b] Determined in stable suspensions. [c] Coefficient of variation.

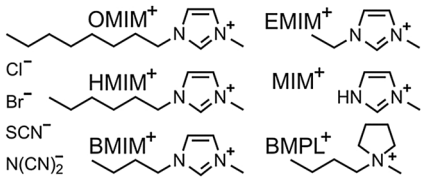

Fig. 1 Chemical structure of IL constituents used in the present study. The anions include chloride, bromide, thiocyanide and dicyanoamide with methylimidazolium, 1-alkyl-3-methylimidazolium and 1-butyl-1-methyl-pyrrolidinium as cations.

were adjusted to pH 4.0 with HCl and filtered prior to sample preparation. The measurements were carried out at a temperature of 25.0 ± 0.2 °C.

2.2 Electrophoresis

A ZetaSizer Nano ZS (Malvern) instrument was used to determine the electrophoretic mobility of the particles. During sample preparation, water was mixed with the appropriate volume of stock electrolyte or IL solutions to reach the desired concentration. The particles were then added from the concentrated stock suspension to get final particle concentrations of 5 mg L^{-1} in the case of amidine and 50 mg L^{-1} for the sulfate latex. The samples were equilibrated for one minute in the instrument prior to the measurements. Five repetitions were performed and averaged.

2.3 Particle aggregation

Time-resolved DLS was used to follow the aggregation process in aqueous particle suspensions. This technique has proved to be most suitable to determine aggregation rates of colloidal particles.[45–47] The instrument used was an ALV/CGS-3 goniometer (ALV) system, equipped with a He/Ne laser of a wavelength of 633 nm and an avalanche photodiode as a detector. Samples were prepared in borosilicate glass cuvettes (Kimble Chase). Before the measurements, the cuvettes were cleaned in piranha solution, which is a mixture of concentrated H_2SO_4 (Carlo Erba) and 30% H_2O_2 (Reactolab) in a volume ratio of 3 : 1. Subsequently, they were washed with water and dried in a dust-free oven at 60 °C. The particle concentrations were varied in the range of 2–10 mg L^{-1} for the amidine latex and 50–200 mg L^{-1} for the sulfate latex, which corresponds to the number concentration range of (0.3–2.0) × 10^{15} m^{-3}. To start the aggregation experiment, the particle stock suspension was injected into a cuvette containing the respective salt solution, and the sample was mixed and inserted in the light scattering system. The correlation function was recorded for 20 seconds at a scattering angle of 90° and the second-order cumulant fit was used to determine the hydrodynamic radius. The change in this quantity was followed in 50–100 subsequent runs. To probe the early stages of the aggregation, the hydrodynamic radius values never increased more than 40% in these experiments. This increase is an adequate compromise between good measurement accuracy and minor interferences of higher aggregates.[45,48] The apparent dynamic aggregation rate coefficient Δ was determined from the initial rate of increase

$$\Delta = \frac{1}{R_h(0)} \cdot \left.\frac{dR_h}{dt}\right|_{t\to 0} \quad (1)$$

where R_h is the hydrodynamic radius and t is the time. The measured apparent rates were then converted to absolute aggregation rate coefficients k by means of the relation

$$k = \frac{\Delta}{\Delta_{fast}} \cdot k_{fast} \quad (2)$$

where Δ_{fast} is the apparent dynamic aggregation rate coefficient in 1.0 M KCl solution, where the aggregation is in the fast regime. The absolute aggregation rate coefficient k_{fast} was previously determined using time-resolved simultaneous static and dynamic light scattering in 1.0 M KCl solutions. In these measurements, the apparent static rate coefficients were obtained from the initial change of the scattered intensity at several scattering angles and plotted against the apparent dynamic aggregation rates. A linear fit was performed on the data and the absolute aggregation rate coefficient was calculated from the intercept.[45] The resulting values were k_{fast} = (3.3 ± 0.2) × 10^{-18} m^3 s^{-1} for the sulfate latex and (3.0 ± 0.2) × 10^{-18} m^3 s^{-1} for the amidine latex.[29] The CCCs were determined from plots of the rate coefficient k *versus* the salt concentration, whereby straight lines were fitted to the experimental points in the slow and fast aggregation regimes. The uncertainty of the CCC determined by this method is about 10%.

2.4 Viscosity

A DV-II Pro viscometer (Brookfield) was used to measure the dynamic viscosities of the IL solutions. The concentration ranges of the monovalent electrolytes were chosen according to the concentrations investigated in the mobility and aggregation measurements, usually up to 1.0 M. In this range, the viscosities varied linearly with the concentration, and the values for the individual samples were obtained from a linear fit of the data.

3. Results and discussion

Surface charge and aggregation rates of sulfate and amidine modified polystyrene latex particles were investigated in the presence of ILs and monovalent electrolytes by electrophoresis and DLS. The principal aim of these experiments was to place some common IL constituents (Fig. 1) into the Hofmeister series. In addition, the influence of the alkyl chain length within the 1-alkyl-3-methylimidazolium series was investigated.

3.1 General trends

Electrophoretic mobilities and aggregation rates of sulfate and amidine latex particles were measured in different ionic environments. Initially, we investigated the effect of anions, namely Cl^-, Br^-, $N(CN)_2^-$ and SCN^-, in the presence of Na^+ as the cation (Fig. 2). Subsequently, the same anions were investigated in the presence of $BMIM^+$ (Fig. 3) and $BMPL^+$ (Fig. 4) as cations. In all systems, the electrophoretic mobility increases with the salt concentration for the sulfate particles and decreases for the amidine particles, sometimes resulting in an isoelectric point (IEP) and a subsequent weak charge reversal. These trends are mainly caused by the progressive screening through the

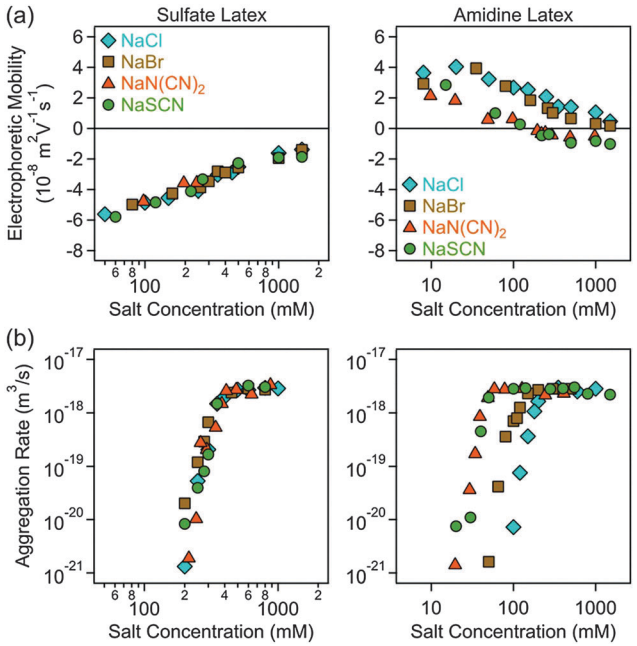

Fig. 2 Electrophoretic mobility (a) and absolute aggregation rate (b) for sulfate (left column) and amidine (right column) latex particles as a function of the salt concentration for different monovalent electrolytes of the sodium cation. The results with the Cl^-, Br^- and SCN^- ions have been already published earlier.[29]

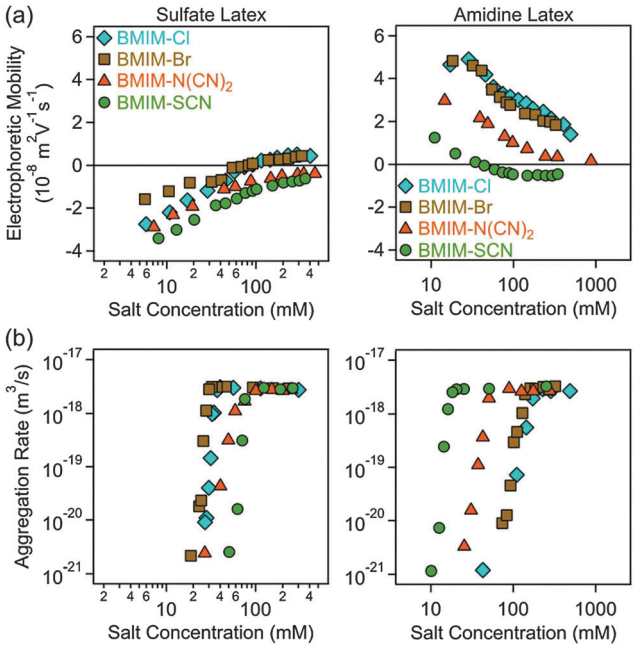

Fig. 3 Electrophoretic mobility (a) and absolute aggregation rate (b) values of sulfate (left column) and amidine (right column) latex particles as a function of the salt concentration in aqueous solutions of different ILs of the $BMIM^+$ cation.

electrolyte and simultaneous adsorption of the counterions. The particle aggregation rates increase rapidly with increasing salt concentration in the slow aggregation regime, and reach a

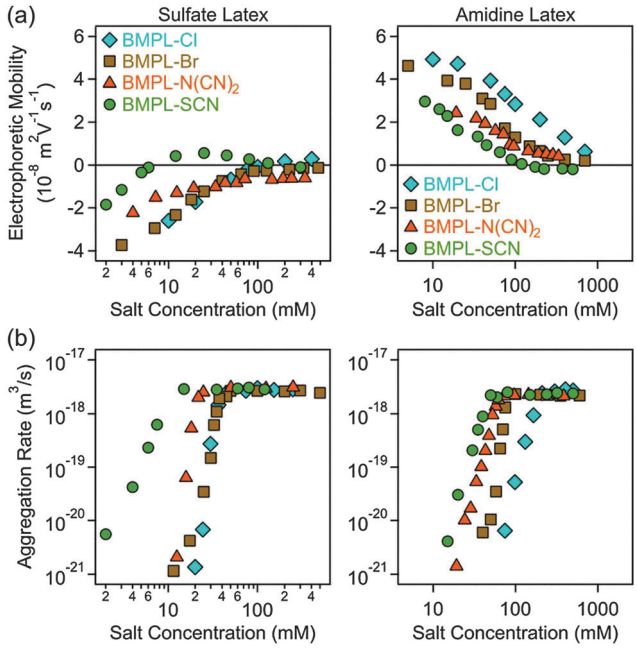

Fig. 4 Electrophoretic mobility (a) and absolute aggregation rate (b) values of sulfate (left column) and amidine (right column) latex particles as a function of the salt concentration for different ILs of the $BMPL^+$ cation.

constant value at higher concentrations in the fast aggregation regime. The CCC is located in the narrow transition zone between these two regimes. This behaviour is typical for charged colloidal particles dispersed in electrolyte solutions and can be predicted by the DLVO theory,[25] in some situations even quantitatively.[49,50] The characteristic influence of the type of ion present on the CCCs will be detailed below. No clear trends were observed in the dependencies of the aggregation rates on the salt concentration in the slow aggregation regimes.

3.2 Fast aggregation regime

The possible influence of the ion type on the fast aggregation rate coefficients measured above the CCCs was addressed. The ions investigated include Cl^-, Br^-, $N(CN)_2^-$ and SCN^- anions, and Na^+, $BMIM^+$ and $BMPL^+$ cations. As one must consider viscosity effects, the absolute rate coefficients in the fast aggregation regime were normalized by Smoluchowski's rate coefficient for diffusion controlled aggregation[51]

$$k_S = \frac{8k_B T}{3\eta} \quad (3)$$

where k_B is the Boltzmann constant, T is the temperature, and η is the dynamic viscosity of the electrolyte solution. The latter value was measured for the respective salt or IL solutions within the appropriate concentration range. No dependence of the normalized fast aggregation rate coefficients on the type of ion is observed, and one finds very similar normalized coefficients for both types of particles (Fig. 5a). Their values were $k_{fast}/k_s = 0.24 \pm 0.01$ and 0.24 ± 0.02 for the sulfate and amidine particles, respectively. These values are comparable to the ones reported earlier for the same particles in the presence of

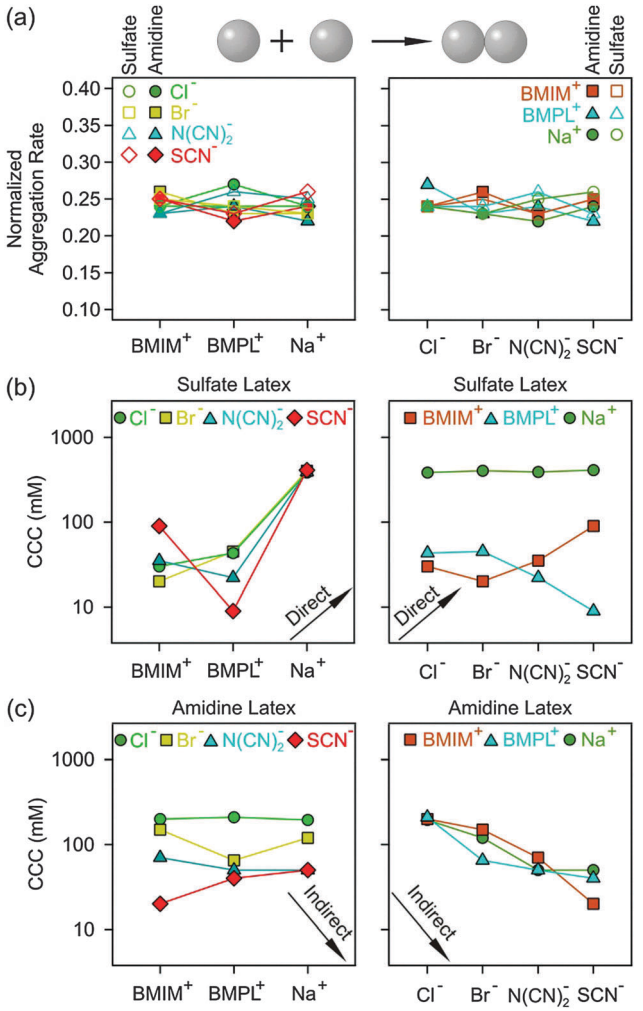

Fig. 5 Normalized fast aggregation rate coefficients (a) and CCC values for sulfate (b) and amidine (c) latex particles in the presence of different cations (left) and anions (right). The arrows indicate the expected trends according to the direct or indirect Hofmeister series. The lines are a guide to the eye.

several simple monovalent electrolytes, which were 0.26 ± 0.01 and 0.23 ± 0.01 for the sulfate and amidine latex, respectively.[29] These findings suggest that the attractive forces (*i.e.*, van der Waals and hydrophobic forces), which determine the fast aggregation rates, do not strongly depend on the type of ion present.

3.3 Ion specific effects

For negatively charged sulfate latex particles, there were no specific effects of the coions, provided Na^+ was used as the counterion. All the anions used, namely Cl^-, Br^-, $N(CN)_2^-$ and SCN^-, adsorb to the particle surface only weakly, and therefore the electrophoretic mobility (Fig. 2a), aggregation rates (Fig. 2b) and CCCs (Fig. 5b) remain the same within the experimental error. With the exception of the $N(CN)_2^-$ anion, the same observation was already reported earlier.[29] For the amidine latexes, the electrophoretic mobilities decrease with the salt level and their values at the same concentration decrease within the series Cl^-, Br^-, $N(CN)_2^-$, and SCN^- (Fig. 2a). The adsorption of $N(CN)_2^-$ and SCN^- ions results in an IEP and a charge reversal, suggesting that these ions are rather hydrophobic and that they adsorb on these particles strongly. Similar charge reversal has been observed with other less solvated monovalent ions.[29,34,52] The trend in the mobilities is also reflected in the CCCs (Fig. 2b and 5c). One observes that the CCC decreases in the same sequence as stated above, namely for Cl^- being the highest and for $N(CN)_2^-$ and SCN^- the lowest. This order can be explained as follows. The hydrophobic counterions, such as $N(CN)_2^-$ and SCN^-, adsorb strongly on the hydrophobic particle surface, leading to a decrease of the surface charge and to lower CCCs. On the other hand, the hydrophilic Cl^- counterion adsorbs weakly leading to highly charged particles, which also have higher CCCs. The observed sequence $Cl^- > Br^- > SCN^-$ reflects the expected indirect Hofmeister series, as reported before.[29] The new finding here is that $N(CN)_2^-$ behaves similar to SCN^-. This observation agrees with earlier protein precipitation experiments.[42]

When the $BMIM^+$ counterion was used, electrophoretic mobilities and aggregation rates of the negatively charged sulfate latex particles were strongly influenced by the type of coion (Fig. 3a and b). The magnitude of the mobility and of the CCCs (Fig. 5b) was significantly lower in the presence of $BMIM^+$ than for Na^+, confirming the considerable adsorption of the $BMIM^+$ counterions to the oppositely charged surface. In these systems, the mobilities and CCCs were sensitive to the type of coion, whereby the CCCs increase in the sequence $Br^- < N(CN)_2^- < SCN^-$. With the exception of the Cl^- ion, this trend reflects the expected direct Hofmeister series for negatively charged hydrophobic surfaces.[33] This finding is in line with recent colloidal probe experiments with hydrophilic silica particles in the presence of the $BMIM^+$ counterions, which reports the strength of the short-range attraction to increase in the sequence $Cl^- < N(CN)_2^- < SCN^-$.[24] Such attraction was significant at salt levels close to the CCCs, and therefore the CCC is expected to decrease in the same sequence as stated above in agreement with the indirect Hofmeister series for negatively charged hydrophilic particles.

A similar sequence of counterions was observed for the amidine particles as in the presence of Na^+. The mobilities (Fig. 3a) and the CCCs (Fig. 5c) decreased again in the sequence $Cl^- > Br^- > N(CN)_2^- > SCN^-$ in agreement with the indirect Hofmeister series for positively charged hydrophobic surfaces.[33] The electrophoretic mobilities remain positive for weakly adsorbing Cl^- and Br^- counterions, while the strongly adsorbing SCN^- ions induce a charge reversal. However, the IEP is situated at much lower concentration than for the Na^+ ions, which suggests that the hydrophobic $BMIM^+$ coion adsorbs to the particle surface, which in turn induces a stronger co-adsorption of SCN^- ions due to ion pair formation on the surface. The formation of ion pairs between cations and anions has been reported in various ILs.[53–57] The IL constituent ions adsorbed on the particle surface may also form ion pairs with the oppositely charged ions. The formation of such surface ion pairs will then influence the surface charge and also the CCC. For the $N(CN)_2^-$ anion, charge neutralization occurs as well, but the adsorption is not strong enough to reverse the particle charge.

For the $BMPL^+$ counterion, specific effects of coions were equally observed for sulfate latex particles. Similar electrophoretic mobilities were measured for Cl^- and Br^-, however, the presence of $N(CN)_2^-$ and SCN^- ions led to higher mobilities (Fig. 4a) and lower CCCs (Fig. 4b and 5b). This trend is opposite to the one observed for $BMIM^+$, and does not follow the anticipated direct Hofmeister series. This reversal of the Hofmeister series could be related to the counterion affinity to the oppositely charged particles and the extent of ion pairing on the surface. The observed trends in the CCCs indicate stronger ion pairing in the BMIM–SCN system than for BMPL–SCN. For the amidine particles, a weak charge reversal is again observed for the SCN^- ions, but the electrophoretic mobilities remain positive for the other counterions (Fig. 4a). The charge reversal occurred at higher concentration than in the $BMIM^+$ system, which may indicate either weaker $BMPL^+$ adsorption on the particle surface or weaker ion pair interactions between $BMPL^+$ and SCN^- ions. Nevertheless, the trends in both the charging and aggregation properties of the amidine particles in the presence of $BMPL^+$ and $BMIM^+$ counterions are similar. Accordingly, the mobilities at the same concentration as well as the CCCs follow $Cl^- > Br^- > N(CN)_2^- > SCN^-$ (Fig. 4a and 5c). This order is in agreement with the indirect Hofmeister series expected for positively charged hydrophobic particles.[31,33]

The observed trends for the cation dependence are summarized in Fig. 5b and c. For the sulfate latex, the presence of the $BMIM^+$ counterion leads to lower CCCs than $BMPL^+$ in the presence of simple anions, while the trend is reversed in the presence of hydrophobic $N(CN)_2^-$ and SCN^- anions. This reversal is probably related to the variable extent of ion pair formation in these systems. No trend with CCCs was observed for amidine latex particles when the coions were varied.

Let us now compare the present results with the ones of an earlier study, which investigated the CCCs of exactly the same particles.[29] In particular, various anions in the presence of Na^+ and various cations in the presence of Cl^- were investigated. Combining the present results with the ones from that study[29] enables us to place the IL constituents into the established Hofmeister series (Fig. 6). For sulfate latex particles, the extended Hofmeister series becomes

$$BMIM^+ < BMPL^+ < N(CH_3)_4^+ < NH_4^+ < Cs^+ < K^+ < Na^+ < Li^+$$

where the hydrophilic Na^+ ions typically lead to the highest CCC, while the hydrophobic IL constituents to lower CCC. $BMIM^+$ and $BMPL^+$ have to be positioned on the left hand side of the series, indicating that they are even more hydrophobic than the $N(CH_3)_4^+$ counterion. The sulfate particles show no effects of coions. The CCCs of amidine latex particles in the presence of different counterions decrease according to the indirect Hofmeister series as

$$H_2PO_4^- > F^- > Cl^- > Br^- > NO_3^- > N(CN)_2^- > SCN^-$$

The $N(CN)_2^-$ counterion has to be placed between NO_3^- and SCN^-. The $BMIM^+$ and $BMPL^+$ coions have again no influence on the CCC of the amidine particles. However, the $N(CH_3)_4^+$ and NH_4^+ coions lead to systematically lower CCCs, probably, due to specific interactions with the amidine groups.

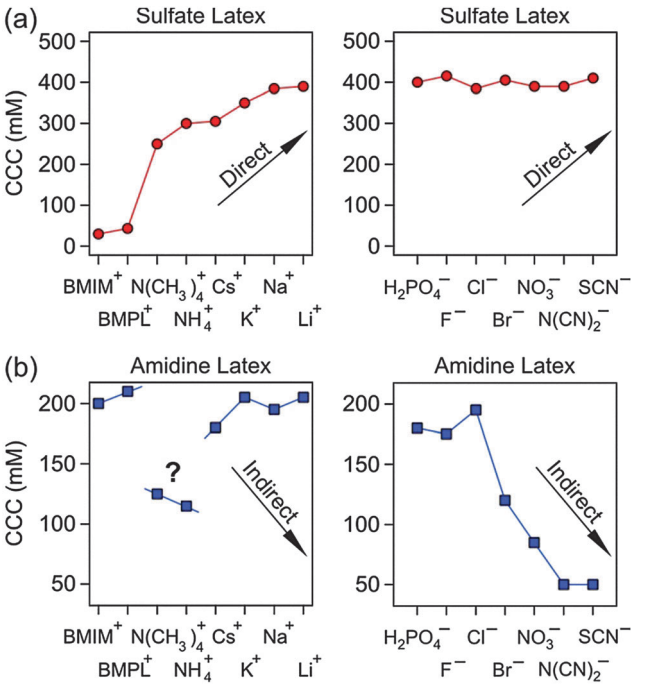

Fig. 6 CCC values for sulfate (a) and amidine (b) latex particles in the presence of different cations (left) and anions (right). The arrows indicate the expected trends according to the direct or indirect Hofmeister series. The lines are a guide to the eye.

3.4 Effect of the alkyl chain length

As shown in the previous section, the hydrophobic $BMIM^+$ counterions strongly adsorb on the negatively charged sulfate latex particles and thus modify the particle charge and their CCCs (Fig. 3a and 5b). To further investigate the effects of cation hydrophobicity on charging and aggregation of these particles, we have studied electrophoretic mobilities and aggregation rates of sulfate latex particles in the presence of 1-alkyl-3-methylimidazolium counterions, namely for MIM^+, $EMIM^+$, $BMIM^+$, $HMIM^+$ and $OMIM^+$. Their hydrophobicity increases from the left to the right due to the increasing length of the alkyl chains (Fig. 1). In all cases, the Cl^- coion was used.

At sufficiently low concentrations, the electrophoretic mobilities increase with the concentration (Fig. 7a). In the presence of MIM^+ and $EMIM^+$, the particles remained negatively charged within the entire range investigated. This increase is primarily due to screening by the increasing salt level, but the adsorption of these ions to the particle surface also contributes to this trend. However, adsorption of these counterions becomes more pronounced for longer aliphatic chains and leads to slight charge reversal for $BMIM^+$. The adsorption of $HMIM^+$ and $OMIM^+$ counterions becomes even more important and induces charge neutralization and a significant charge reversal. At higher concentrations, the mobilities decrease due to screening, as particularly evident in the presence of the $OMIM^+$ cation. A similar charge reversal was already reported for negatively charged kaolinite particles in OMIM–Cl solutions.[58]

The charging behaviour is well-reflected in the respective aggregation rates. For the $BMIM^+$, $EMIM^+$ and MIM^+ cations

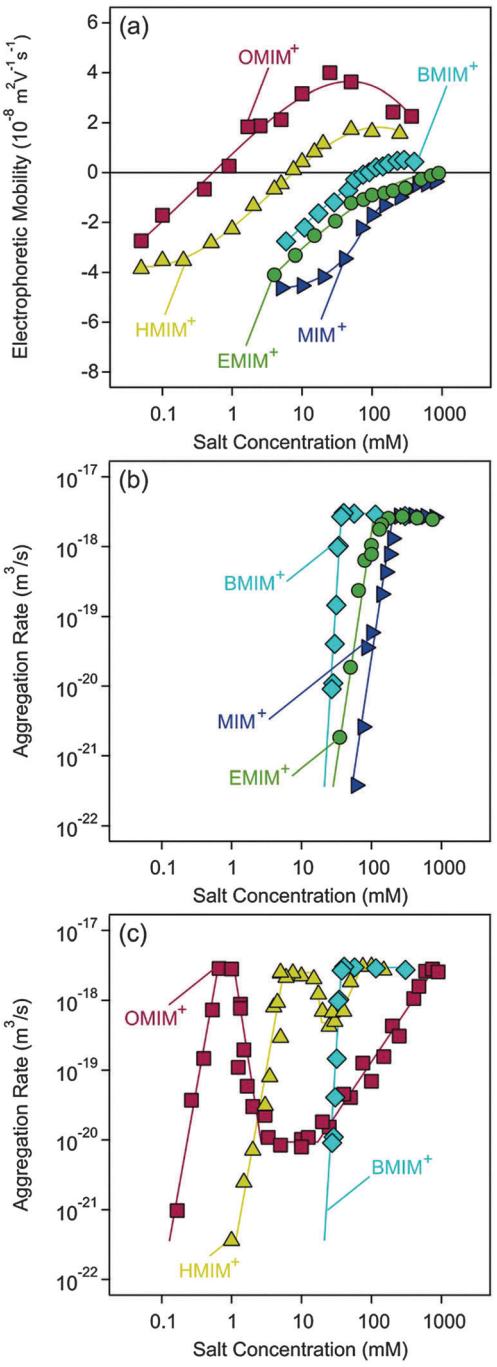

Fig. 7 Electrophoretic mobilities (a) and aggregation rate coefficients (b and c) of sulfate latex particles in the presence of ILs composed of the chloride anion and the 1-alkyl-3-methylimidazolium cation of different alkyl chains. The lines are a guide to the eye.

with short alkyl chains, the aggregation rates (Fig. 7b) show the classical behaviour of slow aggregation at low concentrations and rapid aggregation at high concentrations, with a CCC in between these two regimes. This situation is similar to the systems discussed above. The CCCs decrease systematically with increasing alkyl chain length, which is caused by the increasing adsorption strength due to increasing length of the alkyl chain.

However, the dependence of the aggregation rate on the IL concentration is notably different in the presence of the $OMIM^+$ counterion (Fig. 7c). The aggregation rates are small at low IL concentrations, and they go through a maximum near the IEP. The rate constant at the maximum corresponds to its value in the fast aggregation regime. Upon increasing the IL concentration further, one observes a decrease of the aggregation rate. The rate passes through a minimum and increases again to reach the value in the fast aggregation regime. A similar dependence is observed for the $HMIM^+$ counterion, albeit the intermediate minimum is much less pronounced. This shallower minimum is due to the weaker charge reversal of $HMIM^+$ as revealed by the electrophoresis. Clearly, $OMIM^+$ adsorbs most strongly, and the adsorption strength decreases with decreasing chain length.

One might suspect that the formation of micelles could be relevant in these systems, especially for the cations with a longer apolar alkyl chain. The CMC of OMIM–Cl was reported to be 220 mM and for HMIM–Cl 900 mM.[59,60] The latter value is at the end of the concentration range used in the present study. Therefore, the formation of micelles does not play any role in the adsorption and particle aggregation mechanism in the HMIM–Cl system. For the OMIM–Cl system, the CMC falls into the upper range of the destabilization due to charge screening by the chloride counterions. Again, micellization plays a minor role.

The observed dependence of the aggregation rate on the concentration of 1-alkyl-3-methylimidazolium can be interpreted in terms of a succession of three CCCs. The first CCC occurs at low concentration during the transition from the slow to fast regime. The second CCC is located after the maximum in the IL concentration, whereby the system undergoes a transition from the fast to slow regime. The third CCC is situated at the highest concentrations after the minimum in the aggregation rate, when the aggregation becomes fast again. Comparing the location of the CCCs with the electrophoretic mobilities in the same concentration ranges, one can realize that the first CCC is caused by charge neutralization, the second is connected with the charge reversal process, while the third CCC is due to the screening effect of the counterions on the surface charge.

A stability map of the CCCs *versus* the type of counterion of different chain lengths summarizes this characteristic behaviour well (Fig. 8). Three CCCs are observed for $HMIM^+$ and $OMIM^+$ counterions, while only one CCC is found for MIM^+, $EMIM^+$ and $BMIM^+$. Therefore, this map shows two regions where the dispersions are stable, meaning that the particle aggregation is significantly slower than that in the case of fast aggregation. That region is indicated as unstable. The first stability region in the lower left corner corresponds to the regular stabilization due to the negative charge of the latex particles. The second region on the right hand side corresponds to the positively charged particles after charge reversal, which is induced by the strong adsorption of the less solvated IL cations. The unstable region in the upper part of the map is due to destabilization and screening at high salt concentrations. The narrow unstable channel in the lower right part of the map is due to the destabilization and charge neutralization at the IEP. The first CCC values at low IL concentration in the presence of 1-alkyl-3-methylimidazolium counterions

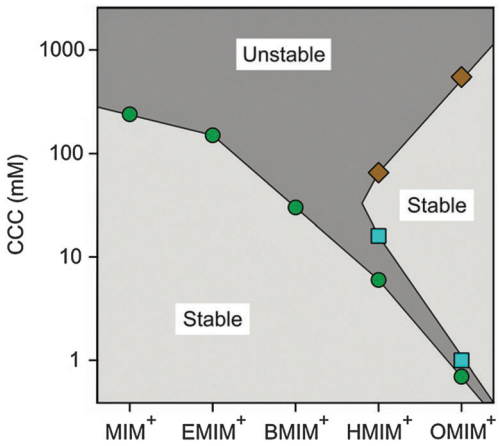

Fig. 8 Stability map including CCC values for sulfate latex particles in the presence of the 1-alkyl-3-methylimidazolium cation based ILs of different alkyl chain lengths with the chloride anion. The circles indicate the first CCC, squares show the second CCC and diamonds refer to the third CCC.

reflect the decreasing chain length and increasing hydrophilicity within the series

$$OMIM^+ < HMIM^+ < BMIM^+ < EMIM^+ < MIM^+$$

On the left hand side of the series, one finds the hydrophobic cations with a longer alkyl chain. They adsorb more strongly to the particle surface, and induce lower CCCs. Those on the right hand side are more hydrophilic and feature a shorter alkyl chain. The latter counterions adsorb more weakly, and lead to higher CCCs. This trend is reminiscent to previous findings for oxide and silver halide particles in the presence of ionic surfactants of variable chain lengths, whereby the IEP or the first CCC shifts towards smaller concentrations with increasing alkyl chain length.[61–64] In addition, the restabilization occurred in all systems containing surfactants with an octyl chain or longer. A subsequent destabilization at high concentrations was also observed, quite in analogy to $OMIM^+$.[64] Enzymatic activity reflects the same order, namely, the proteins lose their activity in the presence of $HMIM^+$ at lower concentration than for $EMIM^+$.[39,40]

Similar stability behaviour was reported for the aggregation of latex particles in the presence of multivalent ions or short-chain oligoamines.[65,66] In particular, the similarity to the system with the oligoamines is striking, and deservers further discussion.[66] These authors have studied electrophoresis and particle aggregation rates for negatively charged sulfate latex particles in the presence of aliphatic oligoamines with the structural formula $H_2NCH_2CH_2(NHCH_2CH_2)_nNH_2$ for n = 0, 1, 2, and 4. Under the mildly acidic conditions used, these oligoamines form multivalent cations. The concentration dependence of electrophoretic mobilities and of the aggregation rate was very similar to the one shown in Fig. 7, and shows an analogous trend with the increasing chain length. Moreover, the stability map of the CCCs *versus* the chain length looks surprisingly similar to Fig. 8. Due to these analogies, one might suspect in these two systems that the underlying mechanisms leading to charge reversal and destabilization are similar. The hydrophobic interaction will become more important with increasing chain length and this aspect might be responsible in both systems for the increased extent of adsorption, which would then induce similar patterns in the charging behaviour and aggregation rates. Moreover, these oligoamines are only partially ionized and their charge could be further reduced by complexation of counterions and ion condensation effects. The interesting consequence of this hypothesis is that the multivalent nature of the longer-chain oligoamines becomes secondary and their increasing hydrophobicity determines the adsorption of these molecules and as a consequence, the aggregation of these particles.

4. Conclusions

The effect of simple monovalent ions and water-miscible ILs on the surface charge and aggregation of polystyrene latex particles was investigated by electrophoresis and time-resolved light scattering in dilute aqueous solutions. From studies performed on negatively charged sulfate latex particles, the Hofmeister series for the cations may be extended as

$$OMIM^+ < HMIM^+ < BMIM^+ < BMPL^+ < EMIM^+ < MIM^+ < N(CH_3)_4^+ < NH_4^+ < Cs^+ < K^+ < Na^+ < Li^+$$

The hydrophobic ions shown on the left hand side lead to the lowest CCCs. The most hydrophobic ones, such as $OMIM^+$ and $HMIM^+$, show more pronounced charge reversal and a subsequent restabilization. The left hand side of the series reflects the known trend of decreasing hydrophilicity with increasing chain length in surfactant solutions. For amidine latex particles, we conclude that the Hofmeister series for the anions should be extended as

$$Cl^- > Br^- > N(CN)_2^- > SCN^-$$

whereby the hydrophobic ions are shown on the right hand side and they lead to the lowest CCCs.

Acknowledgements

The present research was supported by the Swiss National Science Foundation, the University of Geneva and the COST Action CM1206.

References

1 J. P. Hallett and T. Welton, *Chem. Rev.*, 2011, **111**, 3508–3576.
2 A. P. Abbott and K. J. McKenzie, *Phys. Chem. Chem. Phys.*, 2006, **8**, 4265–4279.
3 M. Armand, F. Endres, D. R. MacFarlane, H. Ohno and B. Scrosati, *Nat. Mater.*, 2009, **8**, 621–629.
4 A. Izgorodin, R. Hocking, O. Winther-Jensen, M. Hilder, B. Winther-Jensen and D. R. MacFarlane, *Catal. Today*, 2013, **200**, 36–40.
5 N. V. Plechkova and K. R. Seddon, *Chem. Soc. Rev.*, 2008, **37**, 123–150.

6 E. G. Garcia, A. K. Ressmann, P. Gaertner, R. Zirbs, R. L. Mach, R. Krska, K. Bica and K. Brunner, *Anal. Bioanal. Chem.*, 2014, **406**, 7773–7784.
7 R. Zirbs, K. Strassl, P. Gaertner, C. Schroder and K. Bica, *RSC Adv.*, 2013, **3**, 26010–26016.
8 R. Hayes, G. G. Warr and R. Atkin, *Chem. Rev.*, 2015, **115**, 6357–6426.
9 A. Podgorsek, A. S. Pensado, C. C. Santini, M. F. C. Gomes and A. A. H. Padua, *J. Phys. Chem. C*, 2013, **117**, 3537–3547.
10 P. S. Campbell, C. C. Santini, D. Bouchu, B. Fenet, K. Philippot, B. Chaudret, A. A. H. Padua and Y. Chauvin, *Phys. Chem. Chem. Phys.*, 2010, **12**, 4217–4223.
11 M. Anouti and J. Jacquemin, *Colloids Surf., A*, 2014, **445**, 1–11.
12 P. Wang, S. M. Zakeeruddin, P. Comte, I. Exnar and M. Gratzel, *J. Am. Chem. Soc.*, 2003, **125**, 1166–1167.
13 Z. Zolek-Tryznowska, J. Izdebska and M. Golazbek, *Color. Technol.*, 2014, **130**, 314–318.
14 E. Vanecht, K. Binnemans, S. Patskovsky, M. Meunier, J. W. Seo, L. Stappers and J. Fransaer, *Phys. Chem. Chem. Phys.*, 2012, **14**, 5662–5671.
15 K. Richter, A. Birkner and A. V. Mudring, *Phys. Chem. Chem. Phys.*, 2011, **13**, 7136–7141.
16 L. L. Lazarus, C. T. Riche, N. Malmstadt and R. L. Brutchey, *Langmuir*, 2012, **28**, 15987–15993.
17 G. Salas, A. Podgorsek, P. S. Campbell, C. C. Santini, A. A. H. Padua, M. F. C. Gomes, K. Philippot, B. Chaudret and M. Turmine, *Phys. Chem. Chem. Phys.*, 2011, **13**, 13527–13536.
18 C. Guibert, V. Dupuis, J. Fresnais and V. Peyre, *J. Colloid Interface Sci.*, 2015, **454**, 105–111.
19 J. A. Smith, O. Werzer, G. B. Webber, G. G. Warr and R. Atkin, *J. Phys. Chem. Lett.*, 2010, **1**, 64–68.
20 I. Szilagyi, T. Szabo, A. Desert, G. Trefalt, T. Oncsik and M. Borkovec, *Phys. Chem. Chem. Phys.*, 2014, **16**, 9515–9524.
21 K. Ueno, A. Inaba, M. Kondoh and M. Watanabe, *Langmuir*, 2008, **24**, 5253–5259.
22 J. Nordstrom, L. Aguilera and A. Matic, *Langmuir*, 2012, **28**, 4080–4085.
23 M. Mamusa, J. Siriex-Plenet, F. Cousin, E. Dubois and V. Peyrea, *Soft Matter*, 2014, **10**, 1097–1101.
24 V. Valmacco, G. Trefalt, P. Maroni and M. Borkovec, *Phys. Chem. Chem. Phys.*, 2015, **17**, 16553–16559.
25 D. F. Evans and H. Wennerstrom, *The Colloidal Domain*, John Wiley, New York, 1999.
26 T. Oncsik, G. Trefalt, Z. Csendes, I. Szilagyi and M. Borkovec, *Langmuir*, 2014, **30**, 733–741.
27 C. Schneider, M. Hanisch, B. Wedel, A. Jusufi and M. Ballauff, *J. Colloid Interface Sci.*, 2011, **358**, 62–67.
28 P. Lo Nostro and B. W. Ninham, *Chem. Rev.*, 2012, **112**, 2286–2322.
29 T. Oncsik, G. Trefalt, M. Borkovec and I. Szilagyi, *Langmuir*, 2015, **31**, 3799–3807.
30 D. F. Parsons, M. Bostrom, P. Lo Nostro and B. W. Ninham, *Phys. Chem. Chem. Phys.*, 2011, **13**, 12352–12367.
31 T. Lopez-Leon, M. J. Santander-Ortega, J. L. Ortega-Vinuesa and D. Bastos-Gonzalez, *J. Phys. Chem. C*, 2008, **112**, 16060–16069.
32 J. M. Peula-Garcia, J. L. Ortega-Vinuesa and D. Bastos-Gonzalez, *J. Phys. Chem. C*, 2010, **114**, 11133–11139.
33 N. Schwierz, D. Horinek and R. R. Netz, *Langmuir*, 2010, **26**, 7370–7379.
34 C. Calero, J. Faraudo and D. Bastos-Gonzalez, *J. Am. Chem. Soc.*, 2011, **133**, 15025–15035.
35 M. Lund, R. Vacha and P. Jungwirth, *Langmuir*, 2008, **24**, 3387–3391.
36 F. J. M. Ruiz-Cabello, G. Trefalt, T. Oncsik, I. Szilagyi, P. Maroni and M. Borkovec, *J. Phys. Chem. B*, 2015, **119**, 8184–8193.
37 F. Dumont, J. Warlus and A. Watillon, *J. Colloid Interface Sci.*, 1990, **138**, 543–554.
38 R. Tian, G. Yang, H. Li, X. D. Gao, X. M. Liu, H. L. Zhu and Y. Tang, *Phys. Chem. Chem. Phys.*, 2014, **16**, 8828–8836.
39 C. Lange, G. Patil and R. Rudolph, *Protein Sci.*, 2005, **14**, 2693–2701.
40 Z. Yang, *J. Biotechnol.*, 2009, **144**, 12–22.
41 C. Sanfilippo, N. D'Antona and G. Nicolosi, *Biotechnol. Lett.*, 2004, **26**, 1815–1819.
42 D. Constantinescu, H. Weingartner and C. Herrmann, *Angew. Chem., Int. Ed.*, 2007, **46**, 8887–8889.
43 K. Fujita, D. R. MacFarlane and M. Forsyth, *Chem. Commun.*, 2005, 4804–4806.
44 M. I. Mishchenko, L. D. Travis and A. A. Lacis, *Scattering, Absorption, and Emission of Light by Small Particles*, University Press, Cambridge, 2002.
45 H. Holthoff, S. U. Egelhaaf, M. Borkovec, P. Schurtenberger and H. Sticher, *Langmuir*, 1996, **12**, 5541–5549.
46 K. L. Chen, S. E. Mylon and M. Elimelech, *Langmuir*, 2007, **23**, 5920–5928.
47 A. Zaccone, H. Wu, M. Lattuada and M. Morbidelli, *J. Phys. Chem. B*, 2008, **112**, 1976–1986.
48 M. Schudel, S. H. Behrens, H. Holthoff, R. Kretzschmar and M. Borkovec, *J. Colloid Interface Sci.*, 1997, **196**, 241–253.
49 S. H. Behrens, M. Borkovec and P. Schurtenberger, *Langmuir*, 1998, **14**, 1951–1954.
50 M. Kobayashi, M. Skarba, P. Galletto, D. Cakara and M. Borkovec, *J. Colloid Interface Sci.*, 2005, **292**, 139–147.
51 M. Elimelech, J. Gregory, X. Jia and R. A. Williams, *Particle Deposition and Aggregation: Measurement, Modeling, and Simulation*, Butterworth-Heinemann Ltd., Oxford, 1995.
52 T. Lopez-Leon, J. L. Ortega-Vinuesa and D. Bastos-Gonzalez, *ChemPhysChem*, 2012, **13**, 2382–2391.
53 A. Stoppa, J. Hunger, G. Hefter and R. Buchner, *J. Phys. Chem. B*, 2012, **116**, 7509–7521.
54 R. Sadeghi and N. Ebrahimi, *J. Phys. Chem. B*, 2011, **115**, 13227–13240.
55 M. Bester-Rogac, A. Stoppa, J. Hunger, G. Hefter and R. Buchner, *Phys. Chem. Chem. Phys.*, 2011, **13**, 17588–17598.
56 M. Bester-Rogac, J. Hunger, A. Stoppa and R. Buchner, *J. Chem. Eng. Data*, 2011, **56**, 1261–1267.
57 H. K. Stassen, R. Ludwig, A. Wulf and J. Dupont, *Chem. – Eur. J.*, 2015, **21**, 8324–8335.

58 M. Markiewicz, W. Mrozik, K. Rezwan, J. Thoming, J. Hupka and C. Jungnickel, *Chemosphere*, 2013, **90**, 706–712.
59 U. Preiss, C. Jungnickel, J. Thoming, I. Krossing, J. Luczak, M. Diedenhofen and A. Klamt, *Chem. – Eur. J.*, 2009, **15**, 8880–8885.
60 J. Luczak, J. Hupka, J. Thoming and C. Jungnickel, *Colloids Surf., A*, 2008, **329**, 125–133.
61 D. W. Fuerstenau and M. Colic, *Colloids Surf., A*, 1999, **146**, 33–47.
62 A. Watanabe, *Bull. Inst. Chem. Res., Kyoto Univ.*, 1960, **38**, 179–215.
63 L. Liang and J. J. Morgan, *Aquat. Sci.*, 1990, **52**, 32–55.
64 R. H. Ottewill and M. C. Rastogi, *Trans. Faraday Soc.*, 1960, **56**, 866.
65 P. Sinha, I. Szilagyi, F. J. M. Ruiz-Cabello, P. Maroni and M. Borkovec, *J. Phys. Chem. Lett.*, 2013, **4**, 648–652.
66 I. Szilagyi, A. Polomska, D. Citherlet, A. Sadeghpour and M. Borkovec, *J. Colloid Interface Sci.*, 2013, **392**, 34–41.

CHAPTER 7

Particle Aggregation Mechanisms in Ionic Liquids

Szilagyi, I.; Szabo, T.; Desert, A.; Trefalt, G.; Oncsik, T.; Borkovec, M.

Phys. Chem. Chem. Phys. **2014,** 16, 9515-9524.

PCCP

PAPER

View Article Online
View Journal | View Issue

Particle aggregation mechanisms in ionic liquids†

Cite this: *Phys. Chem. Chem. Phys.*, 2014, **16**, 9515

Istvan Szilagyi, Tamas Szabo, Anthony Desert, Gregor Trefalt, Tamas Oncsik and Michal Borkovec*

Aggregation of sub-micron and nano-sized polystyrene latex particles was studied in room temperature ionic liquids (ILs) and in their water mixtures by time-resolved light scattering. The aggregation rates were found to vary with the IL-to-water molar ratio in a systematic way. At the water side, the aggregation rate is initially small, but increases rapidly with increasing IL content, and reaches a plateau value. This behaviour resembles simple salts, and can be rationalized by the competition of double-layer and van der Waals forces as surmised by the classical theory of Derjaguin, Landau, Verwey, and Overbeek (DLVO). At the IL side, aggregation slows down again. Two generic mechanisms could be identified to be responsible for the stabilization in ILs, namely viscous stabilization and solvation stabilization. Viscous stabilization is important in highly viscous ILs, as it originates from the slowdown of the diffusion controlled aggregation due to the hindrance of the diffusion in a viscous liquid. The solvation stabilization mechanism is system specific, but can lead to a dramatic slowdown of the aggregation rate in ILs. This mechanism is related to repulsive solvation forces that are operational in ILs due to the layering of the ILs close to the surfaces. These two stabilization mechanisms are suspected to be generic, as they both occur in different ILs, and for particles differing in surface functionalities and size.

Received 24th February 2014,
Accepted 4th April 2014

DOI: 10.1039/c4cp00804a

www.rsc.org/pccp

Introduction

Ionic liquids (ILs) have unusual properties, including high chemical stability, low vapour pressure, and a wide electrochemical window.[1–3] Their properties can also be systematically varied through the nature of their ionic constituents. Due to these unique aspects, ILs are developing into promising media for material science applications.[4–6] Among those, particle suspensions in ILs represent an important class of media, as they are relevant in catalysis,[7–11] solar cell development,[12] and mirror design.[13] Such suspensions are also obtained during the synthesis of metal,[14–16] oxide,[17,18] or latex[19] particles in ILs. The stability of such suspensions, or their aggregation state, can be decisive. The presence of aggregates further determines the suspension rheology and controls the formation of particle assemblies, colloidal glasses, and gels.[20–22] Various reports indicate that the nature of ILs and of the particles affects their aggregation state strongly. Silica particles were reported to be unstable in imidazolium-based ILs, while their stabilization could be achieved by surface functionalization.[23] Metal and silica particles were reported to be stable in dry ILs, while small amounts of water induced aggregation.[15,16,24] The presence of alkali metal cations was shown to stabilize particles in ILs.[25] However, this knowledge remains sketchy, and a mechanistic picture of particle aggregation in ILs is lacking.

The Derjaguin, Landau, Verwey, and Overbeek (DLVO) theory was developed to explain the stability of aqueous particle suspensions.[21,23,26,27] This theory represents the interaction potential as a superposition of van der Waals and electric double-layer forces, and explains why aqueous suspensions are stable at low salt levels, and unstable at higher salt levels. At low salt levels, the repulsive double-layer forces dominate and lead to slow aggregation. At higher salt levels, double-layer forces are screened, and the attractive van der Waals forces induce fast aggregation. While this behaviour is well-documented for simple salts,[28–32] a similar scenario might apply to dilute aqueous solutions of ILs.[24] The aggregation remains fast in aqueous suspensions at higher salt levels, since the diffusion is rapid due to the low viscosity of aqueous solutions. On the other hand, the high viscosity of ILs will substantially slow down the diffusion process. This effect will reduce the aggregation rate, and this mechanism will be referred to as *viscous stabilization*. The existence of highly stable particle suspensions in pure ILs contradicts DLVO theory, since the ILs should screen the double-layer forces fully.[23] Stabilization in ILs was attributed to solvation forces originating from their structuring near interfaces.[21,23,24] These forces were measured using the atomic force microscope and they were found to be oscillatory,

Department of Inorganic and Analytical Chemistry, University of Geneva, 30 Quai Ernest-Ansermet, 1205 Geneva, Switzerland.
E-mail: michal.borkovec@unige.ch; Tel: +41 22 379 6405

† Electronic supplementary information (ESI) available. See DOI: 10.1039/c4cp00804a

but overall repulsive.[24,33] This stabilization mechanism will be referred to as *solvation stabilization*.

Here we demonstrate that solvation and viscous stabilization controls the aggregation of particles in ILs. This assertion will be based on detailed measurements of aggregation rates of colloidal particles in IL–water mixtures with time-resolved light scattering. The present article provides the first systematic study of this kind, and shows that these techniques can be used to clarify the mechanisms of particle aggregation processes in ILs.

Methods

The following section summarizes the essential methods and concepts needed to analyse particle aggregation kinetics by time-resolved light scattering. The supplement provides details concerning the materials and experimental protocols used.

Particle aggregation kinetics

Particles suspended in a liquid diffuse due to thermal motion, and attractive van der Waals forces make them stick upon contact. When the suspension is initially composed of isolated particle monomers, they will form aggregates, initially dimers, according to the scheme

$$A + A \rightarrow A_2 \tag{1}$$

The kinetics of this process can be described using the rate equation

$$-\frac{dN_1}{dt} = 2 \cdot \frac{dN_2}{dt} = kN_1^2 \tag{2}$$

where N_1 and N_2 are the number concentrations of the monomers and dimers, respectively, t is the time, and k is the aggregation rate coefficient. Eqn (2) describing aggregation of colloidal particles is exactly the same as in chemical reaction kinetics, except in that field one defines the rate coefficient half as large. The other important difference from the chemical kinetics is that colloidal particles readily form higher order aggregates, such as trimers, tetramers, namely

$$\begin{aligned} A_2 + A &\rightarrow A_3 \\ A_3 + A &\rightarrow A_4 \\ A_2 + A_2 &\rightarrow A_4 \\ &\cdots \end{aligned} \tag{3}$$

Therefore, aggregates keep growing, until they sediment, cream, or interlink to form a gel. By assuming that each of these elementary kinetic steps proceeds with the same rate coefficient k, Smoluchowski has shown that in a suspension initially composed of monomers only, the total number of particles or aggregates $N = N_1 + N_2 + N_3 + \ldots$ decreases as[26,27]

$$N = \frac{N_0}{1 + t/T_{1/2}} \tag{4}$$

where N_0 is the total (or initial) particle concentration $N_0 = N_1 + 2N_2 + 3N_3 + \ldots$ and

$$T_{1/2} = \frac{2}{kN_0} \tag{5}$$

is the half-time of aggregation. This half-time represents the characteristic time, after which the total number of aggregates is reduced by a factor of two. When only monomers and dimers are present, eqn (2) would lead to the same expression for $T_{1/2}$ as eqn (5) up to the factor of 2.

The van der Waals attraction close to contact is normally very strong, which makes the aggregation process irreversible, meaning that aggregated particles do not detach from each other. For weaker attraction forces, as for example, in the case of depletion interactions or critical Casimir forces, the aggregation process may become reversible and lead to equilibrium phase separation.[34–36] Currently, we have no indications that such a situation might be encountered in ILs. Therefore, the irreversible aggregation process always leads to destabilization of a colloidal suspension, whereby the half-time given by eqn (5) sets the corresponding time scale. Depending on the system, however, this half-time may differ by orders of magnitude. When this half-time is large, the suspension is stable, while when it is small, it is unstable. For a half-time that is comparable to the experimental time window, the aggregation process can be followed by various techniques in real time. Initially, particle dimers form, while higher order aggregates occur later (Fig. 1). Correspondingly, one refers to *early stages* and *late stages* of the aggregation. Since the formation of doublets in eqn (1) is a second order kinetic process, the half-time does not only depend on the aggregation rate coefficient k, but also on the particle number concentration N_0. Thus, a suspension can be stabilized by adjusting the conditions such that aggregation rate coefficient is small, by appropriate dilution, or both.

In the case of fast aggregation, one assumes that the diffusing particles do not interact but they stick to each other at every encounter.[26] This model is equivalent to diffusion controlled reaction kinetics or, in colloid language, to a fast aggregation process. Smoluchowski has further shown that the corresponding rate coefficient is given by[26,27]

$$k_S = 16\pi D_1 R_1 = \frac{8k_B T}{3\eta} = 1.23 \times 10^{-17}\ \mathrm{m^3\ s^{-1}} \tag{6}$$

where by D_1 and R_1 denote the diffusion coefficient and the radius of the aggregating particles. The second equality sign in eqn (6) follows from the Stokes–Einstein relation, which relates the former quantities as[26]

$$D_1 = \frac{k_B T}{6\pi\eta R_1} \tag{7}$$

where η is the shear viscosity of the dispersing liquid, T is the absolute temperature, and k_B is the Boltzmann constant. The numerical value given in eqn (6) refers to water at 25 °C, while for ILs this value can be substantially smaller.

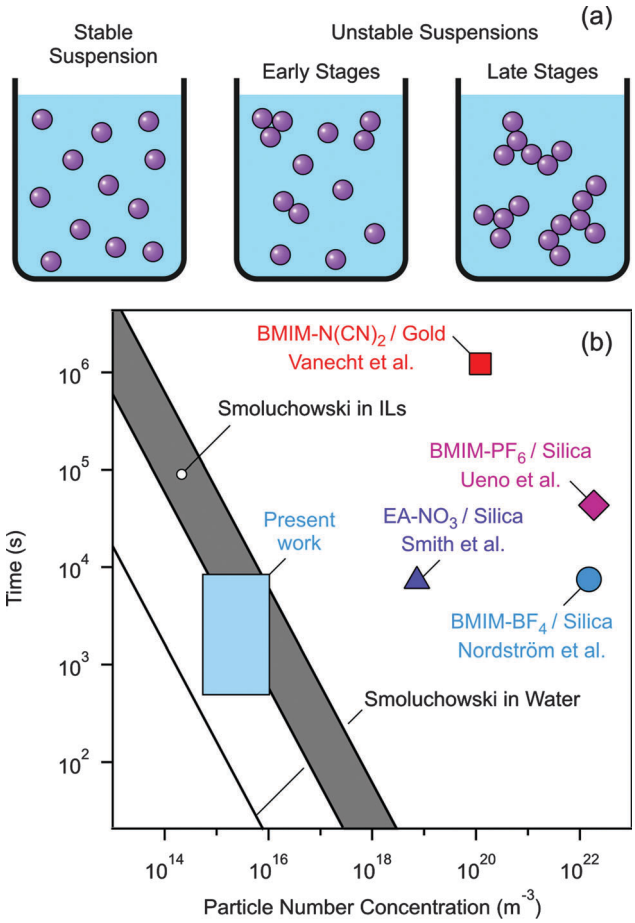

Fig. 1 Particle aggregation in ILs. (a) Schemes depicting the structure of a stable suspension and of unstable suspensions at early and late stages of the aggregation. (b) Aggregation time scale *versus* the particle number concentration. Half-times are calculated using eqn (5) and Smoluchowski's eqn (6) in water (solid line) and in the ILs used in the present study (shaded area). The blue region indicates the conditions of the present experiments. Data points refer to experimental time windows reported by Nordström *et al.*,[25] Smith *et al.*[24] involving ethylammonium ions (EA^+), Vanecht *et al.*,[16] and Ueno *et al.*[23] The other acronyms are defined in Fig. 2 and further details are given in Table S6 (ESI†).

Eqn (5) and (6) can be used to distinguish stable and unstable colloidal particle suspensions in aqueous salt solutions (Fig. 1b). Since viscosities of ILs can be substantially larger than the ones of aqueous solutions,[5,6] the respective boundary is displaced to the right. The stability time windows and the corresponding particle concentrations for stable particle suspensions in ILs reported in the literature are also shown.[16,23–25] The fact that these points cluster above the grey region suggests the importance of solvation stabilization. When the interaction potential acting between the particles is known, aggregation rates could be estimated more accurately.[26,37] We shall not pursue this aspect here, since the information concerning the interaction potentials between particles in ILs is currently incomplete.

Light scattering

Particle suspensions are being routinely characterized by static light scattering (SLS) and dynamic light scattering (DLS).[26,38] When these techniques are employed in a time-resolved fashion, they allow probing particle aggregation processes in detail.[39–42]

SLS measures the light scattering intensity I *versus* the scattering angle θ, which is commonly expressed in terms of the magnitude of the scattering vector

$$q = \frac{4\pi n}{\lambda_0}\sin\frac{\theta}{2} \tag{8}$$

where n is the refractive index of the medium and λ_0 is the wavelength of the incident light in vacuum. The scattering intensity $I(q)$ from a stable and dilute suspension of colloidal particles can be used to evaluate the particle size accurately. For small particles and weak contrast, the angular dependence of the scattering intensity can be calculated within the Rayleigh, Gans, and Debye (RGD) approximation. The contrast is characterized by the difference between the refractive indices of the particles and the dispersing liquid. In the general case, the exact Mie theory for spheres must be used.[43] For quantitative analysis, particle polydispersity and back-reflection correction have to be included.

The scattering intensity from an aggregating suspension varies with time. For a dilute suspension, this quantity can be expressed as

$$I(q,t) = I_1(q)N_1(t) + I_2(q)N_2(t) + \ldots \tag{9}$$

where $I_1(q)$ and $I_2(q)$ are the scattering intensities of the monomer and dimer, respectively. For early stages of aggregation, one can measure the initial apparent static rate Σ, which reflects the rate of change of the scattering intensity normalized by the initial intensity. This quantity can be obtained from eqn (2) and (9) and reads[40]

$$\Sigma = \frac{1}{I(q,0)}\cdot\left.\frac{\mathrm{d}I(q,t)}{\mathrm{d}t}\right|_{t\to 0} = kN_0\left(\frac{I_2(q)}{2I_1(q)} - 1\right) \tag{10}$$

In order to evaluate the aggregation rate coefficient, the optical factor must be known. Within the RGD approximation, this factor is given by[26,40]

$$\frac{I_2(q)}{2I_1(q)} = 1 + \frac{\sin(2qR_1)}{2qR_1} \tag{11}$$

In the general case, the T-matrix theory must be used to evaluate the ratio of scattering intensities.[37,43] At low scattering angles ($q \to 0$), the apparent static rate is always positive, meaning that the scattering intensity increases with time. At larger angles, this quantity can also become negative, which reflects the fact that the scattering intensity may also decrease with time.

DLS measures the intensity autocorrelation function, and from its decay constant one can extract the apparent diffusion coefficient D. In a stable suspension, the particle radius can be directly evaluated from this quantity using the Stokes–Einstein equation (eqn (7)). When a dilute suspension aggregates, the apparent diffusion coefficient can be expressed as[40]

$$D(q,t) = \frac{D_1 I_1(q)N_1(t) + D_2 I_2(q)N_2(t) + \ldots}{I_1(q)N_1(t) + I_2(q)N_2(t) + \ldots} \tag{12}$$

where D_1 and D_2 correspond to the diffusion coefficients of the monomers and dimers, respectively. We prefer to report the apparent hydrodynamic radius $R(q,t)$ that is obtained from the apparent diffusion coefficient $D(q,t)$ using eqn (7). In the early stages of aggregation one can measure the apparent dynamic rate Δ, which corresponds to the initial relative rate of change of the apparent hydrodynamic radius normalized to the initial radius. Following similar arguments as above, this rate can be expressed as[40]

$$\Delta = \frac{1}{R(q,0)} \cdot \left.\frac{\mathrm{d}R(q,t)}{\mathrm{d}t}\right|_{t\to 0} = kN_0\left(1-\frac{1}{\alpha}\right)\frac{I_2(q)}{2I_1(q)} \qquad (13)$$

where $\alpha = D_1/D_2 = R_2/R_1 \simeq 1.39$ is the hydrodynamic factor. The respective hydrodynamic radii of the monomer and the dimer are denoted as R_1 and R_2. The numerical value of this factor α can be estimated from low Reynolds number hydrodynamics.[44] This apparent dynamic rate is always positive, meaning that the hydrodynamic radius always increases with time, as one would intuitively expect. As will be shown in the next section, these light scattering techniques are a powerful means to investigate particle aggregation processes in ILs.

Results and discussion

Aggregation of sub-micron sulphate and amidine latex particles, as well as nano-sized sulphate latex particles, was studied in various ILs and their mixtures with water (Fig. 2a). Many ILs are hygroscopic, and may contain substantial amounts of water.[45] We have therefore systematically studied particle suspensions over a wide range of IL-to-water molar ratios, from dilute solution of ILs in water (water side) to ILs containing small amounts of water (IL side). We have analysed ILs containing the anions tetrafluoroborate, BF_4^-, dicyanamide, $N(CN)_2^-$, and thiocyanate, SCN^-, with 1-butyl-3-methylimidazolium, $BMIM^+$, as the cation. We have further investigated ILs with $N(CN)_2^-$ as the anion, and $BMIM^+$, 1-butyl-3-methylpyridinium dicyanamide, $BMPY^+$, and 1-butyl-1-methylpyrrolidinium, $BMPL^+$ as cations. Comparison experiments were carried out with 1-butylpyridinium tetrafluoroborate, BPY-BF_4, and simple KCl electrolyte solutions. Viscosities, refractive indices, and densities of the IL–water mixtures were determined by standard techniques (Fig. 2b and Fig. S1, ESI†). The viscosities of pure ILs used are 30–150 times larger than the one of water. Refractive indices and densities can be accurately described by ideal mixing laws. We will first summarize how light scattering can be used to characterize these particles and their aggregation kinetics. Subsequently, we will discuss the generic dependence of the aggregation rates on the IL-to-water molar ratio, and finally address system specificities.

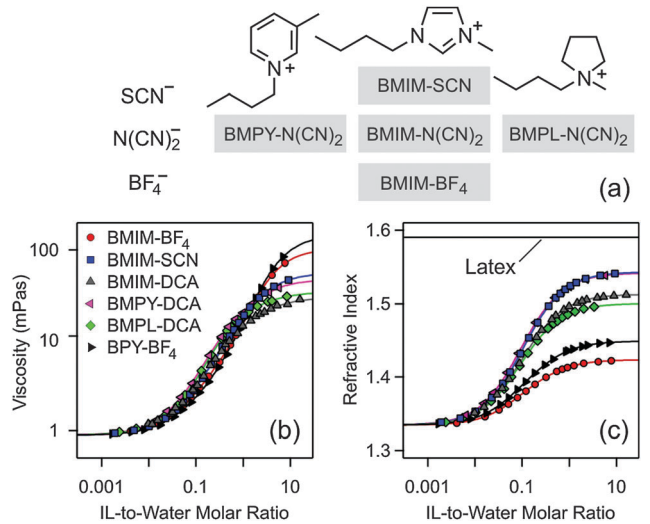

Fig. 2 Properties of ILs used and of their mixtures with water. (a) Structures and abbreviations, (b) shear viscosity, (c) and refractive index measured at 533 nm. The refractive index of the latex particles is also indicated.

Particle characterization by light scattering

We study spherical polystyrene latex particles as model particles. Most experiments were carried out with sub-micron particles having amidine surface modification and a radius of 110 nm and with sulphate surface modification and a radius of 265 nm. Fig. 3a shows measured form factors of the particles in water and in BMIM-SCN whereby the scattering intensity originating from pure ILs was subtracted. This residual scattering can be up to 10 times larger than the one for toluene, probably due to the presence of nm-sized transient clusters that are spontaneously forming in the ILs.[46] However, this residual scattering is still sufficiently small such that the excess scattering from the particles can be easily measured. The form factors are compared with best fits with Mie theory, whereby the refractive index of 1.59 was used for polystyrene.[47] Analogous results of the simpler RGD calculations are also shown. One observes that

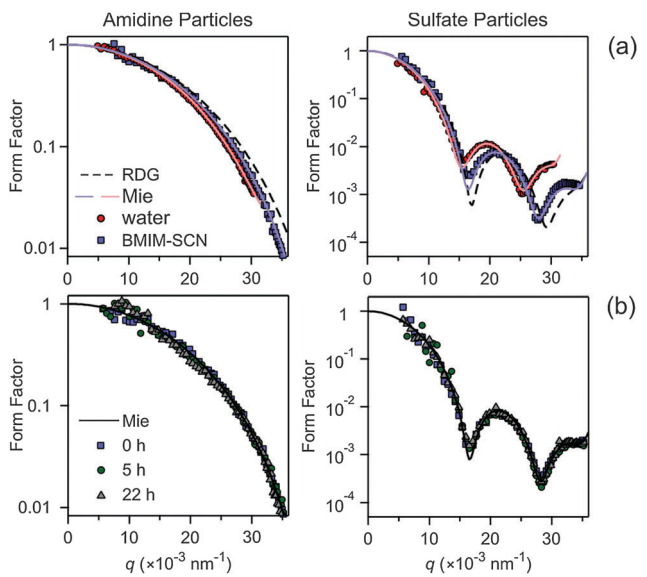

Fig. 3 Monomer form factors $P(q)$ *versus* the magnitude of the scattering vector q of amidine latex particles of 110 nm in radius (left) and sulphate latex of 265 nm (right). (a) The experimental points in water and in pure BMIM-SCN are compared with Mie and RGD theory from which the particle radius can be extracted. (b) No dependence with time of the form factors is observed in BMIM-SCN.

the RGD theory is applicable in ILs, while deviations from this theory are apparent in water, especially for the larger sulphate particles. Mie theory must be used in that case. The fitted particle radii and polydispersities are in excellent agreement with the values obtained by electron microscopy (Table S1, ESI†). RGD theory works well in the IL since the contrast is smaller, meaning that the refractive index of the latex particle is closer to the one of the IL than the one of water (Fig. 2c). Fig. 3b further illustrates that the form factor of the latex particles remains the same over long times. The constancy of this scattering profile confirms that the particles remain stable in the IL and that they neither swell nor dissolve. Hydrodynamic radii were also measured by DLS in these suspensions and they are about 6% larger than the ones obtained by SLS (Table S1, ESI†). This slight increase in radius is probably caused by polydispersity effects or solvation of the surface layer. The absolute scattering intensity remains constant within the experimental error of about 5% over the entire experimental time period, which further demonstrates that sedimentation or creaming effects are negligible in these systems.

Aggregation rates by time-resolved light scattering

The scattering intensity from an aggregating suspension may increase or decrease with time (Fig. 4a). The initial slope of this intensity trace reflects the apparent static rate Σ given in eqn (10) and this quantity can be determined by fitting a straight line to the initial part of the time-dependent scattering intensities. When the scattering intensity decreases with time, this quantity becomes negative. The measured dependence of the apparent static rate Σ on the magnitude of the scattering vector q is compared in Fig. 5a with predictions of RGD theory. This relation agrees well with the experiment for the amidine particles, but the more accurate T-matrix theory must be used for sulphate latex. The deviations are more important in water than in the IL due to larger contrast. The remaining discrepancies are probably related to slight particle asphericity. The respective aggregation rates are obtained by least-squares fit (Table 1). One observes that the aggregation rates in ILs are substantially smaller than the ones in water.

In an aggregating suspension, the apparent hydrodynamic radius always increases with time (Fig. 4b). The apparent dynamic rate Λ can be obtained by fitting straight lines to the initial portion of the hydrodynamic radius trace. The dependence of the apparent dynamic rate Λ on the magnitude of the scattering vector q can be fitted well with eqn (13) whereby the optical factor can be determined by RGD or T-matrix theory (Fig. 5b). When one uses the aggregation rate coefficients obtained from static light scattering, one obtains the hydrodynamic factors. They are summarized in Table 1 and they agree well with the theoretical value of $\alpha = 1.39$. The data points scatter more strongly in the IL due to weaker contrast.

When the optical and hydrodynamic factors are known, the aggregation rate coefficients can also be obtained from the measurement of the apparent dynamic rate at a specific scattering angle. The typical procedure is to perform time-resolved single-angle DLS experiments at various compositions and determine the apparent dynamic rates from the initial slope (Fig. 4c and d).

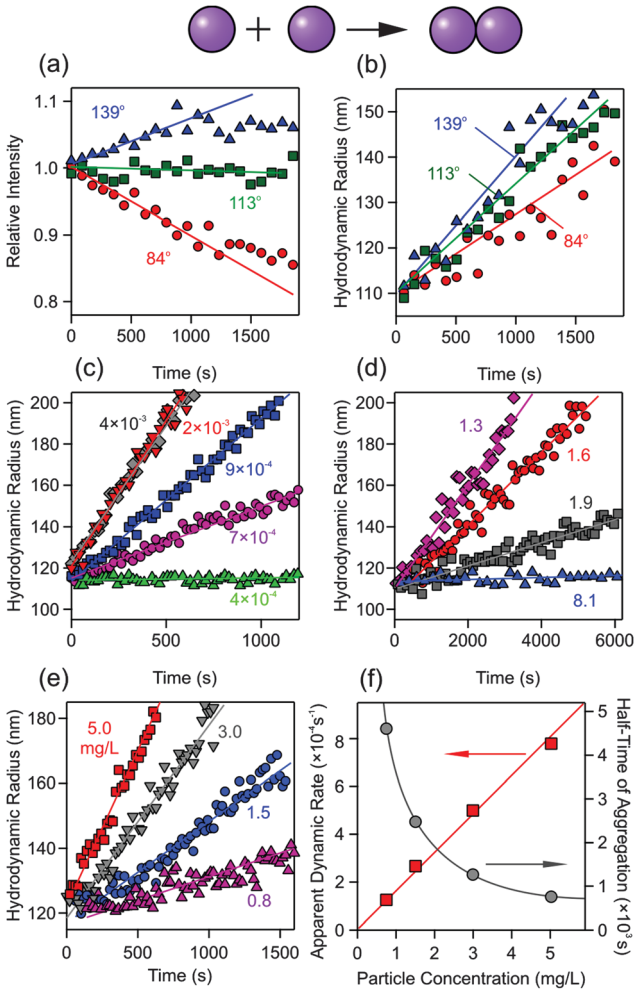

Fig. 4 Time-dependence of the light scattering signal in aggregating particle suspensions in ILs. Amidine latex particles measured at different scattering angles in BMIM-SCN of 0.092 IL-to-water molar ratio with (a) SLS and (b) DLS. Hydrodynamic radius measured using DLS for amidine latex particles in BPY-BF_4–water mixtures at different IL-to-water molar ratios (c) on the water side and (d) on the IL side. Particle concentration dependence for amidine latex particles in BPY-BF_4 on the (e) hydrodynamic radius and (f) the apparent dynamic rate (left axis) and half-time of aggregation (right axis).

The rate coefficients can be extracted from eqn (13) by inserting the known values of the optical and hydrodynamic factors. This single-angle DLS technique was used to measure the rate coefficients in the various IL–water mixtures, and the resulting aggregation rates are in excellent agreement with multi-angle SLS (Table 1).

In order to probe the doublet formation rate, the experiment must be carried out in the early stages of aggregation. This condition can be ensured with time-resolved DLS by satisfying two criteria. First, the initial apparent hydrodynamic radius should agree within experimental error with the corresponding radius in a stable suspension. Second, the relative increase of the apparent radius should be not more than 20–30% of its initial value. Such conditions are best found by varying the particle concentration (Fig. 4e). This figure also indicates that

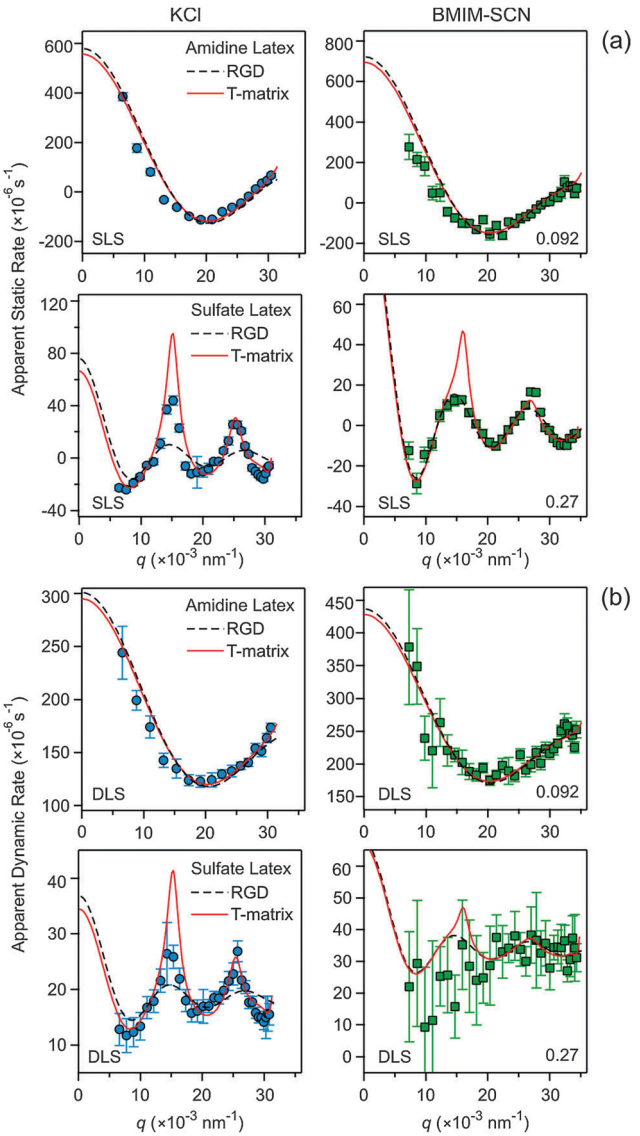

Fig. 5 Apparent aggregation rates *versus* the magnitude of the scattering vector q of amidine and sulphate latex particles measured in 1.0 M KCl (left column) and in BMIM-SCN water mixtures of the IL-to-water molar ratios indicated (right column). Experimental data are compared with RGD (dashed line) and T-matrix (solid line) calculations. The resulting aggregation rates and hydrodynamic factors are given in Table 1. (a) SLS and (b) DLS.

the apparent rate of aggregation is proportional to the particle concentration (Fig. 4f), as stipulated by eqn (13).

Another way to ensure that one focuses on the early stages of the aggregation process is to evaluate the half-time of the aggregation (Fig. 4f). These half-times are also shown in Fig. 1. Since our aim is to measure aggregation rates, we situate ourselves near the unstable region. The appropriate experimental window must be substantially shorter than the half-times, in practice by about a factor 3–5. To estimate the half-time properly, the actual aggregation rate coefficient must be known. However, this quantity is only accessible when the respective light scattering measurements have been completed and not when the experiment is initiated. From this point of view, the criteria concerning the relative increase of the hydrodynamic radius are more practical.

Generic features

Fig. 6a shows the measured aggregation rates for the different latex particles in various ILs and in their water mixtures. The striking aspect is that all systems studied behave similarly. Three main aggregation regimes can be identified. (i) At low IL-to-water ratios, one recovers the classical DLVO regime. In this regime, the aggregation rate increases strongly with the IL content first, and then saturates at a plateau value. The increase in the rate corresponds to slow aggregation, which results from progressive screening of the double-layer repulsion. The plateau reflects fast aggregation, where particle encounters are only limited by their rapid diffusion in water. (ii) At higher IL-to-water ratios, the aggregation rate decreases gradually. This decrease originates from the increasing viscosity, even though the aggregation process remains diffusion controlled. In the systems studied, this mechanism can slow down the aggregation process by almost two orders of magnitude. This regime is referred to as *viscous stabilization*. (iii) At high IL-to-water ratios, which correspond to ILs containing small amounts of water, the aggregation rate decreases rapidly with increasing IL content. This regime reflects stabilization that is specific to the type of the IL, and will be referred to as *solvation stabilization*.

The DLVO regime (i) on the water-rich side is very similar to simple, monovalent salts, like KCl. This fact is not surprising since ILs normally dissociate in water like simple, strong electrolytes.[48] The effect of simple salts on the aggregation of colloidal particles is well documented.[30–32] The transition between slow and fast aggregation can be described by DLVO theory for weakly charged particles.[30,31] Slow aggregation for highly charged particles is often more rapid than predicted

Table 1 Aggregation rates and hydrodynamic factors of sub-micron latex particles measured using time-resolved light scattering

	Amidine latex[a]		Sulphate latex[b]	
Method	KCl[c]	BMIM-SCN[d]	KCl[c]	BMIM-SCN[d]
Multi-angle SLS[e]	$(2.9 \pm 0.1) \times 10^{-18}$	$(8.5 \pm 0.5) \times 10^{-19}$	$(3.3 \pm 0.1) \times 10^{-18}$	$(4.5 \pm 0.9) \times 10^{-19}$
Multi-angle DLS[f]	1.35 ± 0.02	1.43 ± 0.02	1.32 ± 0.02	1.35 ± 0.02
Single-angle DLS[e]	$(3.1 \pm 0.3) \times 10^{-18}$	$(8.3 \pm 0.8) \times 10^{-19}$	$(3.2 \pm 0.2) \times 10^{-18}$	$(3.0 \pm 0.4) \times 10^{-19}$

[a] Amidine latex of 110 nm in radius. [b] Sulphate latex of 265 nm in radius. [c] Measurements were carried out in 1.0 M KCl solutions. [d] IL-to-water molar ratios of 0.092 and 0.27 were used for amidine and sulphate latexes, respectively. [e] Aggregation rate coefficients k in $m^3\ s^{-1}$. [f] Measured hydrodynamic factor α.

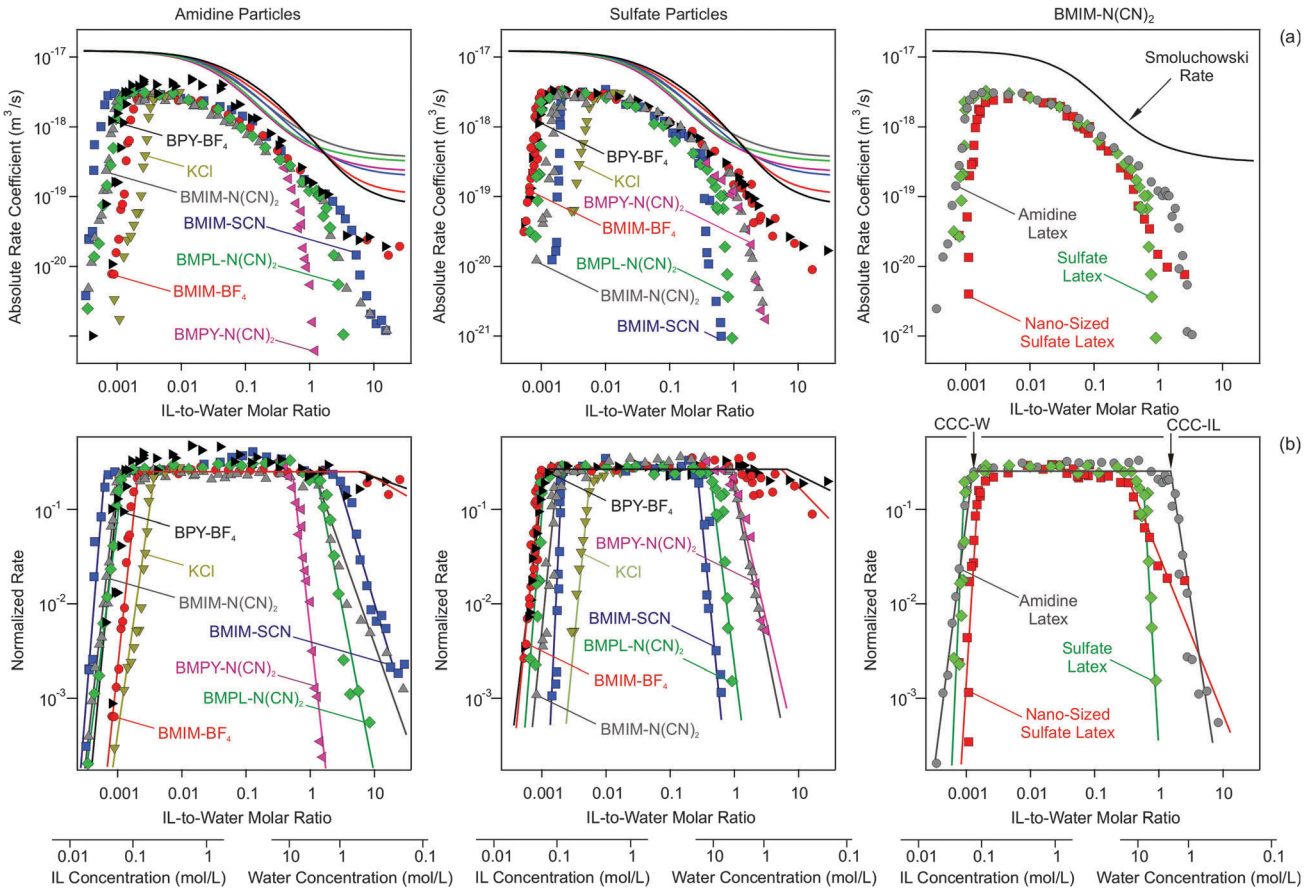

Fig. 6 Aggregation rates of sub-micron latex particles *versus* the IL-to-water molar ratio in various ILs. Molar IL and water concentrations are indicated on separate axes. Amidine (left column) and sulphate latex (middle column) in different ILs, and different particles in BMPL-N(CN)$_2$ with the CCCs indicated for the amidine particles. (a) Aggregation rate coefficient k and (b) the same quantity normalized to the Smoluchowski rate coefficient k_S. Solid lines in (a) correspond to the Smoluchowski rate, while in (b) they serve to guide the eye.

by DLVO theory, which is typically caused by surface charge heterogeneities.[30,32,49]

The importance of viscous stabilization in regime (ii) can be confirmed by comparing the aggregation rate coefficients to the Smoluchowski's value k_S given in eqn (6). Viscosities of the IL–water mixtures increase strongly with increasing IL content (Fig. 2b), and thus the Smoluchowski's rate decreases (Fig. 6a). This point can be better illustrated by plotting the aggregation rate coefficients normalized with the Smoluchowski's value k/k_S (Fig. 6b). The normalized rate coefficient remains constant throughout the entire intermediate concentration regime (ii) within experimental error, which confirms that the aggregation is diffusion controlled. However, the rate coefficient is about a factor of 2–4 smaller than the Smoluchowski's value. Similar discrepancies were reported in aqueous suspensions of latex, silica, or metal oxide particles.[49–52] They can be partly explained by including van der Waals and hydrodynamic interactions in the calculation of the aggregation rate, which results in aggregation rates that are about a factor of two smaller than the Smoluchowski's value. While the Hamaker constant, which defines the strength of the van der Waals force, could vary with the type of IL and its water content, the actual value of the aggregation rate depends only weakly on this constant.[27] The remaining discrepancies probably originate from inaccuracies in the hydrodynamic resistance function at small distances.[52]

The onset of solvation stabilization can be best localized through the abrupt decrease of the normalized rate coefficient at high IL content (Fig. 6b). Solvation stabilization occurring in regime (iii) on the IL-rich side is probably caused by repulsive forces generated by the structuring of the ILs near solid surfaces. This structuring was observed by X-ray reflectivity,[53] and the respective forces could be measured using the surface forces apparatus[54] and the atomic force microscope.[24,33,55] While such solvation forces are oscillatory, they are overall repulsive, and probably responsible for the stabilization of colloidal particles in ILs as suggested earlier.[21] Since we lack reliable models of the interaction potential acting between the particles in IL–water mixtures, we shall not attempt to evaluate the aggregation rates in this regime quantitatively.

The transition between slow and fast aggregation within the DLVO regime at the water rich side occurs in a narrow concentration range, referred to as the critical coagulation concentration (CCC). A similar critical concentration can be identified at the IL rich side, which signals the transition between the solvation and viscous stabilization regime. We distinguish

these two CCCs by referring to CCC-W on the water-rich side, and by CCC-IL on the IL-side. To remain in line with the customary definition of CCC in water, we will express CCC-W as molar concentration of the IL. In analogy, CCC-IL will be expressed as molar concentration of water. The respective molar concentration axes are indicated in Fig. 6. Fig. S2–S4 (ESI†) facilitate conversions to these and other concentration units. The respective CCCs can be inferred from Fig. 6 and they are summarized in Table S5 (ESI†).

Sub-micron amidine latex particles

CCC-W is lower for the ILs than for the simple salts, such as KCl. Charged particles suspended in simple, monovalent salt solutions have CCCs in the range of 0.1–0.5 M.[28,29,56] The corresponding values induced by ILs are consistently lower, around 0.03–0.1 M. This shift is probably related to a stronger affinity of the IL anions to the particle surface than with Cl^-. One further observes that CCC-W increases in the sequence of SCN^-, $N(CN)_2^-$, and BF_4^-, suggesting that the affinity of the surface for these anions decreases in the same way. The effect of the cations on CCC-W is less pronounced.

The CCC-IL can be clearly observed for all ILs studied, except in the presence of the BF_4^- anion. Typical values observed reflect water concentrations of 2–7 M. The ILs containing the BF_4^- anion seem to induce only minor solvation stabilization for the water contents studied, eventually setting in below 1.0 M. This hypothesis seems to be consistent with the absence of aggregation of gold particles in very dry BMIM-BF_4 over time periods that were substantially larger than the half-times estimated using the Smoluchowski relation (Fig. 1b).[16] Silica suspensions were also found to be unstable in BMIM-BF_4.[23] Adopting this hypothesis, CCC-IL increases in the sequence of BF_4^-, SCN^-, and $N(CN)_2^-$. The effect of cations seems to be more important for CCC-IL, since $BMPY^+$ yields the highest value, while $BMIM^+$ and $BMPL^+$ behave similarly.

Sub-micron sulphate latex particles

The values of CCC-W for the sulphate particles are very similar to the values for the amidine particles. This fact can be understood since the magnitudes of the charge densities of both types of particles are comparable (Table S1, ESI†). However, the effects of anions are different. With the $BMIM^+$ cation, one observes the reverse sequence to the amidine particle. The CCC-W thus increases through the anions BF_4^-, $N(CN)_2^-$, and SCN^-. This trend suggests that the affinity of the surface for these anions decreases in the same sequence, and is thus opposite to the one for amidine particles. This reversed trend is probably related to the negative charge of these particles. The effect of cations on CCC-W is again minor, and these values are similar for $BMIM^+$, $BMPL^+$, and BPY^+.

The CCC-IL for the sulphate particles situates in the range 3–13 M, which is somewhat larger than for the amidine particles. As for the amidine particles, the ILs containing the BF_4^- anions lead only to minor suspension stabilization at low water concentrations, around 0.4 M. The CCC-IL increases with BF_4^-, $N(CN)_2^-$, and SCN^-, which reflects the same sequences observed at the water side. The role of cations is less important, one still observes the sequence $BMPY^+$, $BMIM^+$, and $BMPL^+$. These findings suggest again that cations interact with the particle surfaces more weakly than anions.

Nano-sized sulphate latex particles

To address the applicability of our findings to smaller particles, aggregation rates of nano-sized sulphate latex particles with 50 nm radius in BMPL-$N(CN)_2$ and its water mixtures were measured (Table S1, ESI†). Due to the weak scattering power of these particles, the respective measurements are more difficult, especially in ILs. While the overall trends are similar, the present data suggest that the nano-sized particles aggregate more slowly than the sub-micron sized ones on the IL side. This point is in agreement with the observation that suspensions of nano-sized silica particles were more stable than suspensions of larger ones.[21] However, such differences could also be related to different particle concentrations of the samples.

The present scenario is consistent with visual observations of silica particle suspensions in mixtures of ethylammonium nitrate and water by Smith *et al.*[24] These suspensions were stable in pure water and the pure IL, but unstable in the mixtures. Fig. 1 reveals that solvation stabilization must be the relevant stabilization mechanism in that system too. We thus estimate CCC-W to be around 0.1 M and CCC-IL to be around 2 M in that system.

Conclusions

Our light scattering studies demonstrate that colloidal particles suspended in ILs and their water mixtures form aggregates. However, the time scale of this process strongly depends on the particle concentration and on the value of the aggregation rate coefficient. The rate coefficients vary characteristically. At the water side, ILs behave like simple, monovalent salts and the data are in line with the DLVO theory. In this DLVO regime, one observes slow aggregation at low IL content. With increasing IL content, the aggregation rate increases and finally reaches the plateau reflecting fast aggregation. At the IL side, aggregation may proceed again very slowly. Two mechanisms are responsible for this stabilization. The *viscous stabilization* mechanism is important in viscous ILs, and originates from the slowdown of the diffusion process in a viscous liquid. The *solvation stabilization* mechanism is system specific, but can lead to a dramatic slowdown of the aggregation rate. This mechanism is probably related to repulsive solvation forces that are operational in ILs due to strong layering close to surfaces. These two stabilization mechanisms are suspected to be generic, as they are operational in different ILs and for particles with different surface functionalities and of different size. We further suspect that in ILs containing BF_4^- anions the principal mechanism is viscous stabilization, and solvation stabilization is unimportant, unless the IL is extremely dry. On the other hand, ILs containing $N(CN)_2^-$ or SCN^- anions tend to stabilize suspensions by both mechanisms, and solvation stabilization can be even operational in ILs containing 10% of water by mass.

Acknowledgements

Financial support by the Swiss National Science Foundation, Swiss Scientific Exchange Program and the University of Geneva is gratefully acknowledged.

References

1 A. P. Abbott and K. J. McKenzie, *Phys. Chem. Chem. Phys.*, 2006, **8**, 4265–4279.
2 M. Armand, F. Endres, D. R. MacFarlane, H. Ohno and B. Scrosati, *Nat. Mater.*, 2009, **8**, 621–629.
3 F. Endres and S. Z. El Abedin, *Phys. Chem. Chem. Phys.*, 2006, **8**, 2101–2116.
4 N. V. Plechkova and K. R. Seddon, *Chem. Soc. Rev.*, 2008, **37**, 123–150.
5 H. Tokuda, K. Hayamizu, K. Ishii, M. Abu Bin Hasan Susan and M. Watanabe, *J. Phys. Chem. B*, 2004, **108**, 16593–16600.
6 H. Tokuda, K. Hayamizu, K. Ishii, M. A. B. H. Susan and M. Watanabe, *J. Phys. Chem. B*, 2005, **109**, 6103–6110.
7 M. Ruta, G. Laurenczy, P. J. Dyson and L. Kiwi-Minsker, *J. Phys. Chem. C*, 2008, **112**, 17814–17819.
8 J. D. Scholten, B. C. Leal and J. Dupont, *ACS Catal.*, 2012, **2**, 184–200.
9 F. T. Li, X. J. Wang, Y. Zhao, J. X. Liu, Y. J. Hao, R. H. Liu and D. S. Zhao, *Appl. Catal., B*, 2014, **144**, 442–453.
10 X. Yang, Z. F. Fei, D. B. Zhao, W. H. Ang, Y. D. Li and P. J. Dyson, *Inorg. Chem.*, 2008, **47**, 3292–3297.
11 S. Shylesh, D. Hanna, S. Werner and A. T. Bell, *ACS Catal.*, 2012, **2**, 487–493.
12 P. Wang, S. M. Zakeeruddin, P. Comte, I. Exnar and M. Gratzel, *J. Am. Chem. Soc.*, 2003, **125**, 1166–1167.
13 E. F. Borra, O. Seddiki, R. Angel, D. Eisenstein, P. Hickson, K. R. Seddon and S. P. Worden, *Nature*, 2007, **447**, 979–981.
14 H. Itoh, K. Naka and Y. Chujo, *J. Am. Chem. Soc.*, 2004, **126**, 3026–3027.
15 L. L. Lazarus, C. T. Riche, N. Malmstadt and R. L. Brutchey, *Langmuir*, 2012, **28**, 15987–15993.
16 E. Vanecht, K. Binnemans, S. Patskovsky, M. Meunier, J. W. Seo, L. Stappers and J. Fransaer, *Phys. Chem. Chem. Phys.*, 2012, **14**, 5662–5671.
17 Y. Zhou and M. Antonietti, *J. Am. Chem. Soc.*, 2003, **125**, 14960–14961.
18 M. Ramalakshmi, P. Shakkthivel, M. Sundrarajan and S. M. Chen, *Mater. Res. Bull.*, 2013, **48**, 2758–2765.
19 H. Minami, K. Yoshida and M. Okubo, *Macromol. Rapid Commun.*, 2008, **29**, 567–572.
20 Q. M. Ji, S. Acharya, G. J. Richards, S. L. Zhang, J. Vieaud, J. P. Hill and K. Ariga, *Langmuir*, 2013, **29**, 7186–7194.
21 K. Ueno and M. Watanabe, *Langmuir*, 2011, **27**, 9105–9115.
22 S. S. Moganty, S. Srivastava, Y. Y. Lu, J. L. Schaefer, S. A. Rizvi and L. A. Archer, *Chem. Mater.*, 2012, **24**, 1386–1392.
23 K. Ueno, A. Inaba, M. Kondoh and M. Watanabe, *Langmuir*, 2008, **24**, 5253–5259.
24 J. A. Smith, O. Werzer, G. B. Webber, G. G. Warr and R. Atkin, *J. Phys. Chem. Lett.*, 2010, **1**, 64–68.
25 J. Nordström, L. Aguilera and A. Matic, *Langmuir*, 2012, **28**, 4080–4085.
26 W. B. Russel, D. A. Saville and W. R. Schowalter, *Colloidal Dispersions*, Cambridge University Press, Cambridge, 1989.
27 M. Elimelech, J. Gregory, X. Jia and R. A. Williams, *Particle Deposition and Aggregation: Measurement, Modeling, and Simulation*, Butterworth-Heinemann Ltd., Oxford, 1995.
28 T. Lopez-Leon, A. B. Jodar-Reyes, D. Bastos-Gonzalez and J. L. Ortega-Vinuesa, *J. Phys. Chem. B*, 2003, **107**, 5696–5708.
29 D. N. Furlong, A. Launikonis, W. H. F. Sasse and J. V. Sanders, *J. Chem. Soc., Faraday Trans. 1*, 1984, **80**, 571–588.
30 S. H. Behrens, M. Borkovec and P. Schurtenberger, *Langmuir*, 1998, **14**, 1951–1954.
31 M. Kobayashi, M. Skarba, P. Galletto, D. Cakara and M. Borkovec, *J. Colloid Interface Sci.*, 2005, **292**, 139–147.
32 N. Ryde and E. Matijevic, *J. Chem. Soc., Faraday Trans.*, 1994, **90**, 167–171.
33 R. Hayes, G. G. Warr and R. Atkin, *Phys. Chem. Chem. Phys.*, 2010, **12**, 1709–1723.
34 V. J. Anderson and H. N. W. Lekkerkerker, *Nature*, 2002, **416**, 811–815.
35 A. Zaccone, J. J. Crassous and M. Ballauff, *J. Chem. Phys.*, 2013, **138**, 104908.
36 D. Bonn, J. Otwinowski, S. Sacanna, H. Guo, G. Wegdam and P. Schall, *Phys. Rev. Lett.*, 2009, **103**, 156101.
37 W. Lin, M. Kobayashi, M. Skarba, C. Mu, P. Galletto and M. Borkovec, *Langmuir*, 2006, **22**, 1038–1047.
38 B. J. Berne and R. Pecora, *Dynamic Light Scattering*, Robert E. Krieger Publishing, Malabar, 1990.
39 D. A. Weitz, J. S. Huang, M. Y. Lin and J. Sung, *Phys. Rev. Lett.*, 1984, **53**, 1657–1660.
40 H. Holthoff, S. U. Egelhaaf, M. Borkovec, P. Schurtenberger and H. Sticher, *Langmuir*, 1996, **12**, 5541–5549.
41 S. H. Xu and Z. W. Sun, *Soft Matter*, 2011, **7**, 11298–11308.
42 P. Sandkuhler, M. Lattuada, H. Wu, J. Sefcik and M. Morbidelli, *Adv. Colloid Interface Sci.*, 2005, **113**, 65–83.
43 M. I. Mishchenko, L. D. Travis and A. A. Lacis, *Scattering, Absorption, and Emission of Light by Small Particles*, University Press, Cambridge, 2002.
44 W. L. Yu, E. Matijevic and M. Borkovec, *Langmuir*, 2002, **18**, 7853–7860.
45 E. J. Gonzalez, A. Dominguez and E. A. Macedo, *J. Chem. Eng. Data*, 2012, **57**, 2165–2176.
46 S. Chen, S. Zhang, X. M. Liu, J. Wang, J. Wang, K. Dong, J. L. Sun and B. Xu, *Phys. Chem. Chem. Phys.*, 2013, **16**, 5893–5906.
47 X. Y. Ma, J. Q. Lu, R. S. Brock, K. M. Jacobs, P. Yang and X. H. Hu, *Phys. Med. Biol.*, 2003, **48**, 4165–4172.
48 M. Bester-Rogac, A. Stoppa, J. Hunger, G. Hefter and R. Buchner, *Phys. Chem. Chem. Phys.*, 2011, **13**, 17588–17598.
49 M. Schudel, S. H. Behrens, H. Holthoff, R. Kretzschmar and M. Borkovec, *J. Colloid Interface Sci.*, 1997, **196**, 241–253.

50 S. H. Behrens, D. I. Christl, R. Emmerzael, P. Schurtenberger and M. Borkovec, *Langmuir*, 2000, **16**, 2566–2575.
51 M. Kobayashi, F. Juillerat, P. Galletto, P. Bowen and M. Borkovec, *Langmuir*, 2005, **21**, 5761–5769.
52 P. Sinha, I. Szilagyi, F. J. Montes Ruiz-Cabello, P. Maroni and M. Borkovec, *J. Phys. Chem. Lett.*, 2013, **4**, 648–652.
53 M. Mezger, H. Schroder, H. Reichert, S. Schramm, J. S. Okasinski, S. Schoder, V. Honkimaki, M. Deutsch, B. M. Ocko, J. Ralston, M. Rohwerder, M. Stratmann and H. Dosch, *Science*, 2008, **322**, 424–428.
54 R. G. Horn, D. F. Evans and B. W. Ninham, *J. Phys. Chem.*, 1988, **92**, 3531–3537.
55 J. J. Segura, A. Elbourne, E. J. Wanless, G. G. Warr, K. Voitchovsky and R. Atkin, *Phys. Chem. Chem. Phys.*, 2013, **15**, 3320–3328.
56 W. Lin, P. Galletto and M. Borkovec, *Langmuir*, 2004, **20**, 7465–7473.

Supporting Information for

Particle Aggregation Mechanisms in Ionic Liquids

Istvan Szilagyi, Tamas Szabo, Anthony Désert, Gregor Trefalt, Tamas Oncsik, Michal Borkovec*

*Corresponding author: Phone: + 41 22 379 6405, E-mail: michal.borkovec@unige.ch

Materials. Spherical negatively charged sulphate and positively charged amidine functionalized polystyrene latex particles were purchased from Interfacial Dynamics Corporation (Portland, USA). Their size and charge are summarized in Table S1. The manufacturer further reports the density of the latex particles as 1.05 g/cm^3. The purchased aqueous stock suspensions were purified by dialysis against Milli-Q water (Millipore, Molsheim, France). Milli-Q water was used throughout. For the amidine particles, polyvinylidene difluoride membranes and for the sulphate particles cellulose ester membranes, both with a molecular mass cut-off of 300 kg/mol were used (Spectrum Rancho, Dominguez, USA). The dialysis was performed until the conductivity of the surrounding medium reached the value of Milli-Q water. The stock suspension was subsequently diluted for light scattering measurements and adjusted to pH 5.0 by HCl. The precise particle concentration was determined by static light scattering by comparing the scattered intensities with the samples of known particle concentration and with total carbon and nitrogen analysis (TOCV, Shimadzu, Japan).

The following water miscible room temperature ILs were purchased from IoLiTech GmbH (Heilbronn, Germany): 1-butyl-3-methylimidazolium tetrafluoroborate, BMIM-BF_4, 1-butyl-3-methylimidazolium dicyanamide, BMIM-$N(CN)_2$, 1-butyl-3-methylimidazolium thiocyanate, BMIM-SCN, 1-butylpyridinium tetrafluoroborate, BPY-BF_4, 1-butyl-3-methylpyridinium dicyanamide, BMPY-$N(CN)_2$, and 1-butyl-1-methylpyrrolidinium dicyanamide, BMPL-$N(CN)_2$ (Table S2). The ILs were dried under vacuum at 50°C and the final water content was determined by Karl-Fischer titration (Metrohm, Herisau, Switzerland). The water content was below 1 g/L. IL impurities originating from the synthetic procedures are given in Table S3. The dried ILs were handled in a glove box. A precipitate sometimes appeared after mixing the ILs with water, which could be easily detected by light scattering. This precipitate could be removed by leaving the sample standing overnight, and filtering with 0.2 μm syringe filter (Millipore, Molsheim, France). However, the precipitate could not be removed in BMPY-$N(CN)_2$-water mixtures at low IL-to-water ratios, and therefore the aggregation rates could not be determined under these conditions. All experiments are carried out at 25.0±0.2 °C.

Properties of ILs and their water mixtures. Density, refractive index, and viscosity of the ILs and their water mixtures were determined with standard techniques. Densities were measured with a Krüss Easy Dyne K20 tensiometer (Krüss GmbH, Hamburg, Germany) by weighing a silicon crystal cylinder immersed in the IL-water mixture. The uncertainty of the measurements was estimated to be ±0.001 g/cm^3. Data for BMIM-SCN, BMPL-$N(CN)_2$ and BPY-BF_4 were taken from literature.[1-3] The experimental data were fitted with the ideal mixing law

$$\rho = \frac{1}{(1-y)/\rho_{\mathrm{W}} + y/\rho_{\mathrm{IL}}} \tag{1}$$

where y is the mass fraction of the IL, and $\rho_{\mathrm{W}} = 0.997$ g/cm^3 is the density of water and ρ_{IL} are the densities the IL given in Table S2. The ideal mixing law is accurate within 0.7% for all IL-water mixtures studied. The data and fits are shown in Fig. S1.

Refractive index measurements were carried out with an Abbemat-WR/MW automatic multiwavelength refractometer (Anton Paar, Zofingen, Switzerland) at wavelengths of 533 nm and 632 nm, which correspond to the laser wavelength of the light scattering instruments used. The data were fitted with the ideal mixing law

$$n = n_{\mathrm{W}}(1-\phi) + n_{\mathrm{IL}}\phi \tag{2}$$

where ϕ is the volume fraction of the IL, and n_{W} and n_{IL} are the refractive indices of water and the IL, respectively. The refractive index of water is 1.334 at 533 nm and 1.331 at 632 nm, while the ones for the ILs are given in Table S2. The volume fraction was calculated assuming the mixing law eq. (1) for the density. The ideal mixing law for the refractive index is accurate within 0.4% for all IL-water mixtures studied.

Shear viscosities were measured with a Brookfield LVDV-II+ Pro C/P viscometer (Hunter and Caprez, Zumikon, Switzerland) in a cone-plate geometry with the CPE-40 cone. The data were recorded with the IL-water mixture. The shear stress always showed a linear dependence with the shear rate, indicating that the ILs are Newtonian liquids. The viscosities of the IL-water systems were fitted with a polynomial model[4]

$$\eta = \eta_{\mathrm{W}}(1-x) + \eta_{\mathrm{IL}}x + x(1-x)\sum_{i=0}^{4} a_i \left(2x-1\right)^i \tag{3}$$

where x is the mole fraction of IL, η_{W} and η_{IL} are the viscosities of water and pure IL. The viscosity of pure water is 0.890 mPas, while the ones of the ILs are given in Table S2. The fitting parameters a_i are given in Table S4. For some ILs a satisfactory fit could be achieved by setting the higher order coefficients to zero. This model describes the viscosity data within about 1%.

Light Scattering. The size and optical properties of particles were characterized by static light scattering (SLS) in both aqueous electrolyte (KCl, Acros Organics, Geel, Belgium) and IL solutions as well as in pure ILs. The intensity of the scattered light was recorded at several scattering angles with a multi-angle goniometer with 8 photomultiplier detectors (ALV/CGS-8F, Langen, Germany) equipped with a 532 nm solid-state Verdi V2 laser. The measurements in stable suspensions were performed at particle concentrations of 10 mg/L and 50 mg/L for amidine and sulphate latex, respectively. Time-resolved aggregation experiments by multi-angle SLS and DLS were carried out in 1.0 M KCl aqueous electrolyte and in BMIM-SCN solutions at an IL-to-water molar ratio of 0.09 and 0.27 for the amidine and sulphate latex particles, respectively. Particle concentrations of 1.2 and 5.0 mg/L were used for the amidine latex of 110 nm in radius in the presence of KCl and IL respectively, while 1.2 and 25.0 mg/L for sulphate latex particles of 265 nm in radius. Even for the largest particles used, sedimentation or creaming effects are negligible as could be confirmed from the constancy of

the absolute light scattering intensity in stable suspensions over 24 h. Most aggregation measurements were performed at a single scattering angle of 90° on the compact goniometer system (ALV/CGS-3, Langen, Germany). The instrument uses a He/Ne laser operating at 633 nm as a light source and an avalanche photodiode as a detector. The time-resolved DLS experiments were performed in borosilicate glass cuvettes. Cuvettes were cleaned with a hot piranha solution consisting of 30% H_2O_2 and concentrated H_2SO_4 in a volume ratio of 1:3 and rinsed extensively with water followed by drying in dust-free environment. The ILs were mixed with the appropriate amount of water. The experiments were started by adding a small amount of the aqueous particle suspension into the cuvette and mixing with a vortex stirrer. This procedure limited the lowest achievable water content to about 3 g/L. The final particle concentration was about 10 mg/L, which was adequately low to keep the aggregation in its early stages. To obtain reliable results for slow aggregating suspensions, the particle concentration was increased about 10-fold compared to the concentrations used for the other experiments. The scattering signal of the pure ILs was about 3–10 times larger than for toluene. This larger scattering intensity probably originates from the nm-scale structures that spontaneously from in the ILs. However, these scattering intensities are still about three times lower than the one of the suspensions containing nano-sized sulphate latex and at least two orders of magnitude lower than the one for the sub-micron particles. Differential sedimentation effects on the early stages of the aggregation are negligible due to the small particle polydispersity.

References

1 U. Domanska and M. Krolikowska, *J. Solut. Chem.,* 2012, **41**, 1422-1445.
2 E. J. Gonzalez, A. Dominguez and E. A. Macedo, *J. Chem. Eng. Data,* 2012, **57**, 2165-2176.
3 B. Mokhtarani, A. Sharifi, H. R. Mortaheb, M. Mirzaei, M. Mafi and F. Sadeghian, *J. Chem. Thermodyn.,* 2009, **41**, 323-329.
4 O. Redlich and A. T. Kister, *Ind. Eng. Chem.,* 1948, **40**, 345-348.
5 J. Nordstrom, L. Aguilera and A. Matic, *Langmuir,* 2012, **28**, 4080-4085.
6 J. A. Smith, O. Werzer, G. B. Webber, G. G. Warr and R. Atkin, *J. Phys. Chem. Lett.,* 2010, **1**, 64-68.
7 K. Ueno, A. Inaba, M. Kondoh and M. Watanabe, *Langmuir,* 2008, **24**, 5253-5259.
8 E. Vanecht, K. Binnemans, S. Patskovsky, M. Meunier, J. W. Seo, L. Stappers and J. Fransaer, *Phys. Chem. Chem. Phys.,* 2012, **14**, 5662-5671.

Table S1. Properties of particles used.

Latex Particles	Radius (nm)			Polydispersity (%)[d]		Surface Charge (mC/m^2)[e]
	TEM[a]	SLS[b]	DLS[c]	TEM[a]	SLS[b]	
Sulphate	265	263	278	2.0	3.8	–19
Nano-Sized Sulphate	50	56	58	7.9	7.9[f]	–17
Amidine	110	110	117	4.3	7.1	10

[a]Measured by transmission electron microscopy by the manufacturer. Measured in static[b] and dynamic[c] light scattering experiments in stable suspensions. [d]Coefficient of variation. [e]Determined from the electrophoretic mobilities with the standard electrokinetic model in aqueous KCl solutions. [f]The value was kept fixed during the fit.

Table S2. Properties of pure ILs used at 25°C.

Ionic Liquid	Molecular Mass (g/mol)	Density (g/mL)	Refractive index (at 533 nm)	Refractive index (at 633 nm)	Viscosity (mPas)
BMIM-BF_4	226.0	1.201	1.422	1.418	104.0
BMIM-SCN	197.3	1.070	1.542	1.534	56.5
BMIM-$N(CN)_2$	205.3	1.060	1.512	1.505	30.0
BMPY-$N(CN)_2$	216.3	1.054	1.540	1.532	47.5
BMPL-$N(CN)_2$	208.3	1.013	1.499	1.494	34.6
BPY-BF_4	223.0	1.208	1.447	1.441	149.7

Table S3. Impurities of the ILs used as reported by manufacturer (in mg/L).

IL	F^-	Cl^-	Br^-	Na^+	NH_4^+	MIM[a]	MPL[b]	PY[c]
BMIM-SCN	–	690	–	–	2770	9680	–	–
BMIM-$N(CN)_2$	–	9360	30	–	–	180	–	–
BMIM-BF_4	50	10	10	–	–	210	–	–
BMPY-$N(CN)_2$	–	17000	20	2960	–	–	–	7760[d]
BMPL-$N(CN)_2$	–	2870	200	–	–	–	50	–
BPY-BF_4	–	10	–	1000	–	–	–	1000

[a]1-Methylimidazole. [b]1-Methylpyrrolidine. [c]Pyridine. [d]3-Methylpyridine.

Table S4. Parameters of the polynomial model fit of the viscosity as given by eq. (3).

Parameter	BMPL-$N(CN)_2$	BMPY-$N(CN)_2$	BMIM-$N(CN)_2$	BMIM-SCN	BMIM-BF_4	BPY-BF_4
a_0	4.75	–13.2	–4.88	–41.1	–149	–239
a_1	5.71	10.6	4.18	8.80	89.6	171
a_2	–14.3	–5.10	–6.10	–2.44	–14.6	–98.2
a_3	–6.53	–11.4	1.07	0	–27.6	34.9
a_4	0	0	0	0	–17.4	0

Table S5. Critical coagulation concentrations (CCC) for latex particles in IL-water mixtures.

	Amidine Latex		Sulphate Latex	
	CCC-W[a]	CCC-IL[b]	CCC-W[a]	CCC-IL[b]
KCl	0.19±0.01	–[c]	0.30±0.01	–[c]
BMIM-BF_4	0.10±0.01	0.8±0.6	0.050±0.005	0.9±0.6
BMIM-SCN	0.03±0.01	1.8±0.1	0.11±0.002	13±1
BMIM-$N(CN)_2$	0.050±0.005	3.2±0.2	0.093±0.008	5.6±0.6
BMPY-$N(CN)_2$	–[d]	6.7±0.3	–[d]	3.2±0.1
BMPL-$N(CN)_2$	0.060±0.005	2.6±0.2	0.057±0.003	10±0.8
BPY-BF_4	0.060±0.007	0.9±0.6	0.055±0.004	0.8±0.6

[a]Concentration of the ILs in mol/L. [b]Concentration of water in mol/L. [c]There is no such CCC since the solubility limit is reached beforehand. [d]The CCC could not be determined due to formation of precipitates.

Table S6. Properties of the previously published particle suspensions in ILs shown in Fig. 1.

Particle type	Mean Particle Radius (nm)	IL	Time (s)[a]	Particle Concentration (m^{-3})	Reference
Silica[b]	6.0	BMIM-BF_4	7.2×10^4	1.6×10^{22}	Nordström et al.[5]
Silica	580	EA-NO_3[c]	7.2×10^4	7.2×10^{18}	Smith et al.[6]
Silica[d]	62	BMIM-PF_6	4.3×10^4	1.9×10^{22}	Ueno et al.[7]
Gold	3.0	BMIM-$N(CN)_2$	1.2×10^6	1.2×10^{20}	Vanecht et al.[8]

[a]Time over which the suspension was reported to be stable. [b]Fumed silica particle was used and the system contained $LiBF_4$ as well. [c]Ethylammonium nitrate. [d]Silica particles with grafted with poly(methyl methacrylate) on the surface.

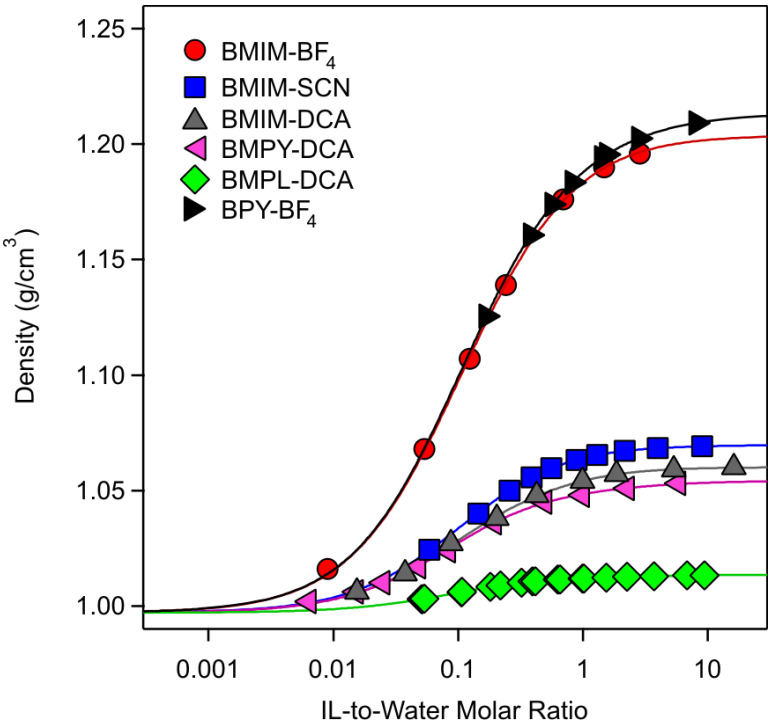

Figure S1. Densities versus the IL-to-water molar ratios. The symbols are experimental data and the lines correspond to the ideal mixing law eq. (1).

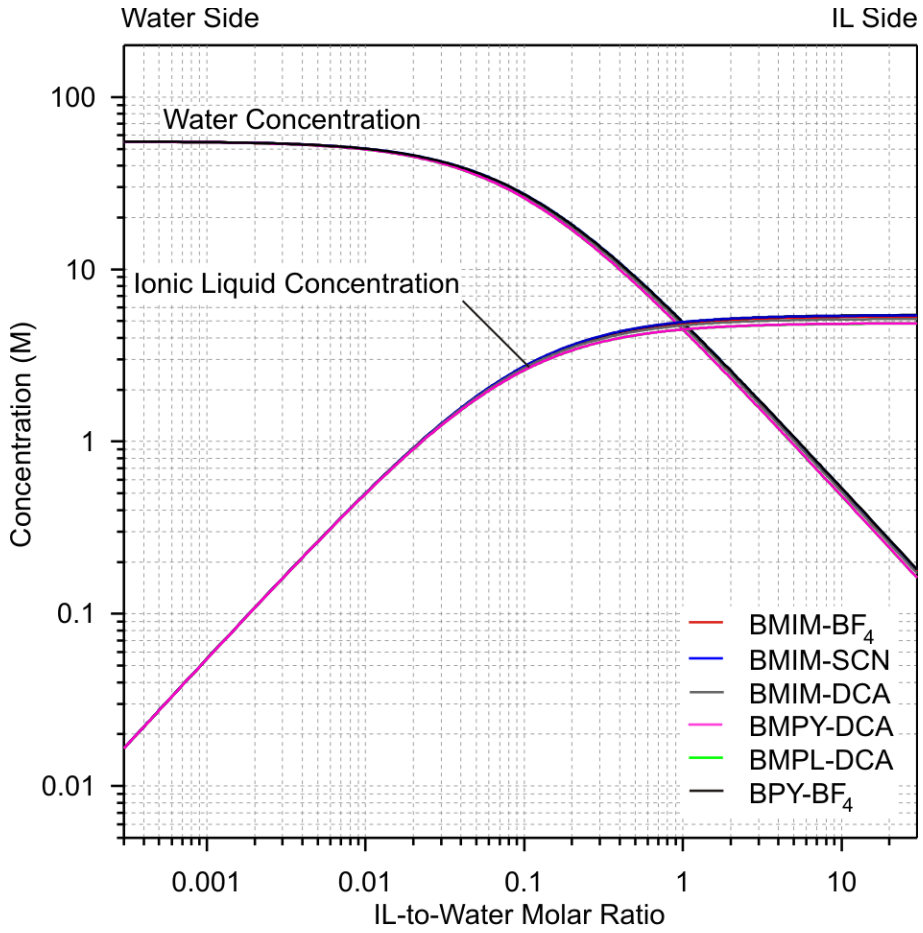

Figure S2. Molar concentrations in IL-water mixtures as a function of the IL-to-water molar ratios. The water and IL molar concentrations are shown. The different lines indicate the different ILs used in the present study.

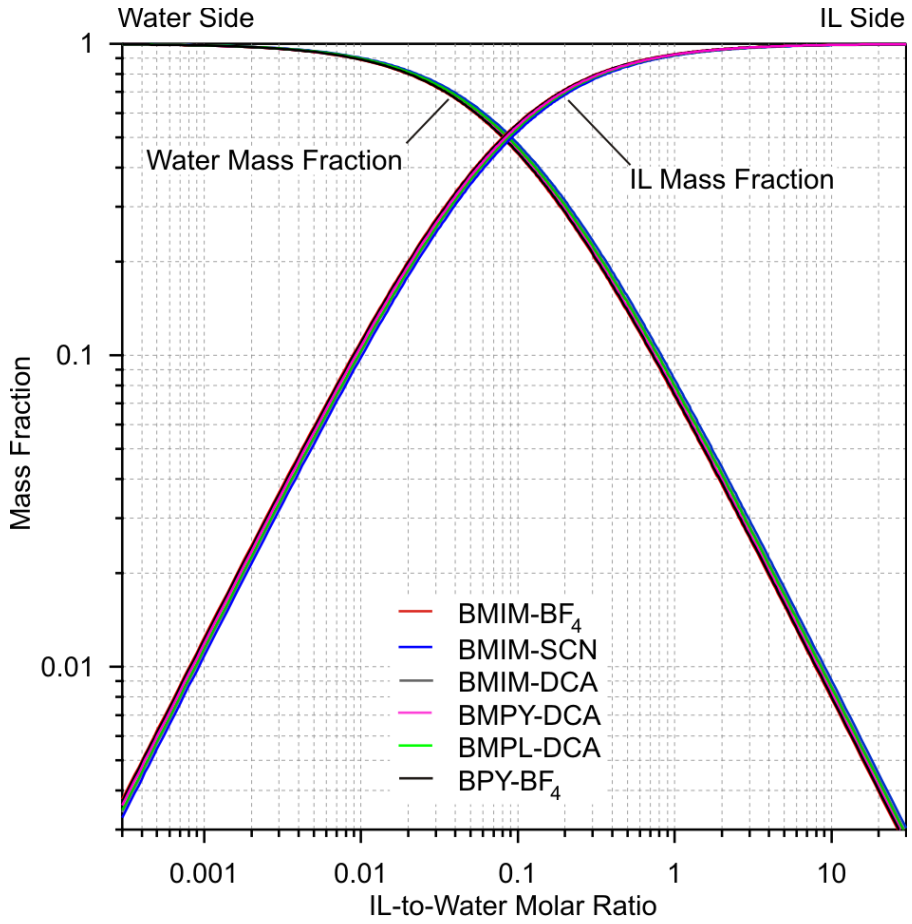

Figure S3. Mass fractions in IL-water mixtures as a function of the IL-to-water molar ratios. The water and IL mass fractions are shown. The different lines indicate the different ILs used in the present study.

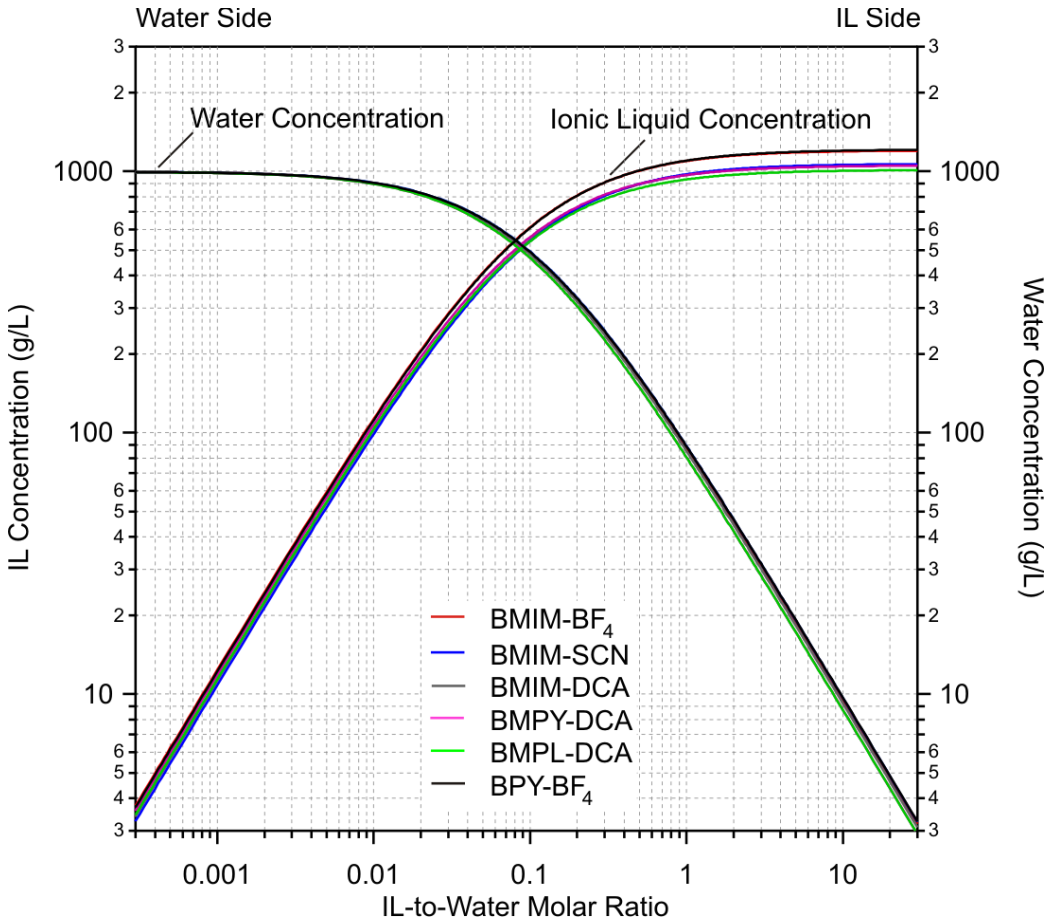

Figure S4. Mass concentrations in IL-water mixtures as a function of the IL-to-water molar ratios. The water and IL mass concentrations are shown. The different lines indicate the different ILs used in the present study.

CHAPTER 8

CONCLUSIONS

Throughout this PhD thesis I demonstrated the applicability of the light scattering techniques for monitoring particle aggregation processes. The appropriate evaluation of the scattered light intensity provided the possibility to determine absolute aggregation rates of suspensions in different ionic environments. In addition, two comparative studies were performed where besides accurate measurements of aggregation rates, direct force measurements were carried out in order to reveal the forces acting between the colloidal particles under different conditions. Based on the obtained force profiles, aggregation rates could be calculated and directly compared to the ones measured by the means of light scattering techniques. Such comparison of aggregation rates using the same type of particles is uniquely done in our laboratory. In most of the cases, the charging behaviour of the different particles was also monitored by electrophoresis, which helped the better understanding of the interactions.

The main part of this thesis was dealing with different ion-specific interactions in particle aggregation. The well-known Schulze-Hardy rule and the Hofmeister series were discussed in comprehensive studies, where several findings helped the better understanding of the interactions of such origins. We demonstrated that the multivalent ions bear with more effective coagulating power than the monovalent ones, as the Schulze-Hardy rule states. Experimental evidence was provided that the viscosity of the medium needs to be carefully taken into account at elevated electrolyte concentrations. Once the salt level increases, the increased viscosity of the different electrolyte solutions can hinder the diffusion, thus the aggregation of the particles. Normalization of the aggregation rates with respect to the Smoluchowski values reveals that at these conditions, the aggregation is still diffusion-controlled and no additional stabilization mechanism is present. Direct force measurements showed that while in case of monovalent and divalent ions the DLVO

theory is capable of predicting the interactions down to distances of few nm, at shorter distances a strong non-DLVO attraction needs to be taken into consideration. For counterions of higher valence, an additional, more long-ranged non-DLVO attractive force is observed, which can be interpreted by surface charge heterogeneities.

In three chapters, I showed that not only multivalent ions can have specific interactions with particle surface, but ions of the same valence too. The hydration state of the different monovalent ions is crucial in determining their coagulating power, in good agreement with the Hofmeister series. However, when they act as co-ions, their chemical nature is rather unimportant. Calculations based on a simplified form of DLVO theory using the measured CCCs and electrophoretic mobilities reveal that the driving forces are mainly of DLVO origin. The shifts in the CCCs originate from the modification of the surface charge. However, the Hamaker constant obtained by fitting was somewhat high, indicating the presence of additional non-DLVO forces. In fact, an additional attractive short-ranged force must be included in the interaction force profiles, as our combined AFM-LS study revealed. The measured and calculated fast aggregation rates are somewhat differ, however, the stability ratios are in excellent agreement. The additional force is essential in predicting the shifts in the CCCs correctly, assumption of forces of only DLVO origin leads to enormously high values.

After several studies on ion-specific effects on particle aggregation induced by well-studied simple and complex electrolytes, I investigated the charging and stability of latex particles in aqueous solutions of ionic liquids. I showed that only small changes in the constituent anions and cations can lead to completely different behavior of the suspension. Investigating the effect of the alkyl chain of the IL constituent cations reveal that the extent of adsorption on oppositely charged surface can lead to not only neutralization and overcharging, but the charge reversal can be so pronounced in case of longer chain lengths that restabilization of the dispersion occurs at intermediate concentrations.

Due to the growing relevance of ionic liquids in materials science applications, in particularly in nanoparticle synthesis, we investigated the stability of colloidal particles in water-miscible ionic liquids through the whole concentration range. Besides the classical DLVO type of suspension behaviour in dilute IL solutions, two types of stabilization mechanisms were established. First, viscous stabilization occurs in highly viscous ILs due to the increased viscosity of the IL-water

mixtures at elevated IL concentrations. This originates from the hindered diffusion of the particles, which results in a slowdown in the aggregation. Second, at even higher IL concentrations solvation stabilization is the driving mechanism, which originates from the layering of the IL constituents on the particle surface. This structure formation results in an overall repulsive interparticle force, preventing the suspensions from the aggregation.

Another important finding, that the comparison of the absolute aggregation rates in all the different systems investigated reveals that the fast rates are independent on the type of ions present in the solution using the same particle, however, the absolute values somewhat differ from particle to particle.

Based on the different studies presented in this thesis, it can be concluded, that ionic additives can be useful in tuning the stability of suspensions. However, ion-specific interactions in the actual systems need to be well understood. Not only the valence of the ions, but their hydration state is crucial as well in determining their stabilization power, which needs to be considered in case of formulation of particle suspensions for given applications.

Acknowledgement

First of all I would like to express my deep gratitude to my supervisor Prof. Michal Borkovec for his guidance and advices concerning the different projects as well as my future career.

I am grateful to Prof. Gérard Hopfgartner and Prof. Paul Dyson for accepting to be member of the committee for my PhD defense.

I would like to express my very special thanks to Dr. Istvan Szilagyi for teaching me the different techniques I have been using, for all the support and fruitful discussions throughout my PhD and for becoming a real friend of mine.

Special thanks to our lovely secretary Anne-Marie Loup for the enourmous amount of effort she made to help me with all the bureaucratic issues, for all the lunch breaks, and for becoming my honorary second mother. Without her, this PhD wouldn't have been possible.

I would like to acknowledge Dr Francisco Javier Ruiz Montes-Cabello for performing and evaluating the AFM force measurements, for all the fruitful discussions and for becoming a really good friend of mine.

Special thanks to Dr Tamas Szabo and Dr Anthony Désert for their huge contribution to the results presented in the seventh chapter.

I would like to thank to Dr. Gregor Trefalt for helping me many times with the data evaluation.

I am thankful to our technician Olivier Vassalli for all the help in the different measurements.

I thank all the former and present members of the LCSC group for the nice athmosphere over the years. In particular, to Javier, Magda, Tamás, Mohsen, Pavel, Marco, David, Paul, Marko and Biljana for all the amazing memories.

I would like to thank to all my friends in Hungary and in Geneva for all the support and funny moments.

I would like to express my deepest gratitude to my family, in particular to my mother, for the support and encouragement in pursuing scientific career.

Last but not least, I would like to dedicate this thesis to the memory of my father.